NASA Conference Publication 2471

Structural Integrity and Durability of Reusable Space Propulsion Systems

Proceedings of a conference held at
NASA Lewis Research Center
Cleveland, Ohio
May 12–13, 1987

NASA

NASA Conference Publication 2471

Structural Integrity and Durability of Reusable Space Propulsion Systems

Proceedings of a conference
held at NASA Lewis Research Center
Cleveland, Ohio
May 12–13, 1987

National Aeronautics
and Space Administration

Scientific and Technical Information Branch

1987

FOREWORD

The space shuttle main engine (SSME), a reusable space propulsion system, is the most sophisticated Earth-to-orbit propulsion system in use today. Since the United States will rely on the shuttle and its derivative versions for space transportation for the next several decades, the National Aeronautics and Space Administration (NASA) is conducting a program which will establish a technology base and develop the analytical tools necessary for an orderly evolution of reusable rocket engines.

A substantial portion of the technology program is devoted to the structural integrity and durability aspects of reusable rocket systems. This effort focuses on the development of accurate analytical models to describe flow fields, aerothermodynamic loads, structural responses, and fatigue/fracture effects. These analytical tools are then applied to the development of life prediction models of engine components and subsystems. The effort is supported by the development of advanced instrumentation with capabilities to verify the models in an SSME-like environment. These instruments have the potential for future use as diagnostic sensors to perform real-time condition monitoring in critical engine components. The research is conducted through in-house activities at the Lewis Research Center, industrial contracts, and university grants.

To provide a forum for representatives from government, industry, and academia to learn about and discuss the latest findings and progress toward improved structural integrity and durability of reusable space propulsion systems, a 2-day conference was held at NASA Lewis in May 1987. This publication contains extended abstracts and figures used for each of the presentations at the conference.

Stanley J. Marsik
Conference Chairman

CONTENTS

ADVANCED EARTH-TO-ORBIT PROPULSION TECHNOLOGY

Frank W. Stephenson
NASA Headquarters
Washington, D.C.

The Structural Integrity and Durability Program is an integral part of a broadly based NASA rocket technology effort addressing reusable Earth-to-orbit (ETO) engine issues which is being conducted through the NASA Marshall Space Flight and Lewis Research Centers. Program funding is provided by the Office of Aeronautics and Space Technology (OAST) and the Office of Space Flight (OSF).

The era of reusable rocket engines was ushered in by the space shuttle main engine (SSME). A small effort aimed at extending reusable engine technology was initiated in the 1970's, but it wasn't until 1980 that full attention was given to this critical area. At that time, it was fully recognized that our ability to characterize, predict, and guarantee the life of reusable rocket engines, such as the SSME, was severely limited. Since that time, a focused program aimed at developing design and analysis tools capable of assuring the life and performance of reusable ETO engines has been strongly supported on a continuous basis. The program has used SSME experience to identify critical life-limited engine components, as well as design and analysis deficiencies, and in part is building on the experience base established in the airbreathing engine community to help correct these deficiencies. The SSME will also be used as a test bed to verify advanced design concepts and to validate improved analytical codes developed under this program.

The ETO program encompasses three major areas: life prediction/extension, performance, and operations. The life prediction/extension efforts are focused on developing an understanding of and analytically simulating internal engine environments, both mechanical and thermal; on defining resulting transient and steady-state loads; on developing analyses for determining component structural response and material behavior; and on ultimately developing life-prediction techniques, especially for combinations of high-cycle and low-cycle fatigue. Engine performance technologies are primarily directed toward extending combustion, stability, heat-transfer, and cooling models to higher pressure operating conditions. Higher temperature turbine blade materials are also being explored to allow higher combustion pressures. Operations technology is directed toward developing health monitoring diagnostic sensors for automated between-flight inspection, servicing, and checkout; for maintenance scheduling; and for in-flight fault-tolerant engine operation. The principal beneficiary of these technology advances will be the next generation of ETO rocket engines, although the SSME has already accrued some benefits. This conference is focused primarily on reviewing the status and results of life extension/prediction technology tasks involving engine hot-gas flow systems.

OVERVIEW OF AEROTHERMODYNAMIC LOADS DEFINITION STUDY

Raymond E. Gaugler
NASA Lewis Research Center
Cleveland, Ohio

The objective of the Aerothermodynamic Loads Definition Study is to develop methods to more accurately predict the operating environment in the space shuttle main engine (SSME) powerhead. Development of time-averaged and time-dependent, three-dimensional viscous computer codes as well as experimental verification and engine diagnostic testing are considered to be essential in achieving that objective. Time-averaged, nonsteady, and transient operating loads must all be well defined in order to accurately predict powerhead life. Improvements in the structural durability of the SSME turbine drive systems will depend on our knowledge of the aerothermodynamic behavior of the flow through the preburner, turbine, turnaround duct, gas manifold, and injector post regions.

The approach taken in this study consists of two parts: (1) to modify/apply/disseminate existing computational fluid dynamics (CFD) tools in response to current needs, and (2) to develop new technology that will enable more accurate computation of the time-average and unsteady aerothermodynamic loads in the SSME powerhead. With the more accurate aerothermodynamic loads predictions providing boundary conditions to improve structural and fatigue life analysis, the goal of improved durability will be met.

This study was begun in October 1983. The initial effort involved the use of existing CFD tools to analyze problems in the fuel and oxidizer turbopump turbines, the fuel turbine turnaround duct, the fuel-side preburner, and the main injector liquid oxygen posts. Results of those efforts have been presented at previous meetings.

At this meeting, some of the currently ongoing tasks will be highlighted, primarily those dealing with the development of new CFD tools. Also included will be a final report on the analytical and experimental study of the main injector liquid oxygen posts.

UNSTEADY STATOR/ROTOR INTERACTION

Philip C.E. Jorgenson and Rodrick V. Chima
NASA Lewis Research Center
Cleveland, Ohio

The major thrust of the computational analysis of turbomachinery to date has been the steady-state solution of isolated blades using mass-averaged inlet and exit conditions. Unsteady flows differ from the steady solution due to interaction of pressure waves and wakes between blade rows. To predict the actual complex flow conditions one must look at the time accurate solution of the entire turbomachine.

ANALYSIS

Many of the numerical tools used in the analysis of isolated blades can be used for time-accurate analysis. Here the quasi-three-dimensional Euler and thin-layer Navier-Stokes equations are solved for unsteady turbomachinery flows. These equations are written in general coordinates for an axisymmetric stream surface, and they account for the effects of blade-row rotation, radius change, and stream-surface thickness (ref. 1).

A four-stage Runge-Kutta scheme based on the work of Jameson (ref. 2) is used to predict time-accurate results. Body-fitted C-type grids were used in this work and were generated using the GRAPE code (GRids about Airfoils using Poisson's Equation) developed by Sorenson (ref. 3).

To predict the interaction between a stator and a rotor in turbomachinery, one must pass flow information to an interface that acts as a moving boundary between the two computational grids. A nonconservative interface formulation is used in this procedure. The solution must be integrated using a constant minimum time step based on the computational domain of two blades. The data management necessary to update the stator and rotor flowfields will be discussed. Currently the code is limited to solving stator/rotor configurations that have equal pitch blades.

RESULTS

The solution procedure has been applied to two test problems. The first is a cascade and the second is a turbine rotor from the space shuttle main engine (SSME). Euler and Navier-Stokes results will be presented.

A model turbine stage made up of two identical cascades of NACA 0012 airfoils was used to develop and test the interface and data management routines. Figure 1 shows the C-grids used in the computation where the second blade row is moving downward. A converged solution can be seen in the periodic loading diagram of the rotor (fig. 2).

The stator inlet Mach number is 1.84. Figure 3 shows relative Mach number contours when the blade rows are aligned. Detached bow shocks form ahead of the stators, interact at mid-passage, and reflect obliquely back to the stator surface. A strong curved shock forms at the stator trailing edge, and the shock curvature generates an entropy layer that convects downstream into the rotor. The stator flowfield is symmetric but the rotor flowfield is asymmetric due to the incidence of the relative flow.

Figure 4 shows relative Mach number contours after the rotor has moved 1/4 pitch downward. The flow between the stator and rotor is subsonic so that pressure waves from the rotor can affect the stator trailing-edge shock, which has moved upstream. The entropy layer from this shock produces a large asymmetry in the rotor flowfield. The flow reaccelerates to supersonic in the rotor passage and produces strong oblique shocks off the rotor trailing edge.

Previous steady-state calculations of the SSME first-stage fuel-side turbine blade (ref. 1) showed a reverse flow region on the pressure surface (fig. 5). Time-accurate results are being generated to determine how that separation is affected by the upstream stator wakes. The grids used for this calculation are shown in figure 6 where the second blade row is the rotor of interest. Euler results are shown in figure 7. There is very little interaction between the blade rows. Viscous results will be shown in the presentation. Currently the numerical procedure works on blade row configurations of equal pitch. The actual SSME stator/rotor blade count is 41:63, which is close to the 2:3 count shown in figure 8. A future goal of this work is to use this solution procedure to solve problems of unequal blade count like the one shown here.

REFERENCES

1. Chima, R.V.: Development of an Explicit Multigrid Algorithm for Quasi-Three-Dimensional Viscous Flows in Turbomachinery. AIAA Paper 86-0032, Jan. 1986. (Also, NASA TM-97128.)

2. Jameson, A., et al.: Numerical Solutions of the Euler Equations by Finite Volume Methods Using Runge-Kutta Time-Stepping Schemes. AIAA Paper 81-1259, June 1981.

3. Sorenson, R.L.: A Computer Program to Generate Two-Dimensional Grids About Airfoils and Other Shapes by the Use of Poisson's Equation. NASA TM-81198, 1980.

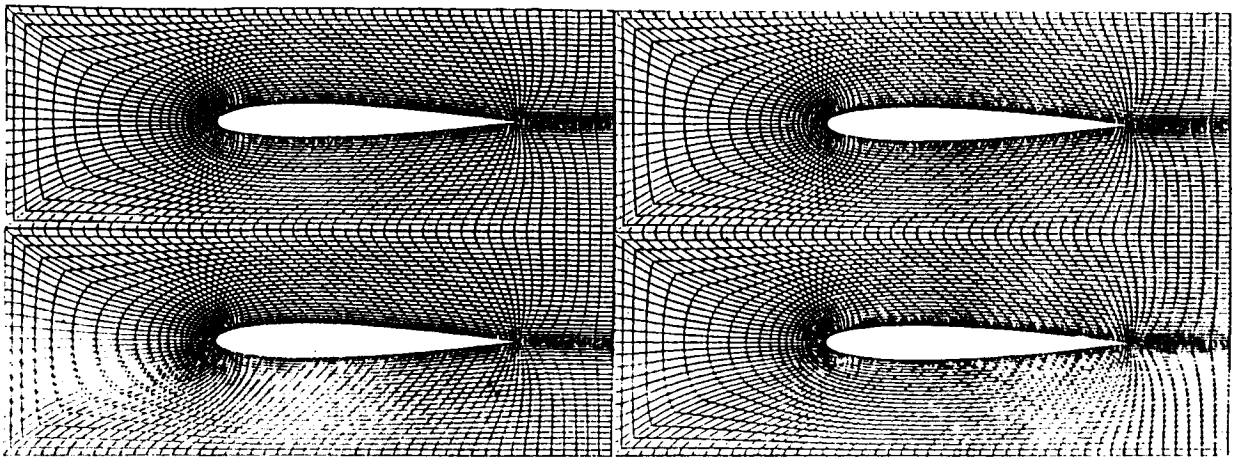

Figure 1.- Computational grids for the NACA 0012 model problem.

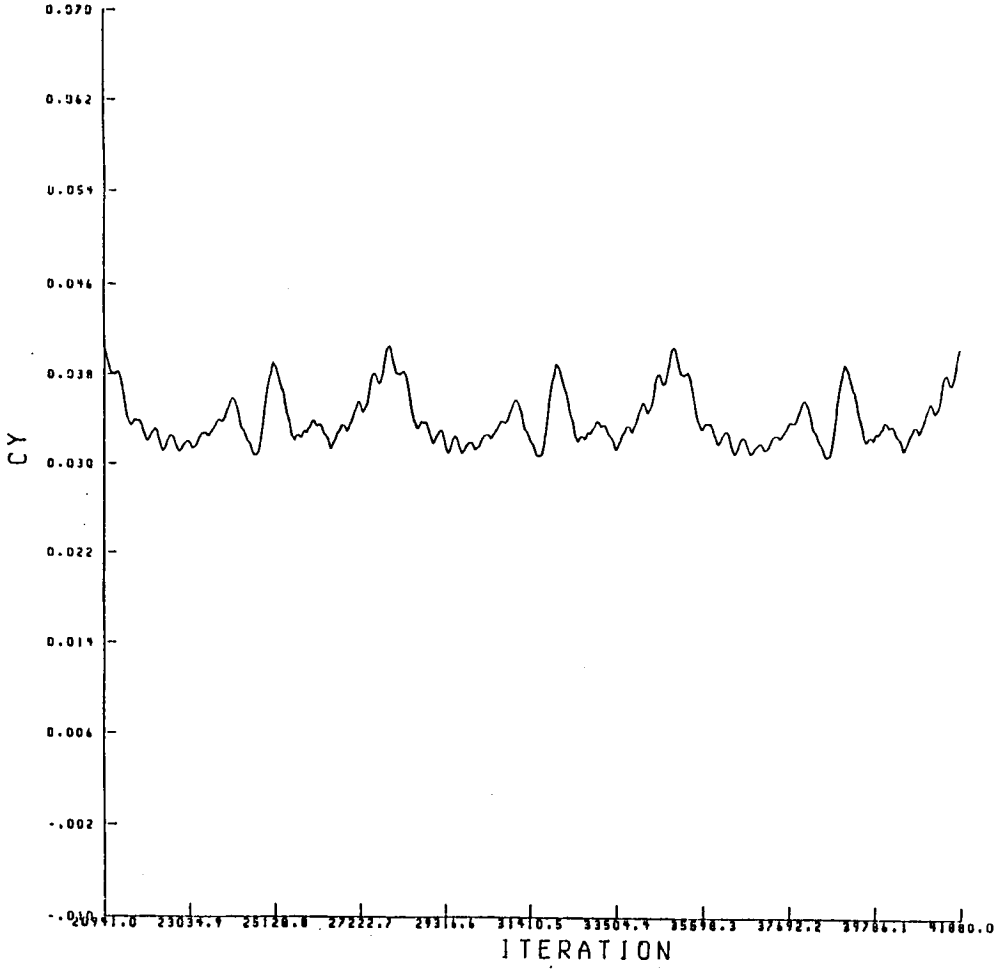

Figure 2. - Loading diagram for the model problem rotor.

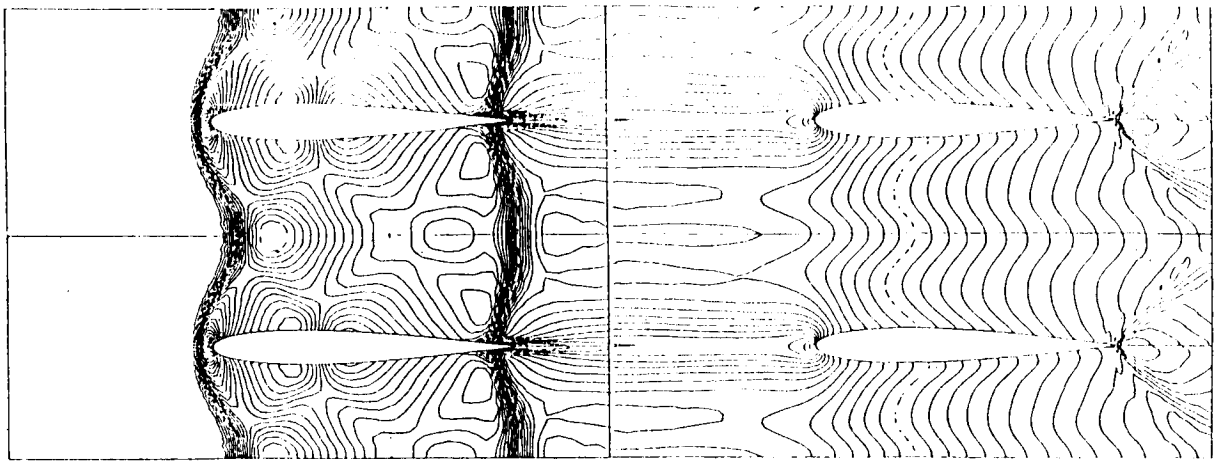

Figure 3.- Mach contours after 1.00 pitch rotation.

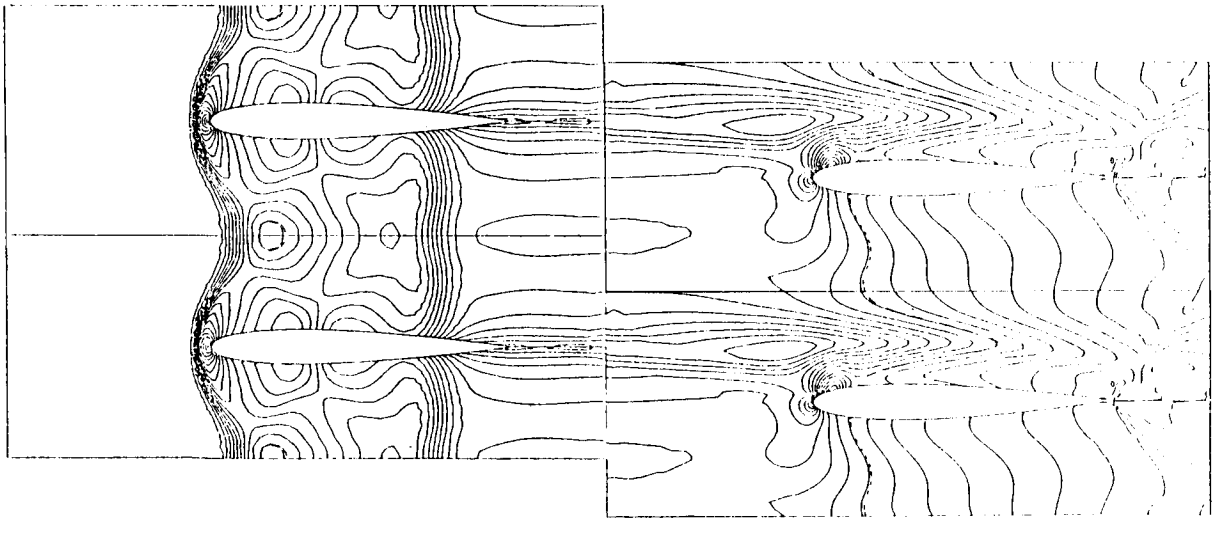

Figure 4.- Mach contours after 1.25 pitch rotations.

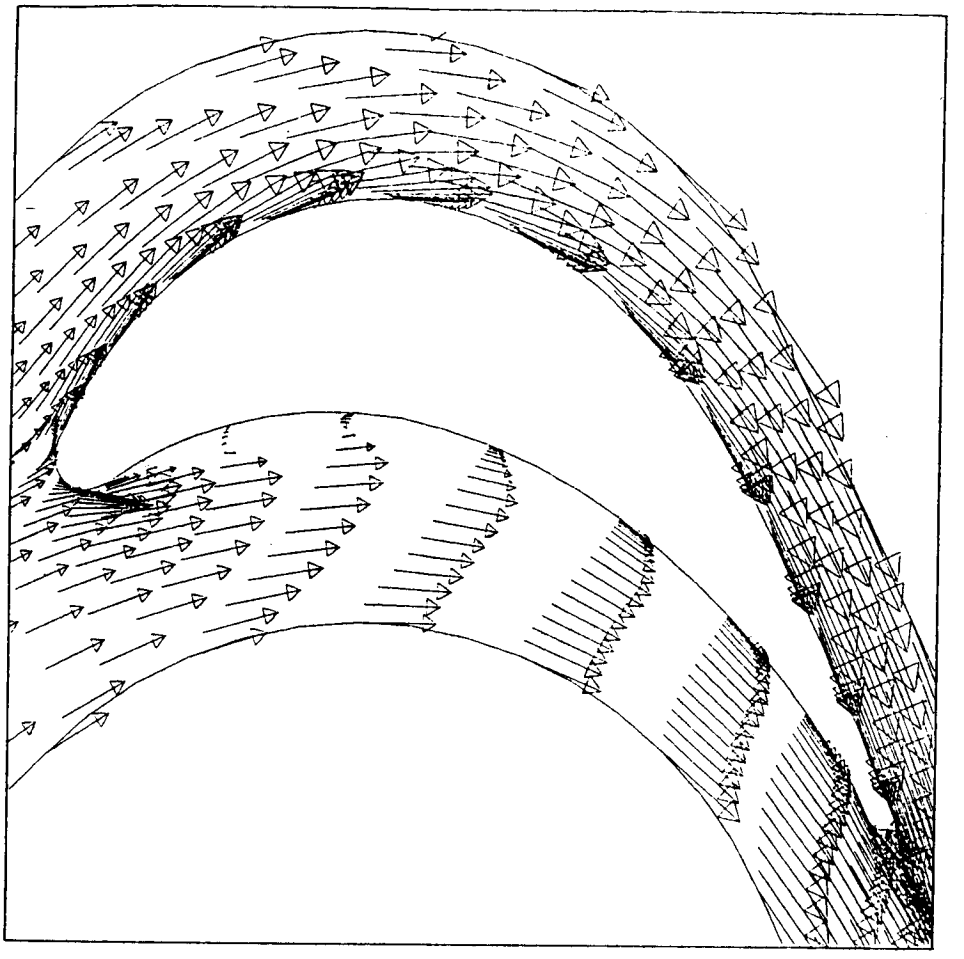

Figure 5. - Steady-state vector plot of SSME turbine rotor.

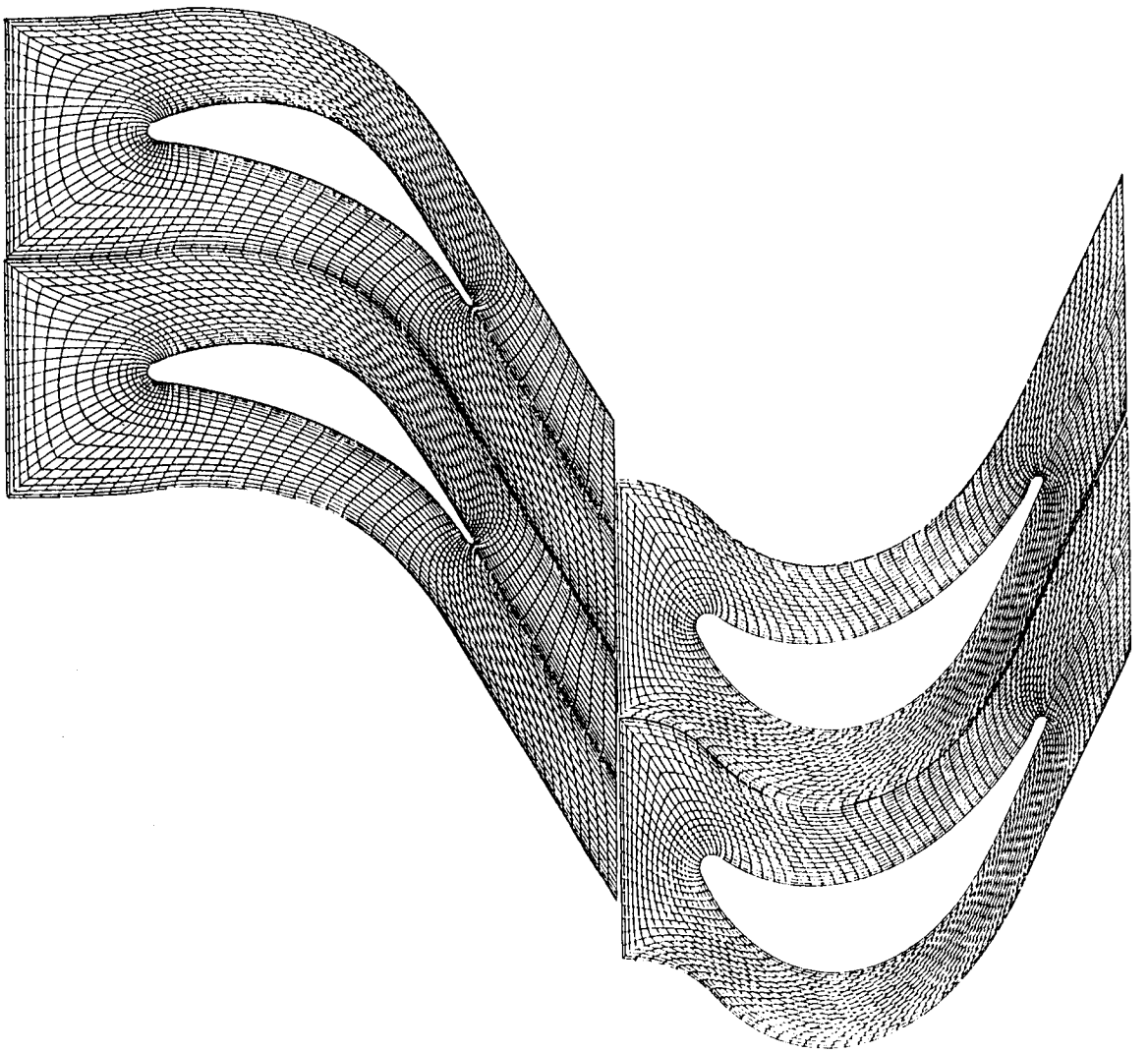

Figure 6. - Computational grids for the time-accurate SSME turbine rotor.

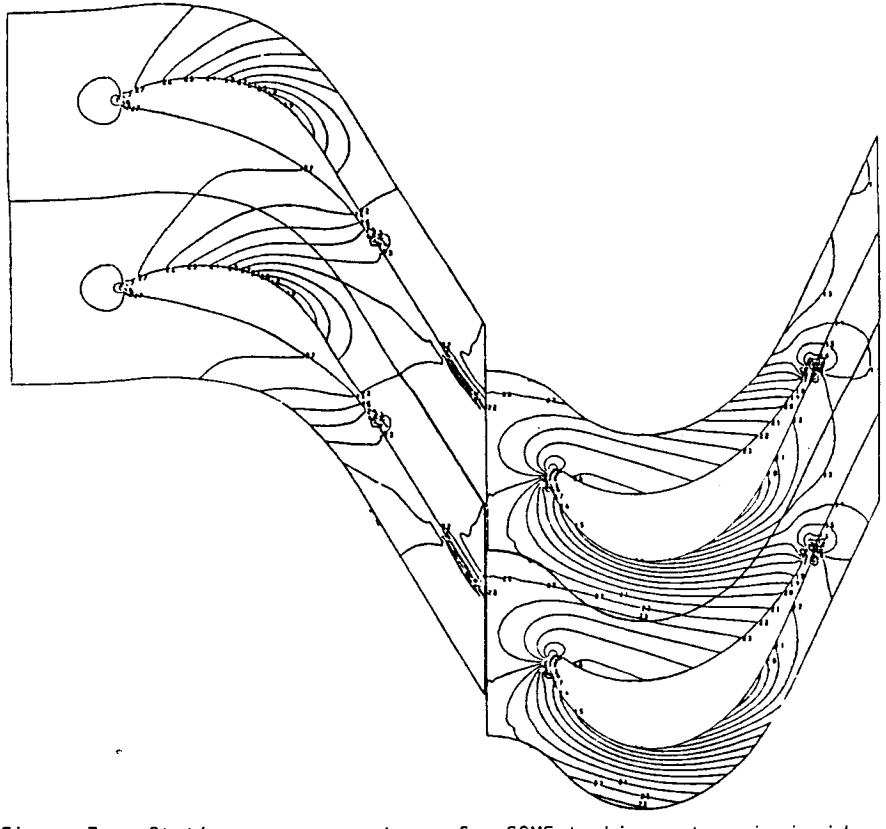

Figure 7. - Static pressure contours for SSME turbine rotor, inviscid.

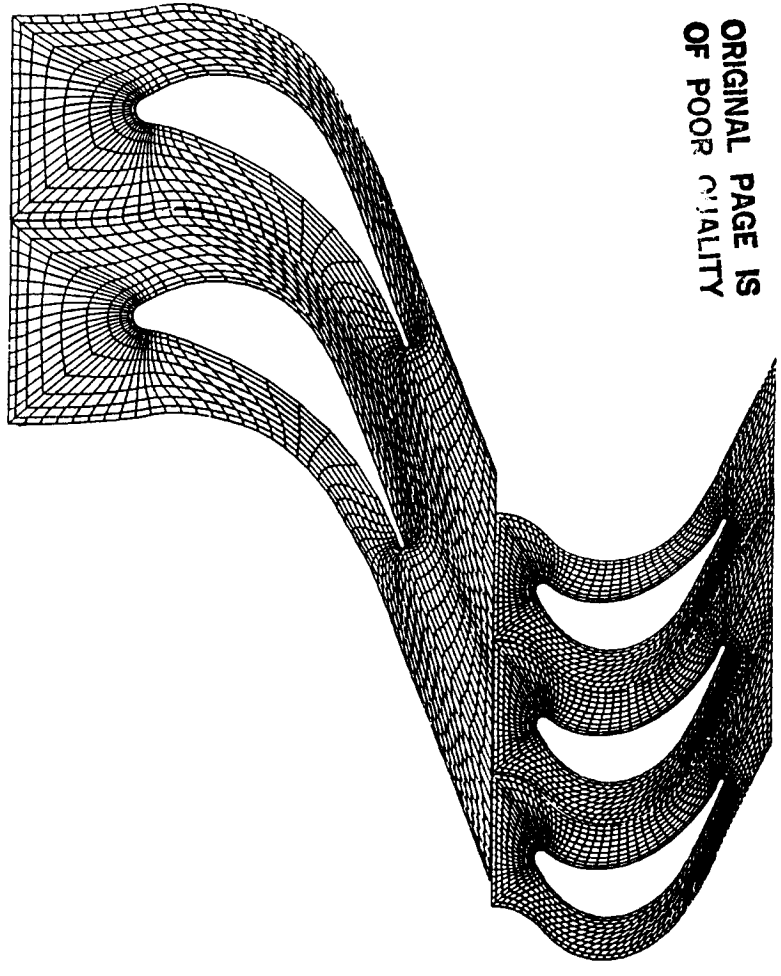

Figure 8. - SSME stator/rotor blade configuration.

SIMULATION OF MULTISTAGE TURBINE FLOWS

John J. Adamczyk
NASA Lewis Research Center
Cleveland, Ohio

and

Richard A. Mulac
Sverdrup Technology, Inc.
Middleburg Heights, Ohio

A flow model has been developed for analyzing multistage turbomachinery flows. This model, referred to as the "average passage" flow model, describes the time-averaged flow field with a typical passage of a blade row embedded within a multistage configuration. The presentation summarizing the work done to date, based on this flow model, will be in two parts. The first part of the talk will address formulation, computer resource requirement, and supporting empirical modeling, and the second part will address code development with an emphasis on multitasking and storage. The presentation will conclude with illustrations from simulations of the space shuttle main engine (SSME) fuel turbine performed to date.

SSME POWERHEAD COMPONENT ARRANGEMENT

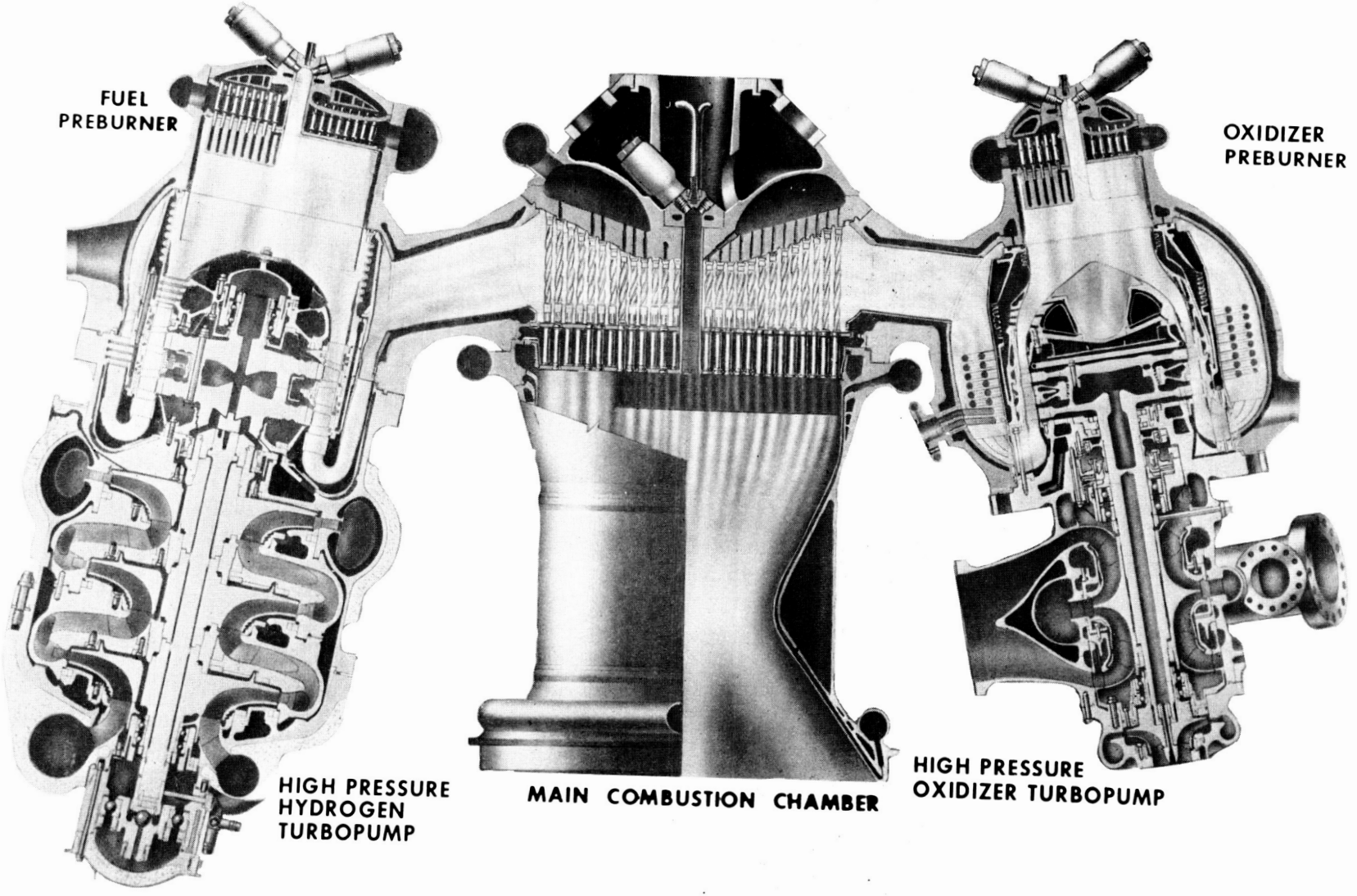

Figure 1.

PREMISE

- HIGH SPEED MULTI – STAGE TURBOMACHINERY FLOWS HAVE TOO MANY LENGTH AND TIME SCALES TO BE AMENABLE TO DIRECT NUMERICAL SIMULATION EVEN ON TODAY'S MOST ADVANCED COMPUTERS

- MODELS OF MULTI – STAGE FLOWS WHICH GIVE AN "AVERAGED" DESCRIPTION OF THE FLOW WITHIN TURBOMACHINERY PROVIDE USEFUL INFORMATION

Figure 2.

OBSERVATION

MOST MODELS CURRENTLY USED TO ANALYZE MULTI – STAGE FLOWS ARE BASED ON AN AXI–SYMMETRIC REPRESENTATION OF THE FLOW WITHIN THESE MACHINES

Figure 3.

QUESTION

GIVEN TODAY'S COMPUTER RESOURCES AND HIGH RESPONSE INSTRUMENTATION, IS IT TIME TO DEVELOPE MODELS WHICH PROVIDE A HIGHER DEGREE OF RESOLUTION OF MULTI – STAGE FLOWS THAN TODAY'S AXISYMMETRIC MODELS?

Figure 4.

CONSTRAINT

- PROPOSED MODEL MUST BE COMPATIBLE WITH THE AVAILABLE COMPUTER RESOURCES AND INSTRUMENTATION LIMITS

- PROPOSED MODEL MUST HAVE A RATIONAL BASIS

Figure 5.

TURBOMACHINERY MODELING EQUATIONS

NAVIER STOKES

(REYNOLDS AVERAGED EQNS.)

ENSEMBLE AVERAGED EQNS.

- DETERMINISTIC FLOW FIELD

TIME AVERAGED EQNS.

- TIME AVERAGED FLOW FIELD

(TYPICAL BLADE PASSAGE FLOW FIELD)

AVERAGE-PASSAGE EQNS.

- BLADE-TO-BLADE PERIODIC FLOW FIELD

CIRCUMFERENTIAL AVERAGED EQNS.

- AXISYMMETRIC FLOW FIELD

QUASI 1-D EQNS.

Figure 6.

THREE-DIMENSIONAL CELL-CENTERED FINITE VOLUME FLOW SOLVER

ADAMCZYK'S AVERAGE-PASSAGE EQUATION SYSTEM

$$(d\lambda\underline{u}/dt) + L(\lambda\underline{u}) + \int \lambda\underline{S}dVol = \int \lambda\underline{K}dVol$$

$$\underline{u}^T = (\rho\,,\ \rho v_r\,,\ r\rho v_\theta\,,\ \rho v_z\,,\ \rho e_o\ )$$

$$L(\lambda\underline{u}) = \int_{dA} (\lambda\underline{F}\cdot d\underline{A}_r + \lambda\underline{G}\cdot d\underline{A}_\theta + \lambda\underline{H}\cdot d\underline{A}_z)$$

$\int \lambda\underline{S}dVol$ - *body forces, energy sources, momentum and energy temporal correlations associated with neighboring blade row (closure term)*

$\int \lambda\underline{K}dVol$ - *source term due to cylindrical coordinate system*

FOR ROTATING SYSTEMS

$$(d\lambda\underline{u}/dt)|abs = (d\lambda\underline{u}/dt)|rel - \Omega(d\lambda\underline{u}/d\theta)|rel$$

$$L(\lambda\underline{u}) = \int_{dA} (\lambda\underline{F}\cdot d\underline{A}_r + \lambda(\underline{G} - r\Omega\underline{u})\cdot d\underline{A}_\theta + \lambda\underline{H}\cdot d\underline{A}_z)$$

Figure 7.

AVERAGE PASSAGE FLOW MODEL
AXIAL MOMENTUM EQN.

$$\frac{\partial}{\partial r}\lambda r\rho uv + \frac{\partial}{\partial \theta}\lambda\rho uw + \frac{\partial}{\partial z}r\lambda(\rho u^2+P) = \text{VISCOUS TERMS} + \text{BODY FORCE} + \text{CORRELATIONS}$$

BODY FORCE = F_1 (NON-AXISYMMETRIC COMPONENT OF THE NEIGHBORING AVERAGE PASSAGE FLOW'S)
+ F_2 (NON-AXISYMMETRIC COMPONENT OF THE "UNSTEADY DETERMINISTIC" FLOW FIELD)
+ F_3 (NON-AXISYMMETRIC COMPONENT OF THE "TIME AVERGE" FLOW FIELD

CORRELATIONS = R_1 (NON-AXISYMMETRIC COMPONENT OF THE NEIGHBORING AVERAGE PASSAGE FLOW'S)
+R_2 (NON-AXISYMMETRIC COMPONENT OF THE "UNSTEADY DETERMINISTIC" FLOW FIELD)
+R_3 (NON-AXISYMMETRIC COMPONENT OF THE "TIME AVERAGE" FLOW FIELD
+R_4 ("TIME" "UNRESOLVED" FLOW)

Figure 8.

CLOSURE STRATEGY

FIELD EQUATION

$$(\partial u^{(1)}/\partial t)\,dV + \vec{L}(u^{(1)}) + \int S^{(1)} dV = 0$$

$$(\partial u^{(2)}/\partial t)\,dV + \vec{L}(u^{(2)}) + \underbrace{\int S^{(2)} dV}_{\text{Source Term}} = 0$$

Figure 9.

CLOSURE STRATEGY

BLADE ROW (1)

$$\vec{L}(u_n^{(1)}) + \int S^{(1)} dV = 0$$

BLADE ROW (2)

$$\vec{L}(u_n^{(2)}) + \int S^{(2)} dV = 0$$

WHERE

$S^{(1),(2)} = S^{(1),(2)}$ (*Body Force, Energy Src, Velocity Cor., Energy Cor.*)

Figure 10.

ASSUME

$$S^{(1)} = S^{(1)}(u_{n-1}^{(2)})$$

$$S^{(2)} = S^{(2)}(u_{n-1}^{(1)})$$

LET A ----> AXISYMMETRIC AVERAGING OPERATOR

THEN

$$A\,L(u_n^{(1)}) + \int S^{(1)}(u_{n-1}^{(2)})\,A\,dV = 0$$

$$A\,L(u_n^{(2)}) + \int S^{(2)}(u_{n-1}^{(1)})\,A\,dV = 0$$

Figure 11.

BUT

$$A\,L(u_n^{(1)}) = L^{(mx)}(A\,u_n^{(1)}) + \int S^{(2)}(u_n^{(1)})\,A\,dV$$

$$A\,L(u_n^{(2)}) = L^{(mx)}(A\,u_n^{(2)}) + \int S^{(1)}(u_n^{(2)})\,A\,dV$$

FINAL RESULT

$$L^{(mx)}(A\,u_n^{(1)}) + \int S^{(2)}(u_n^{(1)})\,A\,dV + \int S^{(1)}(u_{n-1}^{(2)})\,A\,dV = 0$$

$$L^{(mx)}(A\,u_n^{(2)}) + \int S^{(2)}(u_{n-1}^{(1)})\,A\,dV + \int S^{(1)}(u_n^{(2)})\,A\,dV = 0$$

UPON CONVERGENCE

$$A\,u_n^{(1)} = A\,u_n^{(2)}$$

Figure 12.

MODULAR CODE CONSTRUCTION

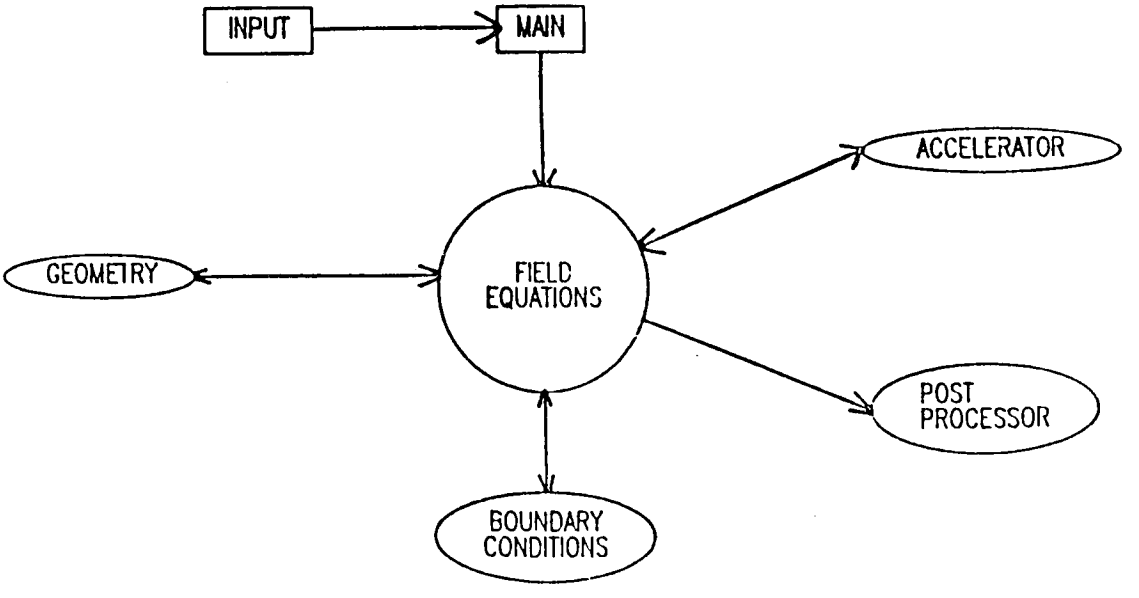

Figure 13.

AVERAGE–PASSAGE EQUATION SYSTEM

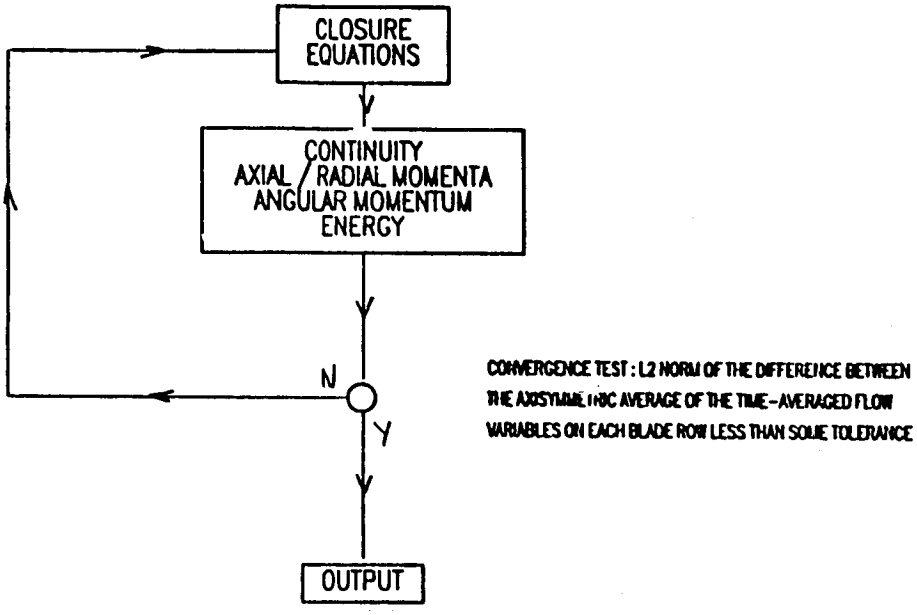

Figure 14.

MULTITASKING OF MULTISTAGE 3-D FLOW FIELD CALCULATION

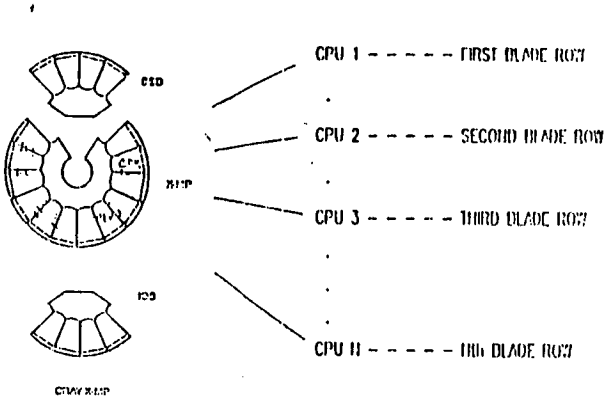

Figure 15.

EVOLUTION OF THE TOTAL TEMPERATURE FIELD WITHIN THE S.S.M.E. FUEL TURBINE

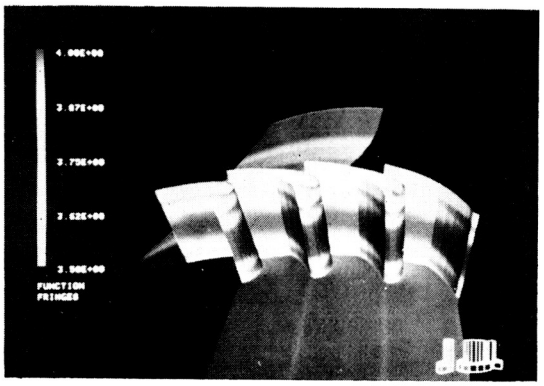

1st VANE
MID PASSAGE

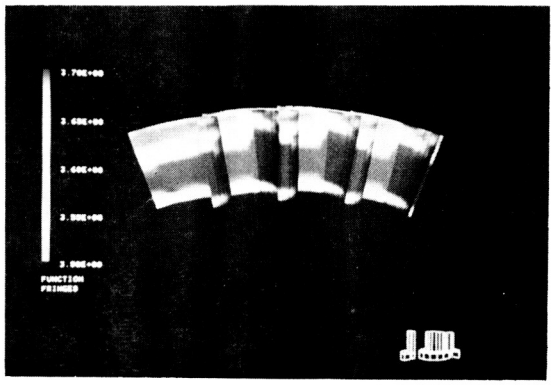

2nd VANE
MID PASSAGE

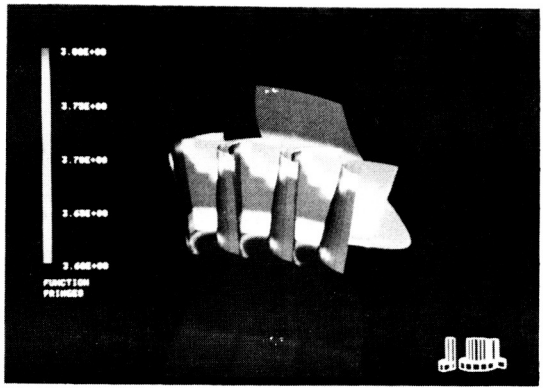

1st ROTOR
MID PASSAGE

2nd ROTOR
MID PASSAGE

SIMULATION PERFORMED ON LEWIS CRAY XMP 24

Figure 16.

PROGRESS IN THE PREDICTION OF UNSTEADY HEAT TRANSFER ON TURBINES BLADES

T. Cebeci
California State University
Long Beach, California

R.J. Simoneau
NASA Lewis Research Center
Cleveland, Ohio

and

A. Krainer and M.F. Platzer
Naval Postgraduate School
Monterey, California

This presentation describes the progress toward developing a general method for predicting unsteady heat transfer on turbine blades subject to blade-passing frequencies and Reynolds numbers relevant to SSME, such as illustrated in figure 1. The method employs an inviscid/viscous interactive procedure (fig. 2) which has been tested extensively for steady subsonic and transonic external airfoil problems. One such example is shown in figure 3. The agreement with experimental data and with Navier-Stokes calculations yields confidence in the method. The present work extends the technique to account for wake generated unsteadiness. The flow reversals around the stagnation point caused by the nonuniform onset velocity are accounted for by using the Characteristic Box scheme developed by Cebeci and Stewartson. The coupling between the inviscid and viscous methods is achieved by using a special procedure, which, with a novel inverse finite-difference boundary-layer method, allows the calculations to be performed for a wide range of flow conditions, including separation.

Preliminary results are presented for the stagnation region of turbine blades for both laminar and turbulent flows. A laminar model problem corresponding to a flow on a circular cylinder which experiences the periodic passing of wakes from turbine blades is presented to demonstrate the ability of the method to calculate flow reversals around the stagnation region. Calculations cover a Strouhal number range of 0.1 to 0.2 and a leading-edge Reynolds number range of 2×10^4 to 4×10^5.

BASIC EQUATIONS

The basic equations are presented in figure 4. As an essential preliminary to more extensive calculations involving complete blades, we consider here the development of an unsteady boundary-layer method for calculating the flow properties near the stagnation region of a blade where the movement of the stagnation point with space and time poses problems. We assume that the external velocity distribution is represented in dimensionless form by a function

(eq. (1)) which allows the variation of the stagnation point and the free-stream velocity.

For a two-dimensional, incompressible time-dependent laminar flow, the boundary-layer equations and their boundary conditions are well known, and for conditions with no mass transfer and specified wall temperature they can be written in the form shown in equations (2) to (6).

The calculation of upstream boundary conditions in the (t,y) plane at some $x = x_0$ when the conditions at a previous time line are known can introduce different problems. To illustrate these difficulties for the case of a moving stagnation point, let us consider equation (1). Since $u_e = 0$ at the stagnation point by definition, its location based on the external streamlines is given by $\xi_s = B(\tau)$.

Figure 5 shows the variation of the stagnation point with time according to the equation with $B(\tau) = 1 + c \sin \omega\tau$, $c = 1$, $\omega = \pi/4$. We see that the stagnation point ξ_s is at 2 when $\tau = -2$ and at 0 when $\tau = 6$, etc. If ξ_s were fixed, we could assume that $u = 0$ at $\xi_s = -1$ for all time and for all y, but this is not the case.

It is more convenient and useful to express equations (2) to (5) in a form more suitable for computation. To achieve this, we introduce the dimensionless variables τ, ξ, η, w, m, and G together with a dimensionless stream function $f(\xi,\eta,\tau)$ and, with $\theta = \partial f/\partial\xi$, write equations (2) to (5) as shown in equations (7) to (9). We use the Characteristic Box method to avoid the numerical problems associated with flow reversals in the stagnation region and to generate the initial conditions on the next time "line." This scheme requires that equations (7) and (8) are expressed in terms of new coordinates. For this purpose, we note the definition of local streamlines and let $d\tau = d\xi/f'$. If the distance in this direction is designated by s and the angle that it makes with the τ-axis by β, then the transformed momentum and energy equations (7) and (8) and their boundary conditions can be written as shown in equations (10) to (13).

MODEL PROBLEM

To illustrate the method we introduce a model problem, which corresponds to a flow on a circular cylinder of diameter D, which experiences the periodic passing of the wakes from the turbine blades (see fig. 6). For a time period t_g the cylinder is subjected to a freestream velocity U_∞ and for t_w it is immersed in a superimposed moving wake which has a motion component u_b. The cycle repeats itself with a so-called blade passing frequency $F[\equiv 1/(t_g + t_w)]$ and is related to the Strouhal number St by FD/U_∞. We assume that the stagnation region of the cylinder is subjected to a velocity which varies in space and time according to equation (1). (The variables are listed in fig. 6.)

Calculations are made for two values of Strouhal number taken equal to 0.1 and 0.2 with the dimensionless minimum wake velocity $u_m = 1/3$ in both cases. The computed values of wall heat flux $G'(0)$ show that they are not influenced by the changes in the freestream velocity and are virtually constant for the range of ξ and τ values considered with $G'(0) \sim 0.50$ for $St = 0.1$ and $G'(0) \sim 0.51$ for $St = 0.2$.

As shown in figure 7, the computed values of wall shear $f''(0)$ for $St = 0.1$ are significantly influenced by the changes in the freestream velocity which causes flow reversals in the velocity profiles around the stagnation point based on the vanishing of the external velocity. The movement of the stagnation point and the resulting flow reversals increase with time and with space. For example, the calculations for steady state have the stagnation point at $\xi = 0$, and, as expected, there is no flow reversal in either side of the stagnation point. At $\tau = 0.05$, the stagnation point moves to $\xi = 0.15$ but the flow reversals in the velocity profiles continue up to and including $\xi = 0.85$ as can be seen from the results shown in figure 8.

CONCLUDING REMARKS

The computed results show that the numerical procedure is able to obtain solutions for a range of blade-passing frequencies of practical relevance. The movement of the stagnation point with space and time and the resulting flow reversals around the stagnation point cause no computational difficulties and the numerical tests show that the accuracy is better than required for practical problems.

GENERAL OBJECTIVE

TO DEVELOP A GENERAL METHOD FOR COMPUTING UNSTEADY HEAT TRANSFER ON TURBINES BLADES SUBJECT TO NONUNIFORM ONSET VELOCITY

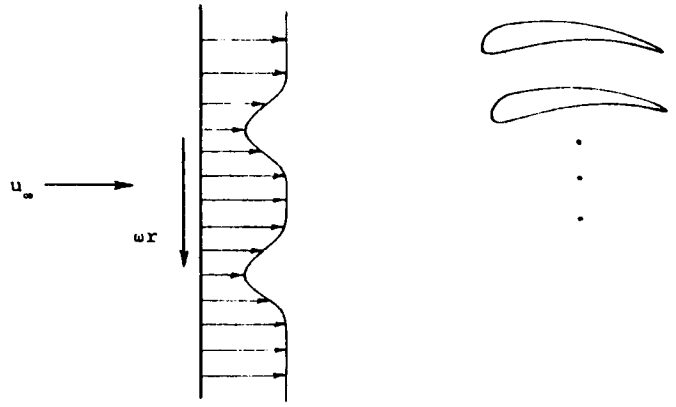

APPROACH

INTERACTIVE BOUNDARY-LAYER THEORY BASED ON THE SOLUTION OF INVISCID AND VISCOUS FLOW EQUATIONS BY A NOVEL COUPLING PROCEDURE

Figure 1. - Approach to rotor wake heat-transfer problem.

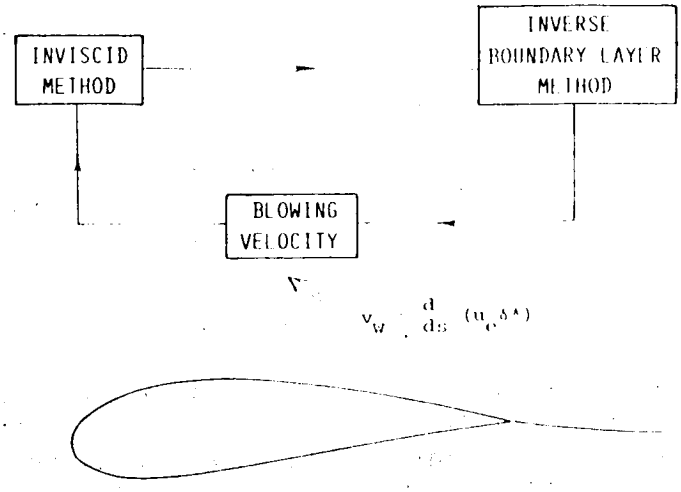

Figure 2. - Interactive scheme. Viscous calculations on the airfoil and in the wake are performed by a series of successive sweeps to establish new boundary conditions for the inviscid method.

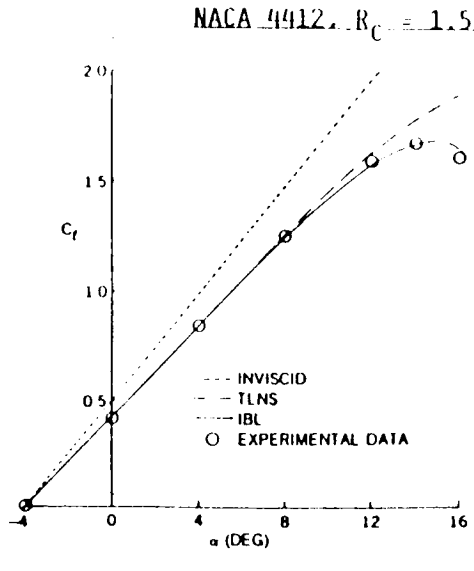

Figure 3. - Typical results for single airfoils.

GENERAL FORM OF EXTERNAL VELOCITY FIELD:

$$\frac{u_e}{u_\infty}(x,t) = A(\xi,\tau)\,[\xi - B(\tau)] \tag{1}$$

BOUNDARY-LAYER EQUATIONS FOR UNSTEADY FLOWS:

$$\frac{\partial u}{\partial x} + \frac{\partial v}{\partial y} = 0 \tag{2}$$

$$\frac{\partial u}{\partial t} + u\frac{\partial u}{\partial x} + v\frac{\partial u}{\partial y} = \frac{\partial u_e}{\partial t} + u_e\frac{\partial u_e}{\partial x} + \nu\frac{\partial}{\partial y}\left(b\frac{\partial u}{\partial y}\right) \tag{3}$$

$$\frac{\partial T}{\partial t} + u\frac{\partial T}{\partial x} + v\frac{\partial T}{\partial y} = \frac{\nu}{Pr}\frac{\partial}{\partial y}\left(c\frac{\partial T}{\partial y}\right) \tag{4}$$

$$y = 0, \quad u = v = 0, \quad T = T_w(x); \tag{5a}$$

$$y = \delta, \quad u = u_e(x,t), \quad T = T_e \tag{5b}$$

$$b = 1 + \frac{\epsilon_m}{\nu}, \quad c = 1 + \frac{\epsilon_m}{\nu}\frac{Pr}{Pr_t} \tag{6}$$

$$(bf'')' + f''\theta + \frac{\partial w}{\partial \tau} + w\frac{\partial w}{\partial \xi} = \frac{\partial f'}{\partial \tau} + f'\frac{\partial f'}{\partial \xi} \tag{7}$$

$$\frac{1}{Pr}(cG')' + G'\theta + m(1 - G)f' = \frac{\partial G}{\partial \tau} + f'\frac{\partial G}{\partial \xi} \tag{8}$$

$$\eta = 0, \quad f = f' = G = 0; \quad \eta = \eta_e, \quad f' = w, \quad G = 1 \tag{9}$$

"CHARACTERISTIC" FORM OF THE EQUATIONS:

WRITE THE EQUATIONS ALONG THE LOCAL STREAMLINES

$$d\tau = d\xi/f'$$

$$(bf'')' + f''\theta + \frac{\partial w}{\partial \tau} + w\frac{\partial w}{\partial \xi} = \lambda\frac{\partial f'}{\partial s} \tag{10}$$

$$\frac{1}{Pr}(cG')' + G'\theta + m(1 - G)f' = \lambda\frac{\partial G}{\partial s} \tag{11}$$

$$\eta = 0, \quad \theta = f' = G = 0, \quad \eta = \eta_e, \quad f' = w, \quad G = 1 \tag{12}$$

$$\lambda = \sqrt{1 + (f')^2}, \qquad \beta = \tan^{-1} f' \tag{13}$$

Figure 4. - Description of the method.

- PRESENT CONTRIBUTION ADDRESSES THE NUMERICAL SOLUTION OF THE BOUNDARY-LAYER EQUATIONS FOR A GIVEN PRESSURE DISTRIBUTION AND ITS EVALUATION FOR MODEL LAMINAR AND TURBULENT FLOWS.

- FOR NONUNIFORM ONSET VELOCITIES, THE STAGNATION POINT LOCATION ξ_s VARIES WITH SPACE AND TIME, I.E. FOR AN OSCILLATING AIRFOIL WHOSE u_e NEAR THE LEADING EDGE IS

$$u_e \sim \frac{z + z_o}{\sqrt{1 + z^2}} \quad (1 + c \sin \omega\tau)$$

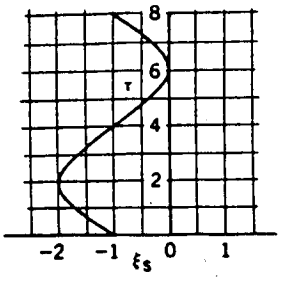

Figure 5. - Variation of stagnation point with time.

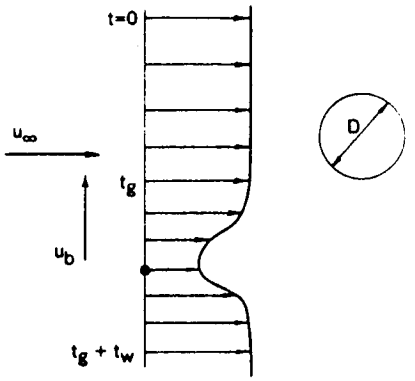

$$A(\tau) = \frac{[h^2 + 10(St)^2(1 - h)^2]^{1/2}}{h} \tag{14}$$

$$B(\tau) = \tan^{-1} [3.3St \ (\frac{1}{h} - 1)] \tag{15}$$

$$h = \frac{1 + u_m}{2} + \frac{1 - u_m}{2} \cos[\pi(1 - 100 \ St\tau)] \tag{16}$$

Figure 6. - Rotor wake model.

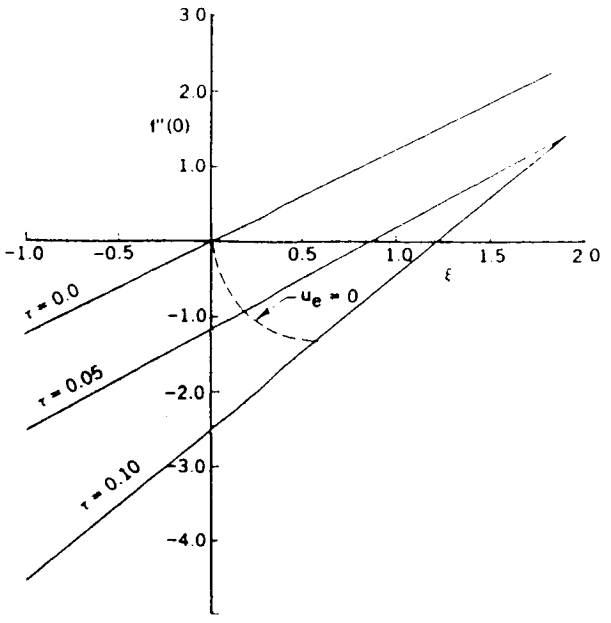

Figure 7. - Shear stress results for rotor wake model.

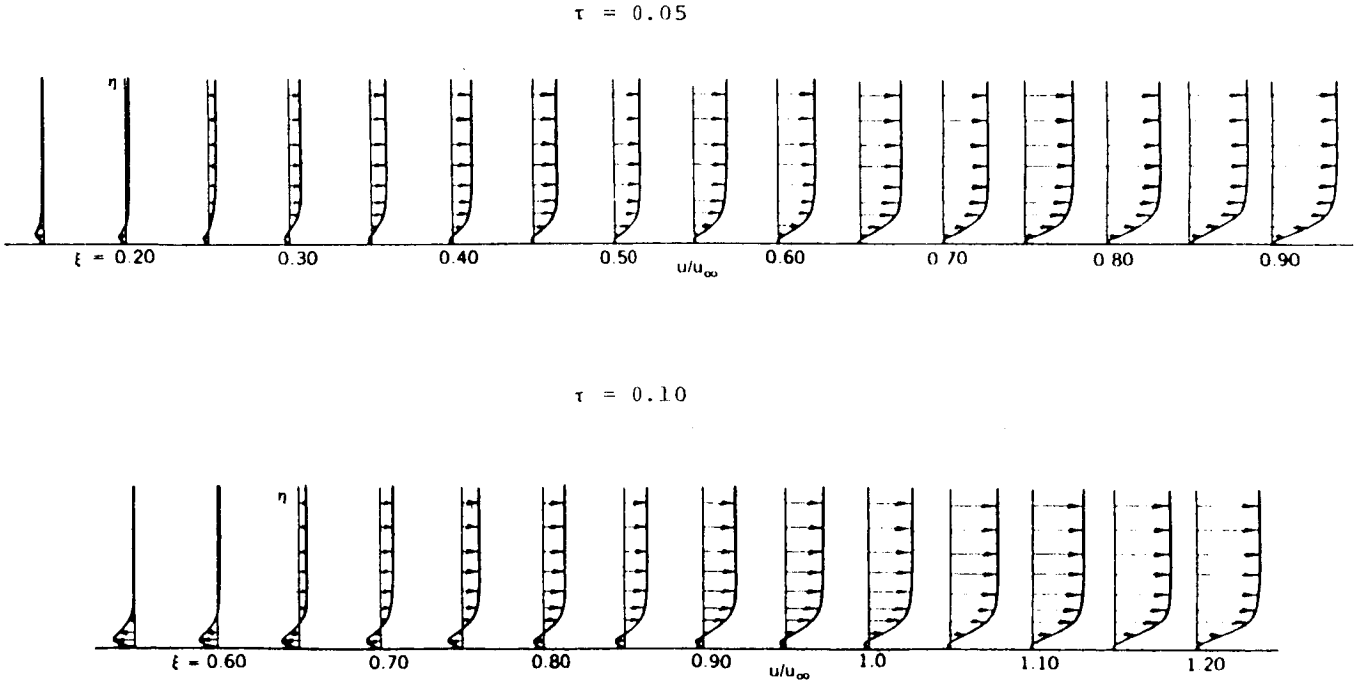

Figure 8. - Flow reversal results for rotor wake model.

EXPERIMENTAL AND THEORETICAL STUDIES OF TIME-AVERAGED AND TIME-RESOLVED ROTOR HEAT TRANSFER

M.G. Dunn, W.J. Rae, and D.L. Rigby
Calspan-University of Buffalo Research Center
Buffalo, New York

CUBRC efforts in support of the SSME structural durability program have concentrated on obtaining detailed time-averaged and time-resolved (or phase-locked) measurements on a full-scale rotating turbine both with and without cold gas injection and on theoretical studies designed to improve the prediction capability for these turbine flows. The experimental efforts have concentrated on use of the Garrett TFE 731-2 hp turbine. However, it has been possible to apply the theoretical efforts to predicting heat-flux distributions obtained for two additional turbines - i.e., (1) the Garrett low aspect ratio turbine (LART) and (2) the Teledyne 702 turbine. In performing these calculations, the ground rules have been that only the turbine inlet parameters and the turbine geometry can be altered in performing the calculations for the respective turbines.

EXPERIMENT

The experimental technique is the short-duration, shock-tunnel approach, in which fast-response, thin-film resistance thermometers are used to measure surface temperature histories at prescribed locations on the turbine component parts. Heat-flux values are then inferred from the temperature histories by using standard data reduction procedures. The turbine being used is the Garrett TFE 731-2 hp stage, and both the nozzle guide vanes and the rotor blades are heavily instrumented with thin-film heat-flux gauges. A detailed description of this instrumentation was previously given (ref. 1) at the 1985 Structural Durability meeting. Depending on how the data from a particular heat-flux gauge are recorded, one can get either time-resolved (or phase-locked) or time-averaged results. Both types of data are illustrated in this presentation.

PREDICTIONS

It is important to be able to predict both the time-resolved and the time-averaged heat-transfer distributions described previously. For the time-averaged prediction, a wide variety of predictive techniques have been developed that range from simple flat-plate correlations to computer codes based on the full three-dimensional Navier-Stokes equations. Between these limits, there exists a substantial body of analytical and numerical methods which account for most of the dominant physical phenomena while still being sufficiently convenient for use by a large fraction of those involved in the field. As part of this NASA effort, several of these midrange methods have been assembled to perform state-of-the-art predictions for several different

turbines. The specific turbines for which these predictions have been performed are (1) the Garrett TFE 731-2, (2) the Garrett low aspect ratio turbine (LART), and (3) the Teledyne 702-hp turbine. Results from the first two turbines were reported in reference 2 and from the third in reference 3. Typical results are given in figures 1 and 2.

Predicting the unsteady flow field is a significantly less developed area of research than is predicting the steady state flow field. Some effort is ongoing within CUBRC to analyze and interpret the unsteady thermal loads on a typical rotating turbine. At this time, the ability to perform phase-locked heat-flux measurements on a turbine rotor is more advanced than the ability to predict same. Figure 3 is a typical phase-locked heat flux distribution obtained at approximately 15 percent wetted distance on a turbine blade suction surface for a rotation speed of 27,000 rpm.

REFERENCES

1. Dunn, M.G.; Rae, W.J.; and George, W.K.: Experimental Measurements and Analysis of Heat Transfer and Gas Dynamics in a Rotating Turbine Stage. Structural Integrity and Durability of Reusable Space Propulsion Systems, NASA CP-2381, 1985, pp. 49-52.

2. Rae, W.J. et al.: Turbine-Stage Heat Transfer: Comparison of Short-Duration Measurements with State-of-the-Art Prediction. AIAA Paper 86-1465, June 1986.

3. Dunn, M.G.; and Chupp, R.E.: Time-Averaged Heat-Flux Distributions and Comparison with Prediction for the Teledyne 702 HP Turbine Stage. To be presented at the 32nd International Gas Turbine Conference, Anaheim, CA, June 1987.

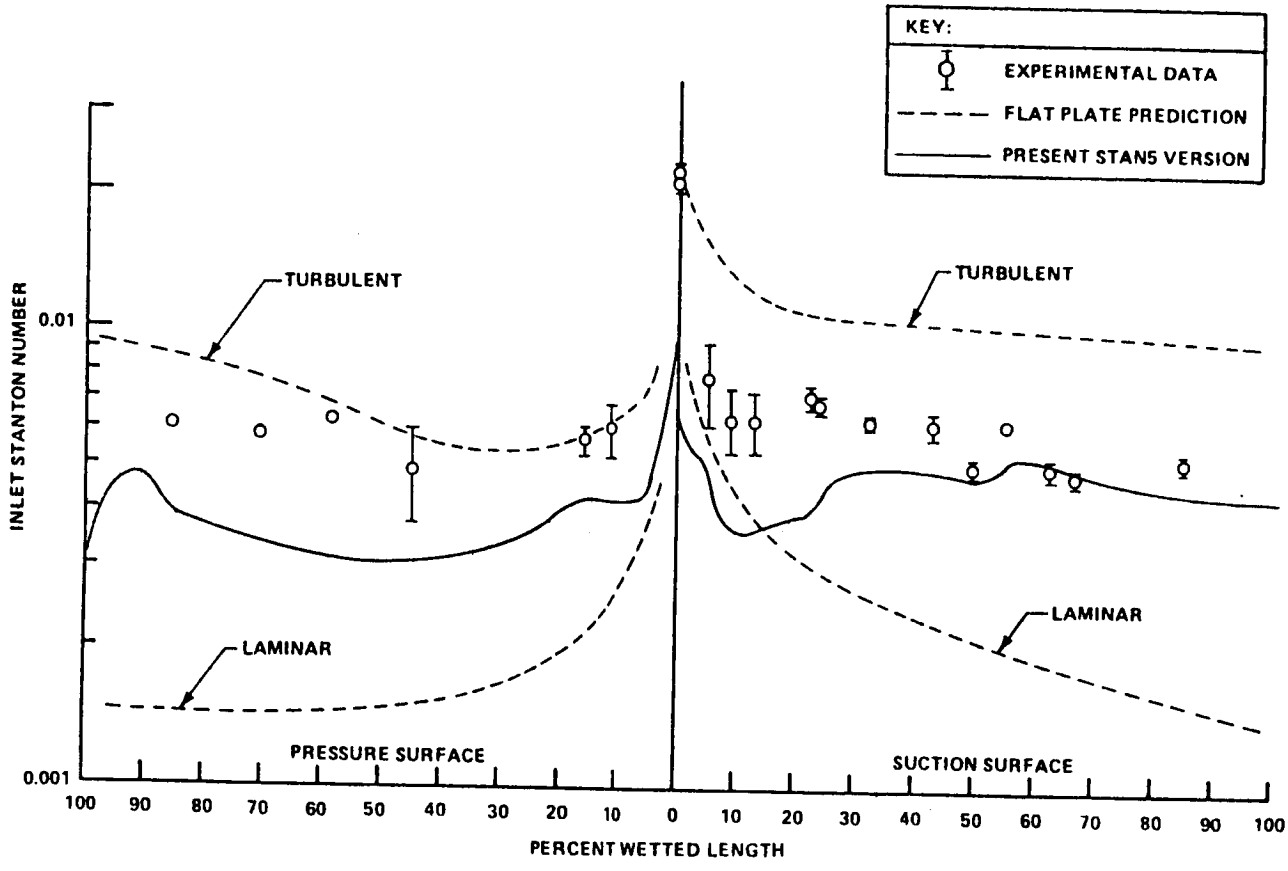

Figure 1.- COMPARISON OF EXPERIMENTAL DATA WITH PREDICTION FOR ROTOR BLADE OF TFE 731-hp TURBINE.

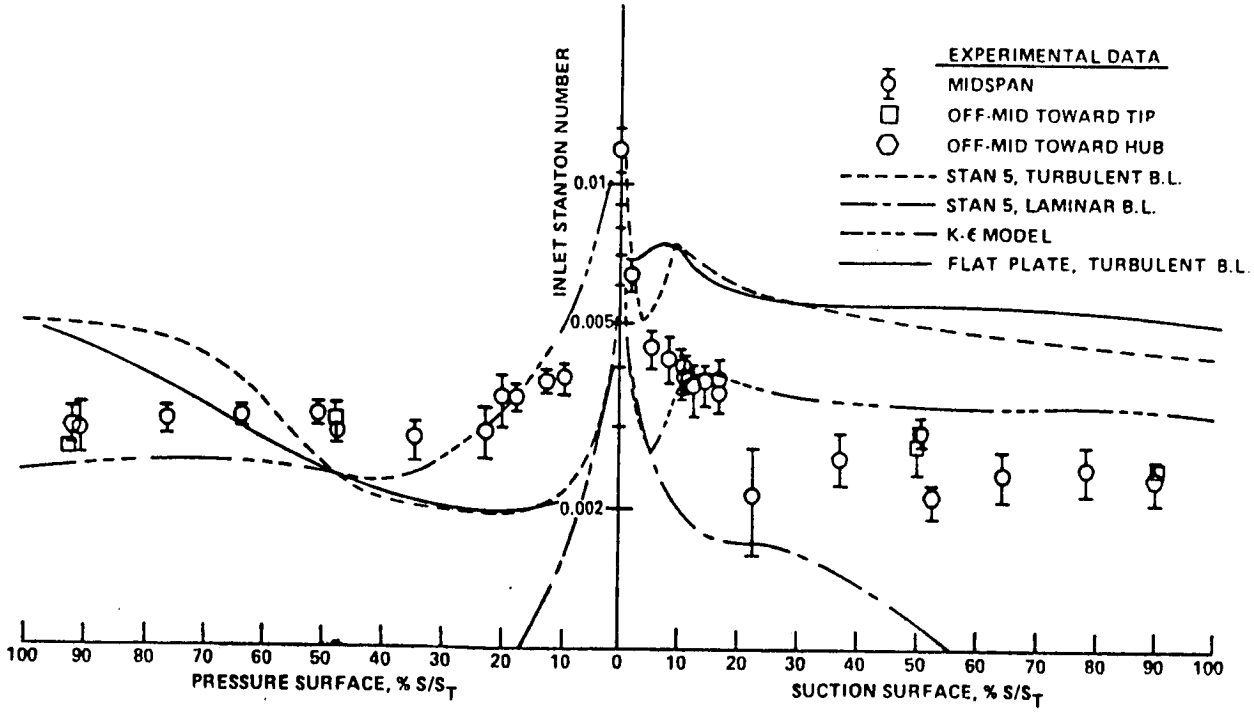

Figure 2. - STANTON NUMBER DISTRIBUTION FOR TELEDYNE 702 BLADE.

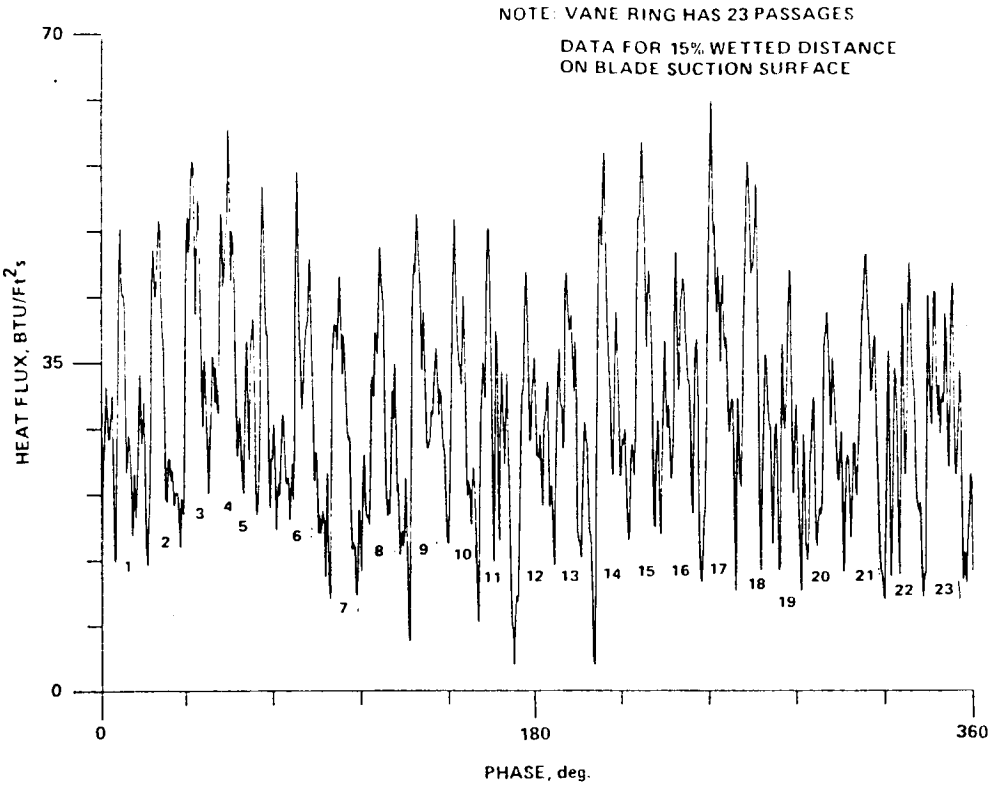

Figure 3. – HEAT-FLUX HISTORY FOR ONE REVOLUTION CALCULATED FROM THREE-POINT FILTERED TEMPERATURE SIGNAL.

ANALYTICAL AND EXPERIMENTAL STUDIES OF FLOW-INDUCED VIBRATION OF SSME COMPONENTS*

S.S. Chen, J.A. Jendrzejczyk, and M.W. Wambsganss
Argonne National Laboratory
Argonne, Illinois

Components of the SSMEs are subjected to a severe environment that includes high-temperature, high-velocity flows. Such flows represent a source of energy that can induce and sustain large-amplitude vibratory stresses and/or result in fluidelastic instabilities. Three components are already known to have experienced failures in evaluation tests as a result of flow-induced structural motion. These components include the liquid-oxygen (LOX) posts, the fuel turbine bellows shield, and the internal inlet tee splitter vane. We have considered the dynamic behavior of each of these components with varying degrees of effort: (1) a theoretical and experimental study of LOX post vibration excited by a fluid flow; (2) an assessment of the internal inlet tee splitter vane vibration (referred to as the "4000-Hz vibration problem"); and (3) a preliminary consideration of the bellows shield problem. This paper summarizes our effort in the resolution of flow-induced vibration problems associated with the SSMEs.

1. An Assessment of LOX Post Vibration: The LOX post vibration problem was assessed. Various excitation mechanisms including vortex shedding, fluidelastic instability, LOX flow-induced instability, acoustic resonance, and turbulent buffeting were considered. A scoping experiment was designed and completed; the experimental data agree well with analytical results (ref. 1). It was concluded that the potential excitation mechanisms for unshielded LOX posts are fluidelastic instability and turbulent buffeting.

2. A Mathematical Model for LOX Posts in Crossflow: A general model, based on unsteady flow theory, for LOX post vibration was developed. The model includes both motion-dependent fluid forces and fluid excitation forces (refs. 1 and 2). In the past, studies of the fluidelastic instability of a tube array in crossflow have been based on three different flow theories: quasi-static flow theory, quasi-steady flow theory, and unsteady flow theory. The quasi-static flow theory predicts fluid-stiffness-controlled instability only and is applicable for high reduced flow velocities. (Reduced flow velocity is equal to the flow velocity divided by oscillation frequency and cylinder diameter.) The quasi-steady flow theory predicts both fluid-stiffness- and fluid-damping-controlled instability. It is applicable for high reduced flow velocities; at low flow velocities it does not predict some of the instability characteristics. Only a complete unsteady flow theory is applicable in all cases.

---

*Work performed for NASA under an agreement with the U.S. Department of Energy.

3. Fluid Excitation Forces: The fluid excitation forces acting on a square array were measured as a function of Reynolds number, incoming flow conditions, and tube location (ref. 3). The main conclusions are as follows:

(1) The fluid forces acting on the first few rows depend on the incoming flow conditions. Once the flow has passed through 3 to 4 rows, the flow and its excitation on the tubes reach a steady-state condition.

(2) In a square array, the RMS values of the lift coefficients are larger than the drag coefficients.

(3) As the flow passes through a tube array, both the turbulence intensity and the resulting fluid excitation forces increase.

(4) The power spectral densities of the fluid excitation forces are fairly flat for reduced frequencies of less than 0.1; they reach a peak at the Strouhal frequency and then decrease drastically with an increase in reduced frequency.

(5) The convection velocity for drag force is higher than that for lift force; it varies from 0.5 to 0.7 of the gap flow velocity.

4. Motion-Dependent Fluid Forces: Motion dependent fluid force components g_j and h_j acting on a group of cylinders in crossflow are given in figure 1. Components g_j and h_j consist of fluid inertia, fluid damping, and fluid stiffness forces. Fluid-damping and fluid-stiffness coefficients for a tube row in crossflow were obtained as a function of reduced flow velocity (ref. 4). Typical results are shown in figure 2 as a function of the reduced flow velocity. In addition, the effects of oscillation amplitude, tube alignment, and flow velocity were studied. From the characteristics of the motion-dependent fluid forces, the stability criteria and the effect of various system parameters can be determined.

5. Splitter Vane Vibration: A preliminary assessment of the excitation mechanism(s) associated with a 4000-Hz vibration of the internal inlet tee splitter vane was made from the available information (unpublished data of Chen's, 1985). The most probable mechanism responsible for the 4000-Hz vibration is a "lock-in" oscillation involving the splitter vanes and the vortex formation in the near-wake of the trailing edges of the vanes. A combination of structural and fluid-dynamic attenuation methods is recommended to eliminate the detrimental vibration.

Even though there are significant gaps in our current knowledge, designers have been able to put together complex, interactive components, such as those of the SSMEs, which operate in severe environments (high temperatures, pressures, and flows) and still provide useful service without significant problems. In many cases, some of the obvious flow-induced vibration effects can be avoided by using common sense and experience without detailed study and calculations. However, in the SSMEs, several vibration problems have been identified which require further consideration. As an example, the shields on the liquid oxygen posts, which have served to reduce the flow-induced vibration problems of the posts to an acceptable level, have caused severe additional loads on other structural components. It would be desirable to redesign the injectors with a detailed consideration of flow induced vibration effects so that the flow shields could be removed. Clearly, there is a need to develop

and perform a prioritized research agenda in flow-induced vibration which will lead to a comprehensive technology base consisting of design data, prediction methods, and computer codes required in the design and evaluation of SSME components.

REFERENCES

1. Chen, S.S.; and Jendrzejczyk, J.A.: Flow-Induced Vibration of the SSME LOX Posts. Flow-Induced Vibration - 1986, ASME Publication PVP-Vol. 104, 1986, pp. 119-125.

2. Chen, S.S.: A General Theory of Dynamic Instability of Tube Arrays in Crossflow. Journal of Fluids and Structures, vol. 1, 1987, pp. 35-53.

3. Chen, S.S.; and Jendrzejczyk, J.A.: Fluid Excitation Forces Acting on a Tube Array. Measuring and Metering of Unsteady Flows, ASME Publication FED-Vol. 40, 1986, pp. 45-55.

4. Jendrzejczyk, J.A.; and Chen, S.S.: Motion-Dependent Fluid Forces Acting on a Tube Row in Crossflow. Argonne National Laboratory Report ANL-86-48, 1986.

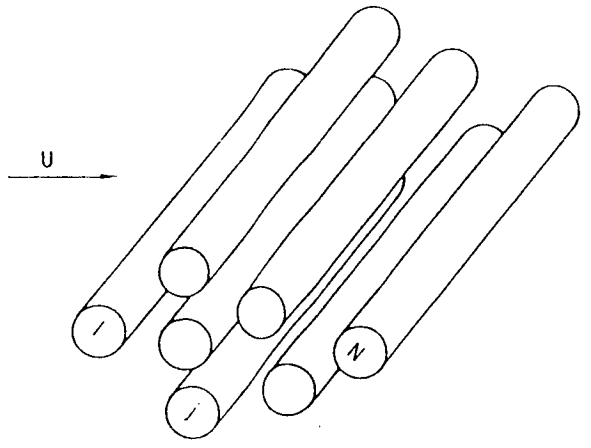

(a) Group of circular cylinders.

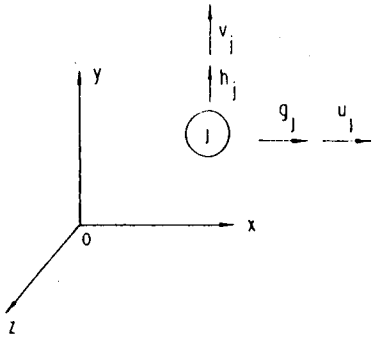

(b) Fluid force and cylinder displacement components.

$$g_j = -\rho\pi R^2 \sum_{k=1}^{n} \left(\alpha_{jk} \frac{\partial^2 u_k}{\partial t^2} + \sigma_{jk} \frac{\partial^2 v_k}{\partial t^2}\right) + \frac{\rho U^2}{\omega} \sum_{j=1}^{n} \left(\alpha'_{jk} \frac{\partial u_j}{\partial t} + \sigma'_{jk} \frac{\partial v_k}{\partial t}\right) + \rho U^2 \sum_{k=1}^{n} \left(\alpha''_{jk} u_k + \sigma''_{jk} v_k\right) ,$$

$$h_j = -\rho\pi R^2 \sum_{k=1}^{n} \left(\tau_{jk} \frac{\partial^2 u_k}{\partial t^2} + \beta_{jk} \frac{\partial^2 v_k}{\partial t^2}\right) + \frac{\rho U^2}{\omega} \sum_{k=1}^{n} \left(\tau'_{jk} \frac{\partial u_j}{\partial t} + \beta'_{jk} \frac{\partial v_k}{\partial t}\right) + \rho U^2 \sum_{k=1}^{n} \left(\tau''_{jk} u_k + \beta''_{jk} v_k\right) .$$

Figure 1. - Schematic of a group of circular cylinders in crossflow and fluid force and displacement components.

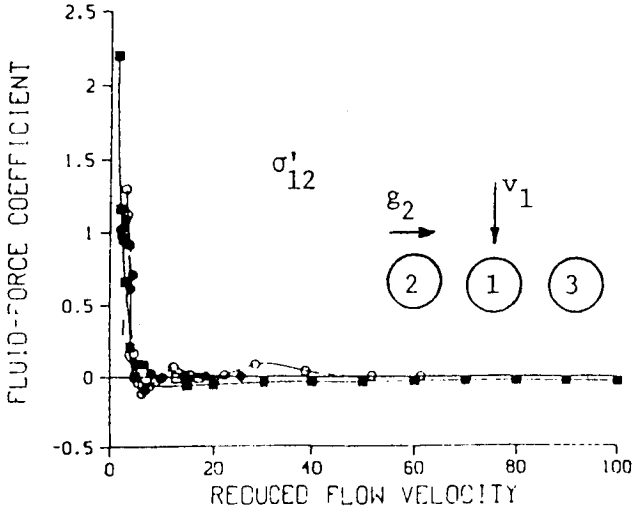

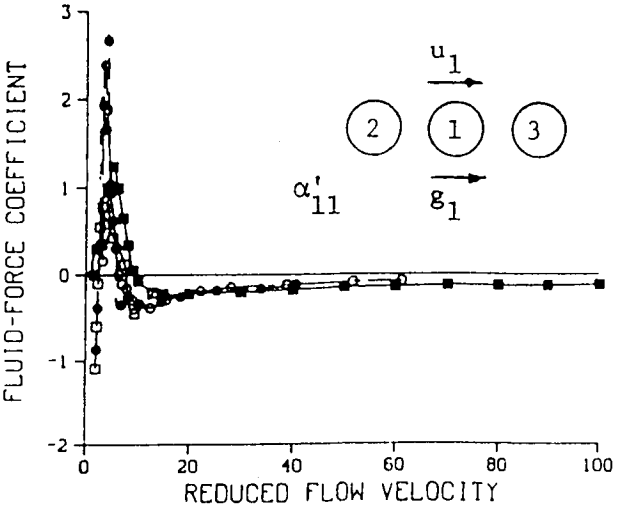

Figure 2. - Fluid-damping coefficients for a row of cylinders obtained at several flow velocities denoted by different symbols.

OVERVIEW OF THE INSTRUMENTATION PROGRAM

William C. Nieberding
NASA Lewis Research Center
Cleveland, Ohio

As you have or will hear in the rest of this conference, one of the major goals of the durability program is to develop computational models of the structural behavior, the fatigue life, and the environmental conditions pertinent to advanced reusable space propulsion systems. In many cases, however, there is very little experimental data available to either verify these models or to use as input conditions to the models.

The instrumentation portion of this durability program is thus aimed primarily at developing sensors and measurement systems capable of obtaining the data necessary for the verification of computational models. Indeed, some of these sensor systems may and probably will find their way into the test bed engine and possibly even into flight engines. The major effort, though, is to develop what is needed for bench mark experiments in research rigs to more fully define the actual conditions experienced in such an engine. In some cases, the research rig itself will turn out to be the test bed engine simply because the conditions cannot be adequately simulated in less extensive facilities.

One of the characteristics of measurement systems needed to verify codes is that the sensors must be totally nonintrusive or at least minimally intrusive so as not to significantly perturb the conditions being measured. The reason for this is that the computer codes do not take the perturbations caused by something like a probe into account. This leads to a heavy emphasis on laser optical techniques and on minimally intrusive sensors.

Another characteristic of such instruments is that they must be highly accurate and produce very high spatial and temporal resolution of the parameter being measured. Verifying codes demands this because the codes usually calculate highly resolved maps of such things as velocity, strain, temperature, etc.

The measurement systems needed generally fall into two broad categories. First there are the measurements needed on the surfaces of components such as turbine blades and vanes. Some of the desired parameters are temperature, strain, and heat flux. Papers on these three measurements are included in this session. The other broad category encompasses those measurements needed in the flow environment around these components. Here, the desired results are highly resolved maps of such parameters as flow velocity, temperature, density, pressure, and species concentration. One of the papers in this session deals with this type of measurement.

In summary, the instrument program is aimed at high-accuracy, high-resolution, minimally intrusive measurements on space propulsion system components. The primary goal is code verification, but some of the results may apply to later flight instruments.

PROGRESS ON THIN-FILM SENSORS FOR SPACE PROPULSION TECHNOLOGY

Walter S. Kim
NASA Lewis Research Center
Cleveland, Ohio

The objective of this work is to develop thin-film thermocouples for SSME components. Thin-film thermocouples have been developed for aircraft gas turbine engines and are in use for temperature measurement on turbine blades to 1800 °F. The technology established for aircraft gas turbine engines will be adapted to the materials and environment encountered in the SSME. Specific goals are to expand the existing in-house thin-film sensor technology and to test the survivability and durability of thin-film sensors in the SSME environment.

STATUS OF WORK

An initial goal of thin-film sensor work was to augment the in-house capability in thin-film sensor technology. A thin-film sensor laboratory was established in a refurbished clean room which has been equipped with a new sputtering system for sputter deposition of both insulator and sensor films (fig. 1). Other equipment installed in the clean room includes a photolithography exposure system for masking sensor patterns, parallel gap welder, and ultrasonic wedge bonder for attaching leadwires to sputtered thin films. A scanning electron microscope was acquired for surface characterization of sputtered films and substrates. Also, a vacuum furnace was acquired to grow oxide coatings in controlled environments.

One major accomplishment was the fabrication and testing of a thin-film thermocouple on SSME HPFTP blade material. The thin-film thermocouple was fabricated on a sample of the HPFTP blade material (MAR M-246 + Hf) following the fabrication process used for aircraft engine turbine blade materials. The test specimen was coated with an MCrAlY anticorrosion coating and oxidized to grow an adherent, electrically insulating surface film of aluminum oxide. This film was augmented with additionally sputtered aluminum oxide upon which a type S thin-film thermocouple was sputter deposited (fig. 2). Junctions between the thin films and the leadwires were formed by parallel gap welding.

This thin-film thermocouple was tested for survivability in severe thermal shock conditions of 2000 °F and liquid nitrogen. This survivability test consisted of soaking the test piece at 2000 °F for 1 hour and then immediately immersing it in a pool of liquid nitrogen. The thin-film thermocouple survived five of these temperature excursions. After these immersion tests, the sensor output signals were recorded while thermal shock cycling the sensor between 2000 °F and liquid nitrogen (fig. 3). Sensor outputs were measured while consecutively soaking and immersing the sensor between those temperature extremes (fig. 4). The thin-film sensor has survived at least six of these thermal shock cycles.

Another major accomplishment was the fabrication of a thin-film thermo couple on a future candidate SSME material (fig. 5). The thin-film thermo couple was deposited on a flat specimen of a single-crystal nickel base superalloy such as PWA 1480. The preliminary tests indicated that this sensor is just as good as the sensor prepared on MAR M-26 (+Hf) specimen. Tests are underway to determine the survivability and durability of this sensor in the same thermal shock cycling conditions. However, the severity of the thermal shocks imposed on these sensors are not as severe as expected in SSME and thus the next step is to test these sensors in the SSME environment simulated in the Turbine Blade Tester at MSFC.

The original plan for testing thin-film sensors in an SSME environment has been modified. The plan to contract for test hardware to test aircraft engine thin-film thermocouples was changed so that in-house fabricated thermocouples on SSME blades will be tested. The current plan is to install thin-film thermocouples on flight-hardware blades and other blades made from candidate material such as single-crystal nickel-base superalloy. We obtained from MSFC a blade holder assembly that was previously used for a thermal barrier coating experiment. Thin-film sensors will be installed on this assembly and will be tested in the Turbine Blade Tester at MSFC.

SUMMARY

Significant progress was made in thin film sensor work by completing the establishment of a thin film sensor laboratory. One accomplishment was the development of a thin-film thermocouple on SSME HPFTP blade material. This sensor was thermal shock cycled for 12 cycles of consecutively soaking the test specimen between 2000 °F and liquid nitrogen. Another accomplishment was the development of a thin-film thermocouple on a candidate SSME material. This thin-film thermocouple has been deposited on single crystal material of nickel-base superalloy, and tests are underway to determine the survivability and durability under thermal shock cycle conditions. Lastly, the original plan to contract to test thin-film thermocouples on turbine blade material in an SSME environment has been changed. The current plan is to install thin-film thermocouples on flight-hardware blades and single-crystal blades mounted on the blade holder assembly obtained from MSFC for testing in their Turbine Blade Tester.

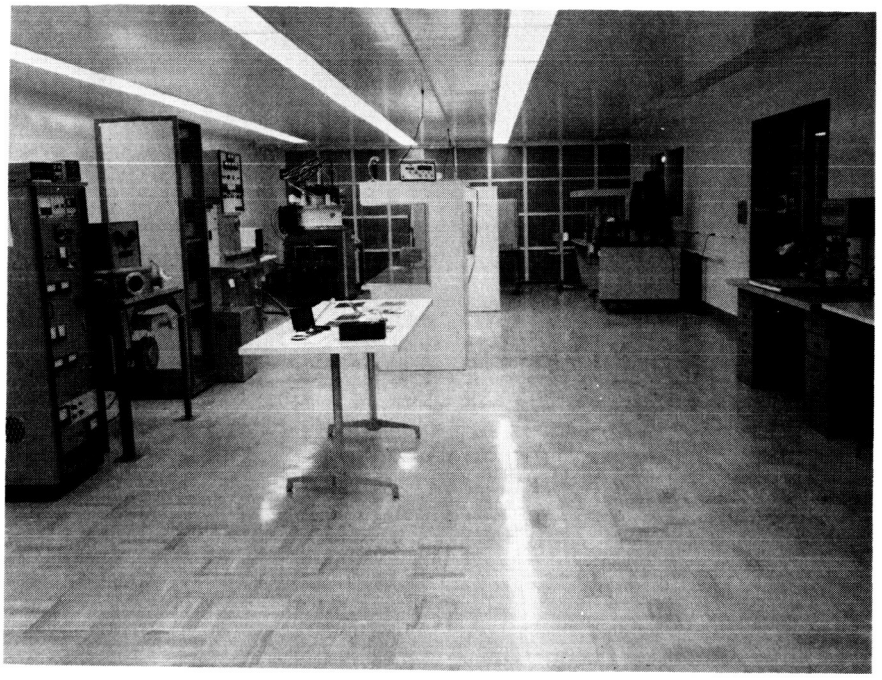

Figure 1. - Thin-film sensor laboratory.

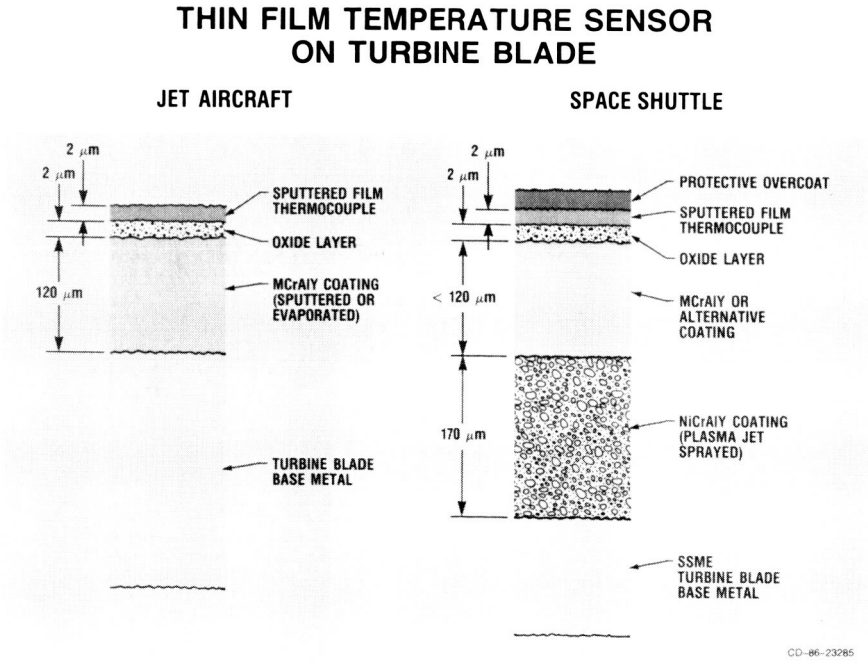

Figure 2. - Basic thin-film thermocouple technology.

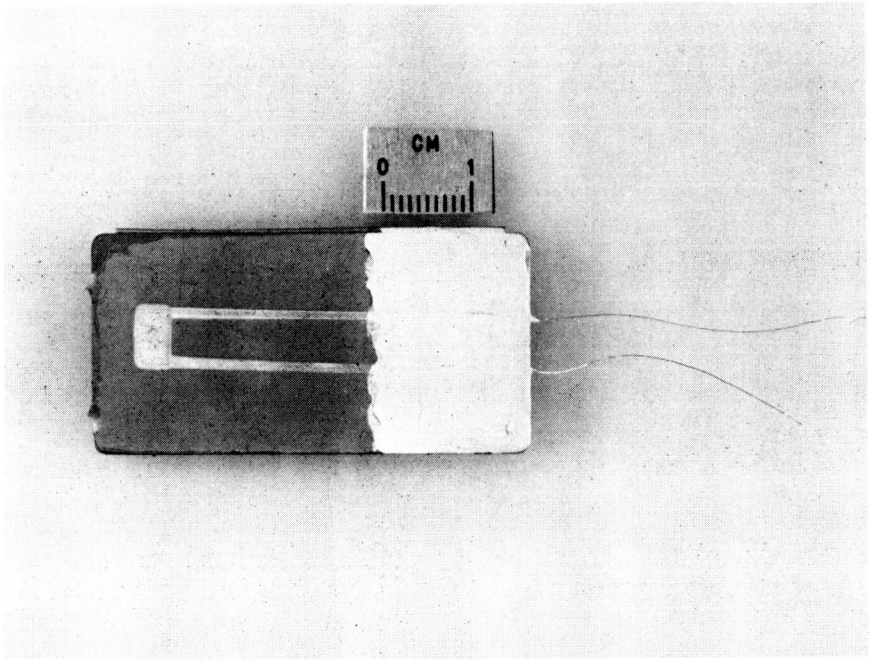

Figure 3. - Thermal-shock-cycled thin-film thermocouple deposited on flat plate of MAR M-246 + Hf.

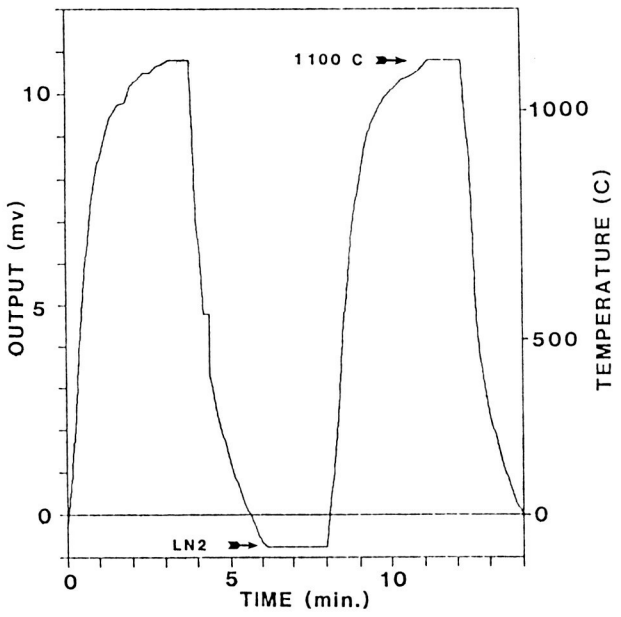

Figure 4. - Signal output of thin-film thermocouple during thermal shock cycling between 2000 °F and liquid nitrogen.

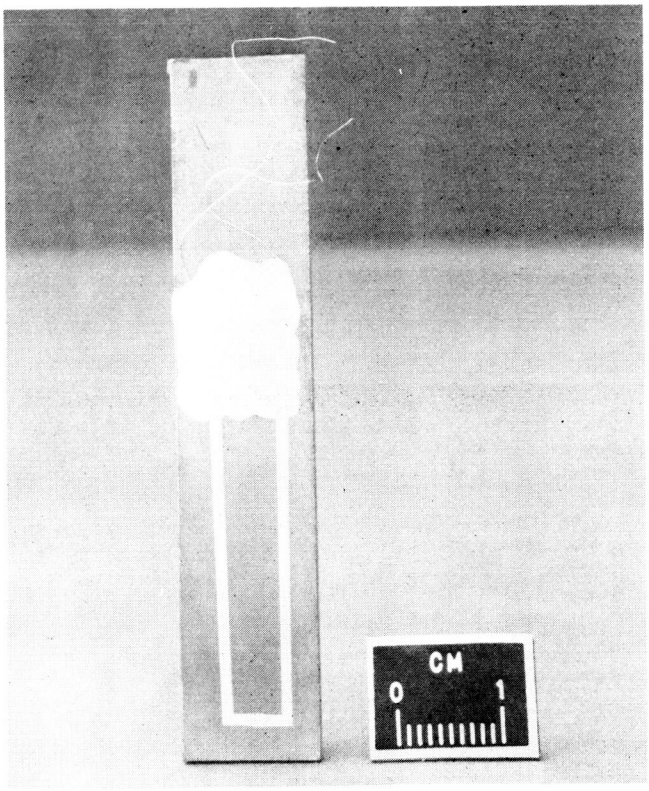

Figure 5. - Thin-film thermocouple on flat bar of single-crystal nickel-base superalloy.

HIGH TEMPERATURE AND PRESSURE LASER DIAGNOSTICS FOR SSME APPLICATIONS

J.W.L. Lewis
University of Tennessee Space Institute
Tullahoma, Tennessee

No paper available at time of printing.

PROGRESS IN OPTICAL STRAIN MEASUREMENT SYSTEM DEVELOPMENT

Christian T. Lant and Walid Qaqish
Sverdrup Technology, Inc.
Middleburg Heights, Ohio

A laser speckle strain measurement system has been built and tested for the NASA Lewis Research Center. The system is based on a speckle shift technique, which automatically corrects for error due to rigid body motion, and provides a near real time measure of strain. This paper covers the first of a multiphase effort in developing an optical strain gauge capable of mapping in two dimensions the strain on the surface of a hot specimen. The objectives of this first phase have been to provide a noncontact, one dimensional, differential strain gauge for experimental purposes, and to determine the maximum open air temperature limit of the system.

BASIC PRINCIPLES

Laser speckle is a phase effect caused by the diffuse reflection of spatially coherent light off of a rough surface. Its characteristically mottled intensity distribution is present in most laser applications. This optical strain measurement system is based on the speckle shift technique of Ichirou Yamaguchi (ref. 1), which utilizes the linear relationship between surface strain and the differential shift of speckle patterns generated by symmetrically incident laser beams. The speckle patterns created by the test specimen are interpreted as higher order interference fringes generated by a random diffraction grating, which is the naturally rough surface of the specimen. Strain induced on the specimen causes a change in spacing of the surface features, which in turn shifts the position of the interference pattern (speckles).

Theory shows that the displacement of a speckle pattern generated by a deformed specimen surface contains terms of translation, rotation, and strain, from which the strain term must be extracted. This extraction relies on the use of two symmetrically incident laser beams reflected sequentially onto a linear photodiode array. After the reference (before-strain) and shifted (after-strain) speckle patterns from each beam are correlated, taking the difference in shift between them leaves only the component due to surface strain.

The system has a gauge length of 5 millimeters given by the laser spot size, and a resolution of 16 microstrain determined by the sensor pitch of the photodiode array and the specimen-to-sensor separation. The theoretical strain measurement error is ±18 microstrain ±0.3 percent of the strain reading.

RESULTS

Uniaxial loads were applied to Inconel 600 test specimens by a testing machine. A number of data runs were performed with the system, confirming the expected response of the system as well as providing first-hand knowledge about sensitive parameters. Tests conducted during Phase I verified the stability

of speckle patterns generated by an oxidized specimen subject to strains over 0.1 percent. Isothermal stress-strain plots as well as measurements of thermal strain showed good results up to temperatures of 450 °C. Stress-strain curves generated by the optical system were compared to data taken from conventional resistance strain gauges. The modulus of elasticity for each set of data was calculated using a least squares fit and compared for each run. Agreement of the optical data was typically within 3 to 10 percent of the measured or handbook values of Young's modulus.

The largest measurement error observed in the testing was due to incomplete cancellation of the out-of-plane term of rigid body motion. The resulting error in strain was caused by the radius of curvature of the laser beams. It was observed that the cause of the excessive out-of-plane motion encountered during testing was poorly machined specimen grips. However, by increasing the radius of curvature of the laser beams, the error due to out-of-plane movement and other rigid body motions can be completely cancelled.

CONCLUSIONS

The results of the test runs show a good response of the system to surface strain. The residual error due to out-of-plane movement of the test specimen can be eliminated through modifications to the optical system. Hysteresis of the optical data over a load cycle is shown to agree very well with resistance gauge data. Strain data is obtainable at temperatures up to 450 °C in the present open-air configuration. Reduction of time-varying thermal gradients near the specimen, which cause decorrelation of the speckle patterns at higher temperatures, can increase the temperature range of the system considerably.

REFERENCES

1. Yamaguchi, I: A Laser-speckle Strain Gauge. J. Phy. E., Sci. Instrum., vol. 14, no. 11, Nov. 1981, pp. 1270-1273.

HEAT FLUX CALIBRATION FACILITY CAPABLE OF SSME CONDITIONS

Curt H. Liebert
NASA Lewis Research Center
Cleveland, Ohio

There is a need to more thoroughly characterize the hostile space shuttle main engine (SSME) turbopump environment. It has been estimated that component surface heat flux in the hot-gas environment is about 10 MW/m^2, and this is about 50 times that encountered in aircraft engines. Also, material temperature transients can be as high as 1000 K in about 1 second. These transients can cause durability problems such as material cracking. Heat flux sensors placed in the turbopump components can partially characterize this environment by measuring surface heat flux. These heat flux data can be used to verify analytical-stress, boundary-layer, and heat-transfer design models.

Preliminary plans were discussed at the first SSME durability conference for designing and fabricating a new facility for the calibration and durability testing of prototype heat flux sensors for the SSME (ref. 1). This facility is necessary for assessment of new heat flux gauge concepts needed in the hostile SSME turbopump environment.

CALIBRATION FACILITY

Figure 1 is a photograph of the calibration facility. A 100 kW Vortek arc-lamp and Anorad high-speed positioning system are shown positioned in the test cell. A Hewlett-Packard 900-236 minicomputer is located in a control room behind the control room window shown in figure 1. The interrelation of calibration facility components is schematically presented in figure 2. The minicomputer is used to control a microcomputer built into the arc-lamp power module. The same minicomputer also controls a microcomputer located in the positioning system apparatus. Prototype heat flux sensors are placed at desired positions in the arc-lamp beam. Thermocouples attached to the heat flux sensor produce voltages which are scanned and read in a multiprogrammer and then stored in the computer. Calculation of heat flux is then performed using the stored voltages after they have been converted to temperature readings.

ARC-LAMP ACCEPTANCE TESTS

The Vortek arc-lamp system design is described in reference 1. Figure 3 presents a comparison of heat flux measurements made in the Lewis facility and previously on an identically designed arc-lamp located in the Vortek facility. (Although the Lewis facility was not completed at this time, there were sufficient apparatuses available to make the test.) The same water-cooled heat flux sensor was used to perform both measurements. The agreement of heat flux data obtained with the two lamps (fig. 3) is satisfactory and demonstrates an ability to repeat the heat flux within experimental error. Heat flux measurements and calibrations in the Lewis facility will also be compared with calibrations

of radiant heat flux sources at Case Western Reserve University and Pratt and Whitney. The comparisons are part of a grant with Case Western Reserve University to develop a credible basis for heat flux calibration at high heat flux loads.

TRANSIENT HEAT FLUX MEASUREMENT AND ACCURACY

It is not feasible to use commercial water-cooled heat flux gauges on SSME turbine surfaces because these gauges are too big and water cooling is not practical. Therefore, heat flux gauge design must be reinvestigated with particular emphasis given to minimally intrusive instrumentation - possibly thin-film or miniature plug-type sensors. To aid in design, a transient heat flux prediction model for heat flow with variable thermal properties has been analytically and experimentally developed. The model characteristics were studied using transient temperature data taken with heat flux gauges designed at Lewis Research enter for flux measurement in rocket engines in 1960 (ref. 2). This study is guiding the design of heat flux gauges for SSME and suggests that SSME heat fluxes can be measured with an accuracy of about ±1 to 20 percent.

REFERENCES

1. Liebert, C.H.: Heat Flux Sensor Calibrator. Structural Integrity and Durability of Reusable Space Propulsion Systems. NASA CP-2381, 1985, pp. 195-198.

2. Liebert, Curt H.; Hatch, J.E.; and Grant, R.W.: Application of Various Techniques for Determining Local Heat Transfer Coefficients in a Rocket Engine From Transient Experimental Data. NASA TN D-277, 1960.

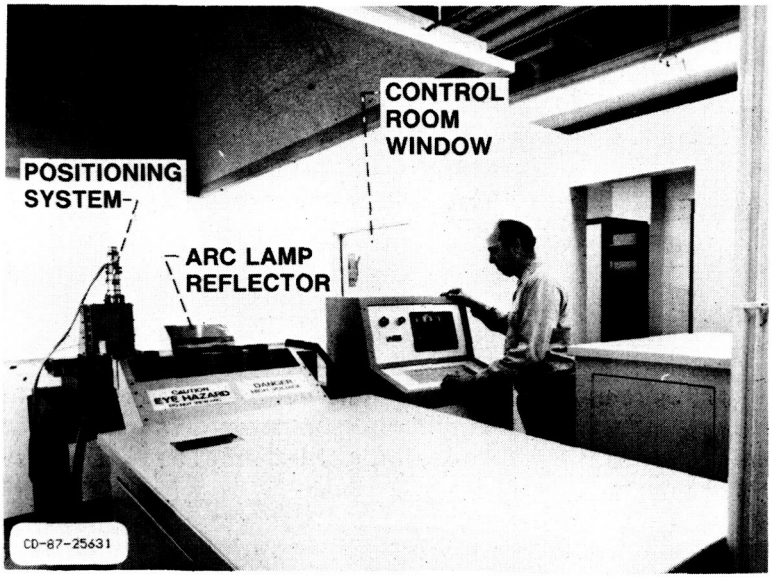

Figure 1. - View of calibration facility.

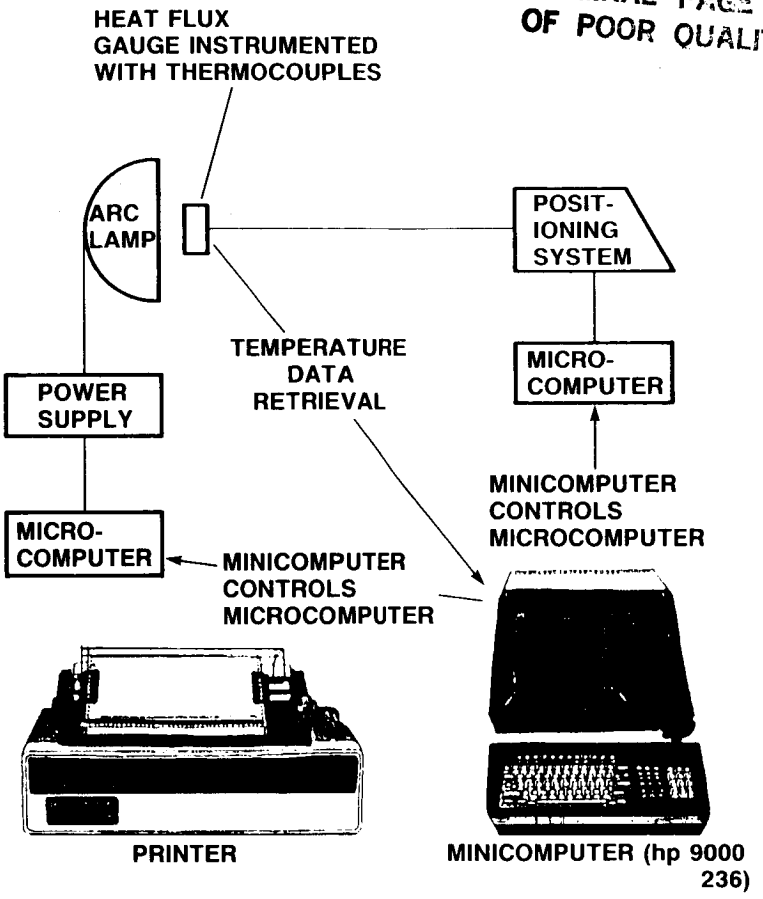

Figure 2. - Interrelation of calibration facility components.

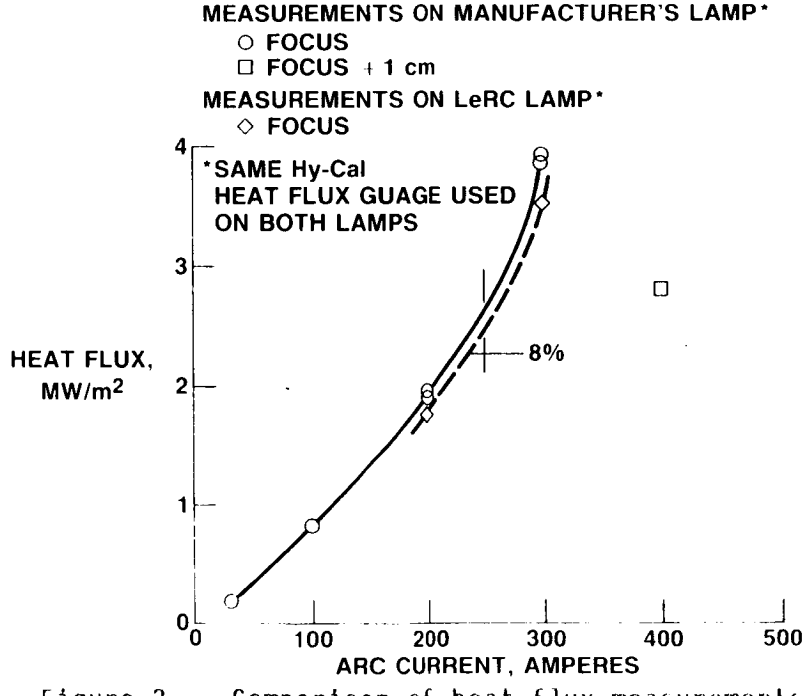

Figure 3. Comparison of heat flux measurements on manufacturer's lamp and Lewis lamp.

NUMERICAL STUDY OF THE EFFECTS OF BOUNDARY CONDITIONS ON THE MEASUREMENT AND CALIBRATION OF GARDON-TYPE HEAT FLUX SENSORS

M. Krane and A. Dybbs
Case Western Reserve University
Cleveland, Ohio

To monitor the high-intensity heat flux conditions that occur in the space shuttle main engine (SSME), it is necessary to use specifically designed heat flux sensors. These sensors, which are of the Gardon-type, are exposed on the measuring face to high-intensity radiative and convective heat fluxes and on the other face to convective cooling. To improve the calibration and measurement accuracy of these gauges, we are studying the effect that the thermal boundary conditions have on gauge performance. In particular, we are studying how convective cooling effects the field inside the sensor and the measured heat flux.

The first phase of this study involves a numerical study of these effects. Subsequent phases will involve experimental verification.

A computer model of the heat transfer around a Gardon-type heat flux sensor was developed. The results of this study will allow us to make corrections both in calibration and applications so that the input (hot-side) heat flux can be determined more accurately.

Two specific geometries are being considered as shown in figure 1:

(1) Heat flux sensor mounted on a flat-plate
(2) Heat flux sensor mounted at the stagnation point of a circular cylinder

Both of these configurations are representative of the use of heat flux sensors in the components of the SSME.

The purpose of the analysis is to obtain a temperature distribution as a function of the boundary conditions. Previous analyses of Gardon sensors have concentrated on the thin-foil part of the sensor, considering it to be attached to an infinite heat sink. This is a reasonable assumption at low temperatures, but at the high temperatures found in the SSME, this assumption is questionable. The results of this analysis will determine (1) how the cooling of a sensor in such extreme environments approximates the "thin-foil" assumption and (2) how nonuniformities in the cooling (caused by convection cooling coefficients being space dependent) effect the measurement of the hot-side heat flux.

The equations for the general case are shown in figure 2. We have not included in this formulation the thermal conductivity variations caused by the thermocouple wires or channels.

As a first test case, the following simplifications were made:

(1) Constant radiant hot-side heat flux
(2) Constant convection cooling coefficients and ambient temperatures
(3) Symmetrical k-distribution (i.e., no thermocouple wire or channels)
(4) Constant thermal conductivity

The first assumption eliminates natural convection or re-radiation cooling. We know how to handle both of these effects. The second and third assumptions eliminate any θ-dependence in the problem so that it is axisymmetric. Finally, the fourth assumption makes the problem a linear one.

A finite-difference model was used to solve the equations shown in figure 2. Several cases have been studied. The results are shown in figures 3 to 5. Figure 3 shows the calibration curves for a typical sensor. The top of the sensor has a convective heat-transfer coefficient $h_{top} = 10$ KW/m^2°K. This figure shows the results of varying the cooling or bottom side heat-transfer coefficient. For these cases, the sensitivity of the sensor decreases with an increase in the cooling heat-transfer coefficient. This result is also shown in figure 4 where the sensor sensitivity is plotted versus the cooling heat-transfer coefficient.

The cases studied in figures 3 and 4 were for radiation and convective heat fluxes at the top face of the sensors to be of the same order of magnitude. If the convective heat flux is small in comparison to the radiation heat flux, then the cooling heat transfer has little effect on the calibration curve. This is shown in figure 5 where the cases of figures 3 and 4 are compared to the case of $h_{top} = 0$ KW//m^2°K with varying cooling h's.

TWO GEOMETRIES:

1. FLAT PLATE

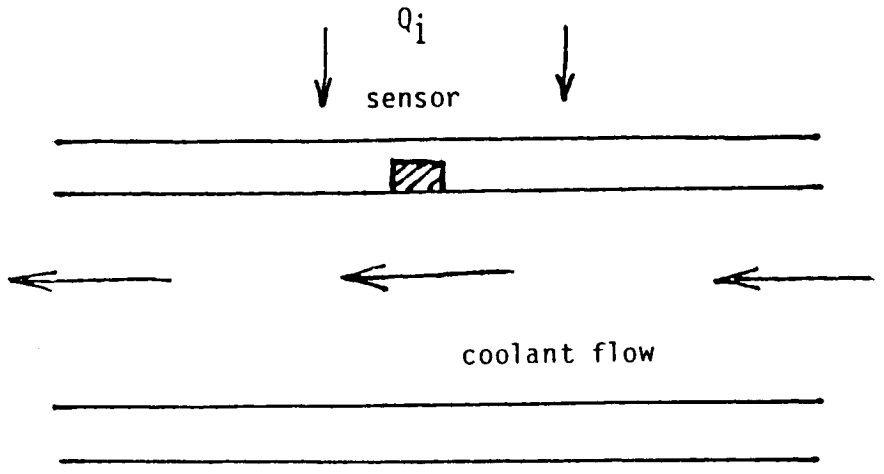

2. CYLINDER

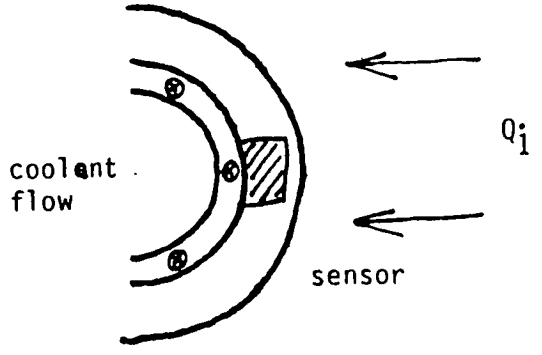

Figure 1. - Heat flux sensor configurations to be considered.

GENERAL CASE

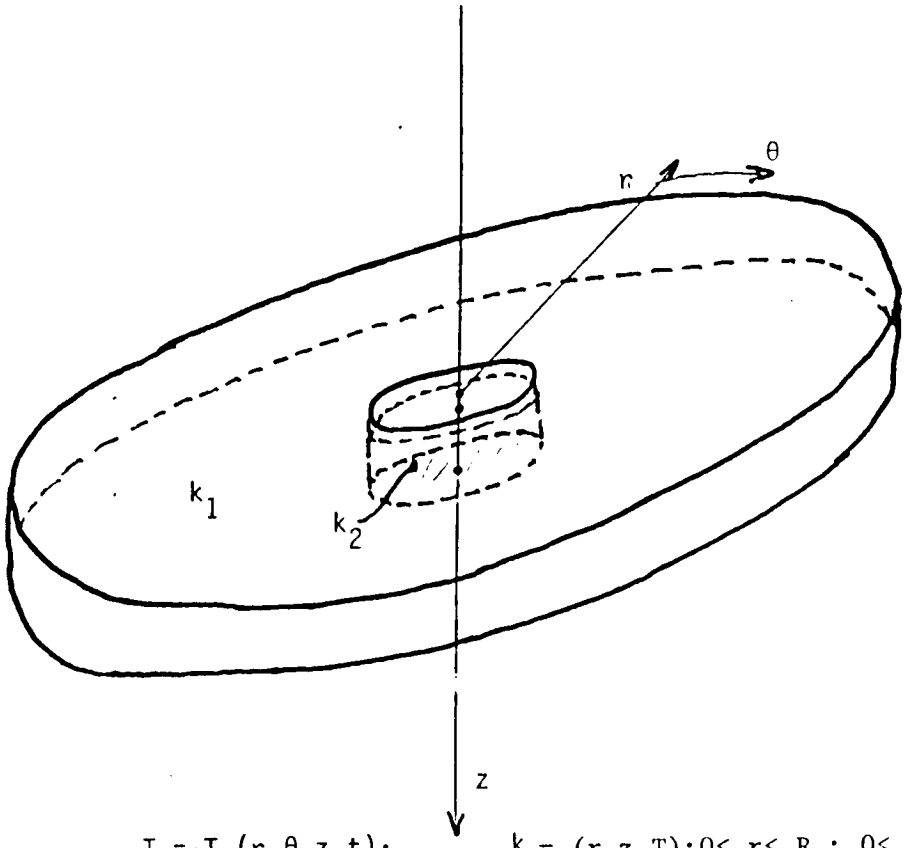

$$T = T(r,\theta,z,t); \qquad k = (r,z,T); 0 \leq r \leq R_a;\ 0 \leq \theta \leq 2\pi;\ 0 \leq z \leq H;\ t \geq 0$$

Equation: $$\frac{\partial^2 T}{\partial r^2} + \frac{1}{r}\frac{\partial T}{\partial r} + \frac{1}{r^2}\frac{\partial^2 T}{\partial \theta^2} + \frac{\partial^2 T}{\partial z^2} = \alpha \frac{\partial T}{\partial t}$$

B.C.: TOP: $$k_1 \frac{\partial T}{\partial z}(r,\theta,0,t) = \alpha Q_i - h_{CT}(T(r,\theta,0,t) - T_{CT}) - \alpha\sigma\,(T^4(r,\theta,0,t) - T_{CT}^4)$$

SIDE: $$k_1 \frac{\partial T}{\partial r}(R_a,\theta,z,t) = -h_{CR}(T(R_a,\theta,z,t) - T_{CR})$$

BOTTOM:
$$\begin{cases} k_1 \dfrac{\partial T}{\partial z}(r,\theta,H,t) = -h_{CB}\,(T(r,\theta,H,t) - T_{CB}) \ ; \ R_s \leq r \leq R_a \\ k_2 \dfrac{\partial T}{\partial z}(r,\theta,H,t) = -h_{CB}\,(T,r,\theta,H,t) - T_{CB} \ ; \ 0 \leq r \leq R_s \end{cases}$$

CENTER: $$|\,T(0,\theta,z,t)\,| < \infty$$

I.C. $$T(r,\theta,z,0) = T_{CI}\,(r,\theta,z)$$

Figure 2. - General case and formulation.

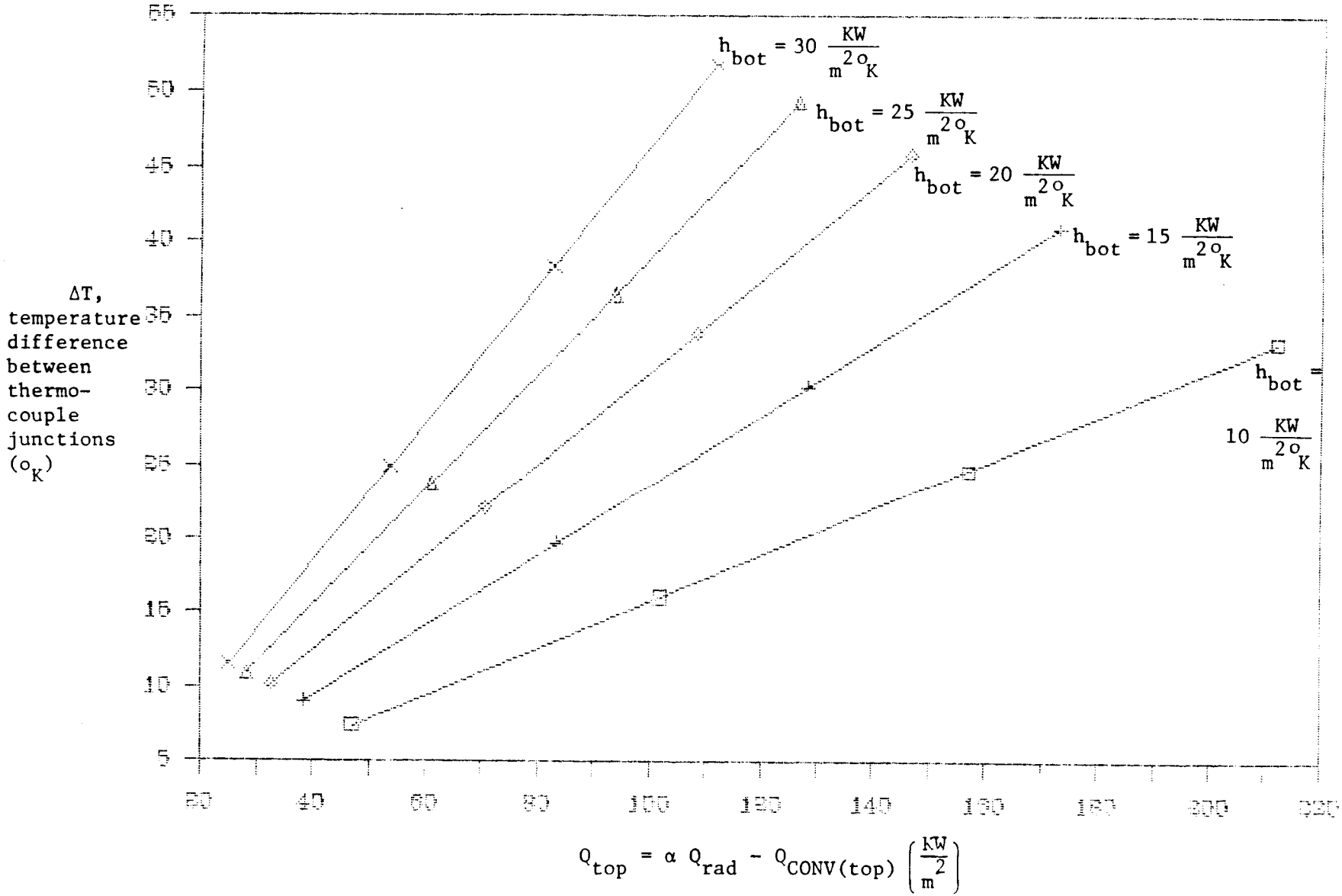

Figure 3. - Calibration curves for several values of h_{bot}. Note that h_{top} = 10 KW/m^2°K is constant and uniform for all cases.

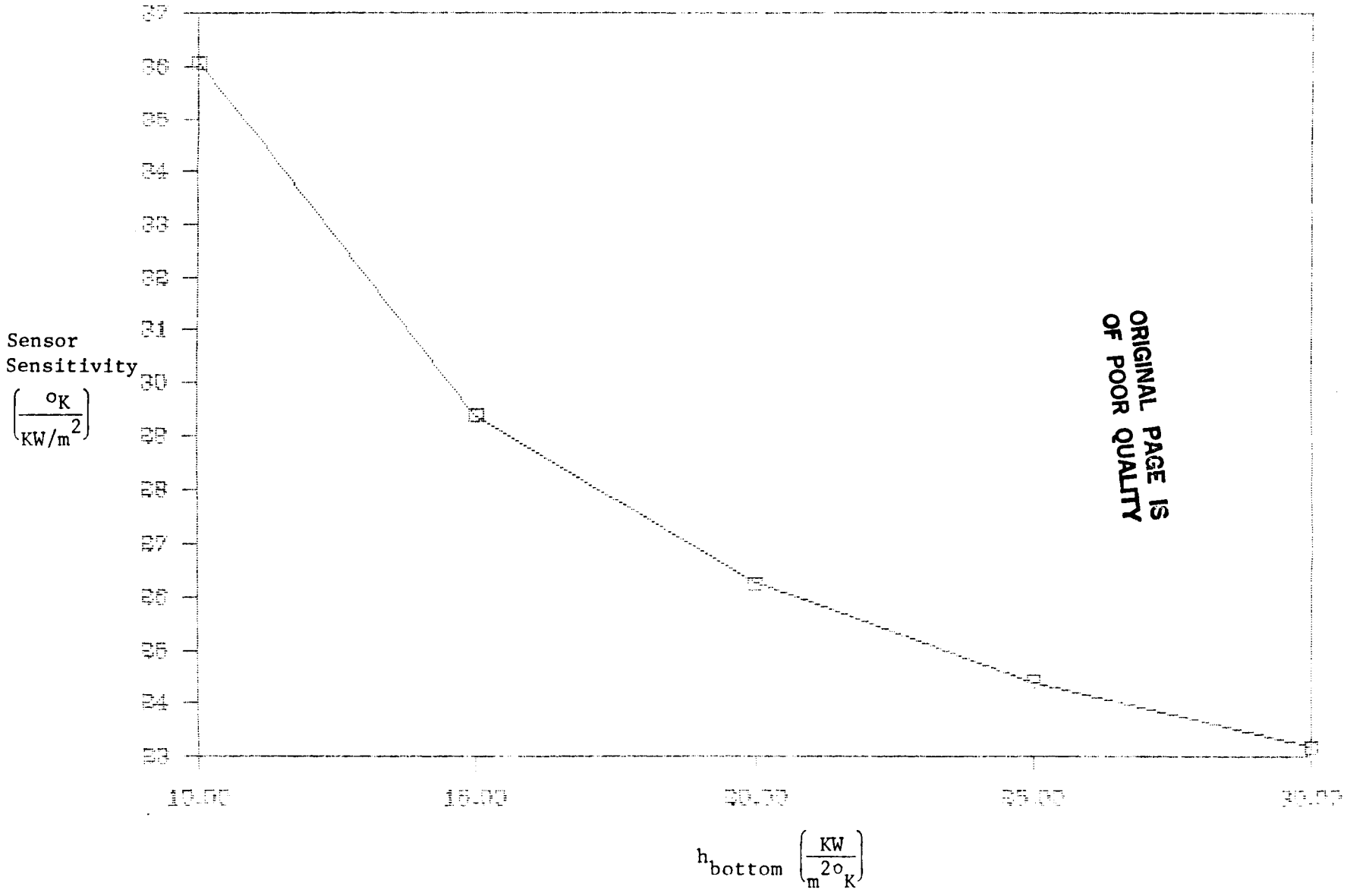

Figure 4. - Variation of sensor sensitivity with h_{bottom}. Note that h_{top} = 10 $KW/m^2 {}^{o}K$ was fixed and uniform in all cases.

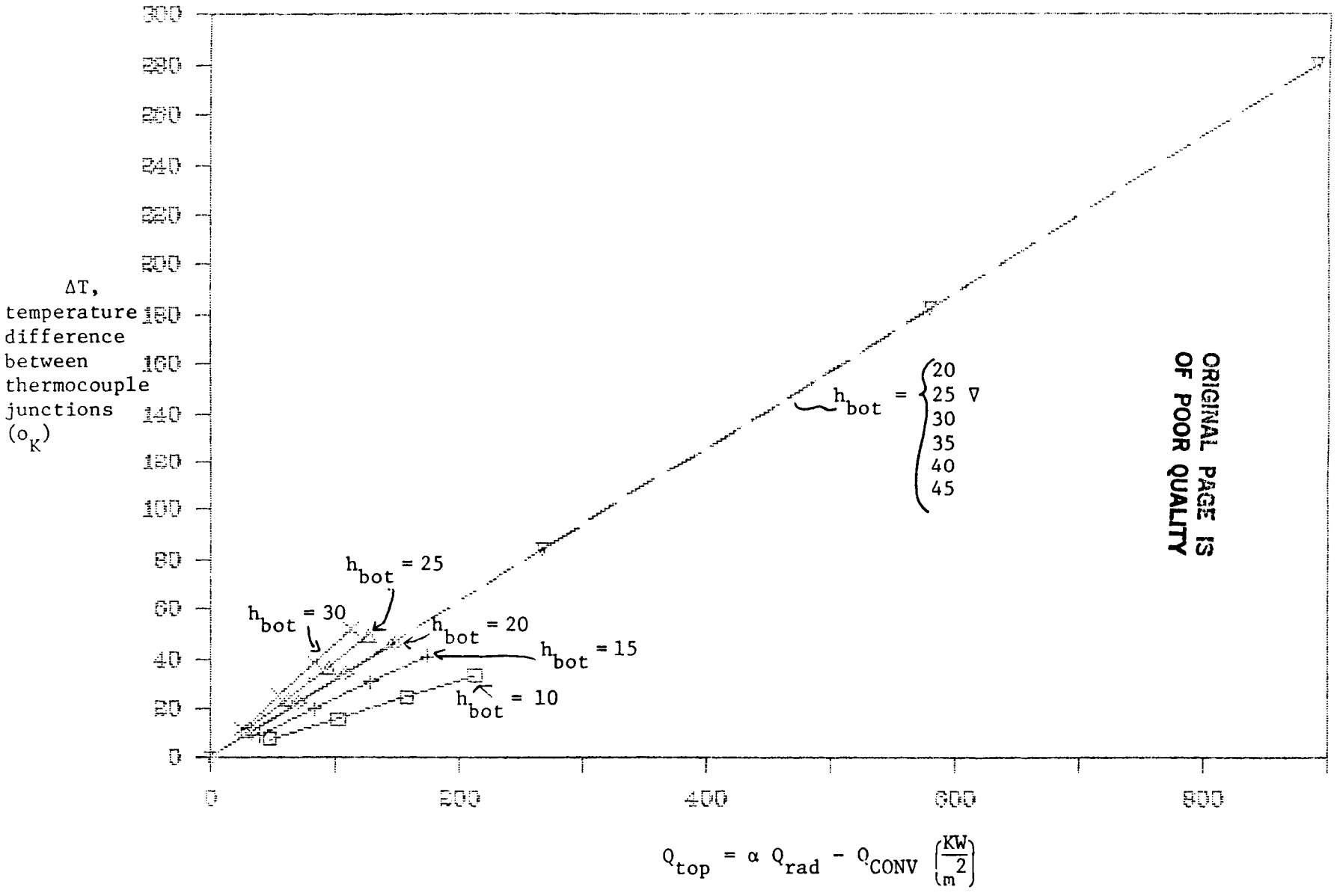

Figure 5. - Comparison of calibration curves for (1) large top-side cooling solid curves (h_{top} = 10 KW/m^2°K) - 5 curves and (2) small top-side cooling broken line (h_{top} = 0 KW/m^2°K) - 5 separate curves all on same line.

OVERVIEW OF FATIGUE, FRACTURE, AND CONSTITUTIVE MODELING PROGRAMS AT LEWIS

Gary R. Halford
NASA Lewis Research Center
Cleveland, Ohio

The objective of the NASA Lewis Research Center's Structural Integrity and Durability program is to develop and verify cyclic constitutive stress strain and crack initiation life prediction models for materials of use in reusable space propulsion systems. Emphasis is on application to those hot gas path components that have demonstrated limited durability (i.e., turbopump blades, LOX posts, and the main combustion chamber liner).

Our approach to meeting the rigorous demands of space propulsion systems has been to borrow from technology developed under aeronautical gas turbine sponsorship. Where the aerotechnology can be used directly, it is being applied; where modifications and extensions are required, these are being pursued; and where no technology exists, it is being developed. A revealing contrast between the severity of aeronautical gas turbine engine operation and that in the turbopumps of the space shuttle main engine (SSME) is illustrated in figure 1.

The program is in its fourth year, and significant progress has been made. Figure 2 lists several major accomplishments that range from development of an understanding of the complex micromechanisms of cyclic deformation in advanced, directional, nickel-base superalloys at high temperatures, to a new generalized mean stress model for fatigue, and to an accurate, shortcut structural analysis computer code for thermally loaded structures.

Durability research programs currently in progress or planned for the immediate future are listed in figure 3. Results of some of these are being presented in the papers that follow in this session. Finally, programs planned tentatively for the more distant future are presented in figure 4.

Considerable interest has been devoted to the single crystal nickel-base superalloy, PWA 1480, in the anticipation that it will provide superior properties to the bill-of-material, MAR M 246 + Hf, for use in turbopump blading. A consensus of much of the work to date on this alloy points up the substantial benefit of reducing voids. Reductions both in numbers of voids and their size should significantly improve high-cycle fatigue resistance and aid in the alleviation of hydrogen interaction problems. Progress toward this end is reported in this session by researchers from Rocketdyne and Carnegie-Mellon University. Their two programs, while not funded currently out of the Lewis Durability program, certainly have a direct bearing upon our research efforts.

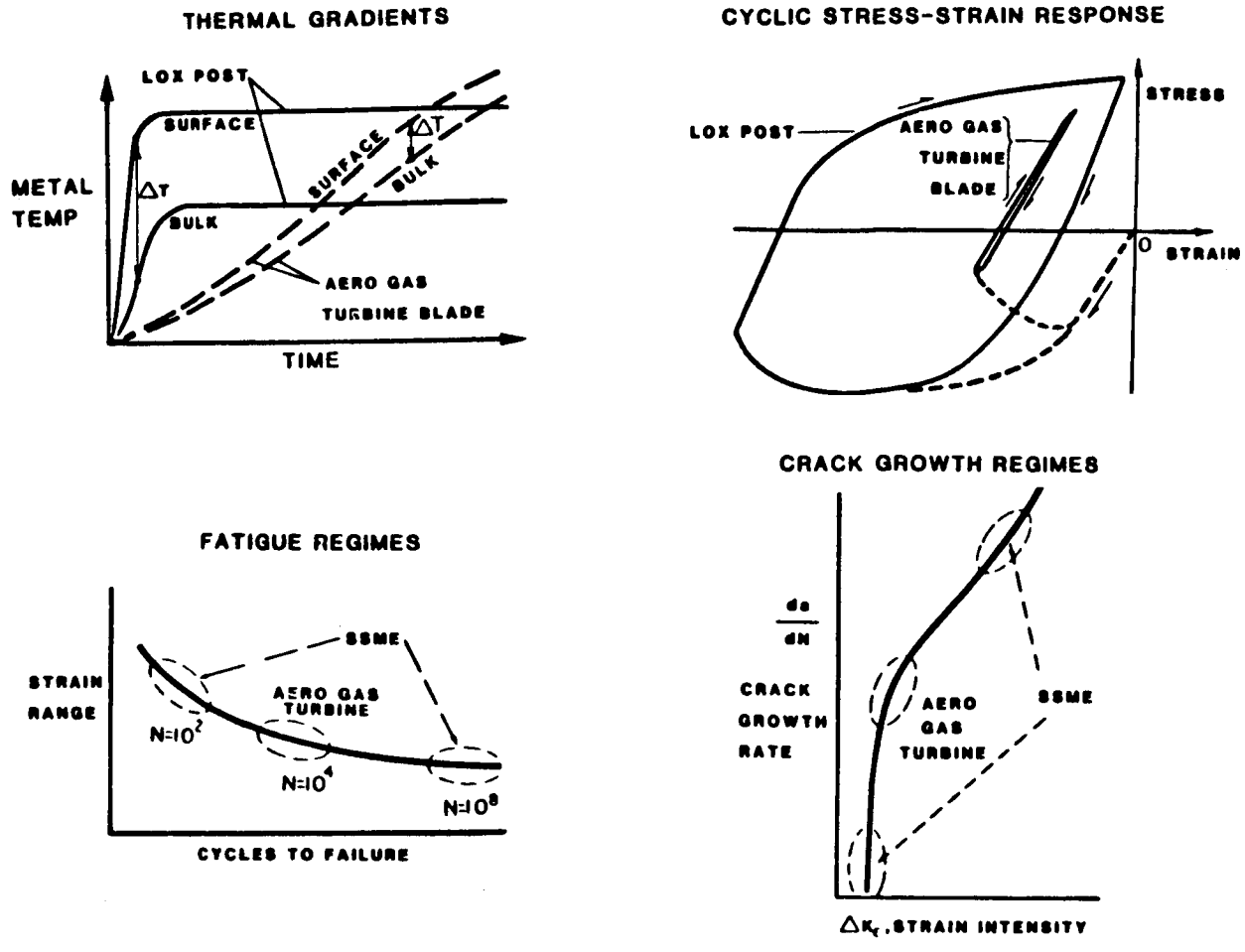

Figure 1. - Thermal loadings, structural response, and durability. (Space shuttle main engine (SSME) compared with aeronautical gas turbine engine)

Hydrogen interaction effects on mechanical strength

- Fatigue loading magnifies extent of hydrogen interaction compared with tensile loading.
- Important micromechanism of hydrogen interaction postulated, i.e., internal voids act as traps for hydrogen and enhance embrittlement.

High mean stress in high cycle fatigue (HCF)

- Factor of two potential increase in HCF strength by reducing void size by factor of four.

Micromechanisms of cyclic deformation in turbopump blading alloys

- Deformation mechanisms leading to low ductility at temperatures where H_2 interaction is greatest have been documented and understood. Improved ductility could lead to reduced H_2 interaction and to improved high cycle fatigue (HCF) resistance.

Cumulative damage rules for HCF/low cycle fatigue (LCF) interactions

- HCF/LCF results for 316 SS, Haynes 188, PWA 1480 show substantial life-degrading interactions
- Simple cumulative damage interaction equations verified and applied in HCF/LCF life extension tradeoff studies

Thermomechanical fatigue (TMF) and relation to isothermal fatigue

- Isothermal fatigue has known limitations for predicting thermomechanical fatigue (TMF) lives
- Newly proposed bithermal fatigue testing technique aids in simplifying TMF investigations
- Newly proposed TMF life prediction model based on application of total strain version of strain range partitioning and bithermal cycling

Advanced structural analysis demonstrations

- Successfully applied advanced constitutive models to analyses of complex mission cycles of SSME turbopump blading, both MAR-M 246 + Hf and PWA 1480
- Verified accuracy of shortcut structural analysis procedure, 10 000 to 1 savings in CPU time

Figure 2. - Accomplishments of structural durability program. (Fatigue/fracture/constitutive modeling)

HCF/LCF interaction under mission-related loading

- Interspersed HCF and LCF loadings
- TMF interaction with HCF loadings
- Generalized creep-fatigue interactions

Application of mechanistically-based constitutive and life models

- Integration of aero-and SSME-based program results
- Pick up where HOST has left off

Macroscopic effects of high pressure H_2 on constitutive and life models

- Competitive procurement package in preparation
- Establish validity of structural durability models developed under program

Structural analyses demonstration program

- GE contract to apply most sophisticated models available to analyze three SSME components, including blade and LOX post

Thermal ratcheting damage analyses

- Interaction of ratchet strains with TMF and HCF
- Application to main combustion chamber materials

Figure 3. - Current and near-term programs. (Fatigue/fracture/constitutive modeling)

Cyclic crack growth under thermomechanical loading conditions

- Application of path-independent integrals to describe crack driving function; pick up where HOST has left off

Application of structural durability analyses to test-bed components

- Improved input information from test-bed instrumentation to provide for more accurate structural durability assessment

Cyclic constitutive and life model development for advanced blade concepts

- Metal matrix composite (MMC) blade materials evaluation

Figure 4. - Long term programs.
(Fatigue/fracture/constitutive modeling)

DEFORMATION AND FATIGUE BEHAVIOR OF SSME TURBOPUMP BLADE MATERIALS

Walter W. Milligan and Stephen D. Antolovich
Georgia Institute of Technology
Atlanta, Georgia

Directionally solidified and single crystal superalloys which are intended for use as turbopump blade materials are anisotropic, both elastically and plastically. Therefore, isotropic constitutive models must be modified. Several models which are now being developed are based on metallurgical theories of deformation in these types of alloys. However, these theories have not been fully justified, and the temperature and strain regimes over which they may be valid are poorly defined. The objective of this work is to study the deformation behavior of the alloys, in order to determine the validity of these models and to thereby support the ongoing research efforts in solid mechanics.

REFERENCES

1. Milligan, W.W.; and Antolovich, S.D.: Yielding and Deformation Behavior of the Single Crystal Superalloy PWA 1480. Metall. Trans. A., vol. 18, no. 1, Jan. 1987, pp. 85-95.

2. Milligan, W.W., Jr.: Yielding and Deformation Behavior of the Single Crystal Nickel-Base Superalloy PWA 1480. (USAAVSCOM TR-86-C-18, Georgia Institute of Technology; NASA Grant NAG3-503) NASA CR-175100, 1986.

3. Huron, E.S.: High Temperature Monotonic and Cyclic Deformation in a Directionally Solidified Nickel-Base Superalloy. (USAAVSCOM TR-86-C-19, Georgia Institute of Technology; NASA Grant NAG3-503) NASA CR-175101, 1986.

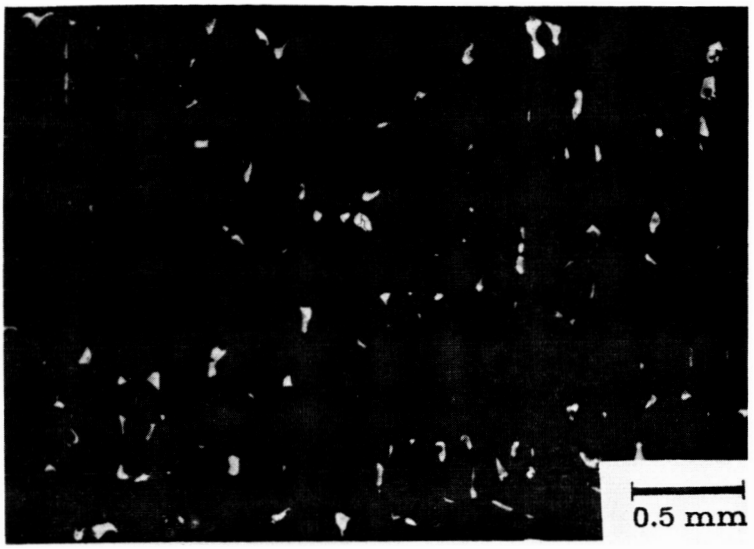

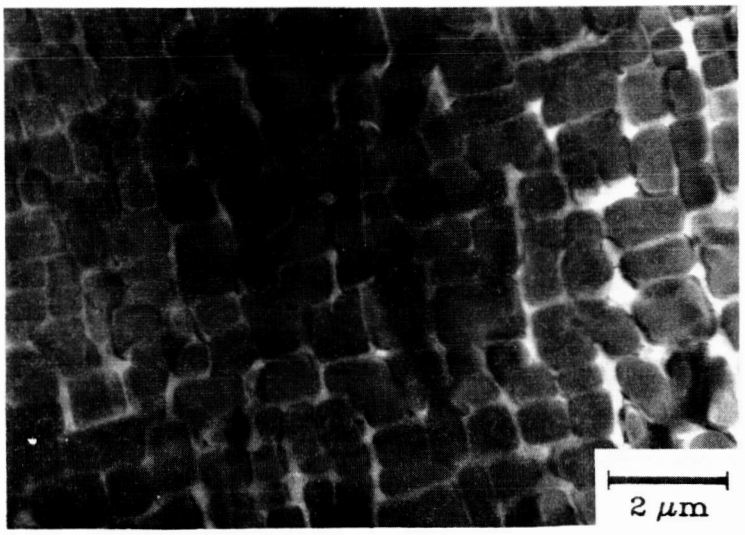

Figure 1. - PWA 1480 initial microstructure.

Classical Plasticity Theory

$$\dot{\epsilon}_t = \frac{\dot{\sigma}}{E} + \dot{\epsilon}_p + \dot{\epsilon}_c$$

Unified Constitutive Theory

$$\dot{\epsilon}_{(in)} = \dot{\epsilon}_t - \frac{\dot{\sigma}}{E} = f^{-1}\left[\frac{\sigma_{ij} - \Omega_{ij}}{K}\right]$$

Figure 2. - Constitutive modeling.

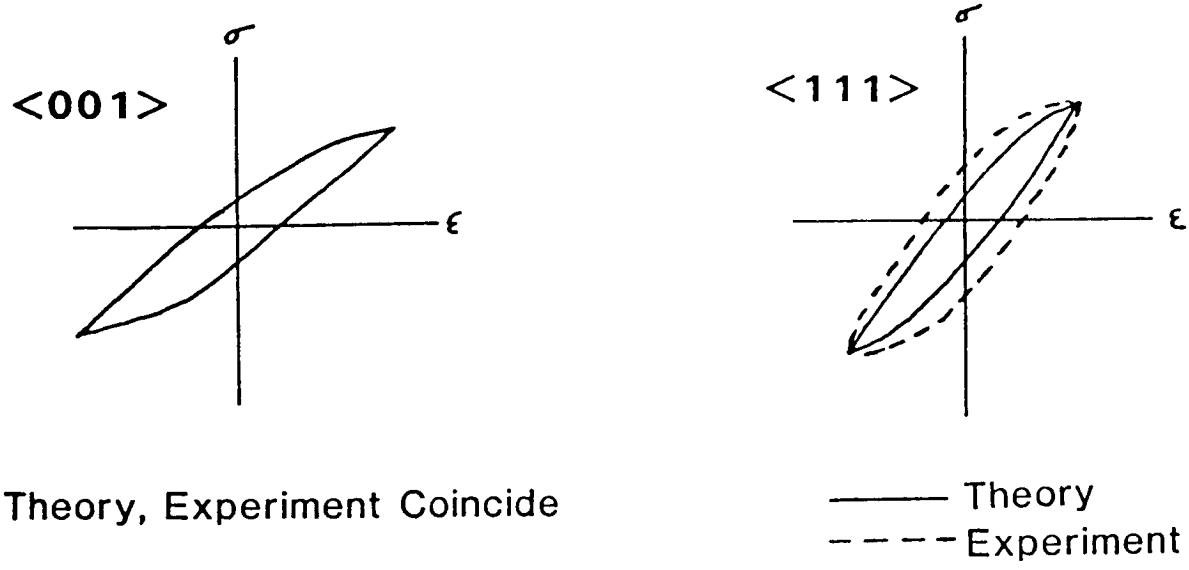

Figure 3. - PWA 1480 at 1600 °F - after K.P. Walker and E. Jordan.

$$\dot{\gamma}_p = \sum_{i=1}^{n} \dot{\gamma}_i \quad ;$$

$$\dot{\gamma}_i = f^{-1}\left[\frac{\underline{\sigma}_i - \underline{\Omega}_i}{K_i}\right]$$

<110>(111)

<112>(111)

<110>(001)

Figure 4. - Unified crystallographic approach.

Crystallographic approach requires physical validation

-Active slip systems

-Cube slip only observed in γ'

-Slip planarity

-Deformation mechanisms

Figure 5.

$$\gamma_o = b\rho_o\lambda \leq 0.006\%$$

γ' must be "overcome" for substantial plasticity

Figure 6. - Deformation mechanisms.

Possibilities:

1. Looping
2. Shearing
3. Climb-assisted Bypass

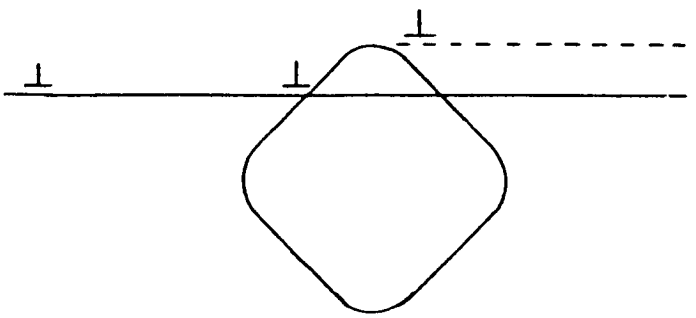

Figure 7.

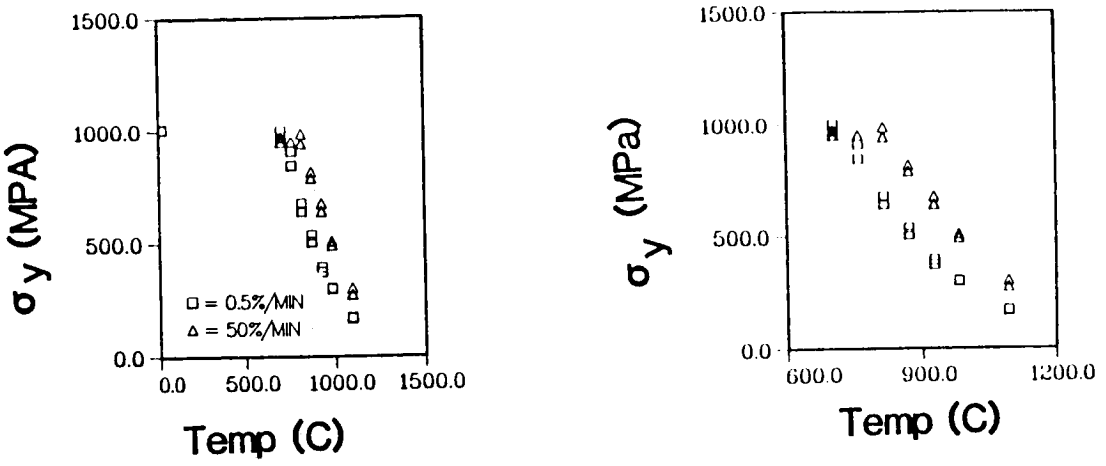

Figure 8. - PWA 1480 yield strength (0.05 percent offset) versus temperature.

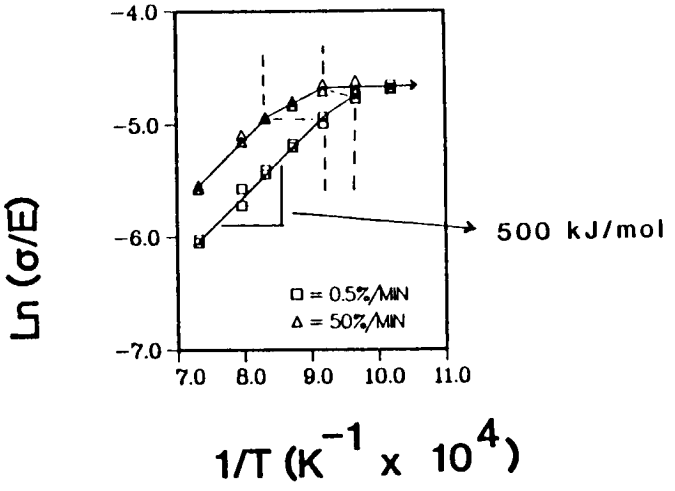

Figure 9. - PWA 1480 modulus normalized yield; strength versus inverse temperature.

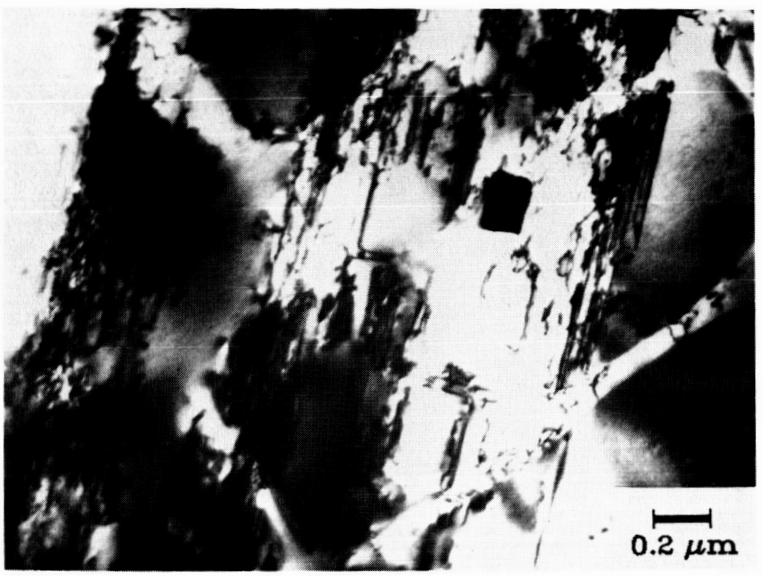

Figure 10. - γ' Shearing by slip bands at low temperatures (0.1 percent ε_p).

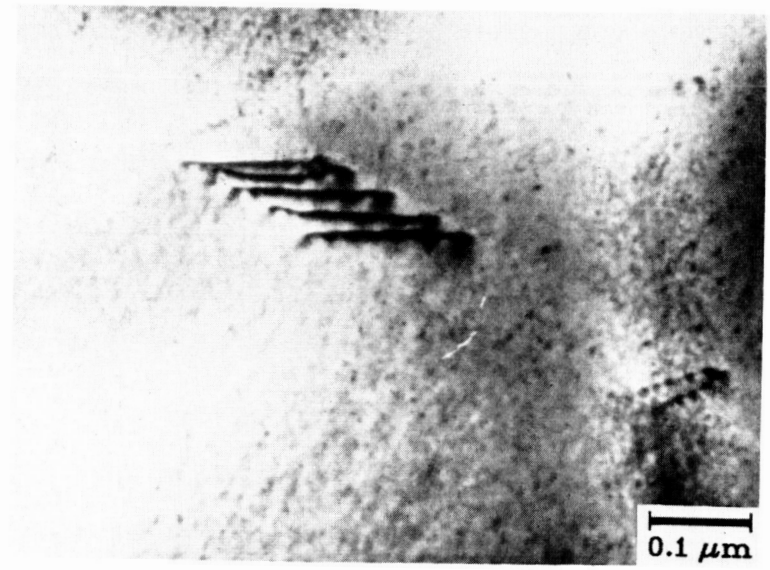

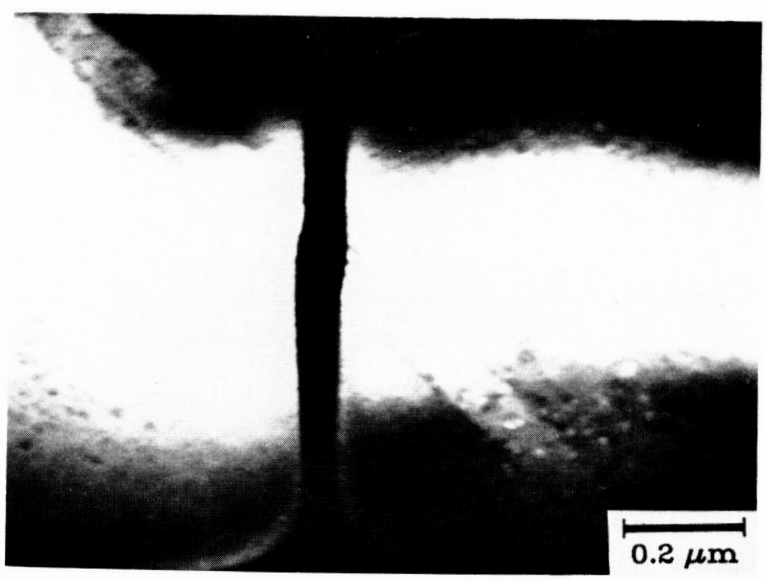

Figure 11. - Shear offsets parallel to $\bar{b}$.

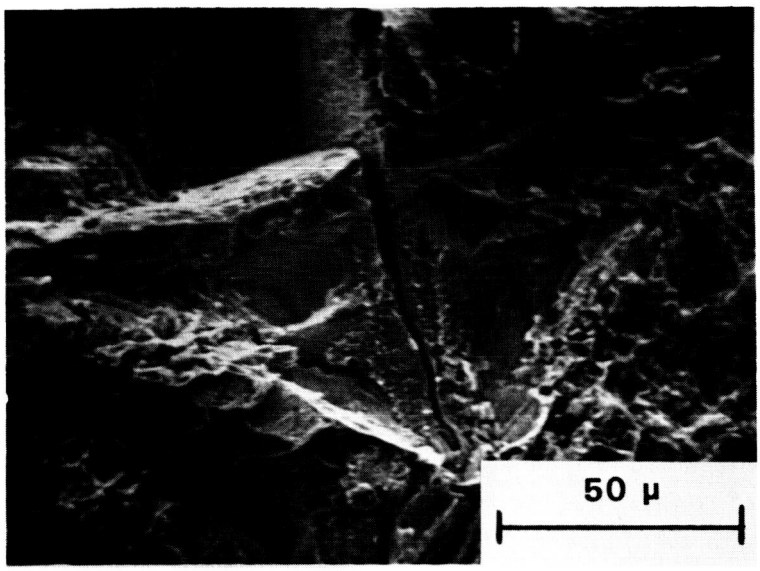

Figure 12. - Typical tensile fracture surface.
(D.S. Mar-M 246 tested at room temperature.)

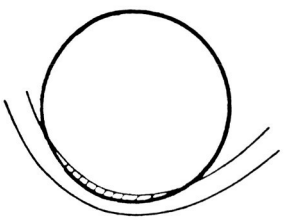

$$(\tau - \tau_p)b + \frac{c}{\Delta x} + \frac{\phi}{r_o} - \gamma = 0$$

$$(\tau - \tau_m)b - \frac{c}{\Delta x} + \frac{\phi}{r_o} = 0$$

$$\tau_c = \frac{\gamma}{2b} - \frac{Gb}{2r_o} + \frac{1}{2}(\tau_m + \tau_p)$$

Figure 13. - Low temperature
(Copley-Kear, Huther-Reppich).

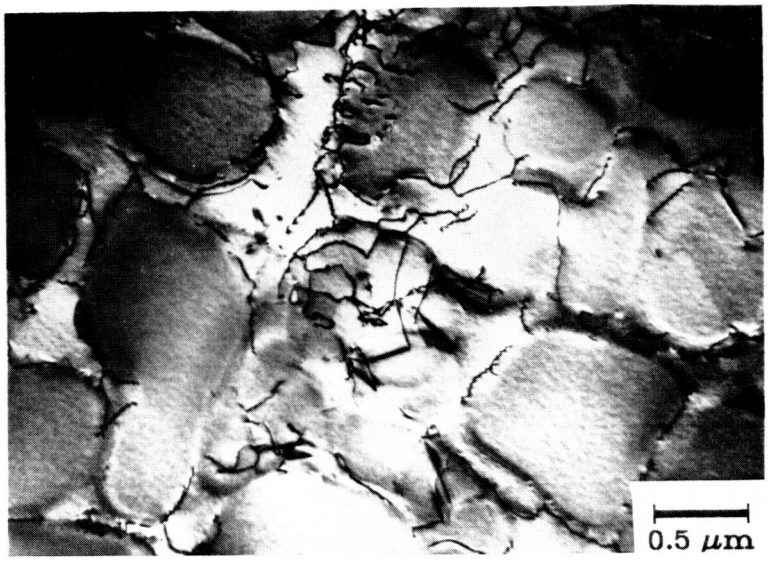

Figure 14. - γ' Bypass at high temperatures (0.3 percent ε_p).

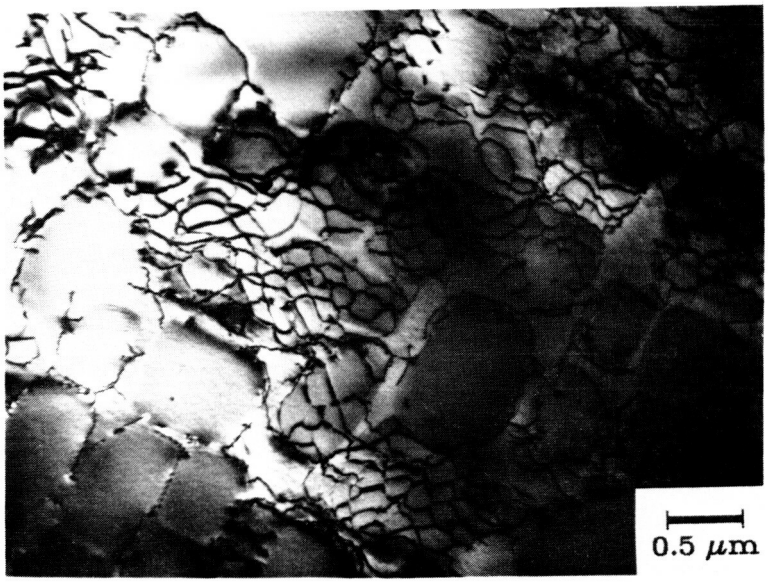

Figure 15. - Interfacial network of dislocations developed at 1093 °C after about 0.25 percent ε_p.

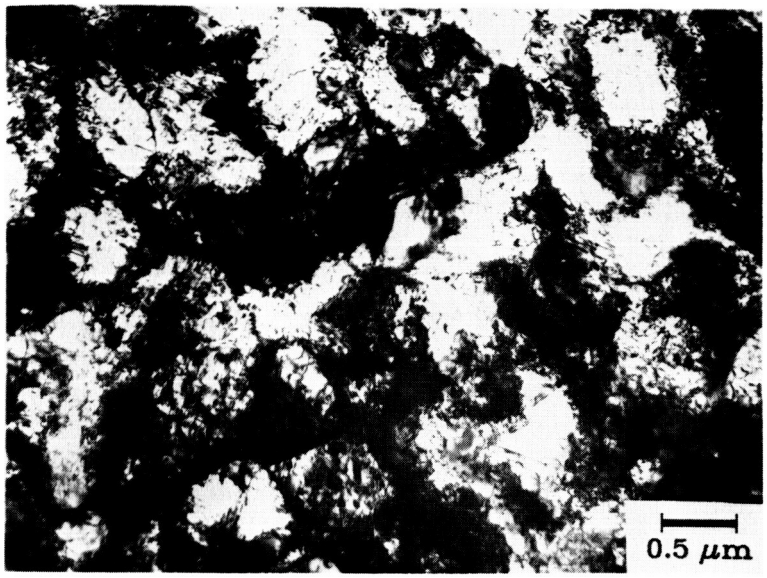

Figure 16. - High dislocation density at failure at 871 °C.

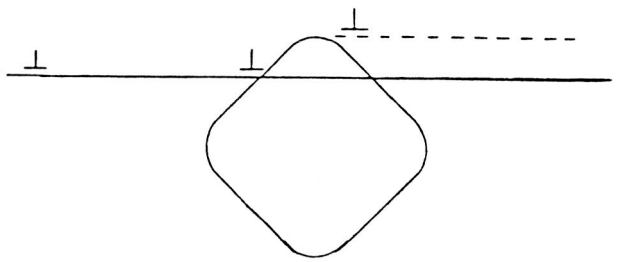

Climb is rate-limiting step

–Controlled by diffusion

$$\tau_c = k_1 Q_D - k_2 T \left| \log(k_3 \dot{\epsilon}) \right|$$

Figure 17. - High temperatures (Brown and Ham, bypass model).

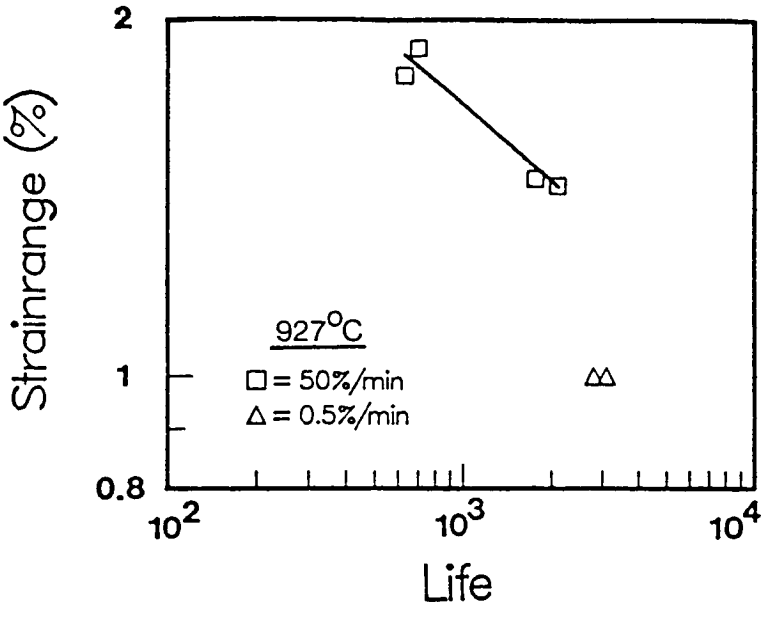

Figure 18. - PWA 1480.

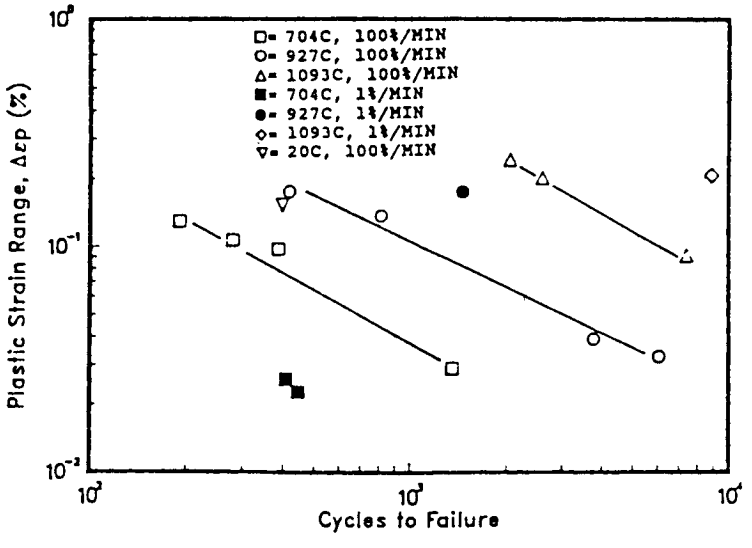

Figure 19. - Mar-M 246.

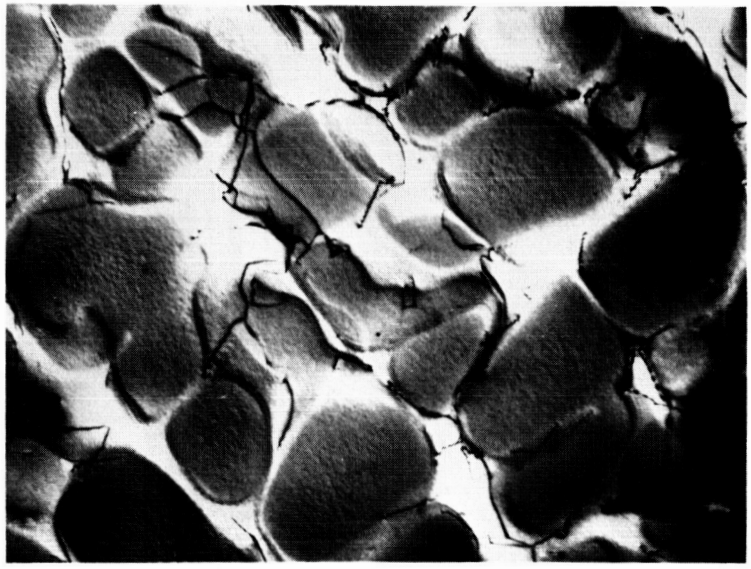

0.5 percent/min

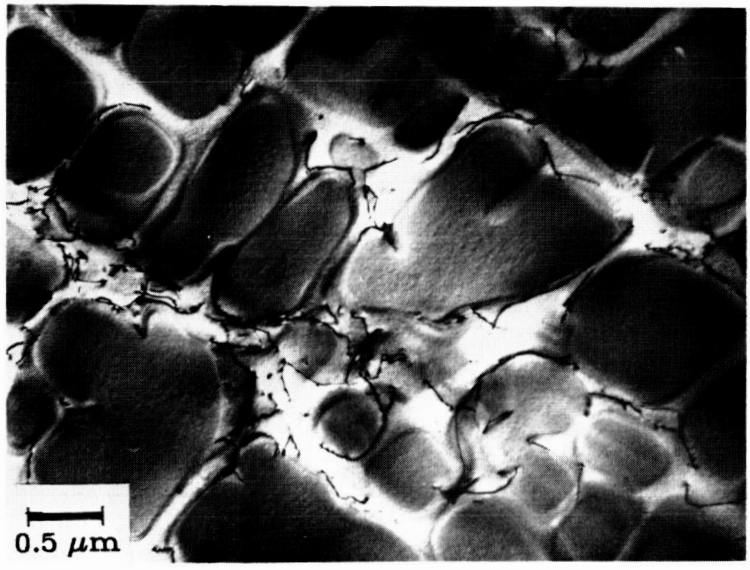

50 percent/min

Figure 20. - 927 °C, $\Delta\varepsilon_p$ = 0.1 percent, N = 4.

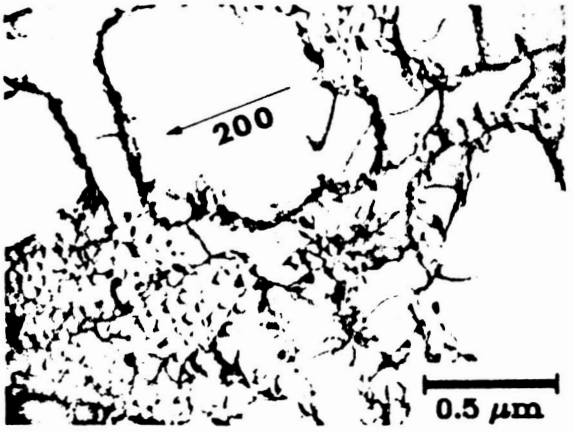

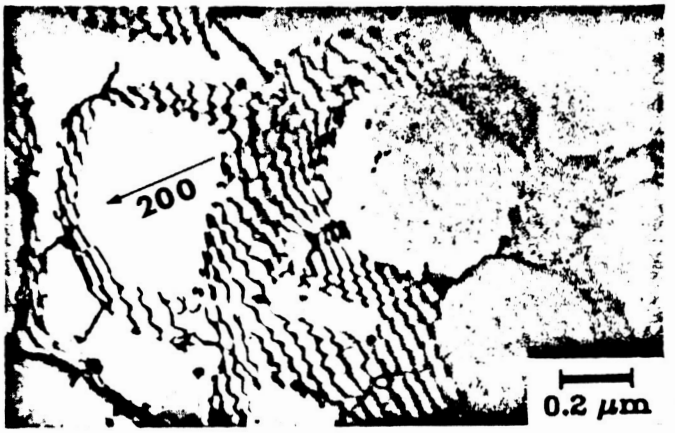

Figure 21. - Mar-M 246 deformation structures after low cycle fatigue at 927 °C.

Original unavailable at time of printing.

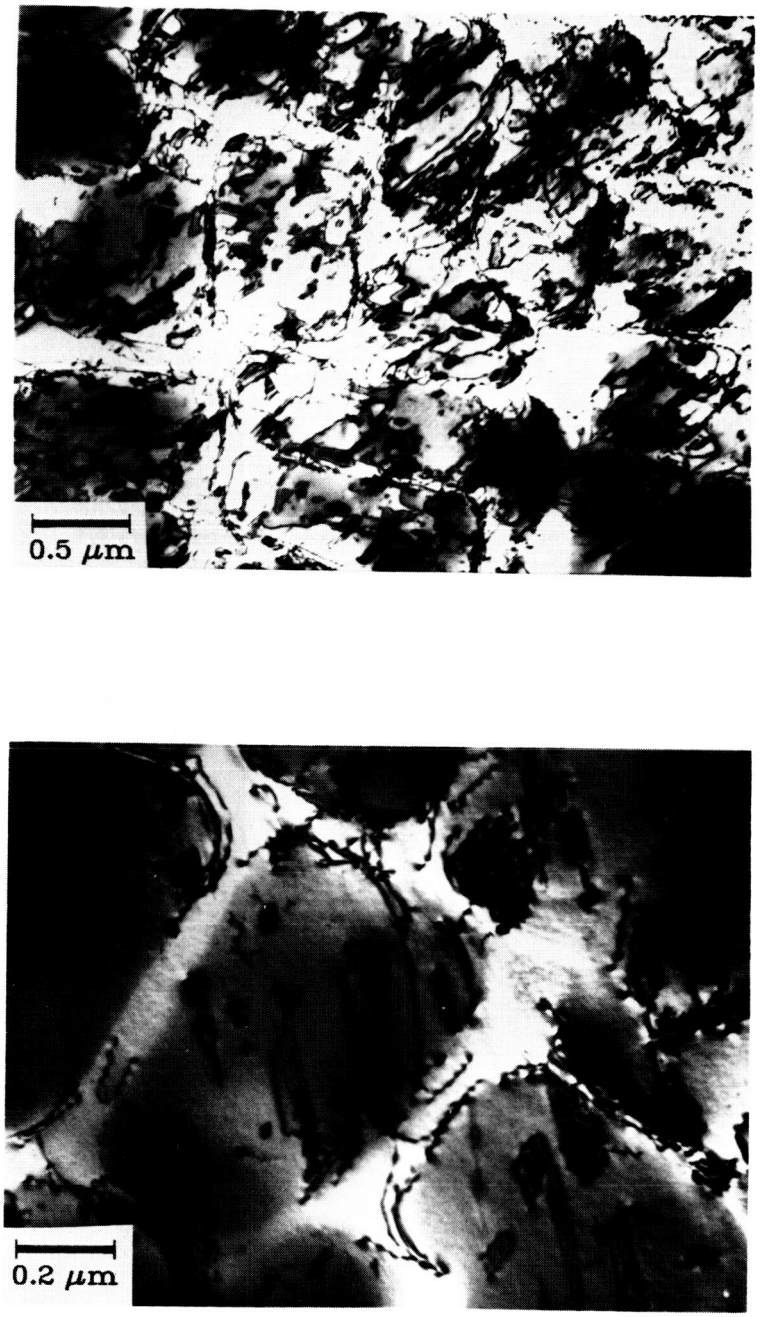

Figure 22. - PWA 1480; 20 °C,
$\Delta\varepsilon_p$ = 0.05 percent, N = 4.

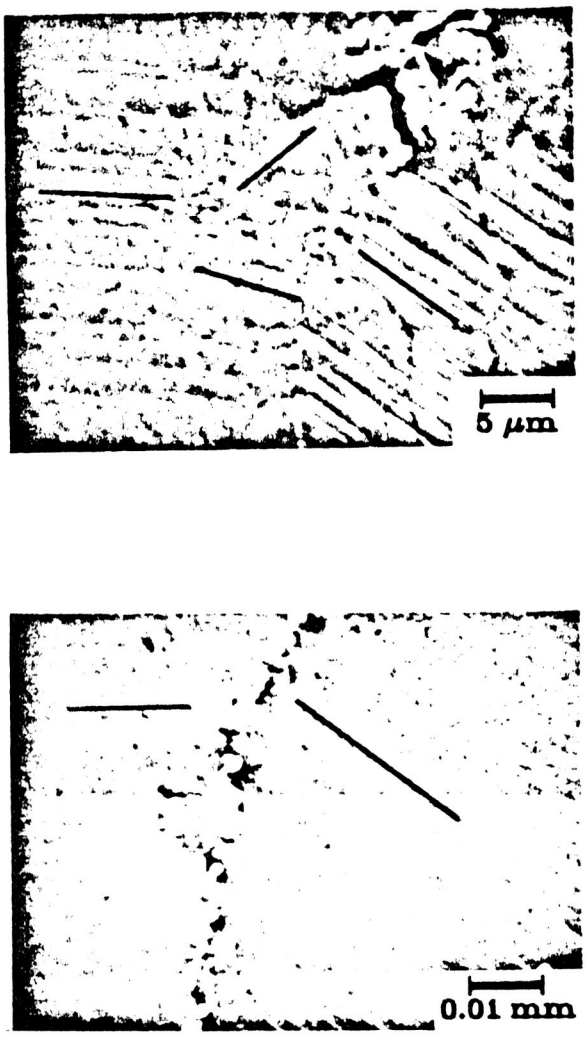

Figure 23. - Surface slip traces after low cycle fatigue at 705 °C, Mar-M 246.

Original unavailable at time of printing.

Deformation during creep,

uniaxial tension and LCF essentially similar

-By-pass at 927 °C

-Shearing at Lower Temps

Figure 24.

Implications

-Unified models justified

-No shearing in (001) crystals at 927 °C

-(123) tests to come

Figure 25.

FATIGUE DAMAGE INTERACTION BEHAVIOR OF PWA 1480

Michael A. McGaw
NASA Lewis Research Center
Cleveland, Ohio

The fatigue damage interaction behavior of PWA 1480 single crystal alloy has been experimentally established for the two-level loading case in which a block of low-cycle fatigue loading is followed by high-cycle fatigue loading to failure. A relative life ratio N1/N2 (where N1 and N2 are the low- and high-cycle fatigue baseline lives, respectively) of approximately 0.002 was explored to assess the interaction behavior. The experimental results thus far show evidence of a loading order interaction effect to a similar degree of detriment as has been observed in polycrystalline materials. Current generation single crystal alloys in general, and PWA 1480 in particular, contain pores; indeed, it was observed in all cases that specimen failure initiated from pores connected with or immediately below the surface. Detailed fractographic and metallographic studies are currently being made to assess the nature of the porosity in terms of its effect on fatigue life.

EXPERIMENTAL RESULTS

Specimens of PWA 1480 were fabricated from slab material. The specimen geometry was solid cylindrical, having a 1-inch uniform axis gauge section and threaded ends. The specimens were within 10° of the 001 crystallographic direction.

Low-cycle fatigue tests were conducted in strain control using a specialized electrohydraulic tension-compression testing system (fig. 1, ref. 1). The specimens were tested at room temperature using a computer-generated sinusoidal waveform command of constant frequency (0.2 Hz). Control and data acquisition were performed by computer using a software system described in reference 2. The strain gauge used for strain measurement and feedback had a gauge length of 0.24 inch. High-cycle fatigue tests were conducted with the same equipment, although under load control. The test waveform was sinusoidal; the frequency was 300 Hz.

The results of this baseline fatigue characterization testing are displayed in figures 2 and 3. Failure in all tests is defined as specimen fracture into two halves.

The interaction tests were based on reference low-cycle and high-cycle fatigue life levels of 3000 and 1.5 million cycles-to-failure, yielding a relative life level ratio of approximately 0.002. As the purpose in this program is to identify potentially deleterious life behavior on a cumulative fatigue basis, the tests were conducted so that the low-cycle fatigue loading was applied first, and the remainder of the test was carried out under high-cycle fatigue loading conditions until failure occurred, whereupon the remaining life fraction was measured.

The results of the interaction testing are displayed in figure 4 (where the data are interpreted in terms of a stress-based life criterion) and figure 5 (where the data are interpreted in terms of a total strain-based life criterion). The solid curves in both figures are predictions made using the Damage Curve Approach (ref. 3), where the average of the low-cycle fatigue lives predicted for the applied cycle parameter (stress or total strain) was used for the low-cycle fatigue reference life N_1 and the same procedure was used for obtaining the high-cycle fatigue reference life N_2.

DISCUSSION AND CONCLUSIONS

A large amount of scatter in the baseline fatigue behavior is observed in figure 3, especially in the 10^6 to 10^8 life range. A number of experiments were performed at nominally the same completely reversed stress range; three failures were obtained in the 10^6 range while two "runouts" were observed at the middle 10^7 range. Scatter, although apparently not to the same degree, was observed in the low-cycle fatigue range as well. A preliminary fractographic analysis of the failed specimens revealed cracks initiating at surface or near-surface porosity in all cases. The nature of the porosity varied widely in terms of pore size, geometry, and orientation with respect to the loading (and crystal growth) direction. Preliminary analysis also indicated a change in fracture surface appearance as a function of life: while the failure always initiated at a pore in the case of low-cycle fatigue, the early propagation was on two intersecting crystallographic planes; in the case of high-cycle fatigue the early propagation was on a singularly dominant crystallographic plane. The actual crack propagation phase of failure observed in these experiments is for all practical matters zero in the context of cyclic life. The stress-strain response observed at the onset of failure gave little or no indication of the impending fracture.

The interaction experiments show an interaction effect produced by cumulative loading, although the precise nature of the interaction effect is not well correlated by current cumulative damage rules, such as the Damage Curve Approach. A difficulty in the study of cumulative fatigue damage has been the compounded scatter observed in such studies; that is, if the reference life levels are known to be within a factor of 2, the loading interaction cannot be known to be anything less than a factor of 2. In fact, the factors of 2 compound one another. Preliminary fractographic analyses reveal fracture surfaces which appear quite planar, being perpendicular to the loading axis for applied low-cycle fatigue ratios less than approximately 0.5.

The fractographic appearance is reminiscent of polycrystalline materials failing in high-cycle fatigue. This fracture morphology was never observed in the baseline experiments. For applied low-cycle fatigue life ratios of approximately 0.5 and greater, the fracture takes on a character similar to that observed in the baseline low-cycle fatigue experiments.

Detailed fractographic and metallographic studies are being made on the failed specimens in an effort to explain the influence of pore size, geometry, and orientation on fatigue life, as well as interaction behavior.

REFERENCES

1. McGaw, M. A.: Lewis' Enhanced Laboratory for Research into the Fatigue and Constitutive Behavior of High Temperature Metals. Turbine Engine Hot Section Technology 1985, NASA CP-2405, 1985, pp. 361-371.

2. McGaw, M. A.; and Bonacuse, P. J.: Automation Software for a Materials Testing Laboratory. Turbine Engine Hot Section Technology 1986, NASA CP-2444, 1986, pp. 399-406.

3. Manson, S. S.; and Halford, G. R.: Practical Implementation of the Double Linear Damage Rule and Damage Curve Approach for Treating Cumulative Fatigue Damage. Int. J. Fract., vol. 17, no. 2, Apr. 1981, pp. 169-192.

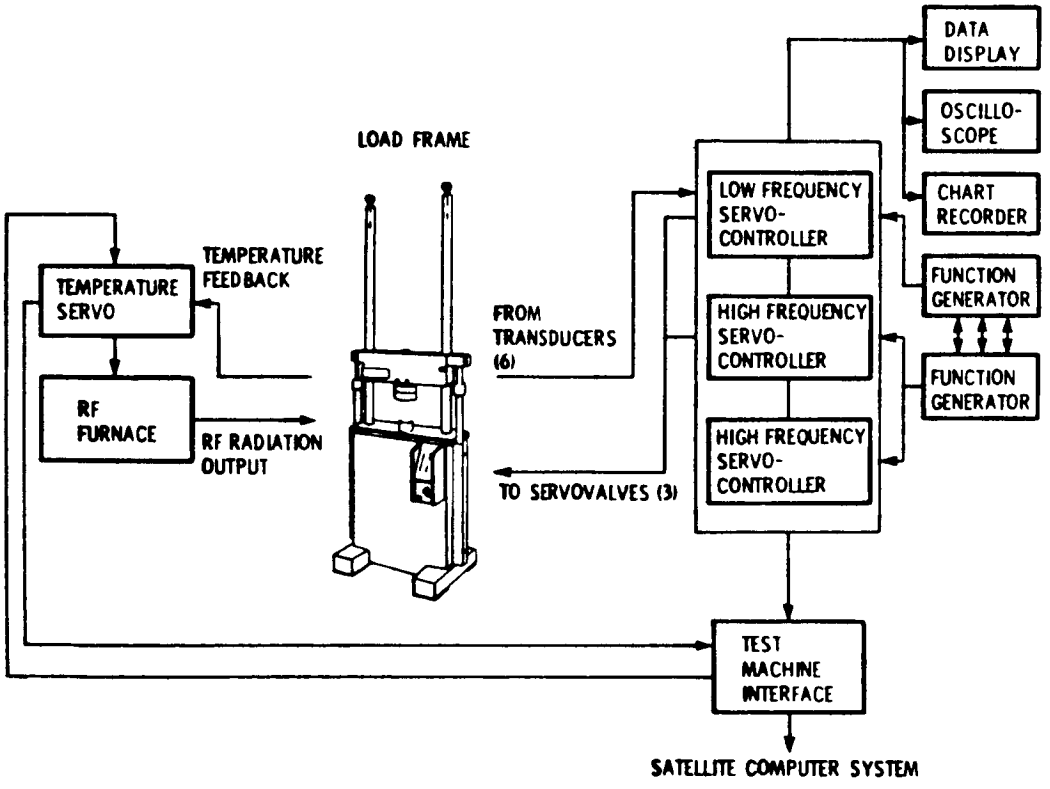

Figure 1. - High-cycle fatigue/low-cycle fatigue materials test system.

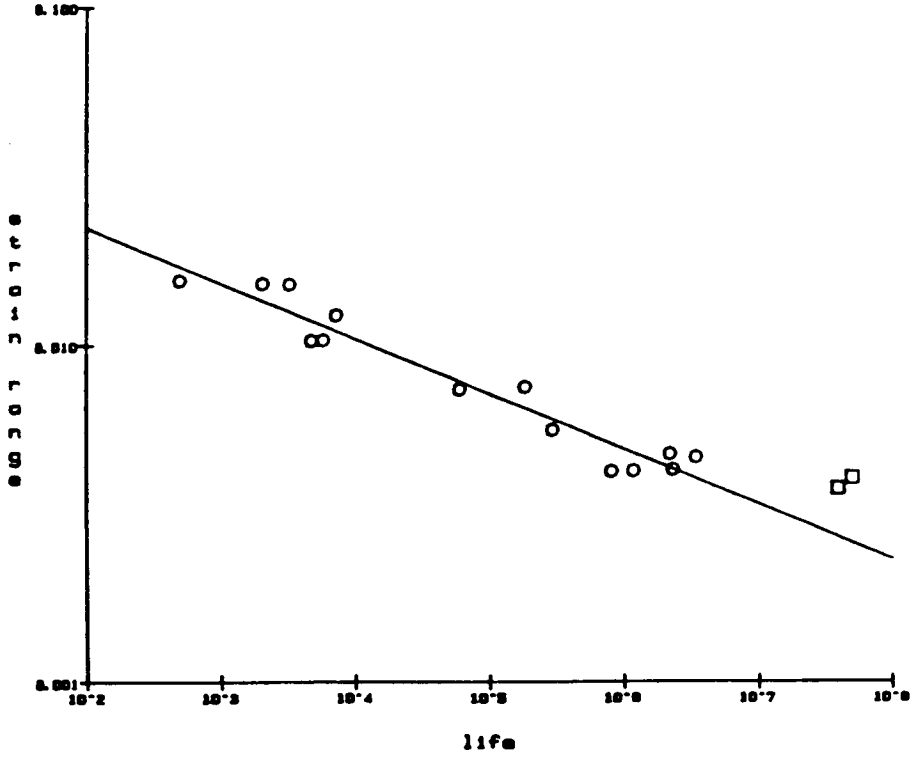

Figure 2. - Fatigue life as function of total strain range. PWA 1480, SC R.T.

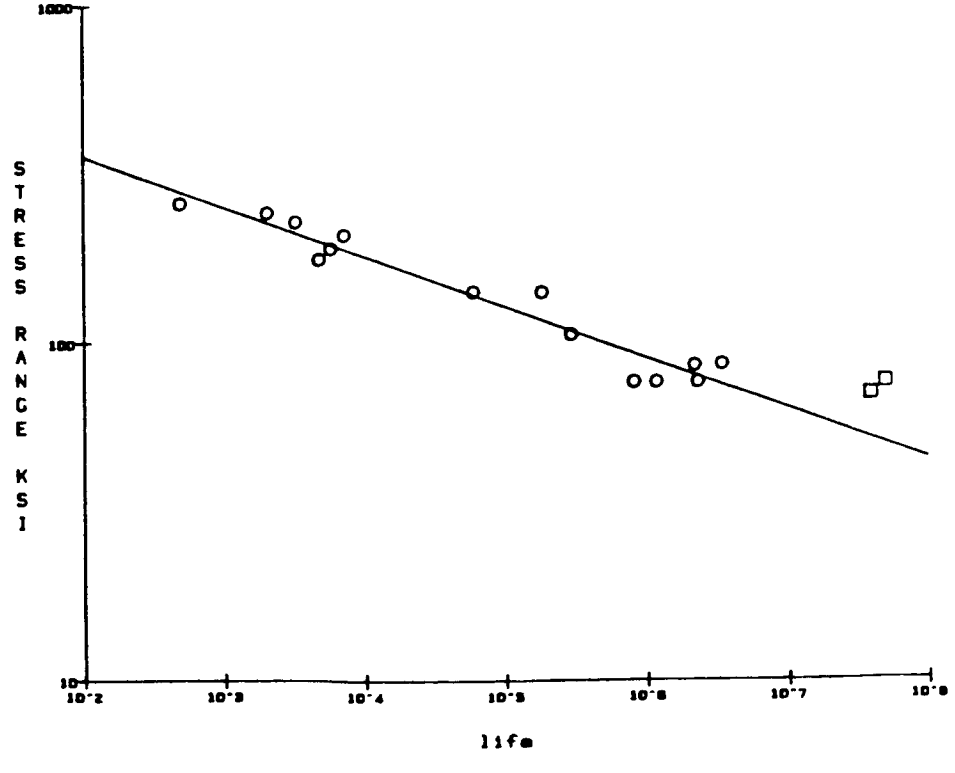

Figure 3. - Fatigue life as function of stress range. PWA 1480, SC R.T.

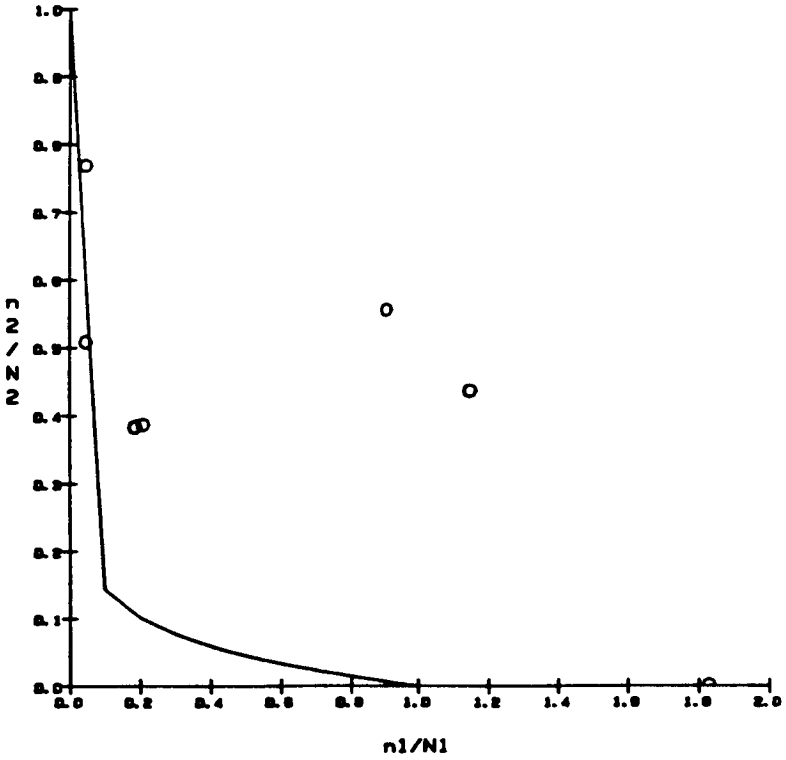

Figure 4. - Results of interaction testing. Data interpreted in terms of stress-based life criterion.

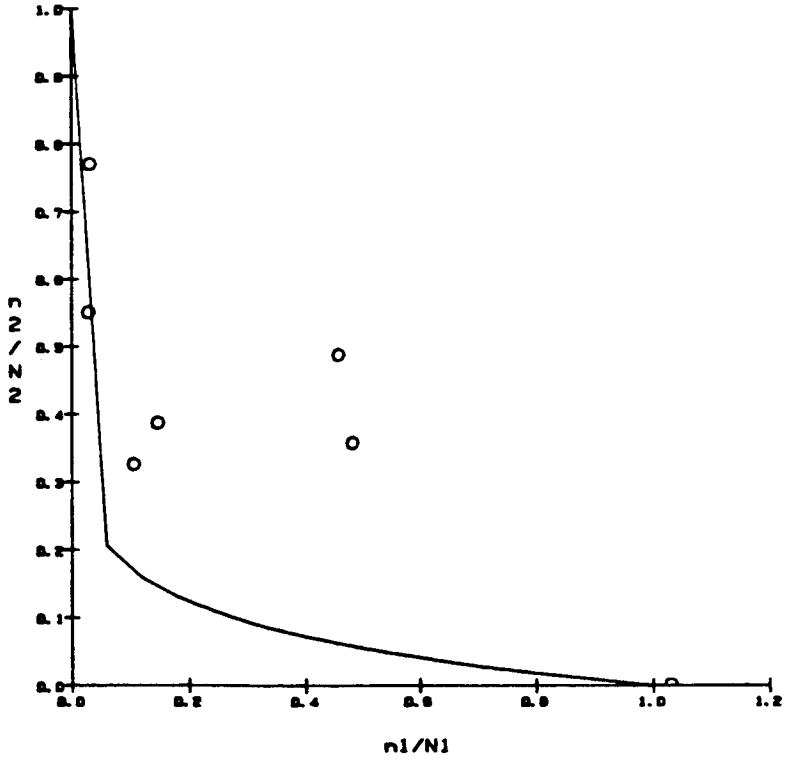

Figure 5. - Results of interaction testing. Data interpreted in terms of total strain-based life criterion.

A NEW FORMULATION OF MEAN STRESS EFFECTS IN FATIGUE

S.S. Manson
Case Western Reserve University
Cleveland, Ohio

and

K.R. Heidmann
Steelcase Corporation
Grand Rapids, Michigan

A common method of treating the mean stress effect on fatigue life is to displace the elastic line on a Manson-Coffin-Basquin diagram while retaining the position of the plastic line. Manson and Halford pointed out that this procedure implies that mean stress significantly affects the cyclic stress-strain curve (ref. 1). Actually, however, they showed experimentally and by more general reasoning, that mean stress has little, if any, effect on the cyclic stress-strain curve. Thus, they concluded that it is necessary to displace the plastic line as well as the elastic line in order to keep the cyclic stress-strain curve unaltered. Another way of expressing the common displacement of the two lines is to keep the lines in place and change the horizontal coordinate to include a term relating to the displacement. Thus, instead of life, $2N_f$, as the horizontal coordinate, a new coordinate can become $2N_f [1 - \sigma_m/\sigma_f]^{1/b}$, thereby displacing both the elastic and plastic lines by an amount $[1 - \sigma_m/\sigma_f]^{1/b}$ where σ_m is the mean stress and σ_f is the intercept of the elastic line at $N_f = 1/2$ cycles and b is the slope of the elastic line.

Such a procedure does not, however, always produce the proper effect on the Goodman diagram in which mean stress is plotted against alternating stress for selected values of life. The Goodman diagram for this case would necessarily be straight lines for all materials. While some materials do, indeed, produce straight lines, others are known to be concave, while still others have convex curvature. In fact, for some materials, the Goodman diagram may be concave for one life level, straight for another life level, and convex for a third life level. A more generalized behavior can, therefore, be achieved by using, as the horizontal coordinate, the parameter

$$2N_f \left[1 - \left(\frac{\sigma_m}{\sigma_f} \right)^{A + B \log N_f} \right]^{1/b}$$

Depending on the values of A and B, the curvature of the Goodman lines can then change according to life level.

We have examined a number of materials for which various degrees of curvature have been observed, as well as one material for which the curvature changed from convex to concave as life was changed.

Figure 1 shows schematically the concept behind the procedure we have developed. Figure 1(a) shows the coordinate axes in a Manson-Coffin-Basquin plot, while figure 1(b) shows an example whereby curvature is altered at different values of life level for particular parameter values of A and B, as shown.

Figure 2 shows the application of this type of analysis to various aluminum and steel alloys for which extensive data are available in the literature. The lines drawn in these figures are derived from the diagrams of figure 1(a) for the specific constants shown for each material. The experimental points are derived from faired curves through the data. Good agreement is seen in all cases. Note especially the 9Ni-4Co-0.45C material for which different curvatures appear at different life levels.

REFERENCE

1. Halford, G.R.; and Manson, S.S.: Discussion of Paper: M. Doner, K.R. Bain, and J.H. Adams; Evaluation of Methods for the Treatment of Mean Stress Effects on Low-Cycle Fatigue. J. Eng. Power, vol. 104, no. 2, Apr. 1982, pp. 403-411: J. Eng. Power, vol. 104, no. 2, Apr. 1982, p. 411.

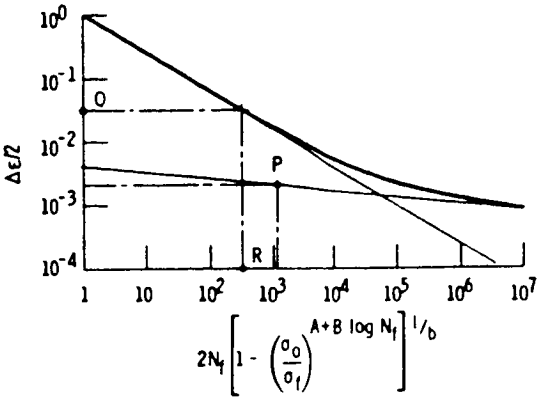

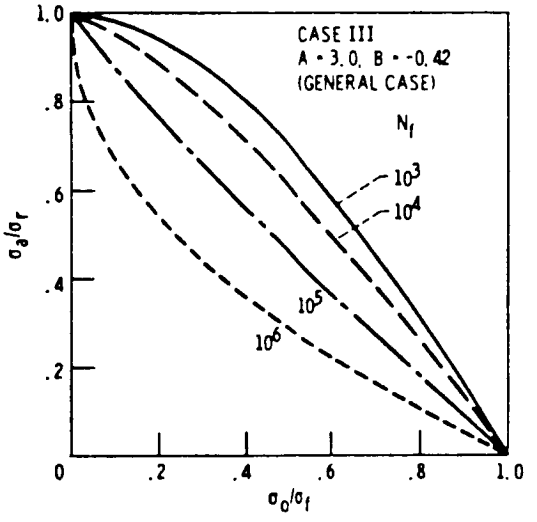

Figure 1. - Framework for new method.

C-2

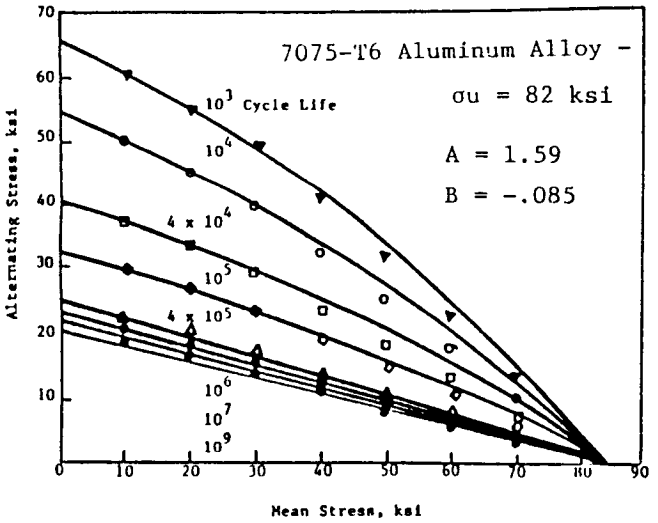

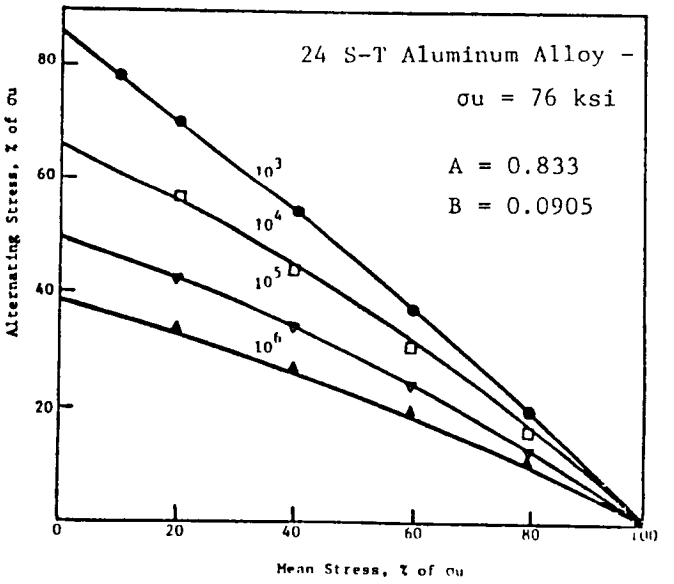

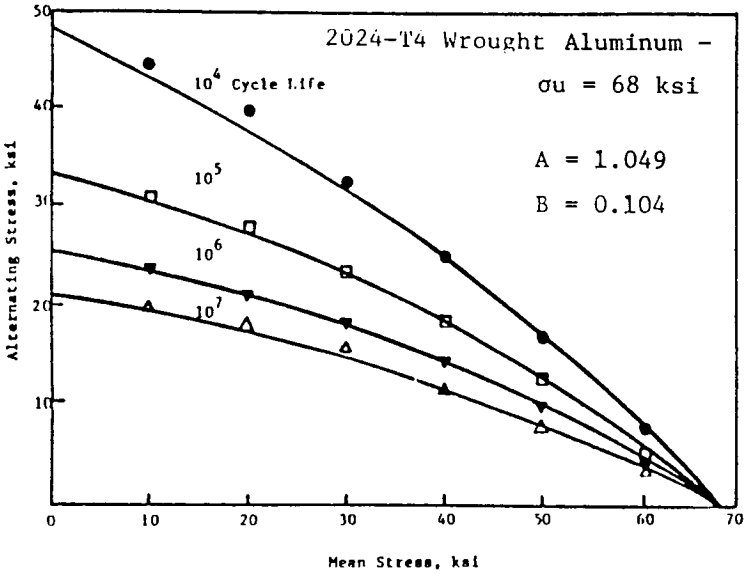

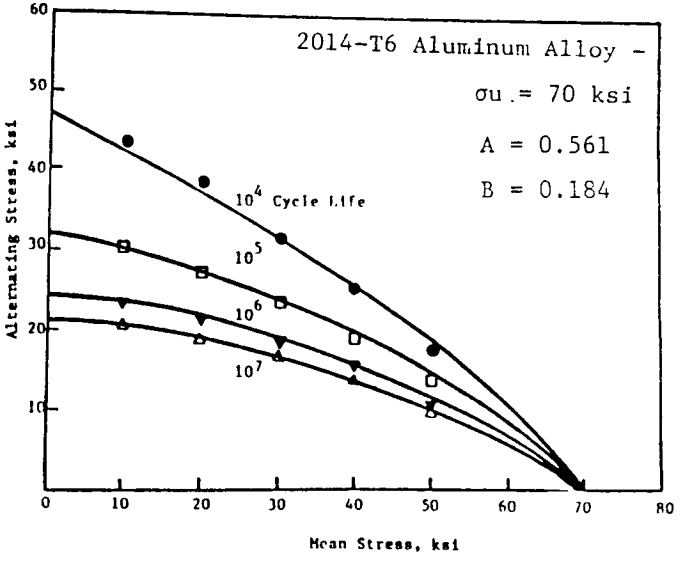

Figure 2. - Comparisons between observed and calculated axial fatigue strengths.
(——— Predictions; ●□Δ From experimental curves)

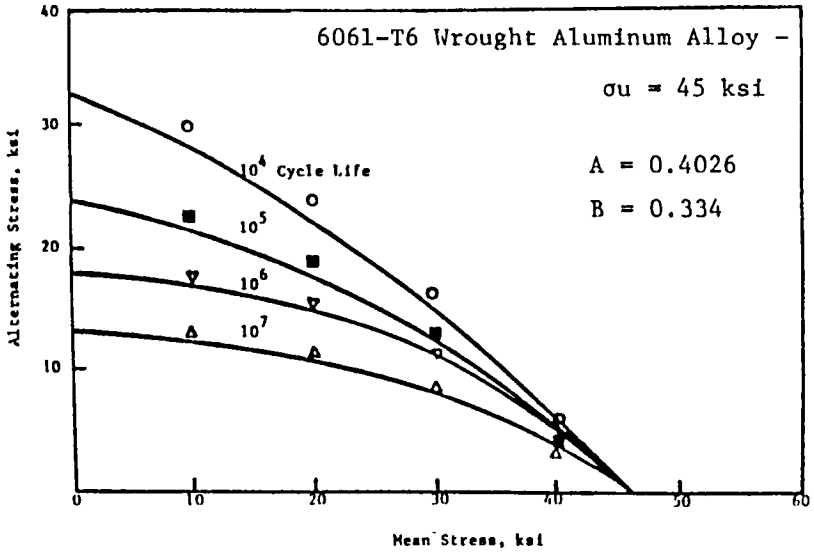

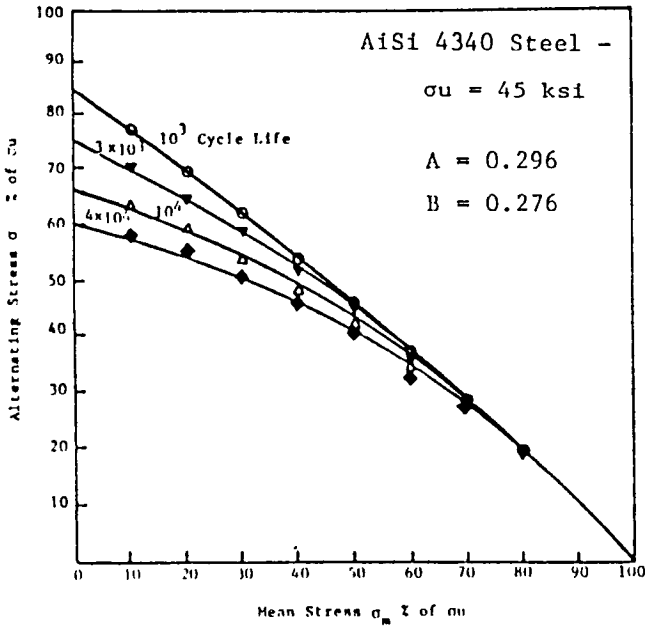

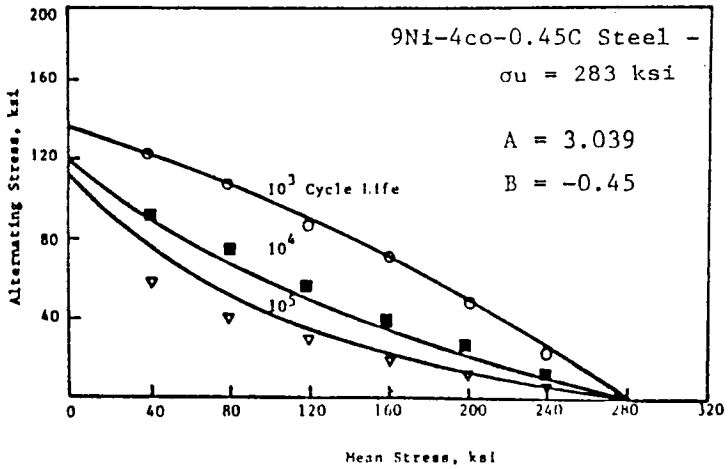

Figure 2. - Continued.

NONLINEAR HEAT TRANSFER AND STRUCTURAL ANALYSES OF SSME TURBINE BLADES

A. Abdul-Aziz
Sverdrup Technology, Inc.
Middleberg Heights, Ohio

and

A. Kaufman (Retired)
NASA Lewis Research Center
Cleveland, Ohio

Three-dimensional nonlinear finite-element heat transfer and structural analyses were performed for the first stage high-pressure fuel turbopump blade of the space shuttle main engine (SSME). Directionally solidified (DS) MAR-M 246 material properties were considered for the analyses. Analytical conditions were based on a typical test stand engine cycle. Blade temperature and stress-strain histories were calculated using MARC finite-element computer code (ref. 1). This study was undertaken to assess the structural response of an SSME turbine blade and to gain greater understanding of blade damage mechanisms, convective cooling effects, and the thermal-mechanical effects.

Hot-gas path components for reusable space propulsion systems operate under extreme gas pressure and temperature. These operating conditions subject the high pressure stage turbine nozzles and blades to severe thermal transients that can result in large inelastic strains and rapid crack initiation. Advances in casting techniques have allowed the development of directionally solidified and single crystal alloys for high temperature components in space propulsion vehicles. Mechanical anisotropy exhibited by these alloys have to be taken into account in the analytical studies. To improve the durability and accuracy of turbine blades and other hot section components, an accurate knowledge of the temperature and stress-strain histories at the critical location for crack initiation is required (fig. 1).

Experimental measurements of gas temperature profiles in the SSME turbopumps are difficult to obtain because of the high gas temperature and severe thermal transients. Turbine blade temperatures are primarily a function of hot gas flow and cooling. The temperature field is determined by the heat transfer from the hot gas to the blade. This heat transfer and its variations are determined by knowledge of the gas film coefficients. Also, the time-temperature history profile at the start transient, steady state, and cutoff is obtained through a combination of analytical and experimental results which is due to the complex flow phenomena through an accelerating turbine.

Temperature-dependent properties for the MAR-M 246 + Hf alloy were mainly provided by Rockwell International Corporation. These elastic properties are summarized in table I. Mean thermal coefficient of expansion data were converted to instantaneous values for MARC input. Longitudinal stress-strain properties, summarized in table II, were used for elastic-plastic region. The mission used for this analysis is shown in figures 2 and 3 in terms of inlet temperature, gas pressure, and revolutions per minute (RPM). This cycle is

applicable to a factory test of the engine; it is also reasonably representative of a flight mission except for the foreshortened steady-state operating time. The major factor inducing fatigue cracking is the transient thermal stresses caused by the sharp ignition and shutoff transients. The finite-element model of the blade in figure 4 was constructed of a three-dimensional eight-node isoparametric brick element. The model consisted of 1-25 elements with 1575 nodes and 4660 unsuppressed degrees of freedom.

Heat transfer coefficients at the blade airfoil (figs. 5(a) and (b)) were predicted by running a boundary layer analysis using a modified version of the STAN5 boundary layer code (refs. 2 and 3). Thermal environment experienced by the platform and shank were obtained from reference 4. Details regarding prediction of heat transfer coefficients at the stagnation region for the airfoil are available in reference 5. Transient results were obtained by scaling steady-state heat transfer coefficients based on transient flow and temperature. Predicted high temperature locations were evaluated for the two temperature spikes shown in figure 2.

The thermal response predicted from the finite-element analysis showed that the leading and trailing edges of the airfoil base are the hottest locations. Temperature distributions showed a cordwise variation at the first ignition spike and a spanwise variation thereafter into the cycle. A uniform temperature distribution was dominant at most of the airfoil surface during cruise except near the base at the platform junction where a mixture of cold and hot gas is present. The coldest spot was always at the blade root because of cooler boundary conditions. Blade temperature is shown in figures 6 through 8.

Elastic-plastic analyses have been conducted for the HPFTB blade with MARC code. Plastic strain calculations were based on incremental plasticity theory using Von Mises Yield criterion, the normality rule and a kinematic hardening model. The material elastic-plastic behavior was specified by the yield strengths and work hardening properties in the longitudinal direction; transverse properties were not available. Creep analyses were not performed at the present time because of inadequate knowledge of the creep characteristics for anisotropic blade material.

Incremental loading included centrifugal and gas pressure loads and metal temperature distributions as calculated from the heat transfer analysis. The same increments were used for the heat transfer and the elastic-plastic structural analysis. Approximately two million words of core storage on the CRAY-XMP computer were needed to run the problem. Analysis required about 4 hours of central processor unit (CPU) time on the CRAY system. The directionality of the elastic material properties causes anisotropic constraints. Lekhnitskii (ref. 6) has derived the generalized elastic strain equations for an anisotropic body with a transverse plane of isotropy. This anisotropic stress-strain law was incorporated in MARC user subroutine HOOKLW.

The colder airfoil base temperatures induce tensile thermal stresses at the critical leading edge location that are additive to the centrifugal stresses. A noticeable discrepancy is seen in the compressive strain region where the reduction in elastic analysis points resulted in failure to capture some of the cycle fluctuation due to transient thermal effects during the rapid engine cooldown. The CPU time for the elastic finite-element analyses amounted to 5 percent of that required for one cycle of the nonlinear finite-element

analysis. The critical location for crack initiation is at the leading edge near the base. Results of both elastic and inelastic structural analyses indicated the region of the finite-element model with the largest total strain range was coincident with the observed crack initiation site.

Radial stress distributions as calculated at the gaussian integration points closest to the suction and pressure surfaces are presented in figures 9 through 11. The stresses primarily reflect the centrifugal and thermal loadings. It is apparent that the analysis would not show a low-cycle fatigue problem if transient thermal effects were not considered.

REFERENCES

1. MARC General Purpose Finite Element Analysis Program. Vol. A: User Information Manual; vol. B: MARC Element Library. MARC Analysis Research Corporation, 1980.

2. Crawford, M.E.; and Kays, W.M.: STAN5 - A Program for Numerical Computation of Two-Dimensional Internal and External Boundary Layer Flows. NASA CR-2742, 1976.

3. Gaugler, R.E.: Some Modification to, and Operational Experiences With, The Two-Dimensional, Finite-Difference, Boundary-Layer Code, STAN5. NASA TM-81631, 1981. (Also, ASME Paper 81-GT-89, Mar. 1981.)

4. Space Shuttle Main Engine, Powerhead Structural Modeling, Stress and Fatigue Life Analysis. (LMSC-HREC-TR-D867333-1, Lockheed Missiles and Space Company; NASA Contract NAS8-34978) NASA CR-170999, 1983.

5. Abdul-Aziz, A.; Tong, M.; and Kaufman, K.: Thermal Finite-Element Analysis of an SSME Turbine Blade. Submitted for Presentation at the 1987 ASME/AIChE National Heat Transfer Conference, on Aug. 9-12, Pittsburgh, PA.

6. Lekhnitskii, S.G.; and Brandstatter, J.J., eds.: Theory of Elasticity of an Anisotropic Elastic Body. Holden-Day, Inc., 1963., pp. 24-25.

TABLE I. - DS MAR-M 246 PHYSICAL PROPERTIES

Temperature, °C	Modulus of elasticity, GPa		Means coefficient of thermal expansion, percent/°C
	Longitudinal	Transverse	
21	131	183	-------
93	120	179	0.00113
204	125	175	.00130
316	124	173	.00133
427	119	166	.00141
538	114	162	.00148
649	109	156	.00149
760	103	149	.00156
671	97	142	.00160

TABLE II. - DS MAR-M 246 STRESS-STRAIN PROPERTIES (LONGITUDINAL)

Plastic strain, percent	Stress, MPa		
	21 °C	649 °C	816 °C
0.1	800	808	875
.2	830	855	930
.4	850	895	965
.6	855	930	970
.8	865	945	975
1.0	870	960	980

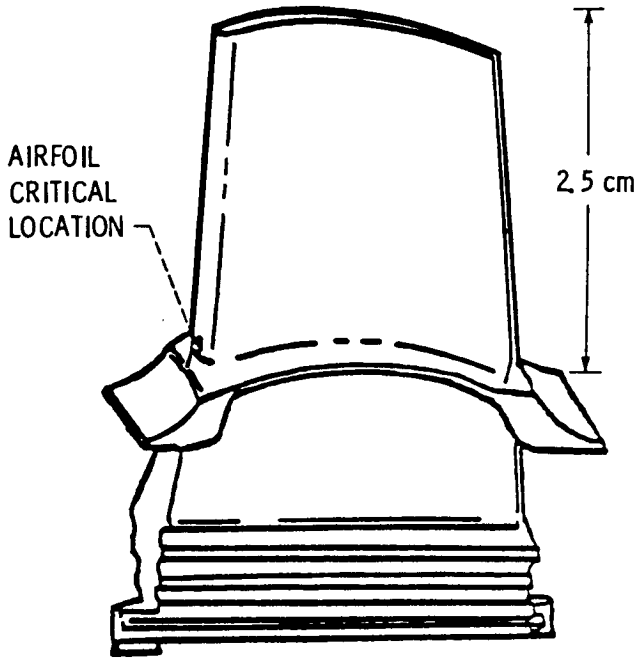

Figure 1. - SSME high-pressure fuel turbopump first stage turbine blade.

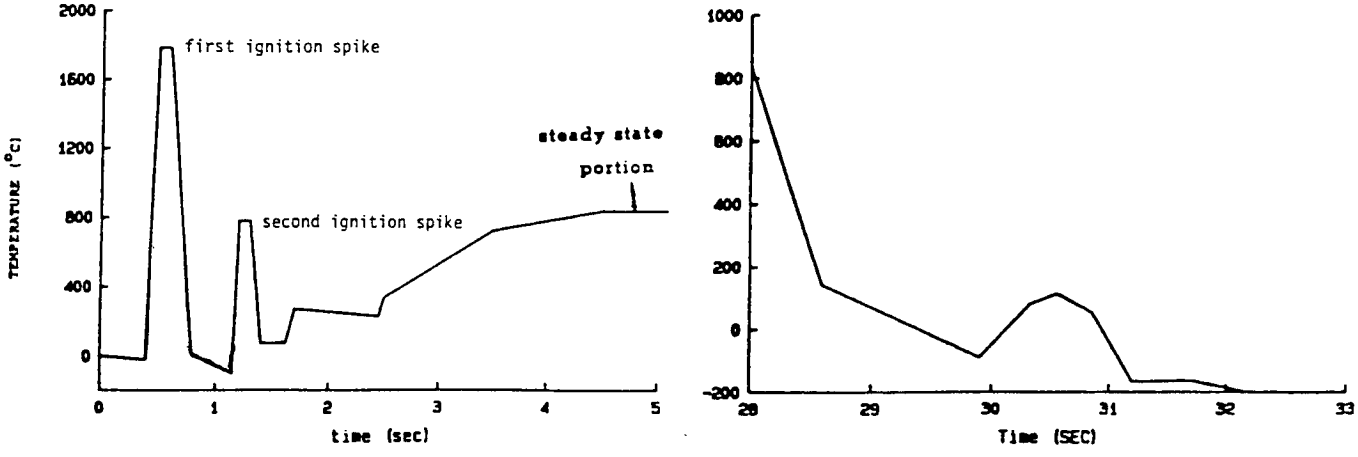

(a) Startup transient.

(b) Cutoff transient.

Figure 2. - Turbine inlet gas temperature for HPFTP.

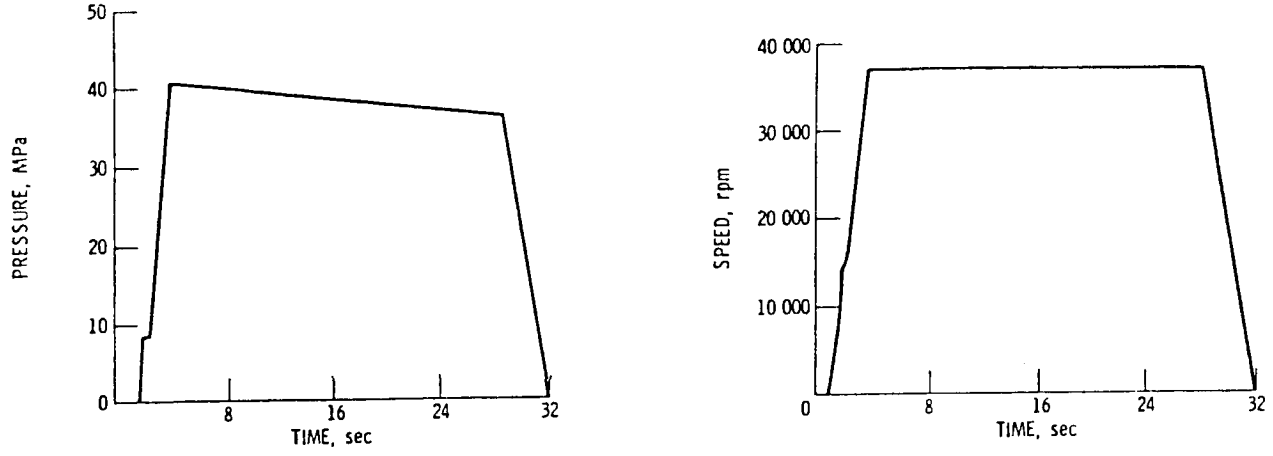

(a) Turbine inlet pressure.

(b) Blade rotational speed.

Figure 3. - Mission cycle used for analysis.

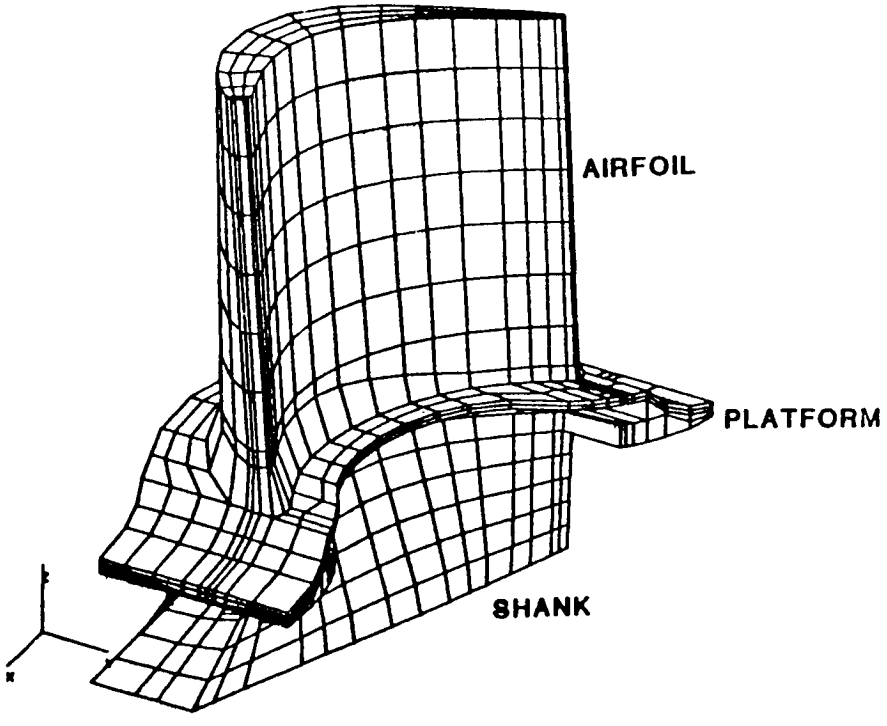

Figure 4. - HPFTP first-stage turbine blade MARC Model. (1575 nodes, 1025 elements)

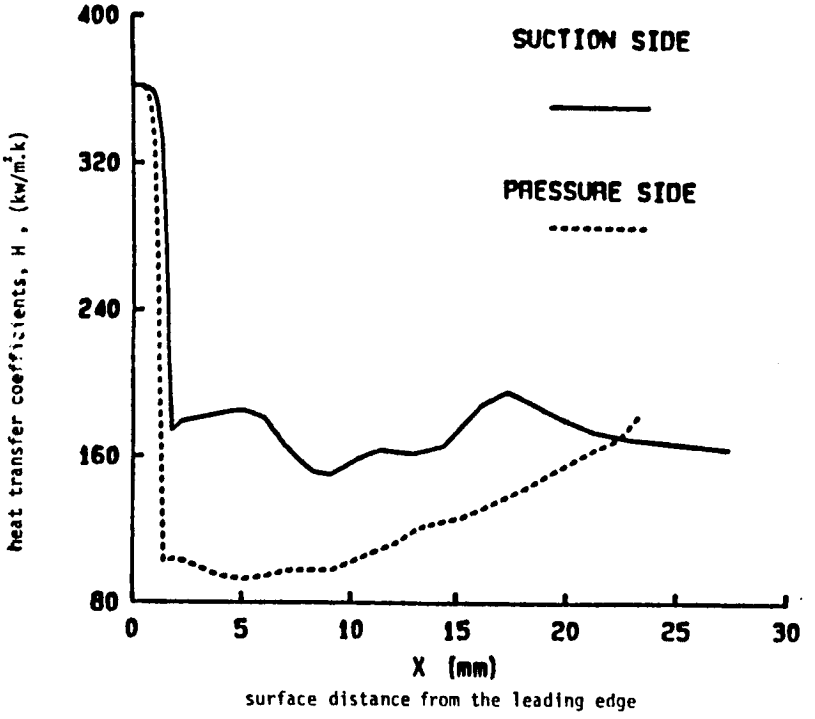

(a) At airfoil root.

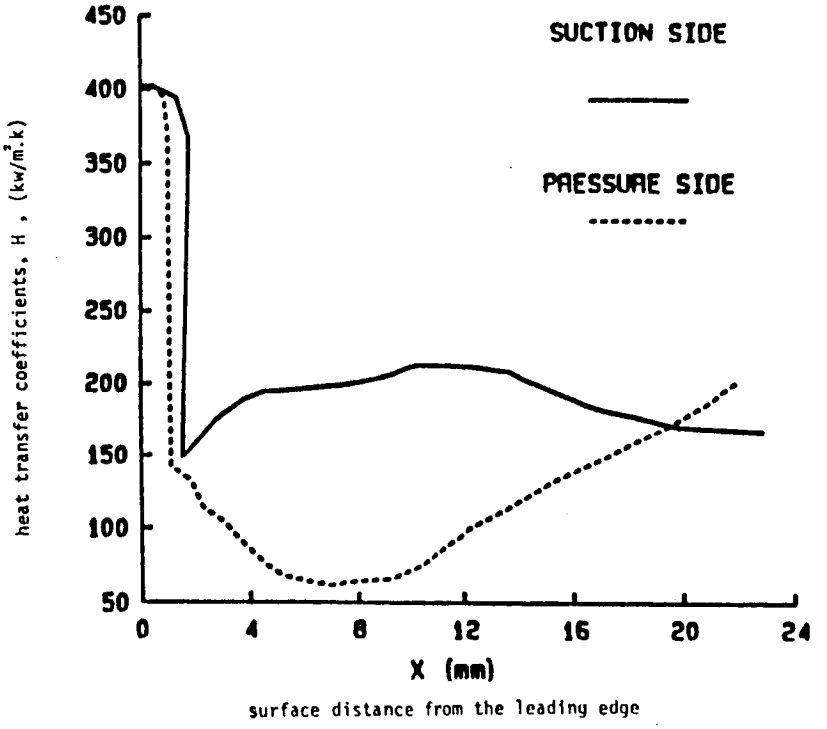

(b) At airfoil tip.

Figure 5. - Distribution of heat transfer coefficients.

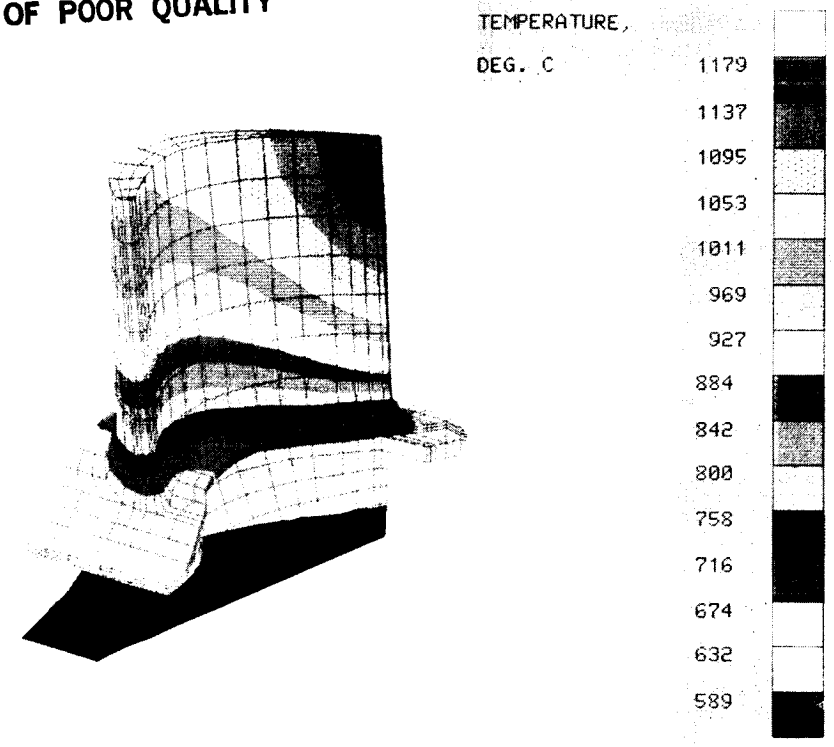

Figure 6. - Temperature contours at first ignition spike.

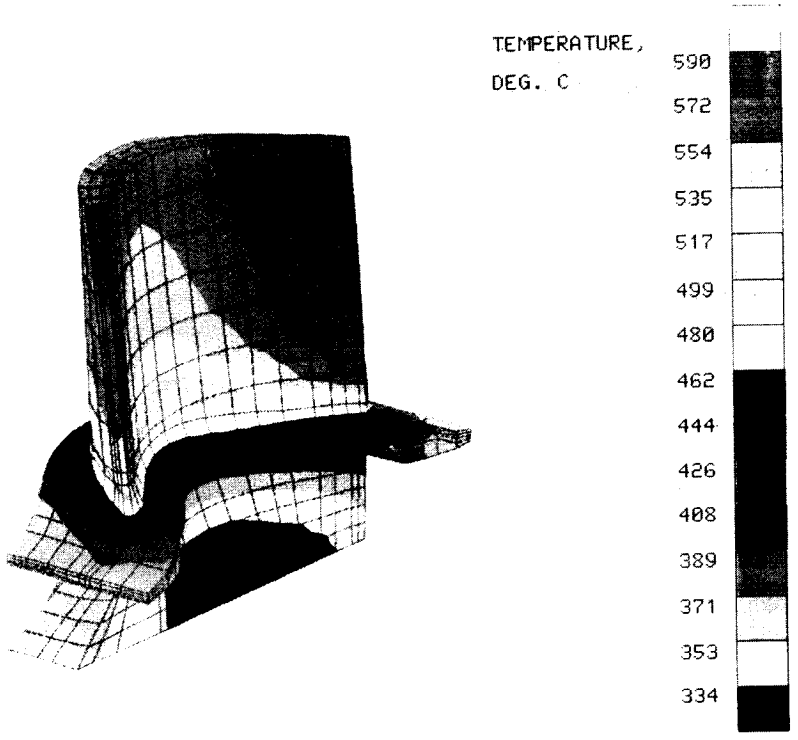

Figure 7. - Temperature at second ignition spike.

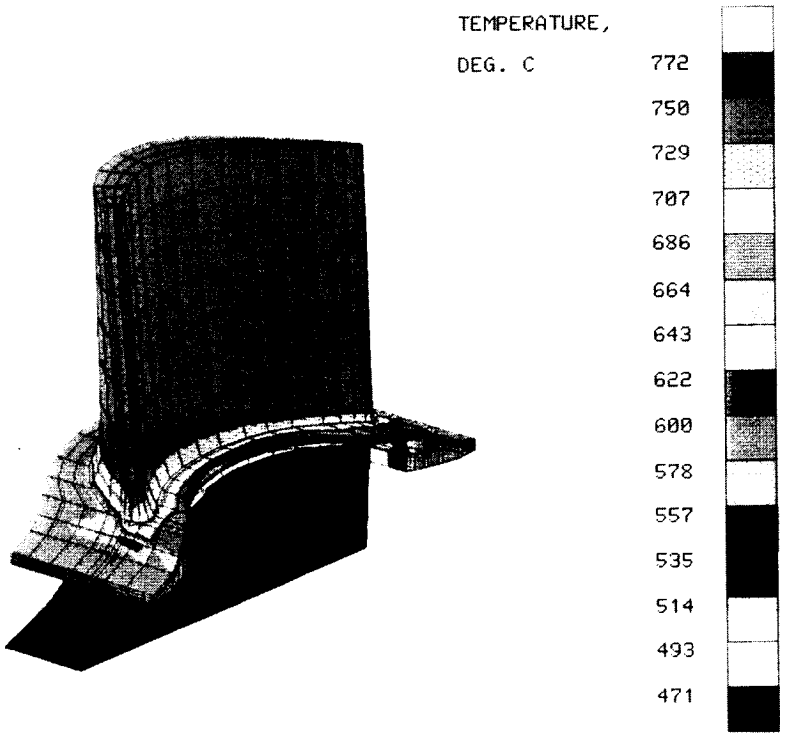

Figure 8. - Temperature contours during cruise.

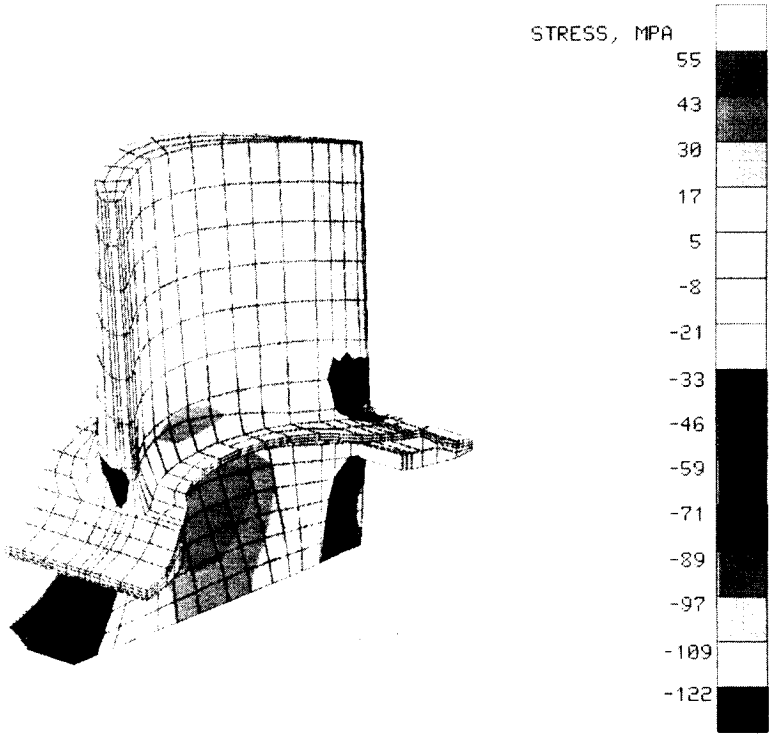

Figure 9. - Radial stresses at first ignition spike.

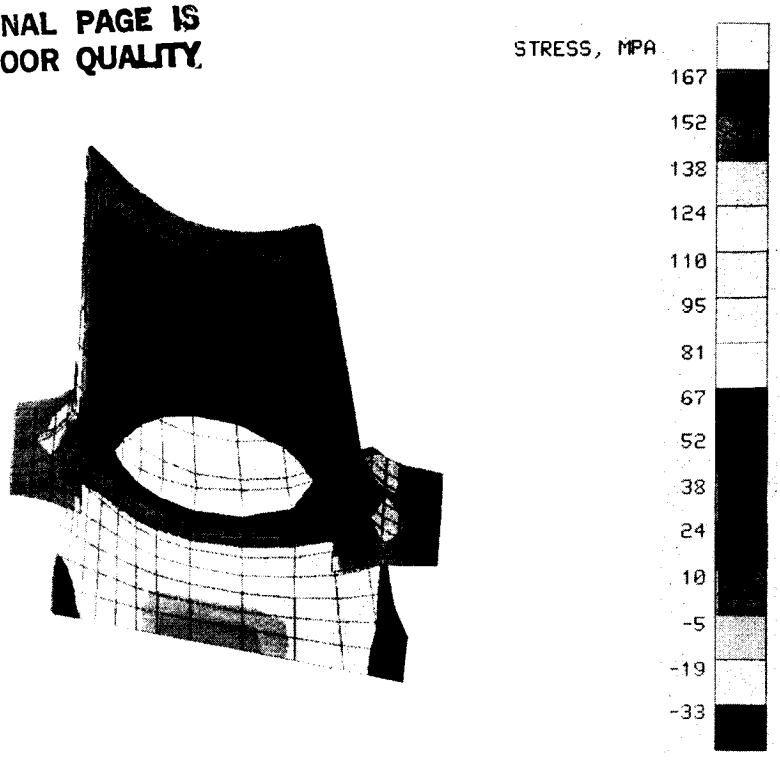

Figure 10. - Radial stresses at second ignition spike.

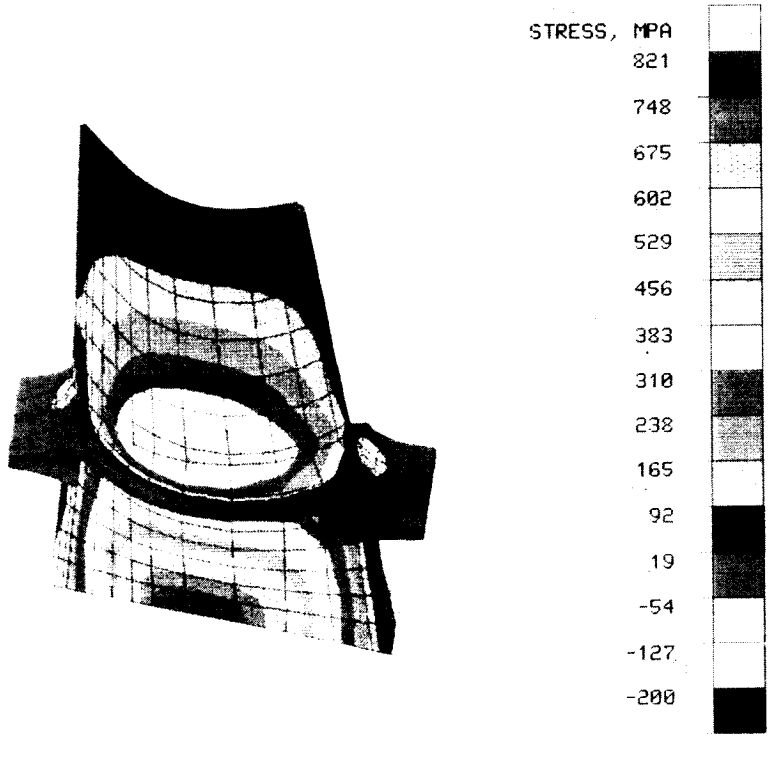

Figure 11. - Radial stresses during cruise.

STRUCTURAL ANALYSIS DEMONSTRATION OF CONSTITUTIVE AND LIFE MODELS

G. Bechtel, T.S. Cook, M.T. Tipton, and R.L. McKnight
General Electric Company
Cincinnati, Ohio

The overall objective of this program is to demonstrate the applicability of NASA-developed advanced constitutive and life damage models for calculating cyclic structural response and crack initiation in selected components of reusable space propulsion systems. The computer model resulting from this program will enable the user to produce an accurate life prediction of hot gas path, life-limiting components of propulsion systems such as the space shuttle main engine (SSME). Program features include:

- Integration of Prior Developed Programs as Basic Approach

  Previously developed computer models addressing constitutive modeling and life damage will be combined in an advanced finite element analysis to generate a sophisticated baseline life prediction program.

- Test Verification of Synthesized Model

  A material data base will be established for the constitutive and life models parametrically involving temperature, strain range, strain rate, mean strain/stress, and dwell time. Structural problems will be run involving cyclic thermomechanical loading and multiaxial stress states. The structural assurance models will be verified for multiaxiality, cumulative damage, and damage mechanism interaction.

- Model Utilization With SSME Components

  The verified computer program will be used to accomplish the life predictions of three SSME critical components as evidence of the model functionality.

Three engine components will be chosen for analysis. Only one of these components has been selected to date - a blade from the high pressure turbopump presently used in the SSME and shown in figure 1. The analysis will be carried out using the properties of PWA 1480, the proposed material for the next generation of blades. Other candidates for the program are a redesigned blade and a nonrotating component. An analysis of these components will be carried out by using properties of appropriate materials that are of a quite different class than the highly anisotropic, single crystal structure of the PWA 1480. This will allow the analysis to test the selected constitutive and life models for quite different microstructures and symmetry classes.

The constitutive model selected for analysis of the anisotropic PWA 1480 is the Stouffer-Dame model. However, the Walker model will be examined to some extent. For the isotropic materials, the model developed by Ramaswamy will be employed, although others may be evaluated depending on data requirements and

what is available. Various damage models will also be investigated, namely continuous damage, hysteresis energy, and strainrange partitioning.

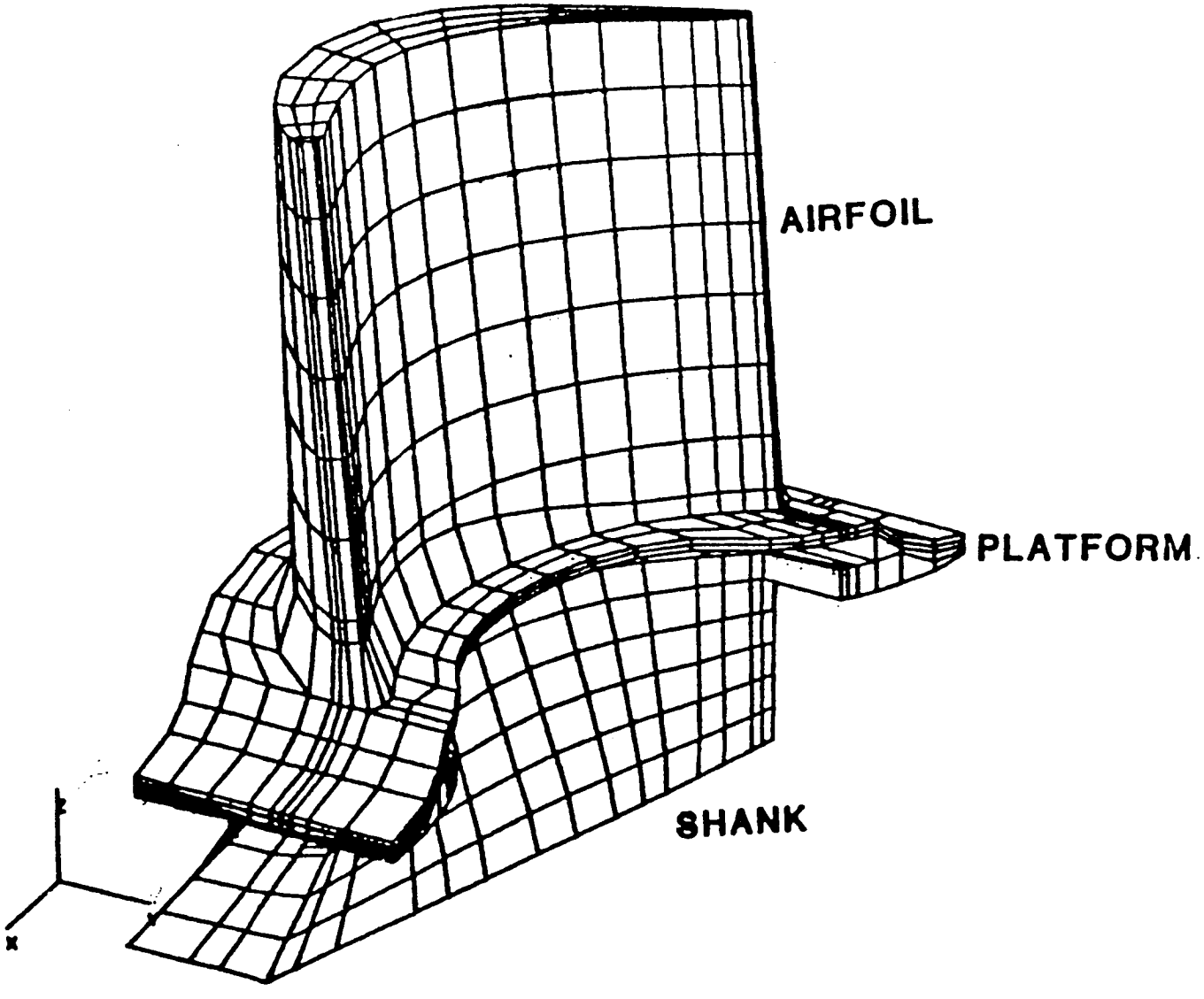

Figure 1.

MECHANICAL PROPERTIES OF HIGH GRADIENT AND HOT ISOSTATICALLY PRESSED PWA 1480

L.G. Fritzemeier and G.D. Schnittgrund
Rockwell International
Canoga Park, California

Single crystal superalloy (specifically, alloy 1480) turbine blades are now in development for application in the high pressure turbopump turbine sections of the SSME. The mechanical and environmental demands placed on these components are quite severe and are significantly different from the requirements of aircraft gas turbine applications for which the alloy was developed. In particular, the extreme thermal transients on start and shutdown and the very high mean stress vibratory loads lead to stronger fatigue excitations than generally encountered in gas turbine engines. In addition, the short design life, about 7.5 hours, of the SSME precludes creep and stress rupture as primary failure mechanisms.

It is recognized that the mechanical properties of single crystal superalloys, especially with respect to life under cyclic loads, are strongly dependent on microstructural defects. Fatigue cracks in single crystal superalloys have been found to initiate at such microstructural anomalies as inclusions, secondary grains and, most frequently, internal porosity. Control or elimination of these defects can be expected to significantly increase the life of single crystal components. The goal of this program is to investigate the potential benefits due to reduction or elimination of casting porosity through high thermal gradient casting and hot isostatic pressing applied to alloy 1480. Additionally, improvement in fatigue life due to alternate heat treatment is being evaluated.

Internal porosity is an inherent feature of single crystal superalloy castings. The bulk of this porosity is formed during solidification and is caused by shrinkage and restricted fluid flow into the interstices of the dendrite arms. Increased casting thermal gradient can refine the microstructure through reduced dendrite arm spacing (DAS) and an attendant decrease in the size and density of the casting porosity. Internal casting porosity can be virtually eliminated by the proper application of hot isostatic pressing (HIP) to the casting. The successful application of HIP to single crystal parts involves overcoming a unique set of obstacles. Temperature control in production HIP vessels is generally not tight enough to control within the as-cast solution heat treatment range of alloy 1480. Cooling rates from temperature are also not rapid enough to provide optimum properties. Post-HIP solution heat treatment cause pore resurgence through Kirkendall diffusion. Improper temperature and pressure application in the HIP cycle can also cause recrystallization around the closing pores. Very small amounts of free carbon in the HIP vessel cause surface carburization. With the successful removal of casting porosity, improvements in fatigue life and increased resistance to hydrogen environment embrittlement (HEE) may be obtainable through tailored heat treatments. Increased slip dispersal through optimum gamma prime distribution will provide improvements in both fatigue and HEE behavior.

This program has been designed to evaluate the potential benefits to alloy 1480 material properties due to high thermal gradient casting, hot isostatic pressing, and alternative heat treatment. Alloy 1480 castings have been obtained from vendors representing the extremes of commercial casting thermal gradients. Quantitative characterization of the DAS and pore distributions has been conducted. A HIP schedule, which avoids the many pitfalls of single crystal HIP has been devised for alloy 1480. In addition, an alternate heat treatment for alloy 1480 has been devised which provides benefits in mechanical properties. The standard gradient cast test material is being evaluated in the standard heat treated condition as a baseline and in the HIP plus alternate heat treated condition. The high gradient cast material is being evaluated in alternate heat treat and HIP plus alternate heat treated conditions. Evaluations focus on demonstration of the benefits due to the applied processes, especially in the area of cyclic life. This interim period report will present current results and procedures derived from the program.

EFFECT OF HYDROGEN ON DEFORMATION STRUCTURE AND PROPERTIES OF CMSX-2 NICKEL-BASE SINGLE-CRYSTAL SUPERALLOY

M. Dollar, I.M. Bernstein, S. Walston,
F. Prinz, and A. Domnanovich
Carnegie Mellon University
Pittsburgh, Pennsylvania

Material used in this study was a heat of the alloy CMSX-2 whose chemical composition is given in Table I. This nickel-based superalloy was provided in the form of [001] oriented single crystals, solutionized for 3 hrs at *1315*°C. It was then usually heat treated as follows: *1050*°C/16h/air cool + *850*°C/48h/air cool. The resulting microstructure is dominated by cuboidal, ordered γ' precipitates with a volume fraction of about 75% and an average size of 0.5 μm (Figure 1).

In previous studies (1,2) of hydrogen effects in the alloy we have shown that a high hydrogen fugacity environment can degrade room temperature mechanical properties. Hydrogen was introduced by cathodic potentiostatic charging in a mixture of two molten salts, 57% sodium bisulfate and 43% potassium bisulfate at *150*°C for 5 hrs. The most significant effects of such charging were on tensile behavior, where a 34% loss of homogeneous elongation was found and on push-pull fatigue behavior where a several-fold decrease of the accumulated plastic strain to fracture resulted, over a wide plastic strain range down to 0.02%. A detailed microscopic interpretation of these hydrogen-induced effects was limited by the fact that the hydrogen introduced by the molten salt charging resided primarily in a surface layer about 50 μm in depth.

To better understand and control the role of hydrogen, high pressure, high temperature hydrogen charging was carried out at Sandia National Laboratory-Livermore, CA. This entailed gas phase charging for 15 days at *300*°C under a pressure of 138MPa, and furnace cooling to room temperature in 16 hrs. under pressure. A resultant, uniform hydrogen concentration of the order of 5000 appm across the entire cross-section of 3 mm thick samples was obtained by such a procedure.

As shown in Tables II and III, and in Figure 2, this charging mode more dramatically changes tensile and fatigue behavior than molten salt charging. The presence of this significant amount of dissolved hydrogen, while not significantly changing the relatively high yield strength, does promote significant work hardening, in contrast to hydrogen-free material where softening is found, and also dramatically reduces the true uniform elongation to almost zero. In fatigue, the number of cycles to failure now drops two order of magnitude and the occurrence of strain localization is more pronounced then in either the hydrogen-free case, or when the hydrogen was localized at the surface.

TEM and SEM evidence provides a picture of how hydrogen can affect the deformation structure and the fracture of CMSX-2 and can be used to correlate changes in mechanical properties with the presence of hydrogen in both the γ and γ' phases. In brief, the most compelling hydrogen induced-changes in deformation structure are : i) enhanced dislocation accumulation in the γ matrix; and ii) more extensive cross-slip of superdislocations in the γ' precipitates. These are shown in Figures 3 and 4, respectively (for comparison see also Figures 5 and 6 which illustrate the deformation structure of H-free material). The enhanced dislocation density in γ acts to decrease the mean free path of a superdislocation, while easier cross slip hinders superdislocation movement by providing pinning points in the form of sessile jobs. Both processes contribute to the increase of flow stress and the notable work hardening that occurs prior to fracture.

Previously (1,2), examination of fractured tensile samples revealed that uncharged samples fractured predominantly along planes parallel to multiple, crystallographic {111} slip systems. The fractured surface was jagged and significant localized and general ductility was observed. In the present study, the hydrogen-charged samples were found to be much more brittle in appearance with a fracture surface that was quite planar and oriented normal to the tensile axis. A most striking SEM observation was that microcracks appear to follow <001> oriented γ/γ' interfaces (Figure 7) suggesting that preferrential cracking parallel to {001} planes occurs. However, TEM observations strongly suggests that a difference exists in the macroscopic and microscopic nature of hydrogen-induced crack initiation and propagation. In particular, Figure 8 clearly shows that cracking is associated with processes in the γ, manifested as localized tearing in thin foils. While at first sight these appear to follow {001} planes, in reality they are comprised of short segments on multiple {111} planes. While tearing in thin foils is clearly not identical with microcracking in bulk material, it is suggestive and we believe accurately so, that embrittlement results from hydrogen-enhanced strain localization, resulting in dislocation intensification in the narrow ribbons of γ and premature plastic failure due to strain exhaustion and the apparent mode I fracture.

This work is being supported by NASA-Lewis under the technical direction of Dr. Robert Dreshfield.

References

1. Bernstein, I.M., et al.: Proceedings of the 1986 NASA Conference on Advanced Earth-to-Orbit Propulsion Technology, May 1986.

2. Baker, C.L., et al.: to be published in Metall. Trans., 1987

TABLE I

CMSX-2 Composition (wt. %)

Cr	8.0
W	8.0
Ta	6.0
Al	5.6
Co	4.6
Ti	1.07
Mo	0.6
Fe	0.08
Si	0.015
Ni	balance
C	15 ppm
S	10 ppm
N	4 ppm
O	2 ppm

TABLE II

Tensile Behavior as a Function of Charging Condition

Charging Conditions	YS (MPa) (0.2% offset)	UTS (MPa)	Homogeneous Elongation (%)	Elongation Loss (%)
uncharged	917	987	21.7	---
molten salt 5h at 150°C	856	976	14.4	33.6
gas phase 5 days at 138MPa & 300°C	935	1123	1.2	94.5

TABLE III

Fatigue Behavior as a Function of Plastic Strain Range and Charging Conditions

$\Delta\epsilon_p$(%)	Charging Conditions	Cycles to Failure uncharged	charged	n_u/n_c	Accum. Plastic Strain ($n \times \Delta\epsilon_p$) (%) uncharged	charged
0.4	molten salt 5h at 150°C	57	16	3.6	46	13
0.2		131	57	2.3	52	23
0.1		214	80	2.7	43	16
0.02		3348	1260	2.7	137	53
0.02	gas phase 15 days at 138MPa & 300°C	6664	21	317	267	.84
0.02		3085	16	193	123	.56
0.02		2483	29	86	99	1.16

R = −1, Room Temperature Testing

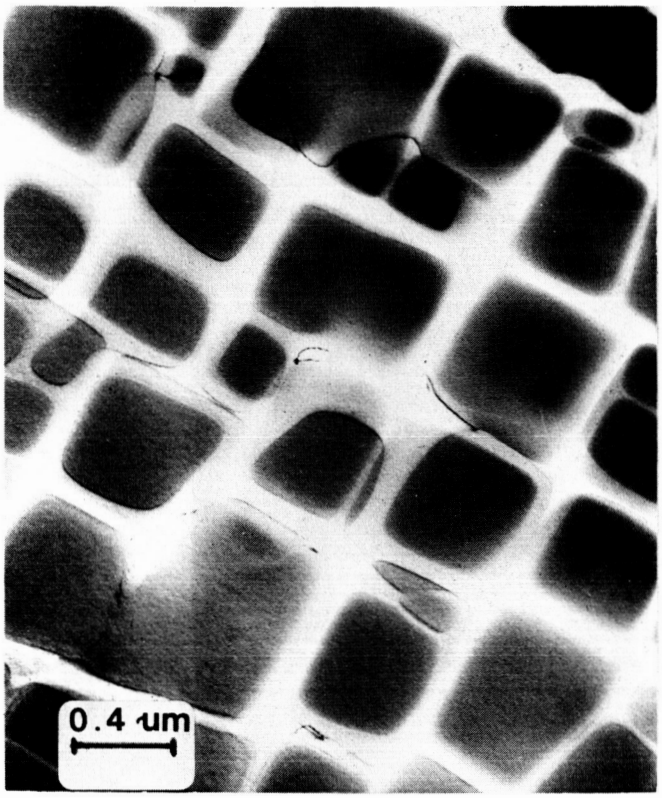

ORIGINAL PAGE IS
OF POOR QUALITY

Figure 1. - TEM micrograph, initial microstructure of CMSX-2.

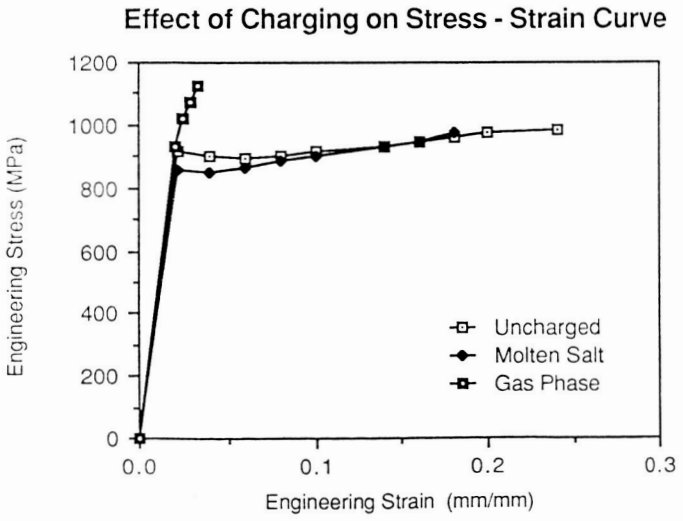

Figure 2. - Influence of hydrogen charging on tensile behavior of CMSX-2.

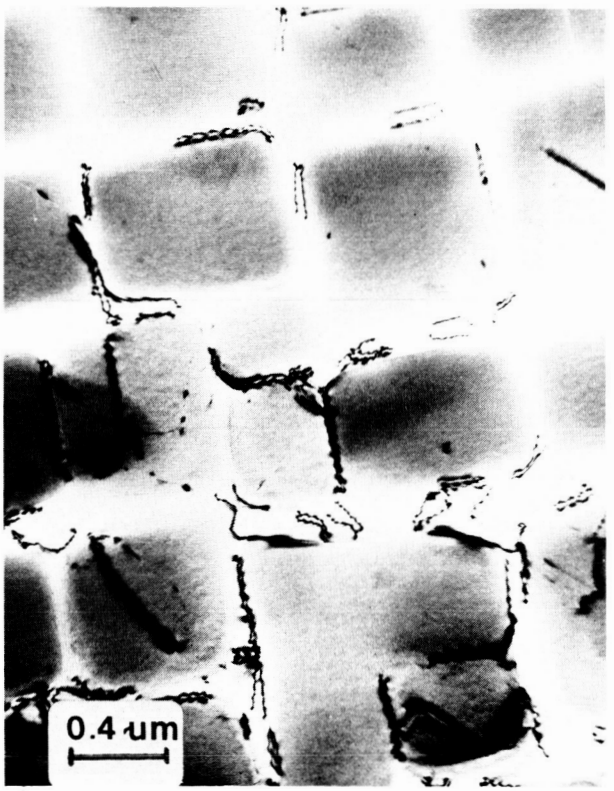

Figure 3. - Typical deformation structure of hydrogen-charged CMSX-2; ε = 0.8 percent.

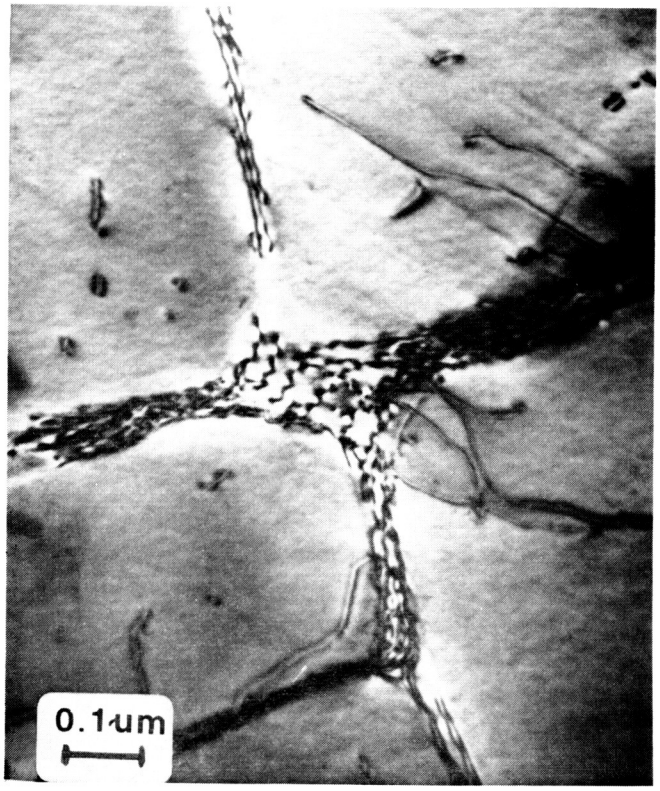

Figure 4. - Typical deformation structure of hydrogen-charged CMSX-2; ε = 1.2 percent.

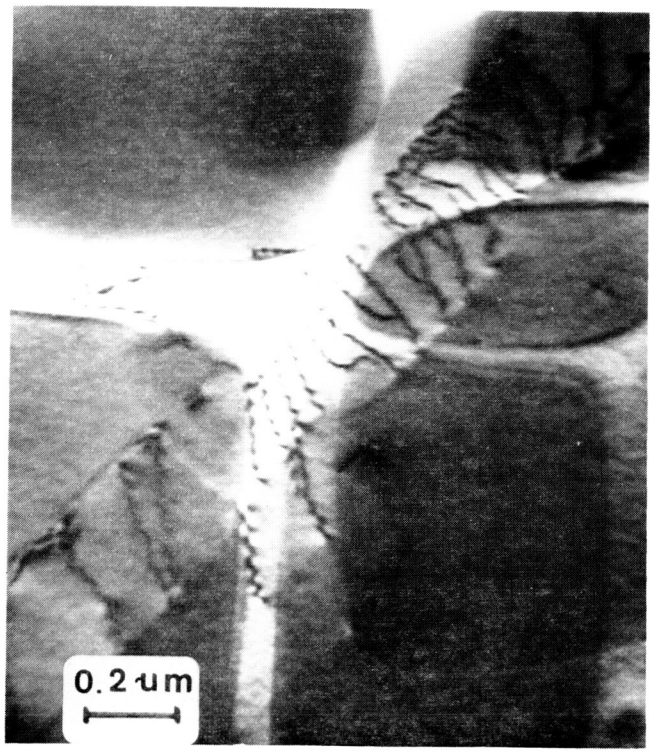

Figure 5. - Typical deformation structure of hydrogen-free CMSX-2; ε = 4 percent.

Figure 6. - Typical deformation structure of hydrogen-free CMSX-2; ε = 5 percent; (foil cut parallel to (111) slip plane).

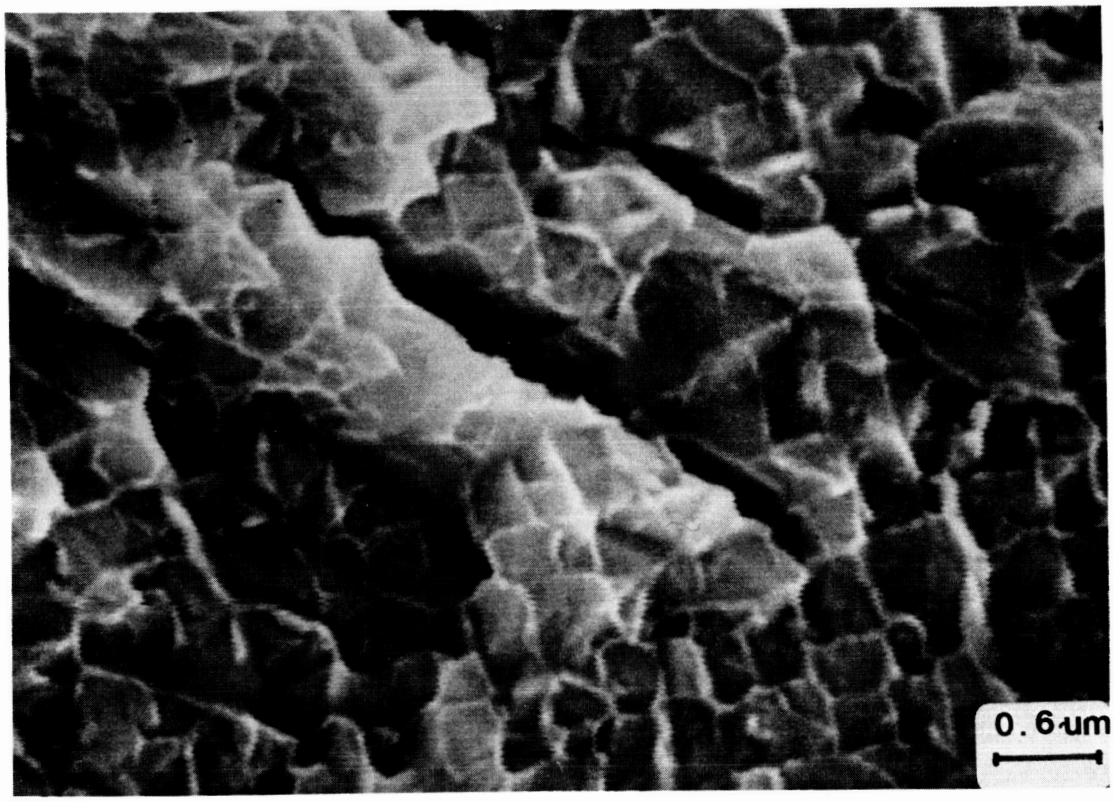

Figure 7. - Fracture surface of hydrogen-charged CMSX-2.

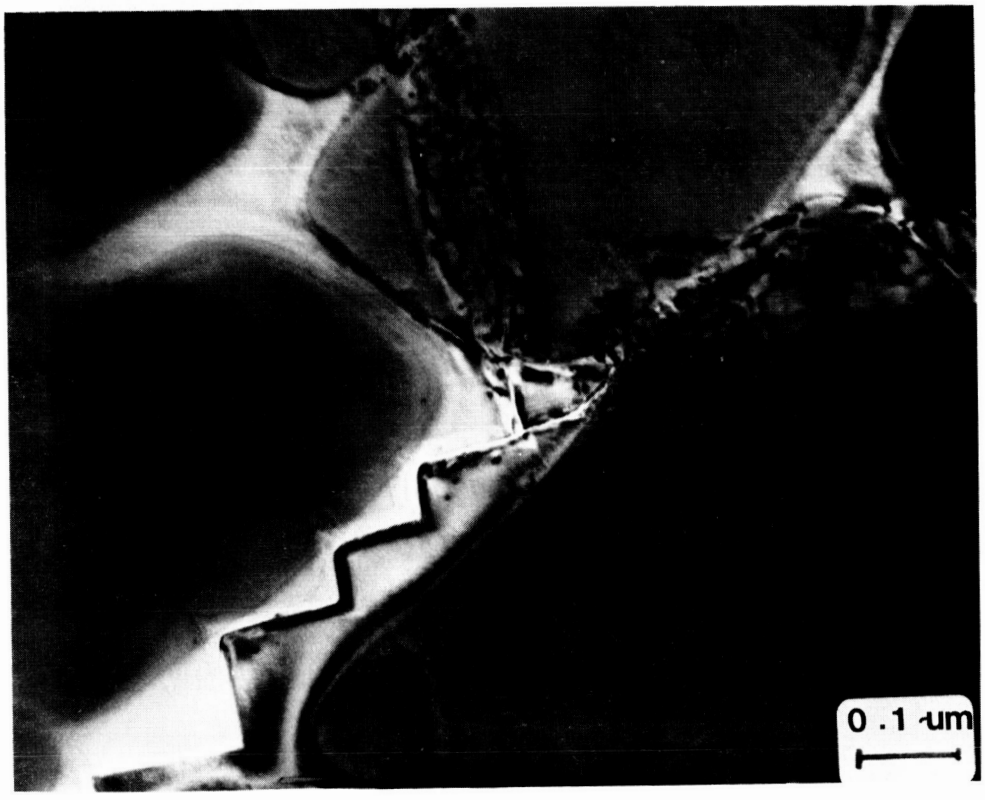

Figure 8. - Tearing in a thin foil cut close to fracture surface. (Material was hydrogen-charged.)

PROBABILISTIC STRUCTURAL ANALYSIS TO EVALUATE THE STRUCTURAL DURABILITY OF SSME CRITICAL COMPONENTS

Christos C. Chamis
NASA Lewis Research Center
Cleveland, Ohio

It is becoming increasingly evident that deterministic structural analysis methods will not be sufficient to design critical structural components for upgraded space shuttle main engines (SSME). Structural components in the SSME are subjected to a variety of complex (cyclic and transient) loading conditions including high temperatures and severe thermal gradients. Most of these are quantifiable only as best engineering estimates. These complex loading conditions subject the component material to coupled nonlinear behavior which depends on stress, temperature, and time. The nonuniform nature of this coupled nonlinear material behavior makes it very difficult to characterize experimentally and perhaps impossible to describe deterministically.

In addition, critical SSME structural components are relatively small. Fabrication tolerances on these components, which in essence are small thickness variations, can have significant effects on the component structural response. Fabrication tolerances by their very nature are statistical. Furthermore, the attachment of the components to the structural system generally differs by some indeterminant degree from what is assumed for design purposes. In summary, all four fundamental aspects - (1) loading conditions, (2) material behavior, (3) geometric configuration, and (4) attachment - on which structural analyses are based, are of statistical nature. One direct way to formally account for all these statistical aspects is to develop probabilistic structural analysis methods where all participating variables are described by appropriate probabilistic functions.

NASA Lewis Research Center is currently developing probabilistic structural analysis methods for select SSME structural components. Briefly, the deterministic, three-dimensional, inelastic analysis methodology developed under the Hot Section Technology ((HOST) and R&T Base Programs) is being augmented to accommodate the complex probabilistic loading spectra, the thermoviscoplastic material behavior, and the material degradation associated with the environment of space propulsion system structural components representative of the SSME such as turbine blades, transfer ducts, and liquid-oxygen posts (fig. 1).

The development of probabilistic structural analysis methodology consists of the following program elements: (1) composite load spectra, (2) probabilistic structural analysis methods, (3) probabilistic finite element theory - new variational principles, and (4) probabilistic structural analysis application. In addition, the program includes deterministic analysis elements: (1) development of structural tailoring computer codes (SSME/STAEBL), (2) development of dynamic creep buckling/ratcheting theory, (3) evaluation of the dynamic characteristics of single-crystal SSME blades, (4) development of SSME blade

damper technology, and (5) development of integrated boundary elements for hot-fluid structure interaction.

The SSME Structural Durability Program is multidisciplinary integrated and is a joint effort of NASA Lewis in-house research, contracts, grants, and support service personnel (table I). The research activities in the various program elements have collectively led to significant technical progress. The objective of the presentations included in this session is to summarize the highlights of this technical progress.

TABLE I. - COMPUTER CODES DEVELOPMENT SUMMARY

Code	Description	Status
NESSUS	Nonlinear evaluations of stochastic structures under stress	Initial version operational
CLS	Composite load spectra probabilistic load simulation	Initial version operational
SSME/STAEBL	Structural tailoring of SSME turbopump blade	Code available for release
VATFEL	Variational theory for probabilistic finite elements	Near completion
DYCREBURT	Dynamic creep buckling/ratcheting theory	Near completion
BEFSIN	Boundary elements for fluid structure interaction	Planning phase
NL-COBSTRAN	Nonlinear structural analysis for high-temperature metal matrix composite turbine blades	Operational

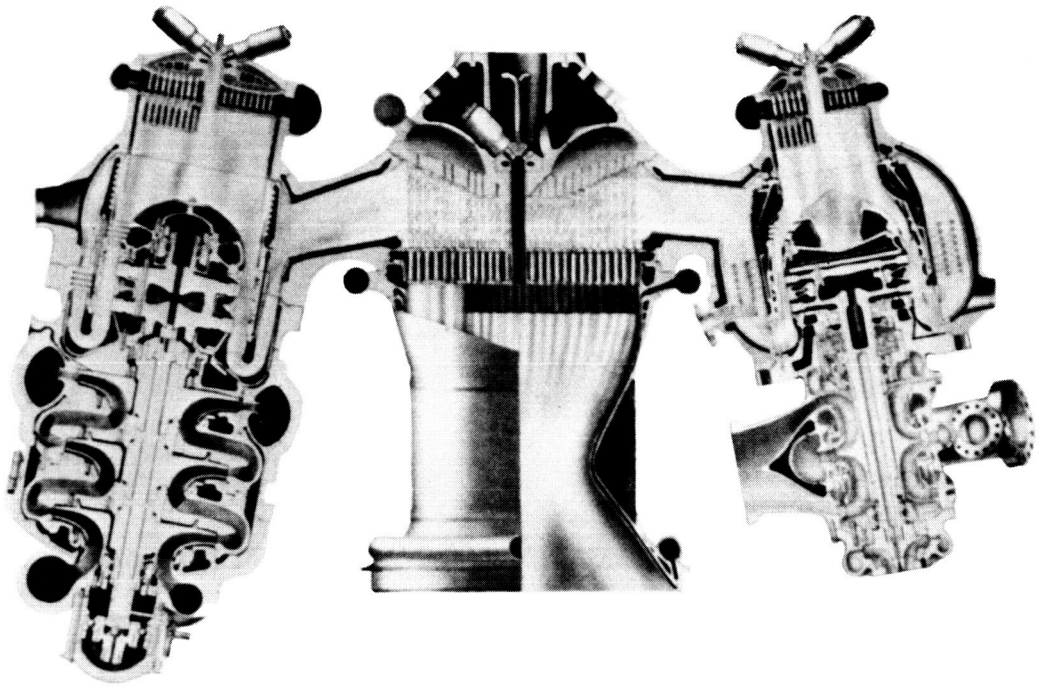

SSME POWERHEAD COMPONENT ARRANGEMENT

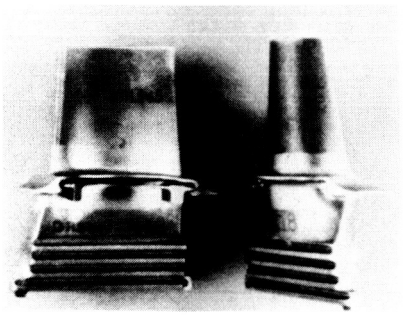

HIGH PRESSURE TURBOPUMP
BLADE

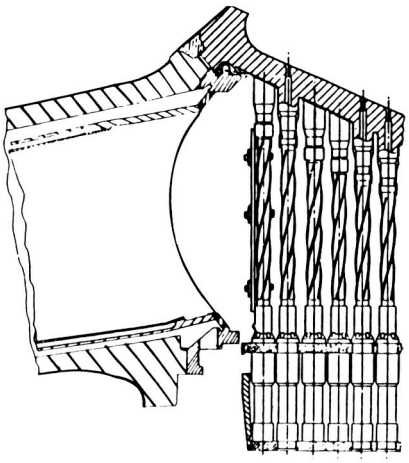

LOX POSTS

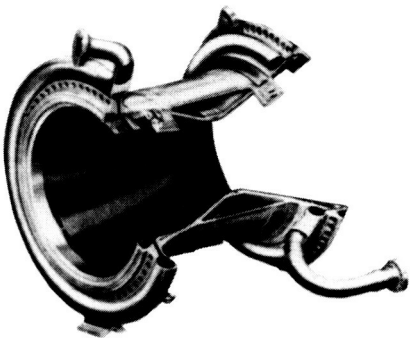

MAIN COMBUSTION CHAMBER

FIGURE 1. - PSAM WILL BE INITIALLY DEVELOPED FOR SELECT SSME STRUCTURAL COMPONENTS.

PROBABILISTIC STRUCTURAL ANALYSIS METHODS FOR SELECT SPACE PROPULSION SYSTEM STRUCTURAL COMPONENTS (PSAM)

T.A. Cruse
Southwest Research Institute
San Antonio, Texas

The objective of this 5-year contract effort[1] is the development of several modular structural analysis packages capable of predicting the probabilistic response distribution for key structural variables such as maximum stress, natural frequencies, transient response, etc. The structural analysis packages are to include stochastic modeling of loads, material properties, geometry (tolerances), and boundary conditions. As shown in figure 1, the solution is to be in terms of the cumulative probability of exceedance distribution (CDF) and confidence bounds. Two methods of probability modeling are to be included as well as three types of structural models - probabilistic finite-element method (PFEM); probabilistic approximate analysis methods (PAAM); and probabilistic boundary element methods (PBEM).

The purpose in doing probabilistic structural analysis is to provide the designer with a more realistic ability to assess the importance of uncertainty in the response of a high performance structure. PSAM tools will estimate structural safety and reliability, while providing the engineer with information on the confidence that should be given to the predicted behavior. Perhaps most critically, the PSAM results will directly provide information on the sensitivity of the design response to those variables which are seen to be uncertain. Design situations where the performance of the structure strongly depends on variables whose values are uncertain can be identified and corrective steps taken.

The PSAM tools will reflect three levels of user-defined uncertainties, as shown in figure 2. The first level is one in which the uncertainty is from part to part or application to application. Thus, for example, one turbine blade has a different fundamental frequency from a second, randomly selected, blade. The second level of uncertainty reflects the fact that the statistics on loading or material behavior or tolerances may vary from one region of the structure to another. The third, and most detailed, level of uncertainty is within the local behavior of a continuum. In this level, for example, the strains within a structure are to be randomly correlated to the displacement derivatives; the stresses are to be randomly correlated with the strains; and so on.

Three major analysis codes are to be developed following the schedule shown in figure 3. The first of these, the PFEM code, has been under development for just over 2 years. A linear version of that code has been developed (fig. 4). Validation studies have been initiated and the code will be applied this year to an SSME turbine blade analysis. The PAAM modeling effort will not

---

[1]Work done under NASA Contract NAS3-24389.

be initiated until FY 88. Following a 1-year study of advanced analysis methods, the development of a probabilistic boundary element code has been initiated. The PBEM code structure will follow that being established for the PFEM code NESSUS.

The current NESSUS (Numerical Evaluation of Stochastic Structures Under Stress) code structure is shown in figure 4. The code currently consists of four major modules: NESSUS/EXPERT, NESSUS/FPI, NESSUS/PRE, and NESSUS/FEM. The EXPERT module provides a user interface to NESSUS to facilitate the development and interpretation of probabilistic data. Fast Probability Integration (FPI) is the currently used reliability estimation algorithm for assessing response distributions and confidence levels. The PRE module reduces random fields with partial correlations to a set of independent random field variables using modal analysis methods. The finite-element method (FEM) module provides a rapid solution method especially developed to perform sensitivity analysis of a structural model. Two subsequent presentations in this same volume will discuss the FPI and EXPERT modules, and then the PRE and FEM modules.

Figure 5 illustrates the team approach being used in the PSAM contract effort. SwRI is responsible for the system integration and code validation efforts, as well as the development of the FPI and EXPERT modules. MARC Analysis Research Corporation is responsible for the FEM and PRE modules. Rocketdyne Division has defined four verification problems and will apply the NESSUS codes to the probabilistic modeling of these applications. Their presentation follows those of SwRI and MARC. Professors Wirsching (University of Arizona) and Atluri (Georgia Institute of Technology) and their graduate students are providing support on the development of advanced reliability and finite-element methods, respectively. Their presentations conclude the set of PSAM presentations.

The goal of the PSAM contract is being attained. A clear methodology for the probabilistic simulation of structural response is established. A linear modeling capability for static and vibrating systems exists and has been forwarded to NASA. The current effort is focusing on a fuller integration of NESSUS/FEM and NESSUS/FPI algorithms in order to more accurately and efficiently define the tails of the distributions. MARC is developing nonlinear solution procedures for probabilistic structures, as well as improving the FEM technology being used. The resulting structural analysis methods are seen to be capable of providing new and very significant insight into the reliable performance of complex structural systems.

PROBABILISTIC DESIGN METHODS WILL SIMULATE "REAL WORLD" STRUCTURAL RESPONSES

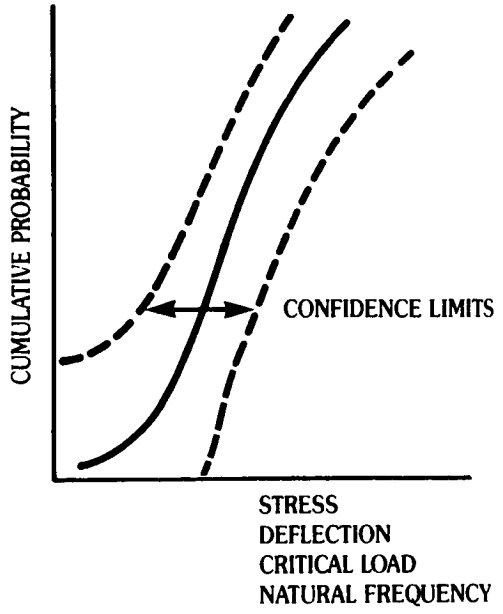

DUE TO DESIGN UNCERTAINTIES:

- LOADING
- MATERIAL BEHAVIOR
- GEOMETRY, TOLERANCES
- BOUNDARY CONDITIONS

FIGURE 1.

NESSUS TO HAVE THREE LEVELS OF MODELING SOPHISTICATION

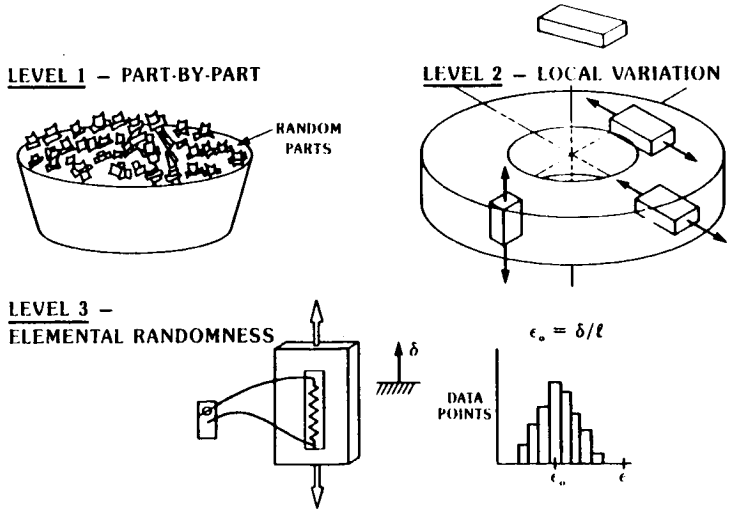

FIGURE 2.

PSAM EFFORT INVOLVES THREE MAJOR ANALYSIS CODES (NESSUS)

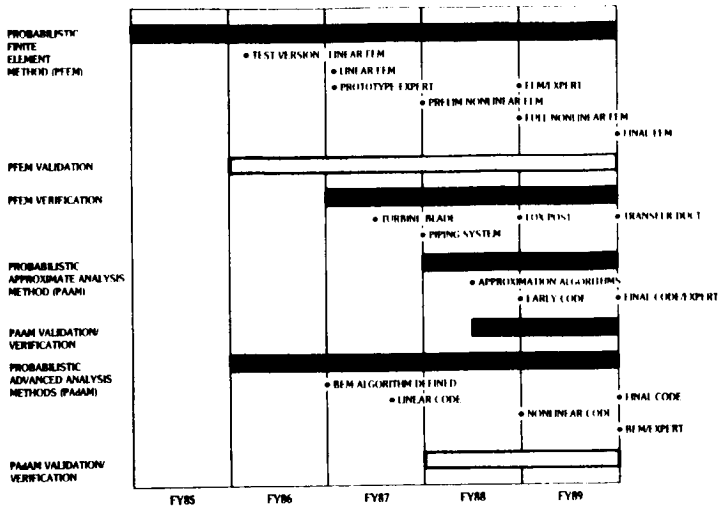

FIGURE 3.

PSAM INTEGRATES FEM TECHNOLOGY WITH PROBABILISTIC METHODS

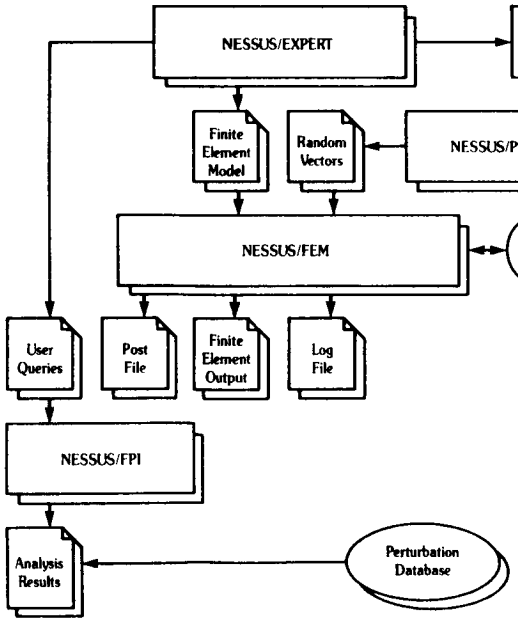

- NESSUS/FEM COMPUTES SENSITIVITY DATA
- NESSUS/PRE ANALYZES CORRELATION MODELS
- NESSUS/EXPERT PROVIDES USER INTERFACE
- NESSUS/FPI COMPUTES PROBABILISTIC RESULTS

FIGURE 4.

PSAM IS A TEAM EFFORT

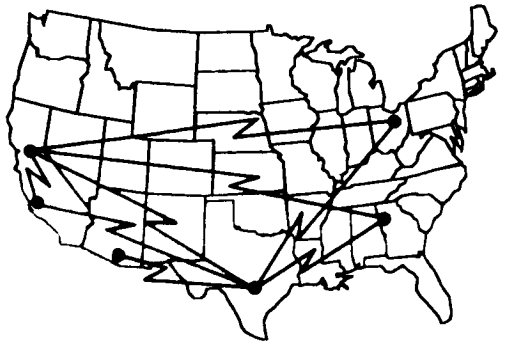

SOUTHWEST RESEARCH INSTITUTE
- PROGRAM MANAGEMENT
- SOFTWARE INTEGRATION
- PROBABILISTIC METHODS
- ADVANCED METHODS

MARC ANALYSIS RESEARCH CORP.
- NESSUS DEVELOPMENT
- ADVANCED FEM DEVELOPMENT
- NESSUS VALIDATION

ROCKETDYNE DIVISION
- VERIFICATION STUDIES
- VERIFICATION APPLICATIONS

PROF. PAUL WIRSCHING (UNIV. OF ARIZONA)
- ADVANCED RELIABILITY METHODS
- STATISTICAL MODELING

PROF. SATYA ATLURI (GEORGIA TECH)
- HYBRID FEM DEVELOPMENT
- STOCHASTIC MECHANICS MODELING

FIGURE 5.

THE NESSUS FINITE-ELEMENT CODE*

J.B. Dias, J.C. Nagtegaal, and S. Nakazawa
MARC Analysis Research Corporation
Palo Alto, California

The NESSUS finite element code is being developed by MARC Analysis Research Corporation as part of the probabilistic structural analysis (PSAM) effort, coordinated by Southwest Research Institute for the NASA Lewis Research Center. The objective of this development is to provide a new analysis tool which integrates the structural modeling versatility of a modern finite element code with the latest advances in the area of probabilistic modeling and structural reliability. Version 2.0 of the NESSUS finite element code was released to the members of the PSAM team last February, and is currently being exercised on a set of problems which are representative of typical SSME applications. NESSUS 2.0 allows linear elastostatic and eigenvalue analysis of structures with uncertain geometry, material properties and boundary conditions, which are subjected to a random mechanical and thermal loading environment.

The NESSUS finite element code is a key component in a broader software system consisting of five major modules. NESSUS/EXPERT is an expert system under development at Southwest Research Institute, with the objective of centralizing all component-specific knowledge useful for conducting probabilistic analysis of typical SSME components. NESSUS/FEM contains the finite element code used for the structural analysis and parameter sensitivity evaluation of these components. The task of parametrizing a finite element mesh in terms of the random variables present is facilitated with the use of the probabilistic data preprocessor in NESSUS/PRE. An external database file is used for managing the bulk of the data generated by NESSUS/FEM. To complete the analysis, Southwest Research Institute has developed the probabilistic analysis module NESSUS/FPI, which extracts from the database the information needed for generating probability distributions for the desired response variables.

Probabilistic finite element analysis involves the computation of the effects of small variations of the random variables on the overall response of the structure. Since probabilistic models of realistic structures often require large finite element models parameterized by many random variables, this step is very computation-intensive and will tend to govern the solution cost. The strategy adopted in the NESSUS finite element code is based on an iterative algorithm akin to the modified Newton method. With this approach, all computations on the perturbed system can be performed at the element level, resulting in substantial savings on memory requirements. This approach also eliminates the need to compute and store explicit partial derivatives of the element matrices and vectors, or to assemble these into additional global arrays. As a result, the perturbation of the element parameters can be made independent of element formulation, allowing the introduction of the newest element technology into the existing algorithm with a minimal amount of new software development. Significant improvements in convergence speed have been

*Work performed under NASA contract NAS3-24389.

demonstrated with the use of modern algorithms for nonlinear programming, which have been implemented in NESSUS within the past year.

The iterative algorithms implemented in the NESSUS finite element code can be shown to be inherently consistent, but must satisfy known stability conditions in order to achieve convergence. In most cases this will not present a problem, since loss of stability will only occur for very large stiffness changes, which are well beyond the range of uncertainty observed in the physical structure. However, there are ill-conditioned problems for which even seemingly small perturbations will engender large changes in some stiffness terms. This is often the case when constraint equations are present in the problem formulation. Such problems are typically encountered in the analysis of strongly anisotropic or incompressible materials (e.g. composites, rubber mounts and seals), deviatoric rate-independent plasticity, or the thin limit of the Reissner-Mindlin shell theory. A solution to this problem will involve the development of smart adaptive algorithms for selecting the perturbation size in order to ensure convergence of the algorithm.

Significant progress was made over the last year on issues related to the modeling of probabilistic structures and the development of a good user interface. It was soon realized that classical shell theories lack the generality needed to capture localized effects which are often important in the analysis of SSME-related components. This resulted in the development of a new family of finite elements based on an assumed strain formulation and designed to achieve superior performance in bending problems. These elements allow the definition of continuous pressure fields at the surface nodes using a new boundary identification algorithm. Current development efforts are aimed at enhancing the element's thermal strain response and extending the new formulation to problems involving material nonlinearity.

The external database file is used for retaining a permanent record of the parameter sensitivity data generated by the NESSUS code. This database resides in a binary (unformatted) direct-access file, and is structured as a two-way ordered linked list. This type of data structure allows the insertion, deletion and replacement of individual entries without the need to move large blocks of data. It is therefore possible to maintain and expand an existing database with additional results obtained in the course of multiple runs of the NESSUS finite element code. Each database file is self-contained, allowing direct access to the perturbation data from within other modules in the NESSUS system.

Planned developments for the coming year include extending the capabilities of the NESSUS code to perform probabilistic analysis in situations involving material nonlinearity and transient dynamics. This will require tracking separate time-histories for all perturbed problems and transferring perturbation data between increments. The ability to conduct random vibration analysis on uncertain structures is also planned for the near future. The development of probabilistic finite deformation analysis in NESSUS is currently planned for the fourth year of the PSAM effort.

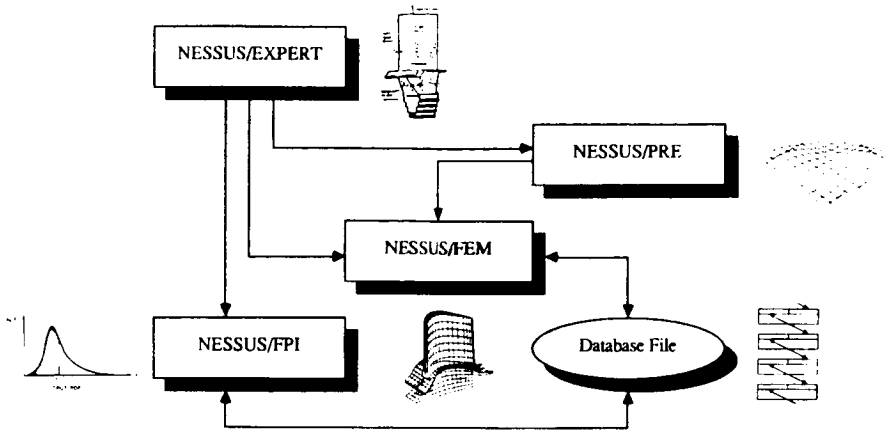

FIGURE 1: AN OVERVIEW OF THE NESSUS CODE

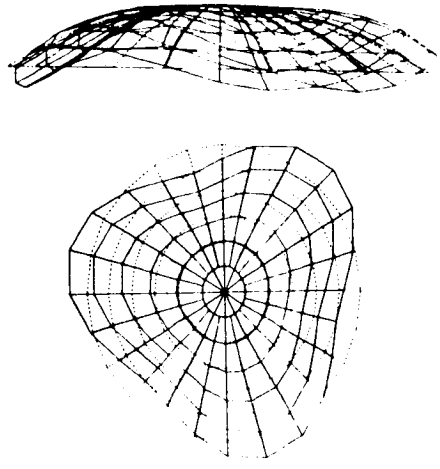

FIGURE 2: UNCOUPLED RANDOM VARIABLES USED TO CHARACTERIZE GEOMETRICAL UNCERTAINTY MAY BE IDENTIFIED WITH SIMPLE GEOMETRY IMPERFECTIONS

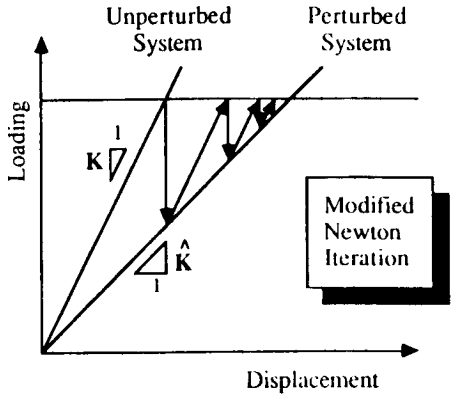

FIGURE 3: GRAPHICAL INTERPRETATION OF MODIFIED NEWTON ITERATION

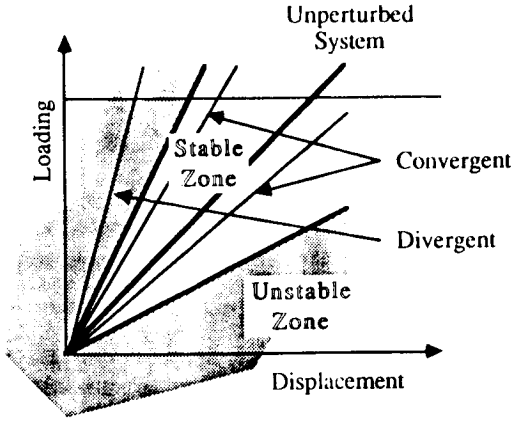

FIGURE 4: STABILITY BOUNDS DEFINE THE ALLOWABLE RANGE OF PERTURBATION SIZES WHICH ARE CONVERGENT WITH THE MODIFIED NEWTON ALGORITHM

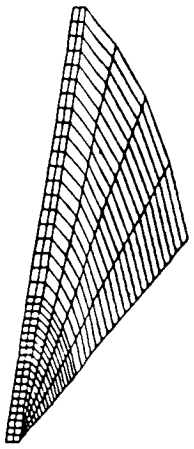

FIGURE 5: LOCALIZED THERMAL AND MECHANICAL EFFECTS CRUCIAL TO THE ANALYSIS OF COMPONENTS SUCH AS THIS BLISTER SPECIMEN MODEL CANNOT BE ADEQUATELY CAPTURED USING SIMPLIFIED SHELL-BASED MODELS

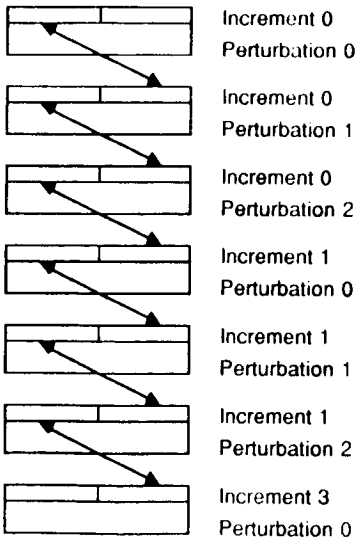

FIGURE 6: AN EXTERNAL DATABASE FILE IS USED TO RETAIN A PERMANENT RECORD OF THE PARAMETER SENSITIVITY DATA GENERATED BY THE NESSUS CODE

PROBABILISTIC STRUCTURAL ANALYSIS VERIFICATION STUDIES

K.R. Rajagopal
Rocketdyne Division, Rockwell International
Canoga Park, California

The space propulsion system components are subjected to complex mechanical and thermal loading. Typically, these components are analyzed using the state of the art deterministic methodologies in linear and nonlinear structural analysis domain. The components are then designed using a factor of safety approach. The purpose for doing a probabilistic structural analysis of space propulsion system components has been explained in one of the earlier papers on PSAM appearing in this same volume.

During the first year and part of the second year of the contract, identification and definition of environments and analysis techniques that are used to analyze the typical space propulsion system components were discussed and presented (Ref. 1). The basic objective of the verification efforts is to apply the probabilistic structural analysis methods developed and implemented in NESSUS (Numerical Evaluation of Stochastic Structures Under Stress) code to typical space propulsion components (Figure 1). The chosen typical components are turbine blade, high pressure duct, Lox post, and transfer tube liners. Since analysis options of increasing levels of sophistication are implemented in NESSUS incrementally, the verification efforts are also tailored to have increasing levels of sophistication during the progression of the contract. The current released version of the code is limited to linear structural analysis.

Considering turbine blade component first, several simple verification studies were conducted. The studies exercised the solid element type, typical random variables, and various solution strategies. The results of the simple verification studies (Ref. 2) aided in establishing confidence in the code, identified its limitations in user interface, finite element and analysis deficiencies. The studies conducted on simple models so far indicate that for the chosen random variables and their normal range of perturbation found in practice, the implemented solution strategies were adequate. On the other hand, the studies also showed that when the perturbations were large, in the context of doing a sensitivity analysis over a wide range, the implemented solution strategies did not converge, and in some cases divergence occurred. The divergence or slow convergence issue has been addressed in the development of fully integrated probabilistic structural analysis package that causes the reformulation of the system equations as needed for convergence.

The studies included geometry perturbation (variations in tilt angle), material orientation perturbation ($\pm 10°$), material property perturbation and load (centrifugal load, pressure, temperature) perturbations. The studies resulted in improved user interfaces and hastened the implementation of more advanced solid elements that behave better in a variety of stress fields including temperature gradients.

Several simple verification studies have been conducted on frequency extraction of the perturbed structure using perturbation technique, which is of special interest in turbine blade components. Based on the review of results, strategies for improvements in accuracy and a reduction in computing time to obtain the frequencies of perturbed structure are being sought.

A solid finite element turbine blade model, representative of blades found in space propulsion system components, has been generated and is currently being exercised (Figure 3). A basic set of random variables, consistent with first cut design requirements, have been identified (Figure 3). These random variables will be used in the study to determine the probability density function (PDF) of stress at critical areas and the PDF of frequencies. Some of the other important random variables such as variables contributing to the damper effectiveness, dynamic pressure, support conditions and transient conditions that are necessary for the final design are not considered in the initial exercise.

Following the turbine blade analysis, verification efforts on other typical components such as high pressure ducts (Figure 4), Lox post (Figure 5), and transfer tube liners (Figure 6) will follow. The random variables and solution types have been carefully chosen to exercise and verify a wide range of analysis options and element types that are being developed in NESSUS and also in determining the probabilistic response of primary component specific design parameters.

References

1. Probabilistic Structural Analysis Methods for Select Space Propulsion System Components (PSAM). First Annual Report, NASA Contract NAS3-24389, March 1986.
2. Probabilistic Structural Analysis Methods for Select Space Propulsion System Components (PSAM). Second Annual Report, NASA Contract NAS3-24389, November 1986.

VERIFICATION ANALYSES
OBJECTIVE

TO APPLY THE METHODS DEVELOPED TO THE ANALYSIS OF
TYPICAL SPACE PROPULSION SYSTEM COMPONENTS

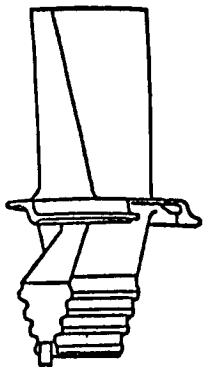

TURBINE BLADE

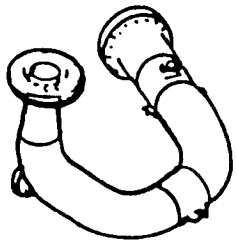

HIGH PRESSURE DUCT

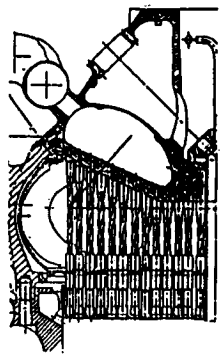

LOX POST

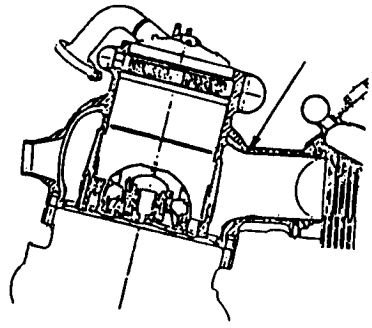

TRANSFER TUBE LINER

FIGURE 1.

SIMPLE VERIFICATION STUDIES
OBJECTIVES

- SHAKEOUT OF ANALYSIS METHODS/CODE/USER OPTIONS
- SELECTION AND EXERCISE OF COMPONENT SPECIFIC KEY RANDOM VARIABLES ON SIMPLISTIC MODELS
- RESULTS IN IDENTIFICATION OF LIMITS AND IMPROVEMENTS IN

ELEMENT TECHNOLOGY	ALGORITHIMIC BEHAVIOR	USER INTERFACE
· SOLID ELEMENT ENHANCEMENTS	· CONVERGENCE AND ACCURACY	· IMPROVEMENTS IN INPUTS
· TEMPERATURE GRADIENT MODELING	· STIFFENING OR SOFTENING STRUCTURE	· SOLUTION STRATEGY RECOMMENDATION

FIGURE 2.

TURBINE BLADE ANALYSIS

- RANDOM VARIABLES
  - GEOMETRY
  - MATERIAL ORIENTATION
  - MATERIAL PROPERTIES
- STEADY STATE
  - CENTRIFUGAL LOAD
  - TEMPERATURE
  - STATIC PRESSURE AND ΔP
- RESPONSE VARIABLES
  - CENTRIFUGAL STRESS AND PRESSURE STRESS
  - FREQUENCY

- 3-D SOLID MODEL

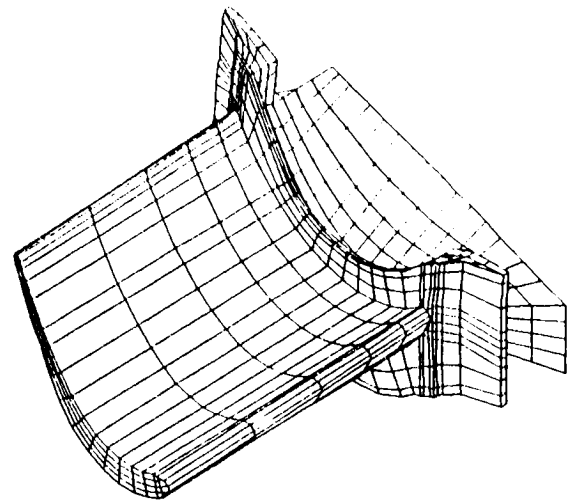

FIGURE 3.

HIGH PRESSURE DUCTS

- DYNAMIC ANALYSIS WILL BE EMPHASIZED
- RANDOM VARIABLES
  - DAMPING
  - SUPPORT VIBRATION
  - ACCELERATION
  - GIMBAL
  - MISALIGNMENT
- RESPONSE VARIABLE
  - STRESS AT CRITICAL AREAS

- 3-D LINE ELEMENT MODEL

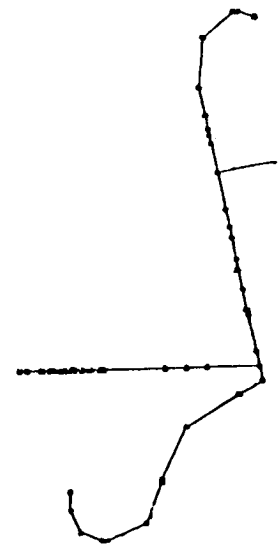

FIGURE 4.

LOX POST ANALYSIS
STATIC MATERIAL NONLINEAR ANALYSIS

- RANDOM VARIABLES
  - STRESS-STRAIN LAW

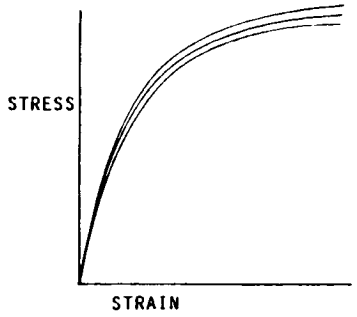

  - TEMPERATURE
- RESPONSE VARIABLE
  - TOTAL INELASTIC STRAIN AT CRITICAL AREAS

- 2-D AXISYMMETRIC MODEL

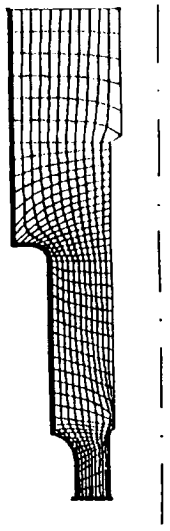

FIGURE 5.

TRANSFER TUBE ANALYSIS
STATIC GEOMETRIC NONLINEAR ANALYSIS

- RANDOM VARIABLES
  - MATERIAL PROPERTIES
  - THICKNESS
  - NODAL COORDINATES
  - BOUNDARY CONDITION FLEXIBILITY
  - TEMPERATURE
- VARIABLE TO BE DETERMINED
  - BUCKLING LOAD

- 3-D THIN SHELL MODEL

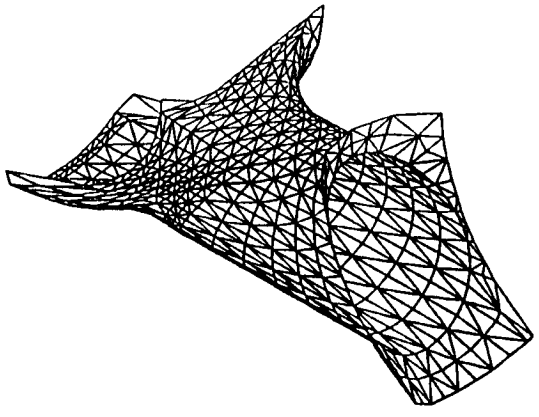

FIGURE 6.

NESSUS/EXPERT AND NESSUS/FPI IN THE PROBABILISTIC STRUCTURAL ANALYSIS METHODS (PSAM) PROGRAM

O.H. Burnside
Southwest Research Institute
San Antonio, Texas

NESSUS (Numerical Evaluation of Stochastic Structures under Stress) is the primary computer code being developed in the NASA PSAM project. It consists of four modules NESSUS/EXPERT, NESSUS/FPI, NESSUS/PRE and NESSUS/FEM. This presentation concentrates on EXPERT and FPI, while PRE and FEM are discussed in another presentation.

One challenge of the PSAM effort is the effective integration of advanced finite element and probabilistic methods. A code with linear static and dynamic capabilities has been provided to NASA. However, it is clear that, in the final version, the user must be provided with an interface program to effectively use features such as nonlinear analysis and confidence band estimation. Such an interface program will also expedite the process of conducting the analyses necessary for NESSUS verification.

To provide an effective interface between NESSUS and the user, an expert system module called NESSUS/EXPERT is being developed. That system uses the CLIPS artificial intelligence code developed at NASA-JSC. The code is compatible with FORTRAN, the standard language for codes in PSAM. The user interacts with the CLIPS inference engine, which is linked to the knowledge database as shown in Figure 1.

The essential features of EXPERT are its automated user input and automated results. The EXPERT module will provide the user with features such as interactive HELP, data set consistency checking, and defaults for the statistical models of random variables. EXPERT will also assist the analyst in managing the large database produced in perturbing the random variables. Such variables may include material properties, geometry, boundary conditions and loading. Because of the potentially large number of random variables, this process must be automated to free the analyst from basically a bookkeeping task. For analysis of certain critical SSME components, EXPERT will choose component specific perturbations. For example, in the case of a turbine blade shown in Figure 2, perturbations may be applied directly to parameters defining the blades geometry such as the twist and tilt angles and blade thickness.

The perturbation database generated by NESSUS/FEM and managed in EXPERT is used to develop the so-called response or performance model in the random variables. Figure 3 illustrates such a model in which natural frequency is a random function of material modulus. It is from this performance model that the probabilistic response is computed. Two independent probabilistic methods are available in PSAM for the computation of the probabilistic structural response. These are the Fast Probability Integration (FPI) method and Monte Carlo simulation. FPI is classified as an advanced reliability method and has been developed over the past ten years by researchers addressing the reliability of civil engineering structures. Monte Carlo is a well-established technique for computing probabilities by conducting a number of deterministic analyses with specified input distributional information.

For structural systems, the probability of failure is generally low. In such situations, Monte Carlo is inefficient since a large number of simulations are required to confidently predict low probability levels. The efficiency of FPI, on the other hand, is not tied to the probability level and can accurately predict the tails of the response distribution. However, Monte Carlo is still useful in PSAM to check the accuracy and robustness of the FPI algorithms. For a given performance function, FPI can compute point probability estimates or obtain full distributional information in terms of the cumulative probability distribution. In general, the performance function may be nonlinear in the random variables and contain mixed probability distribution types. Figure 4 qualitatively compares typical FPI and Monte Carlo results and illustrates the increasing inaccuracy in Monte Carlo at the low probability levels.

The process used by FPI to make the probability estimates may be considered a problem of constrained minimization. This is illustrated in Figure 5. Let us assume that material density and modulus of elasticity are random variables in an eigen-frequency analysis. The response function at a particular frequency is shown, with the lines of constant probability given by the circles. The design or most probable point is defined as the point with the highest joint distribution at a given value of the response function. The design point is geometrically located at the minimum distance β, called the safety index. In a first-order reliability analysis, β is related to the probability of exceeding the specified frequency.

The FPI algorithm uses an efficient iteration technique to converge to the most probable point. The first estimate of the design points uses the NESSUS-generated database at the mean state. From this initial guess, the automated algorithms in FPI use successive NESSUS perturbations at other points to converge to the design point as illustrated in Figure 6. Convergence is usually obtained in several (three to five) iterations. This procedure gives the probability of exceedence at a particular value of the response function. This is called a point probability estimate. Cumulative distributional information can be obtained by running FPI at several values of the response variables as shown on Figure 4.

In summary, the NESSUS/EXPERT and NESSUS/FPI modules provide the designer/analyst with computational methodologies and software for effectively and efficiently evaluating design sensitivities and uncertainties and quantifying the structural performance of SSME components.

EXPERT KNOWLEDGE WILL GOVERN USER INTERFACE

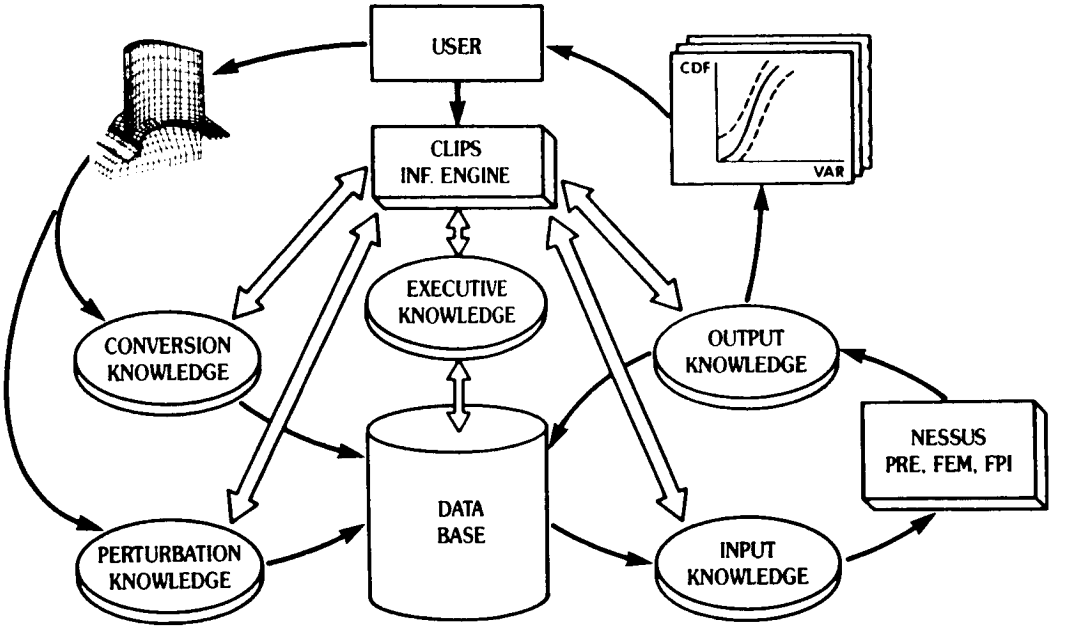

FIGURE 1.

NESSUS PERTURBATIONS TO BE AUTOMATED

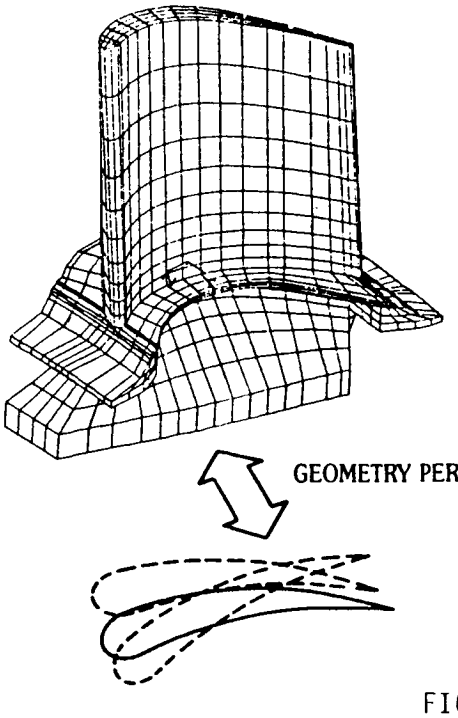

MATERIAL PROPERTIES

- ANISOTROPIC CONSTANTS
- ANISOTROPIC ORIENTATIONS
- STRESS–STRAIN CURVES

GEOMETRY

- TWIST
- TILT
- THICKNESS
- ETC.

BOUNDARY CONDITIONS

- LOADS
- CONSTRAINTS

FIGURE 2.

FPI CODE RELIES ON RESPONSE MODEL

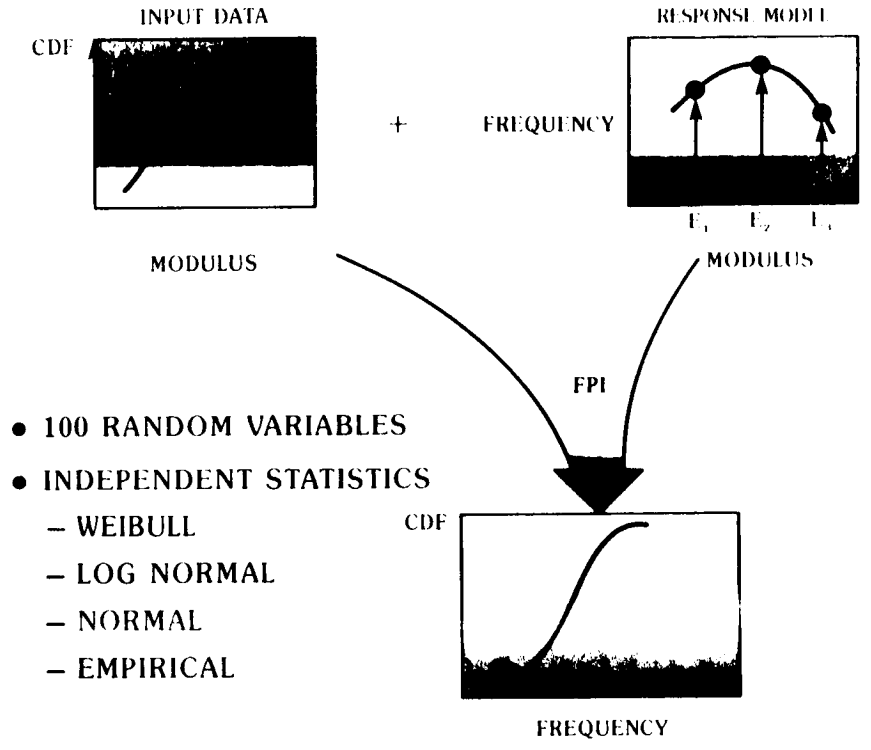

FIGURE 3.

FPI CODE VALIDATED BY MONTE CARLO

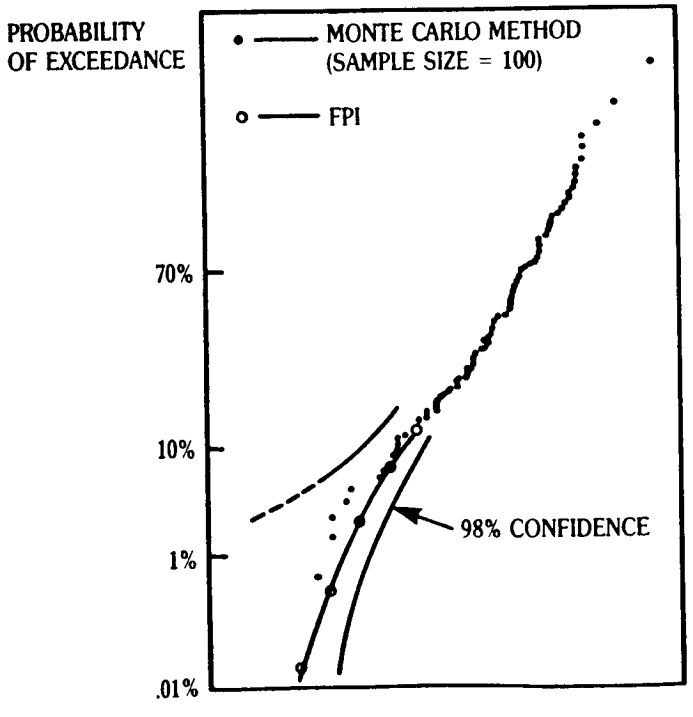

FPI ATTRIBUTES

- UP TO 100 TIMES FASTER THAN MC
- EFFICIENCY INDEPENDENT OF PROBABILITY LEVEL
- CAN USE LINEAR/QUADRATIC DESIGN SENSITIVITY DATA
- CAN BE COUPLED TO FEM
- USES ANY INPUT STATISTICS
- COMPUTES RISK LEVEL
- ESTIMATES CONFIDENCE BANDS

FIGURE 4.

FPI ALGORITHM APPROXIMATES NONNORMAL VARIABLES

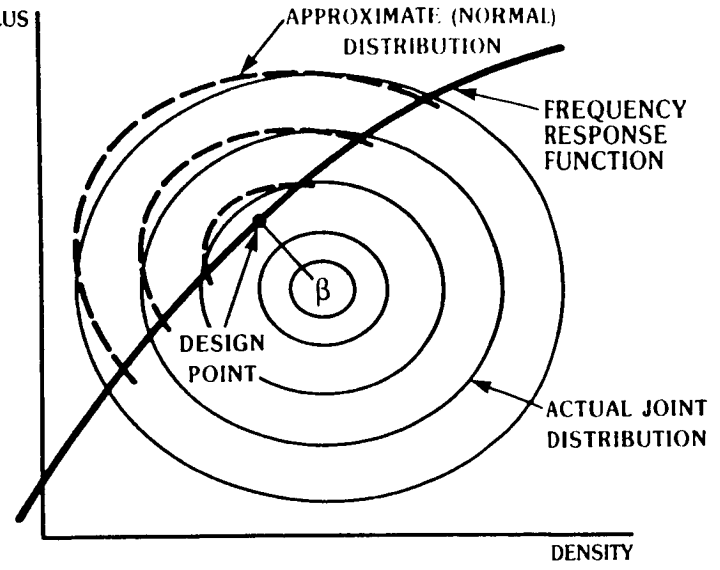

- APPROXIMATIONS BASED ON EQUAL CDF NEAR DESIGN POINT
- AREA OF EXCEEDANCE CALCULATED FOR EQUIVALENT NORMAL DISTRIBUTIONS
- ERRORS GREATEST AWAY FROM DESIGN POINT
- ERROR PROBABILITIES ARE SMALL
- PROBABILITY GIVEN FROM β DISTANCE

FIGURE 5.

FPI ALGORITHM ITERATES TO MAXIMUM LIKELIHOOD POINT

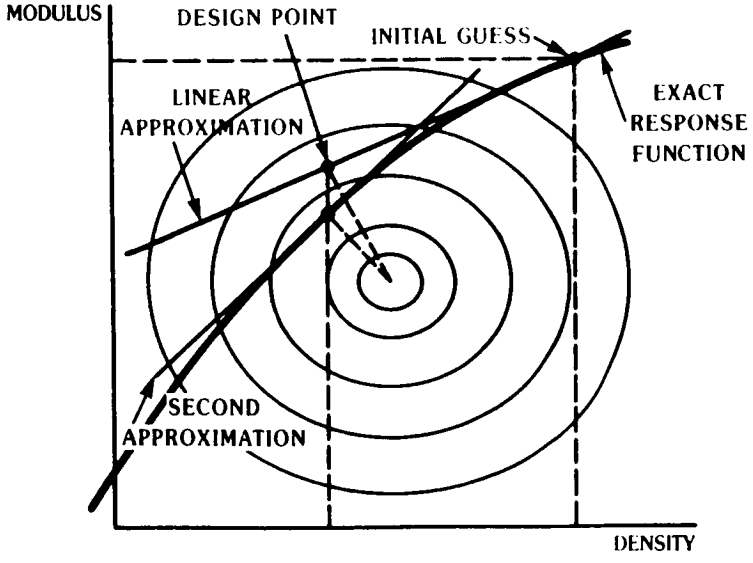

- ESTIMATE LINEAR RESPONSE FUNCTION
- CALCULATE MOST LIKELY DESIGN POINT
- SHIFT RESPONSE FUNCTION SURFACE
- RECOMPUTE DESIGN POINT

FIGURE 6.

ADVANCED PROBABILISTIC METHOD DEVELOPMENT

P.H. Wirsching
The University of Arizona
Tucson, Arizona

Advanced structural reliability methods are utilized on the PSAM project to provide a tool for analysis and design of space propulsion system hardware. The role of the effort at the University of Arizona is to provide reliability technology support to this project. Reliability refers, in general, to application of probabilistic and statistical methods to manage uncertainties in engineering design.

PSAM computer programs will provide a design tool for analyzing uncertainty associated with thermal and mechanical loading, material behavior, geometry, and the analysis methods used. Specifically, reliability methods are employed (a) to perform sensitivity analyses (a study of the importance of each design factor), (b) to establish the distribution of a critical response variable, (e.g., stress, deflection), (c) to perform reliability assessment, and (d) ultimately to produce a design which will minimize cost and/or weight (Fig. 1).

Uncertainties in the design factors of space propulsion hardware, as defined in Fig. 1, are described by probability models constructed using statistical analysis of data. Two examples are provided in Fig. 2 and Fig. 3. Turbine blade twist (a geometric variable) has a statistical distribution (Fig. 2), and significant variability in material properties are observed in laboratory tests (Fig. 3). Statistical methods are employed to produce a probability model, i.e., a statistical synthesis or summary of each design variable (e.g., each X_i in Fig. 4) in a format suitable for reliability analysis and ultimately, design decisions.

Given the probability model for each random variable, and the design equation, i.e., how the variables are related (e.g., through the NESSUS/FEM computer code), two basic methods for computing the distribution of a response variable are available. They are, fast probability integration (FPI), (Fig. 4) and Monte Carlo (Fig. 5). FPI is a complex numerical algorithm which provides "fast" probability calculations, accurate to about ± 5% (See Refs. 1 and 2).

The NESSUS generated perturbed data set, an example of which is shown in Fig. 5, is used as a function of the input variables. Monte Carlo produces an exact solution, but it is expensive to run. There are a large number of different Monte Carlo schemes available; methods of improving efficiency of Monte Carlo, tailored for PSAM application, are being studied. Availability of the response function shown in Fig. 5 is a requirement for performing a fast Monte Carlo analysis. The NESSUS-generated, approximate response function can be used to replace the "exact" simulation models needed by Monte Carlo methods.

The result of PSAM analysis is a distribution of a response variable. But for design purposes, it is often important to be able to specify also the confidence associated with a probability statement. Confidence intervals provide a quantitative description of the quality of the results of the probabilistic analyses (Fig. 6). Efficient methods for constructing confidence intervals are being studied.

In summary, the University of Arizona effort on PSAM is to provide technical support in statistical characterization of design variables, advanced reliability analysis methods, and confidence interval construction (Fig. 7).

REFERENCES

1. Wu, Y.T., "Demonstration of a New Fast Probability Integration Method for Reliability Analysis," Journal of Engineering for Industry, Vol. 109, No. 1, Feb. 1987, pp. 24-28.

2. Wu. Y.T. and Wirsching, P.H., "New Algorithm for Structural Reliability Estimation," to be published in the ASCE Journal of Engineering Mechanics, 1987.

RELIABILITY METHODS ARE EFFECTIVE TOOLS FOR DESIGNERS

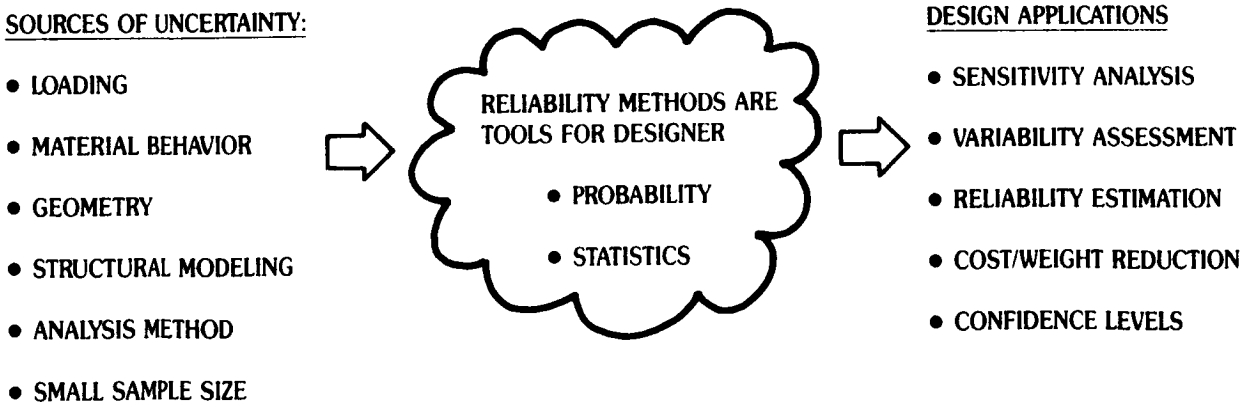

FIGURE 1.

STATISTICAL METHODS TRANSLATE DATA IN MODELS

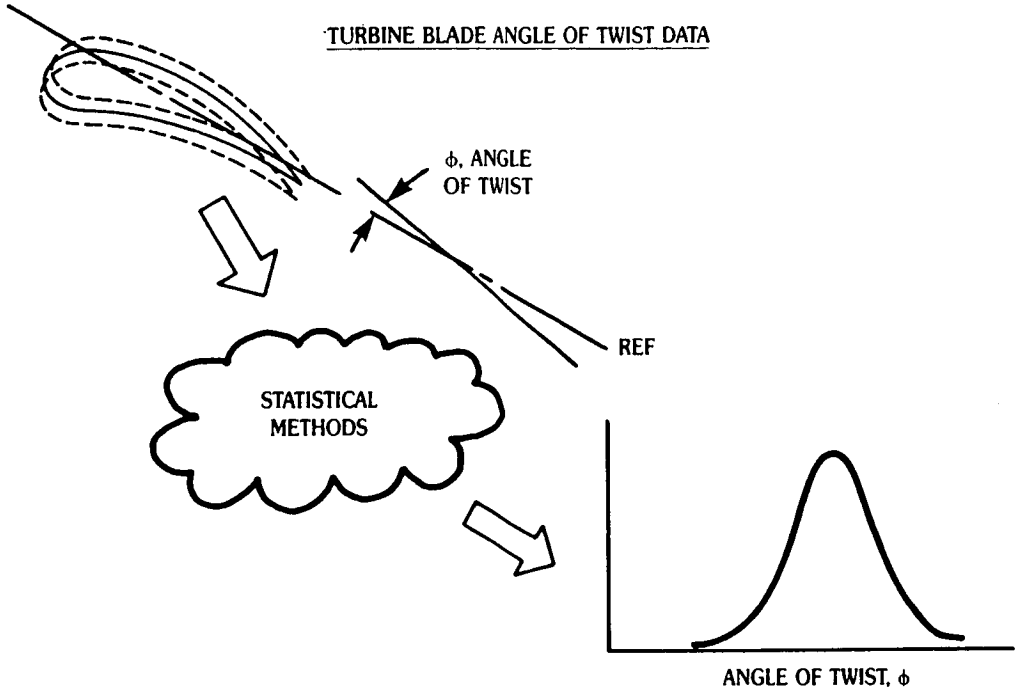

FIGURE 2.

MATERIAL PROPERTIES EXHIBIT SIGNIFICANT VARIABILITY

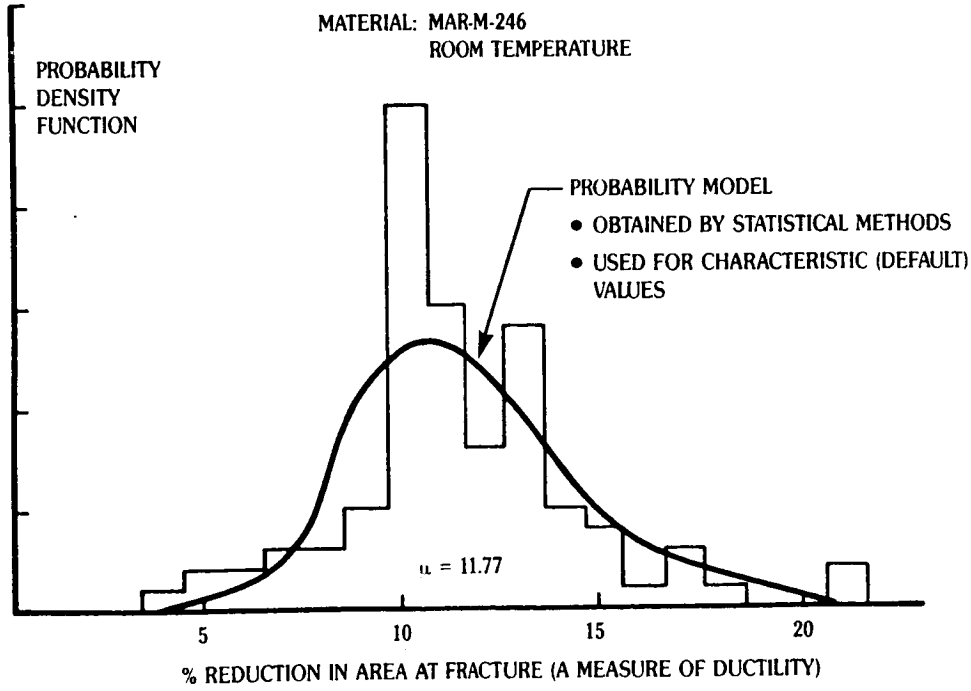

FIGURE 3.

FPI ALGORITHM IMPROVEMENTS DEMONSTRATED

- ENHANCED DISTRIBUTION LIBRARY
  - MATERIAL BEHAVIOR
  - LOADING UNCERTAINTY
- IMPROVED ACCURACY
- VALIDATION PROBLEMS
  - HIGHLY NONLINEAR
  - MANY VARIABLES

FATIGUE DAMAGE PREDICTION MODEL

$$D = X_1 + N_o \left[\frac{X_2}{X_3 (X_4 X_5)^{\gamma}} + \frac{1 - X_2}{X_6 (X_4 X_5)^{\eta}} \right]$$

EACH X_i HAS DIFFERENT DISTRIBUTION

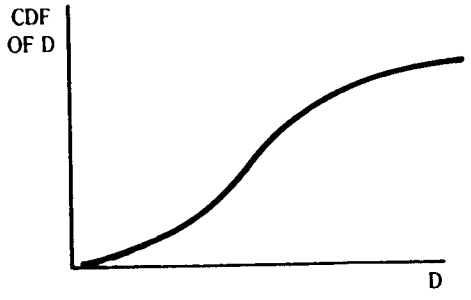

- ACCURACY OF FPI ± 5%
- RELATIVE COMPUTER TIME

  FPI = 1

  MONTE CARLO = 60
  (CONVENTIONAL)

FIGURE 4.

FAST MONTE CARLO ALGORITHM(S) ESTABLISHED

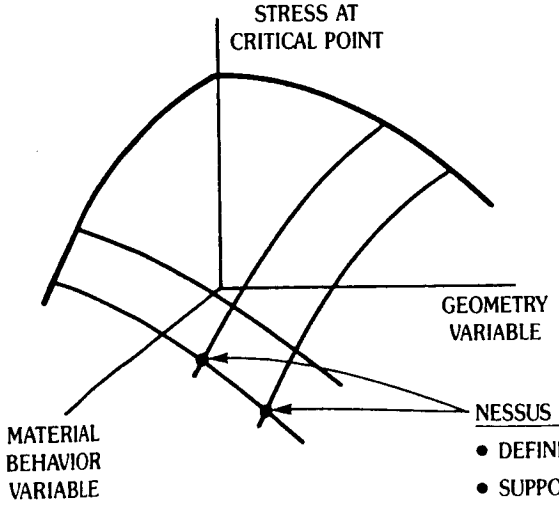

- AN INDEPENDENT CHECK ON FPI
- CONVERGES TO EXACT SOLUTION
- MORE EXPENSIVE THAN FPI
- USES NESSUS DATA BASE
- SEVERAL MONTE CARLO METHODS AVAILABLE
- RELATIVE MERITS OF EACH METHOD UNDER STUDY

NESSUS GENERATED DATA

- DEFINES RESPONSE SURFACE
- SUPPORTS MONTE CARLO SIMULATION

FIGURE 5.

WHAT IS OUR CONFIDENCE IN THE ANSWER?

PROBLEM:

PROB [NATURAL FREQUENCY OF BLADE, Ω < FREQUENCY LIMIT, Ω_L] ?

VARIABLES:

- GEOMETRY
- STIFFNESS
- MASS

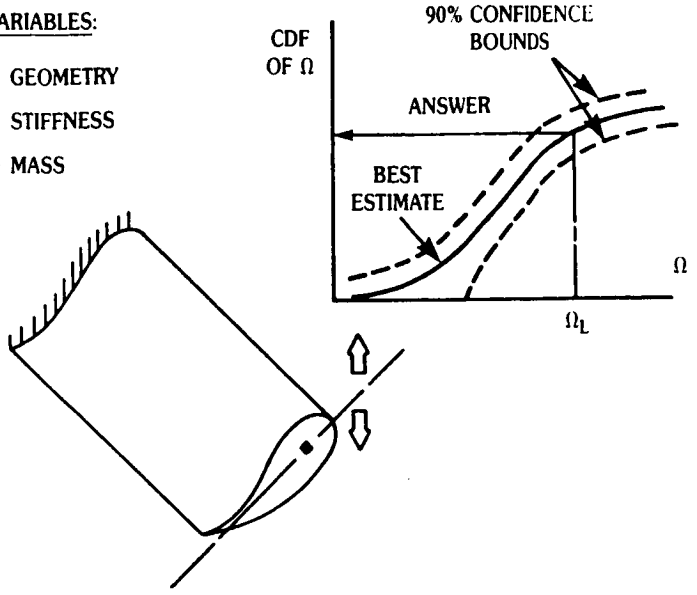

CONFIDENCE

- DIFFICULT ANALYSIS PROBLEM
- APPROXIMATE METHOD DEFINED
- USES NESSUS DATA BASE
- GIVES INTERVAL ESTIMATES
  - PROBABILITY
  - VARIABILITY

FIGURE 6.

UA PROVIDES RELIABILITY TECHNOLOGY SUPPORT

- LITERATURE REVIEW
- STATISTICAL METHODS TO PRODUCE MODELS
  - GEOMETRY
  - MATERIAL BEHAVIOR
- DISTRIBUTIONAL CHOICES FOR DESIGN VARIABLES AND RESPONSES
- RELIABILITY ASSESSMENT METHODS
  - FPI
  - MONTE CARLO
- CONFIDENCE INTERVALS ON PROBABIILTY ESTIMATES

FIGURE 7.

STOCHASTIC AND HYBRID-STRESS PLATE/SHELL FINITE ELEMENTS FOR HOT-SECTION COMPONENTS

S.N. Atluri
Georgia Institute of Technology
Atlanta, Georgia

The research effort in the Center for the Advancement of Computational Mechanics at Georgia Tech has two main thrusts. The first of these is the development of special approaches for the numerical stress analysis of solids and structures whose material and geometric properties are uncertain. The second seeks to develop and implement high-efficiency plate and shell elements.

For a structure in which all loads, material properties and boundary conditions are certain, i.e. possess no random nature, it is possible to solve for precise values of displacement, stress and strain. On the other hand, for a structure in which material properties are uncertain, it is necessary to describe the structural response, e.g. displacement, in a manner which both incorporates and quantifies the resulting uncertainty. To this end the finite element methodology has been re-formulated so as to allow for the determination of a statistical description of stress, strain, etc. in terms of their means, variances and intercorrelations.

The stochastic element method, currently being implemented, will be able to more accurately portray the probabilistic nature of stress, strain, and displacement in actual structures.

In analyses of plate- and shell-like structures which exhibit strong gradients in stress, strain, or temperature through the thickness, accuracy demands that so-called 'degenerate' 3-D elements be used, as opposed to conventional plate or shell elements. The degenerate plate/shell elements currently available, however, admit aspect ratios only up to about 10 to 1 before their performance begins to degrade. As a consequence, use of degenerate shell elements has heretofore been too costly, except for simplified problems.

Current research has provided a hybrid-stress shell element whose behavior is acceptable for aspect ratios as high as 30 to 1. Thus, substantially more complex analyses will be practicable as soon as this element is fully implemented.

An additional advantage of the hybrid approach is that it permits more accurate stress-recovery at the upper and lower surfaces of the shell, an important consideration in high thickness-gradient applications.

The software associated with the above research is being implemented in the form of extensions to the Nessus code, developed jointly by Southwest Research Institute and MARC Analysis Corporation. The implementation is being carried out in the Center for the Advancement of Computational Mechanics at Georgia Tech. The hybrid shell element has been successfully tested in several small-deformation elastic analyses; implementation of the remaining capabilities is underway. The theoretical formulation of the stochastic elements is essentially complete; its implementation is just beginning.

Acknowledgements: The contributions to this effort from Messrs. K. L. Chen and T. Fitzgerald, and Drs. K. W. Reed and C.-T. Yang are sincerely acknowledged.

PROBABILISTIC FINITE ELEMENTS*

Ted Belytschko and Wing Kam Liu
Northwestern University
Evanston, Illinois

In the design of critical components, such as rocket engine parts, we often find large uncertainties in material properties and loads, particularly when considering the ultimate capacity of the components. One reason for this is that the extreme conditions, such as temperature or load, are not known, nor are the material properties at extreme temperatures as well established. Therefore, a single finite element analysis of a component may be quite misleading since it gives no information on the range of responses that can be expected.

Although analysts often try to guard against this shortcoming by varying several of the parameters either arbitrarily or on the basis of their intuition, a more rational and methodical approach to dealing with this difficulty would be very useful. The probabilistic finite element method (PFEM) has been developed in response to these needs.

In PFEM [1-3], finite element methods have been efficiently combined with second-order perturbation techniques to provide an effective method for informing the designer of the range of response which are likely in a given problem. The designer must provide as input the statistical character of the input variables, such as yield strength, load magnitude, and Young's modulus, by specifying their mean values and their variances. The output then consists of the mean response and the variance in the response. Thus the designer is given a much broader picture of the predicted performance than with simply a single response curve. These methods are applicable to a wide class of problems, provided that the scale of randomness is not too large and the probabilistic density functions possess decaying tails. By incorporating the computational techniques we have developed in the past 3 years for efficiency, the probabilistic finite element methods are capable of handling large systems with many sources of uncertainties.

Sample results for an elastic-plastic ten-bar structure and an elastic-plastic plane continuum with a circular hole subject to cyclic loadings with the yield stress on the random field are depicted in Figs. 1-4. For the ten-bar structure, a 5% coefficient of variation in the yield stresss gives a 13% coefficient of variation in the displacement of node 1 and an 11% coefficient of variation in the stress of element 1. For this example, along with many others (not shown here), PFEM compares very well with the Monte Carlo Simulation (MCS) and the Hermite Gauss Quadrature (HGQ) (see Fig. 2). This is an example where a situation where a small variance in the yield strength can result in a much larger variance in the response. It should be noted that the ratios of computer time are 1 to 400 when the PFEM is compared to MCS.

---

*Work performed under NASA Grant NAG3-535 administered by NASA Lewis Laboratories.

As for the elastic/plastic continuum problem, the mean displacement and stress are sinusoidal, resembling closely the forcing function (Fig. 4). The variances are close to zero until the plate begins to yield in compression. After this, the variance jumps to a higher value and remains steady until the yielding in tension begins. This phenomenon repeats every cycle.

A third numerical example for PFEM methods is a turbine blade problem. Some results for the turbine blade model shown in Fig. 5 will be presented. The blade is subjected to a random impulsive load and the yield stress is random.

A natural extension of these methods would be to consider fatigue and failure analysis. Finite element methods, such as PFEM, for analyzing fatigue and fracture in a probabilistic manner, are very scarce. The fracture related quantities such as fracture toughness, size and orientation of the cracks, are usually hard to determine exactly. These and other quantities, which govern the crack growth, can be treated by finite elements in a similar manner, although it woud be necessary to incorporate first and second order reliability methods and to embed singularities in the variational statements to correctly represent cracks. The experience obtained so far suggest that this is a logical extension of PFEM.

REFERENCES

1. Liu, W. K., Belytschko, T. and Mani, A., "Random Field Finite Elements," International Journal for Numerical Methods in Engineering, Vol. 23, 1986, pp. 1831-1845.

2. Liu, W. K., Belytschko, T. and Mani, A., "Probabilistic Finite Elements for Nonlinear Structural Dynamics," Computer Methods in Applied Mechanics and Engineering, Vol. 56, 1986, pp. 61-81.

3. Liu, W. K., Belytschko, T. and Mani, A., "Applications of Probabilistic Finite Element Methods in Elastic/Plastic Dynamics," Engineering for Industry, ASME, Vol. 109/1, pp. 2-8.

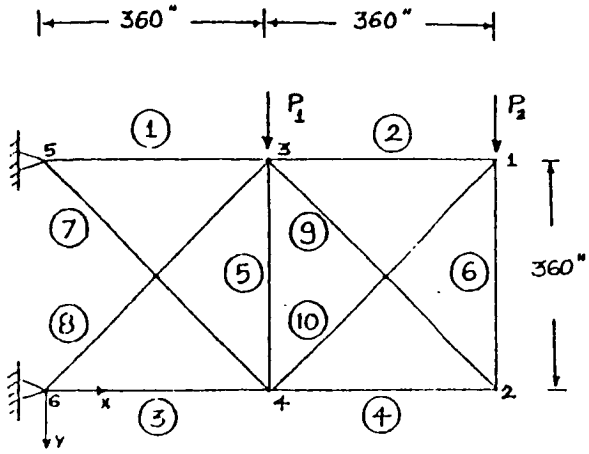

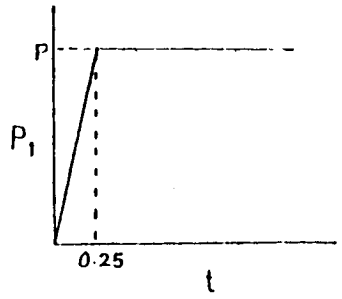

$E = 30.0 \times 10^6$

$E_T = 30.0 \times 10^4$

$A = 6.0$

$\rho = 0.30$

$\sigma_Y = 15000.0$

$P = 175.0 \times 10^3$

$P_2 = 0.0$

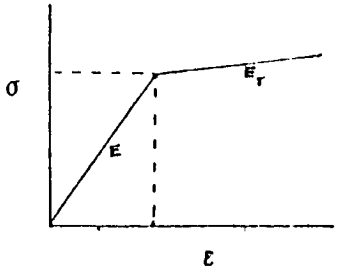

Problem Statement of a Ten-Bar Nonlinear Structure.

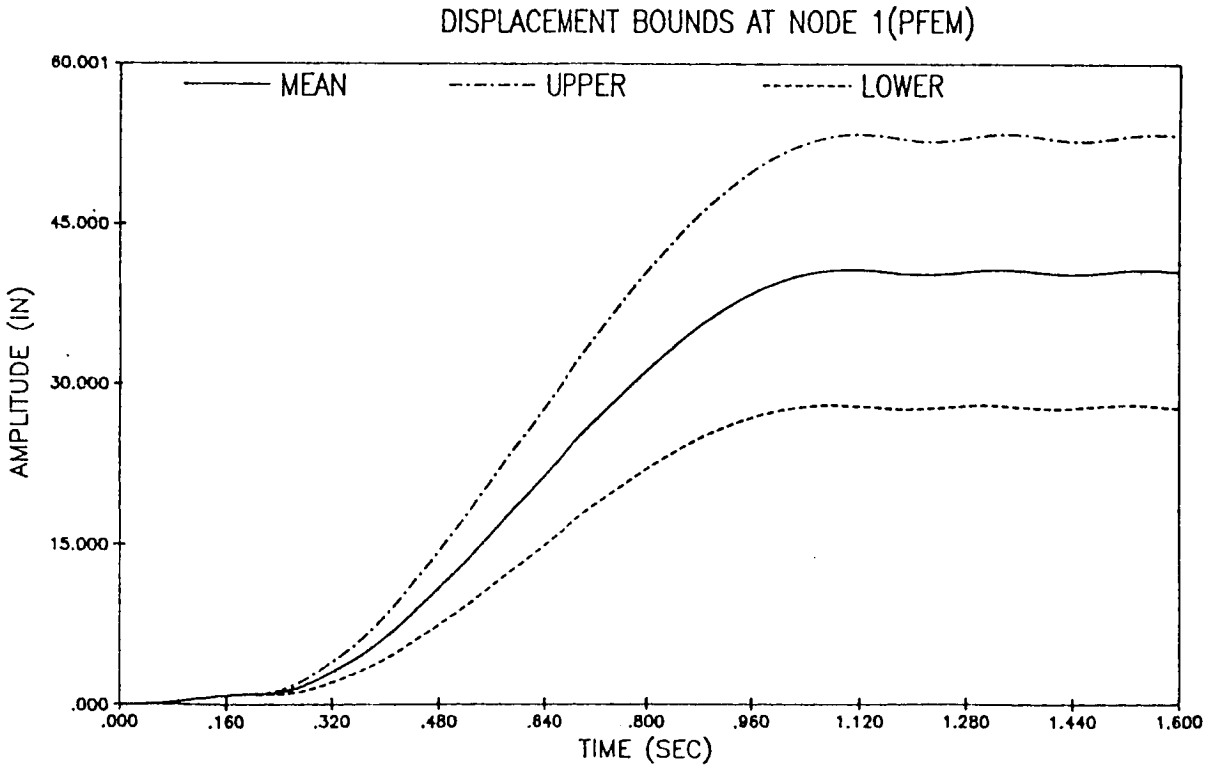

Fig. 1

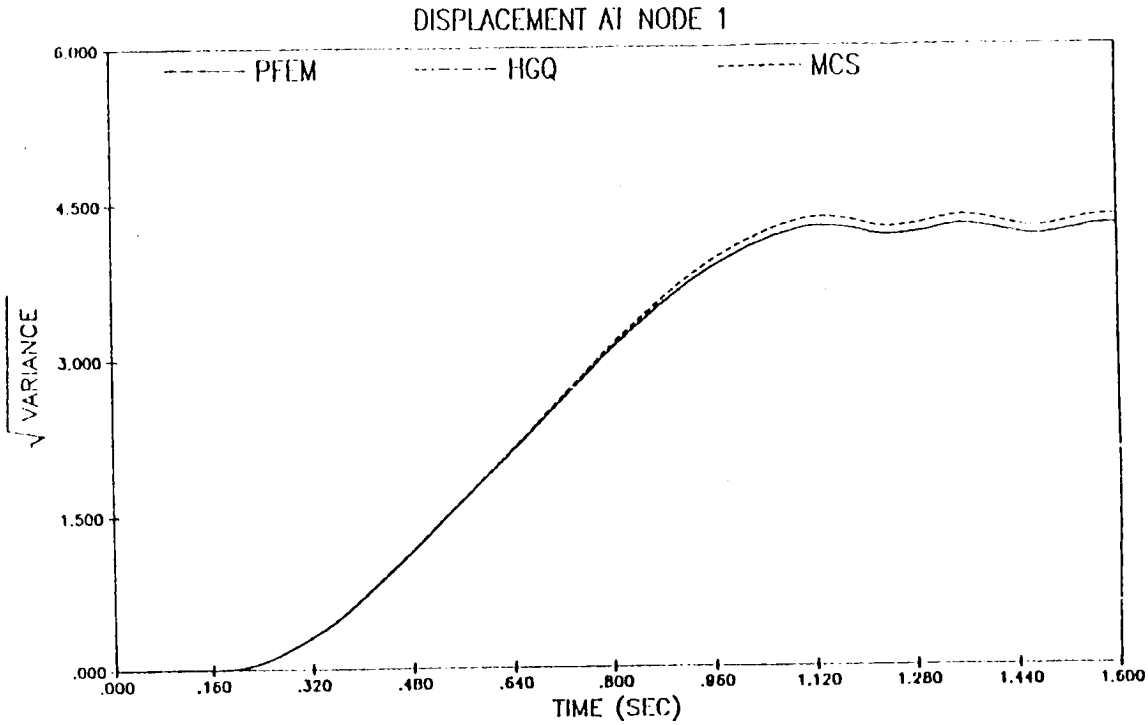

Comparison of the Variance of the y-displacement of Node 1 Using (1) Probabilistic Finite Element Method (PFEM); (2) Hermite Gauss Quadrature (HGQ); and (3) Monte Carlo Simulation (MCS).

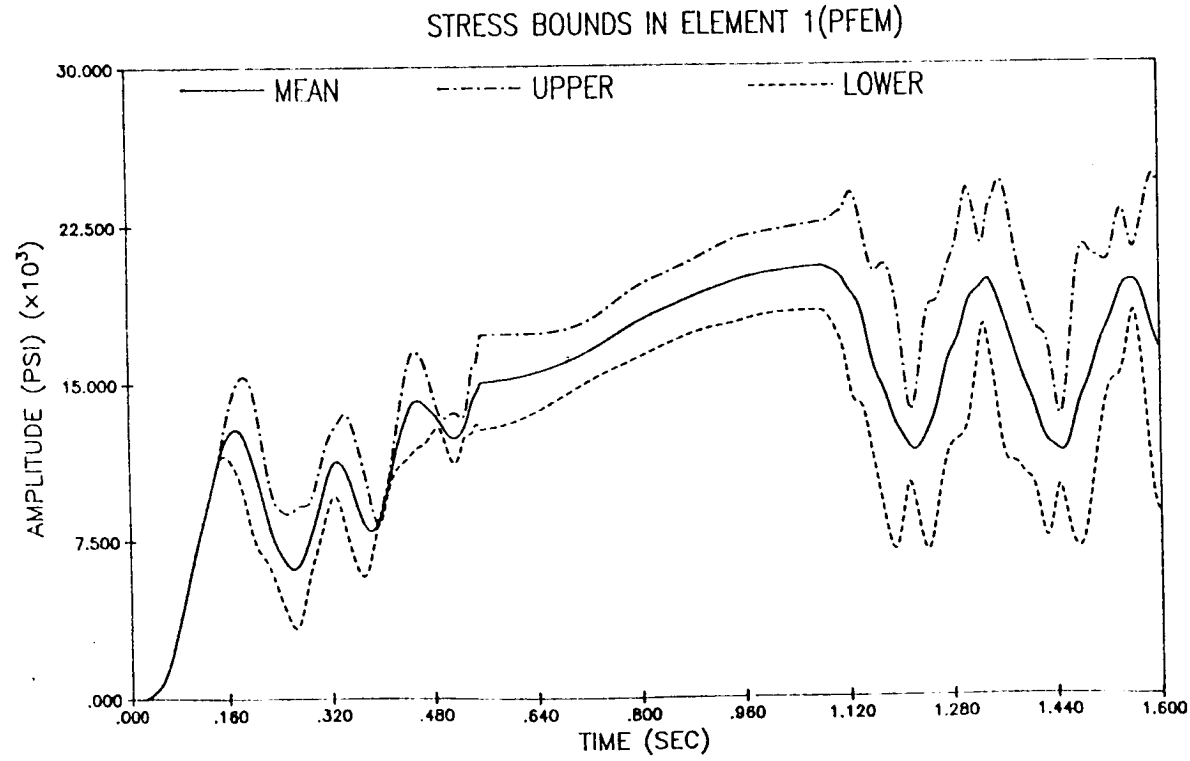

± 3 Sigma Bounds of the Stress in Member 1 using Probabilistic Finite Element Methods (PFEM)

Fig. 2

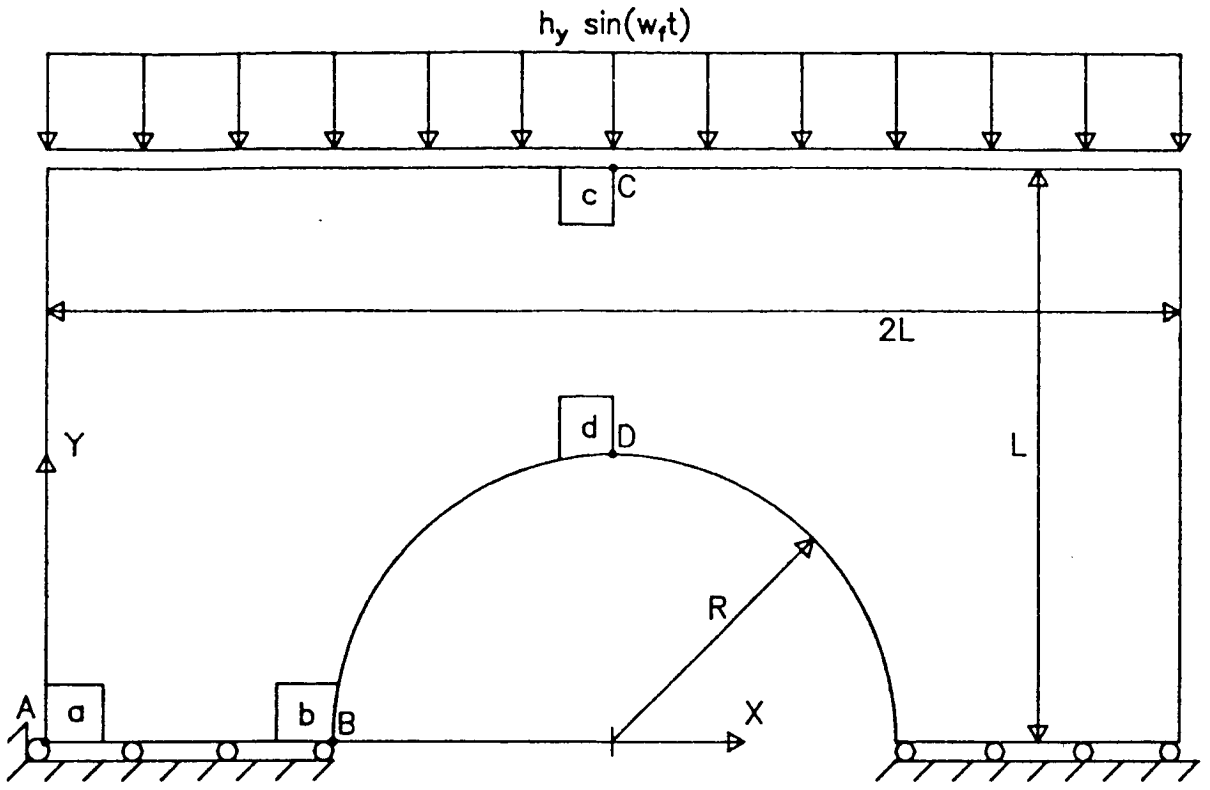

Problem Constants

$E = 3.0X10^7$ lb/in^2
Density = 0.3 lb/in^3
Thickness = 1.0 in
L = 6.0 in
R = 3.0 in
Poissons Ratio = 0.3
h_y = 2000.0 lb/in
w_f = 1500.0 rad/sec
Delta t = $1.0X10^{-4}$ sec
Rayleigh Damping Parameters
$e_0 = 0.0 \quad e_1 = 1.5X10^{-6}$

Mesh Data

4 Node 2D Plane Strain Continuum Element in Radial Mesh
784 Nodes, 720 Elements
Point a = Element 1
Point b = Element 15
Point c = Element 346
Point d = Element 360
Point A = Node 1
Point B = Node 16
Point C = Node 385
Point D = Node 400

Random Load

24 Random Variables
Coefficient of Variation = 0.1
Mean Load = 2000.0 lb/in
Spatial Correlation
$R(x_i,x_j) = \exp(-abs(x_i-x_j)/L_F)$

Random Material

15 Random Variables
Coefficient of Variation = 0.1
Mean Youngs Mod. = $3.0X10^7$ lb/in^2
Spatial Correlation
$R(x_i,x_j) = \exp(-abs(x_i-x_j)/L_E)$

Fig. 3 Problem Statement: Plain Strain Continuum with a Circular Hole.

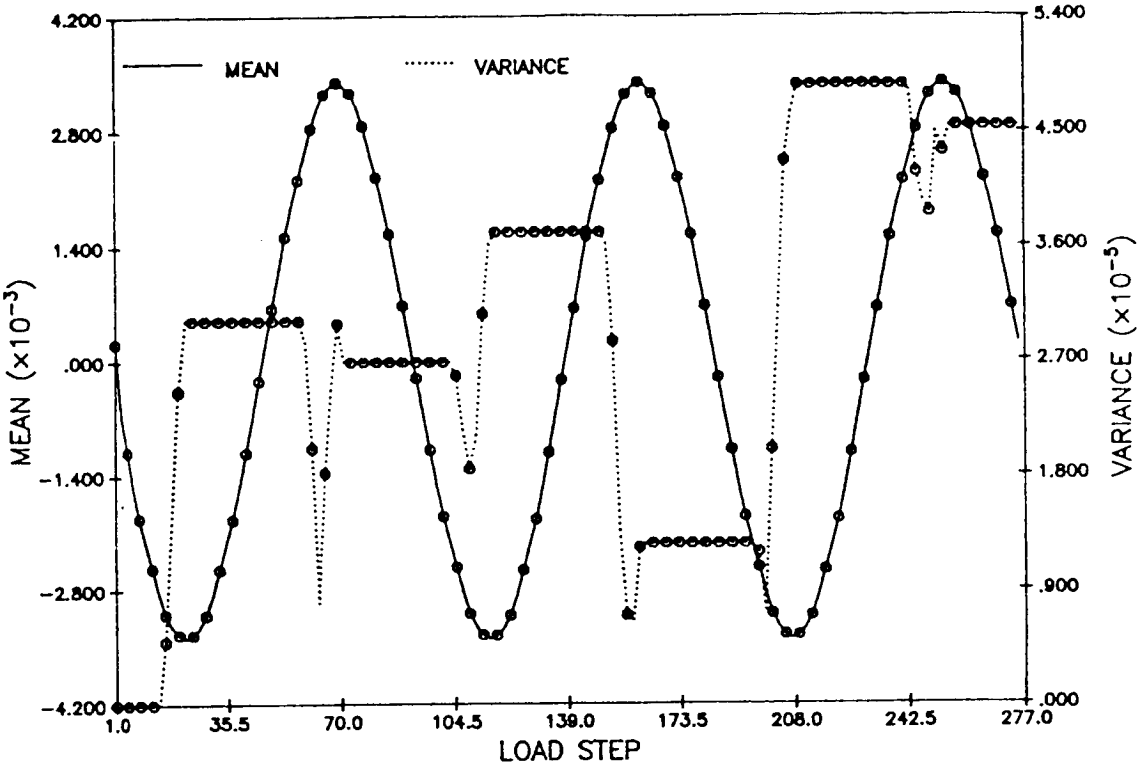

Fig. 4a Mean and Variance of Node 400 y-Displacement versus Load Steps.

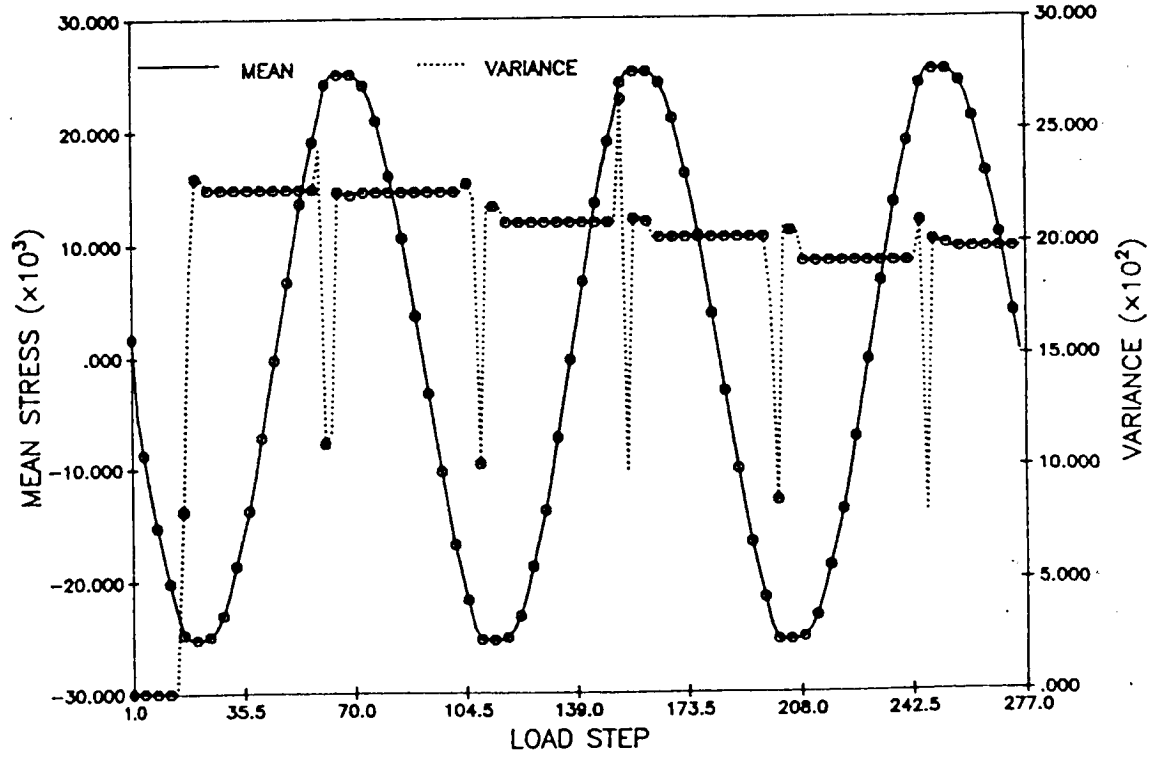

Fig. 4b Mean and Variance of Stress in Element 15 versus Load Steps.

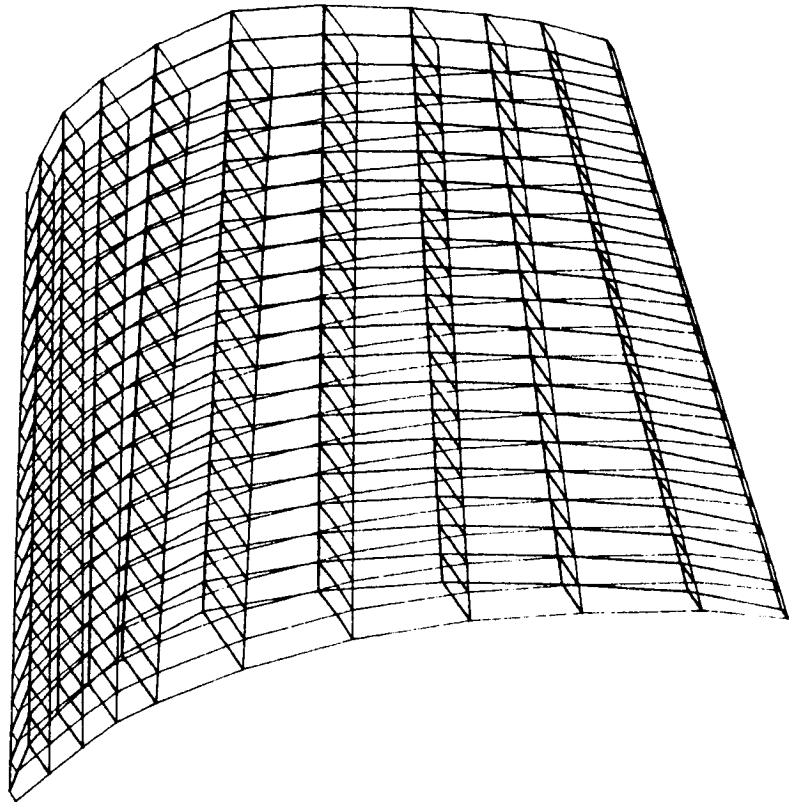

Fig. 5a

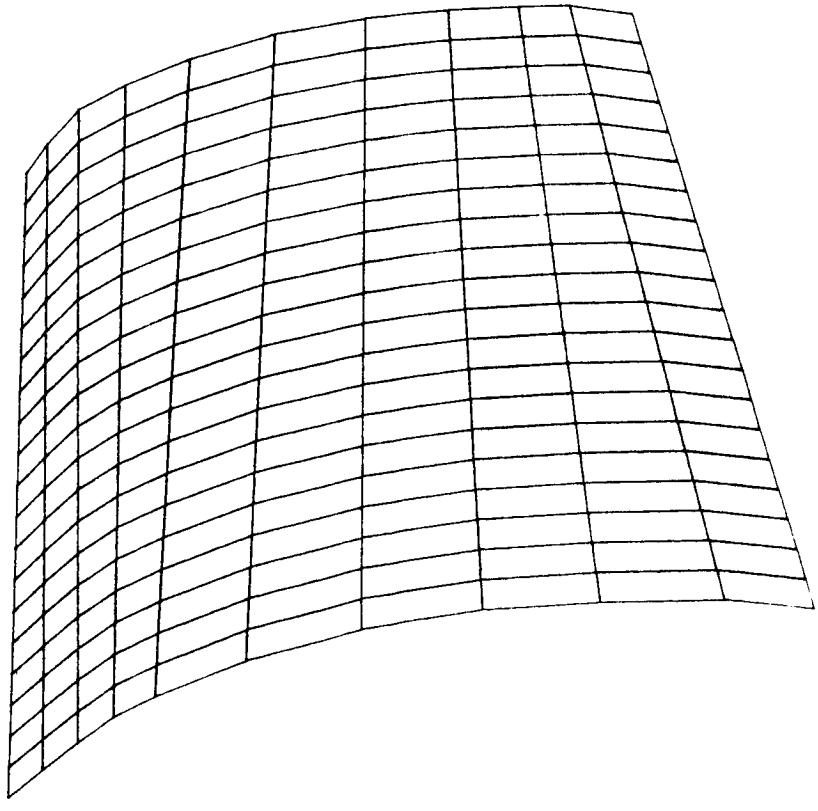

Fig. 5b

PROBABILISTIC SSME BLADES STRUCTURAL RESPONSE UNDER RANDOM PULSE LOADING

Michael Shiao, Robert Rubinstein, and Vinod K. Nagpal
Sverdrup Technology, Inc.
Lewis Research Center Group
Cleveland, Ohio

The purpose of this work is to develop models of random impacts on a Space Shuttle Main Engine (SSME) turbopump blade and to predict the probabilistic structural response of the blade to these impacts. The random loading is caused by the impact of debris. The probabilistic structural response is characterized by distribution functions for stress and displacements as functions of the loading parameters which determine the random pulse model. These parameters include pulse arrival, amplitude, and location. The analysis can be extended to predict level crossing rates. This requires knowledge of the joint distribution of the response and its derivative.

The model of random impacts chosen allows the pulse arrivals, pulse amplitudes, and pulse locations to be random. Specifically, the pulse arrivals are assumed to be governed by a Poisson process, which is characterized by a mean arrival rate. The pulse intensity is modelled as a normally distributed random variable with a zero mean chosen independently at each arrival. The standard deviation of the distribution is a measure of pulse intensity. Several different models were used for the pulse locations. For example, three points near the blade tip were chosen at which pulses were allowed to arrive with equal probability. Again, the locations were chosen independently at each arrival.

The structural response was analyzed both by direct Monte Carlo simulation and by a semi-analytical method. In the Monte Carlo method, appropriate random number generators were used to develop simulated pulse arrival processes. These processes were used as forcing functions in a dynamic analysis of the SSME blade implemented by the computer code STAEBL (Structural Tailoring of Engine Blades). The dynamic analysis originally used by this program was a modal superposition based on up to five modes; this analysis was replaced by a direct time integration which used the Newmark Beta Algorithm.

In the semi-analytical method, the classic analysis of shot noise by S. O. Rice was generalized to the present problem. This analysis requires that the unit pulse response of the blade be known at each point where a pulse can arrive. The unit response was found by numerical simulation using the STAEBL code. Once the unit pulse response is known, all required distribution functions are developed analytically.

Comparisons between the Monte Carlo studies and the semi-analytical method showed excellent agreement. Of course, the semi-analytical method has the advantage of requiring considerably less computer time to implement.

An analysis was begun of the joint distribution of response and its time derivative. This joint distribution can be used to predict level crossing rates which are frequently used in fatigue life predictions. The joint distributions were evaluated both by direct simulation and semi-analytically. In this case, the Monte Carlo simulations require very long integration times to produce smooth distributions.

Possible extensions of this work include clustering effects in level crossings, direct simulation of the level crossing process, and analysis of the distribution of extreme values.

OBJECTIVE

Estimate the influence of random loading on

SSME blade responses

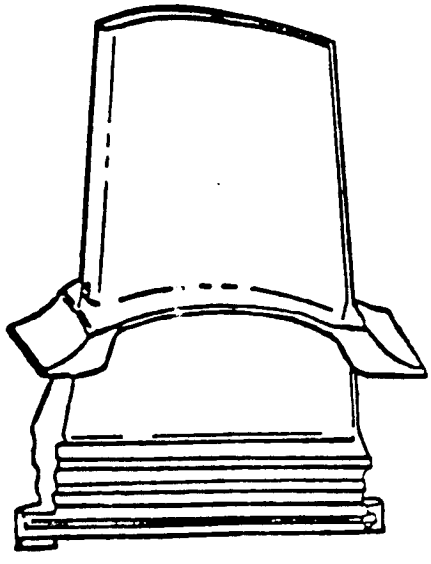

SSME BLADE

RANDOM LOADINGS

1. Pulse
2. Pressure
3. Temperature
4. Centrifugal

RANDOM IMPULSE LOADING

- o Poisson arrival pattern
- o Random impulse amplitude
- o Random impulse location

RANDOM STRUCTURAL RESPONSES

- o Natural Frequency
- o Root Stress
- o Tip Displacement

RANDOM RESPONSES DUE TO RANDOM IMPULSE LOADING

- Three Response Models

(1) $Y_1(t) = \Sigma\ h(t-t_k)$

$h(t)$ = Unit Impulse Response

t_k = A Poisson Process

(2) $Y_2(t) = \Sigma\ a_k\ h(t-t_k)$

a_k = Random Amplitude

(3) $Y_3(t) = \Sigma\ a_k\ h_k(t-t_k)$

$h_k(t)$ = Ranodm Unit Impulse Response (Random Pulse Location)

Probabilistic characteristics of model 1 and 2 are partially known

PROBABILITY CHARACTER OF SSME BLADE RESPONSE SUBJECTED TO RANDOM PULSE LOADING

- Model 1

$$Y(t) = \sum h(t-t_k)$$

- Probability Density Function of $Y(t)$

$$f_Y(y) = e^{-\lambda T} \sum_{k=0}^{\infty} \frac{g_k(y)\ (\lambda T)^k}{k!}$$

- Joint Probability Density Function of $Y(t)$ and $\dot{Y}(t)$

$$f_{Y\dot{Y}}(y,\dot{y}) = e^{-\lambda T} \sum_{k=0}^{\infty} \frac{g_k^*(y,\dot{y})\ (\lambda T)^k}{k!}$$

where λ = Poisson Arrival Rate

T = Unit Impulse Response Duration

$g_k(y)$ = k-Fold Convolution of Probability Density function of $h(t)$

$g_k^*(y,\dot{y})$ = k-Fold Convolution of Joint Probability density function of $h(t)$ and $\dot{h}(t)$

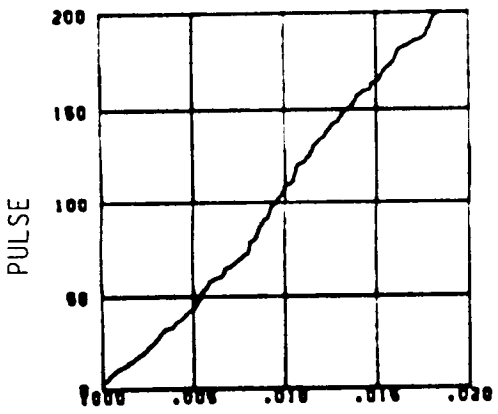

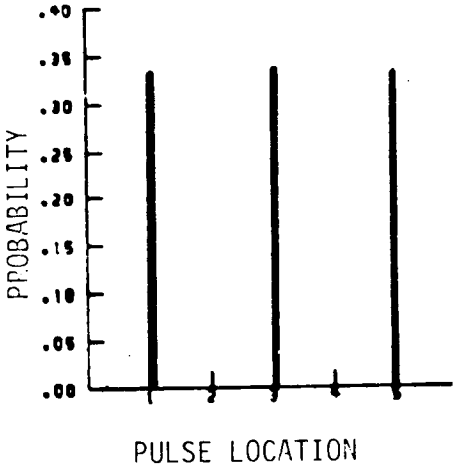

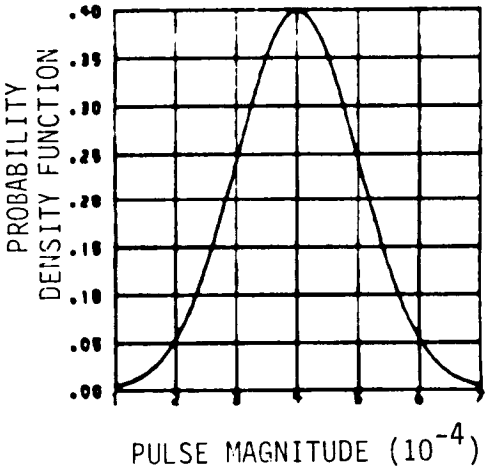

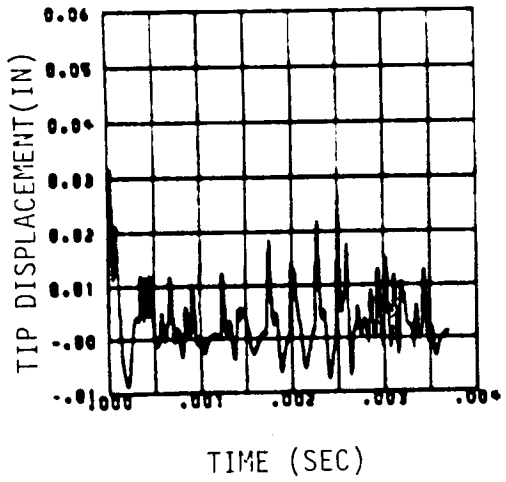

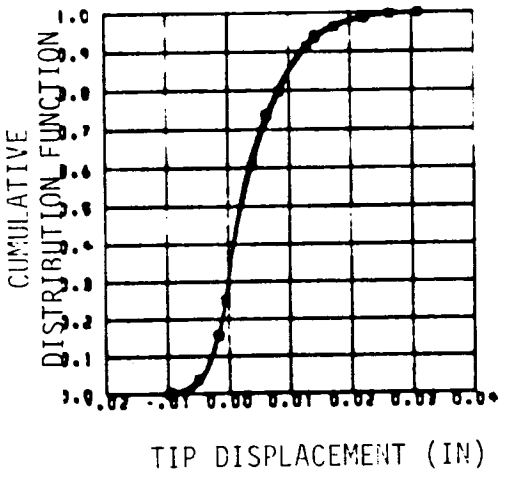

POISSON MEAN ARRIVAL RATE

= 5000/sec

o -- Semi-Analytical Result

□ -- Simulation Result

EXAMPLE 1 (MODEL 3)

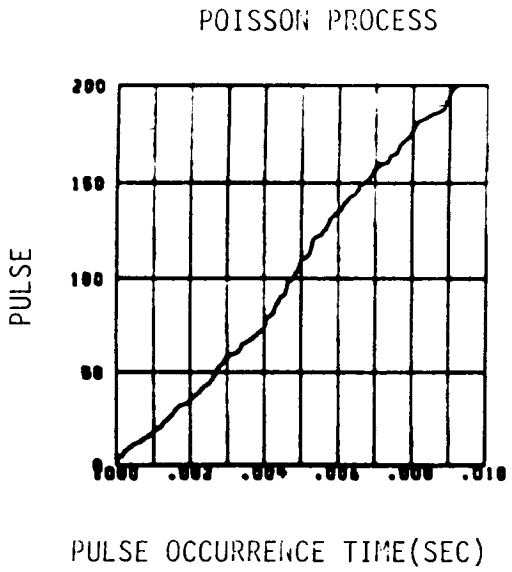

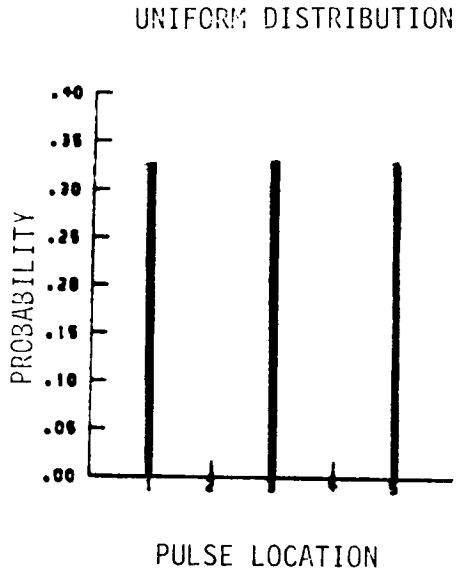

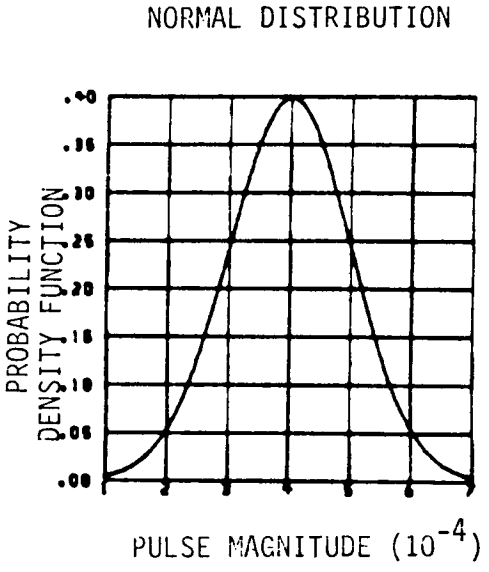

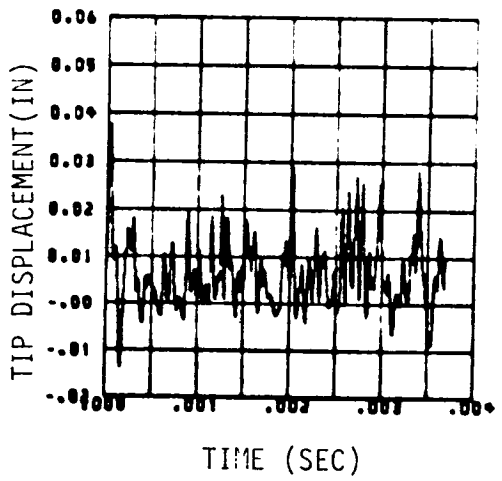

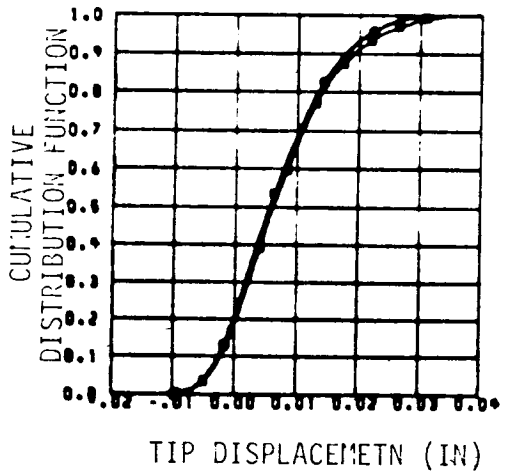

POISSON MEAN ARRIVAL RATE
= 10000/sec

o --Semi-Analytical Result

□ --Simulation Result

EXAMPLE 2 (MODEL 3)

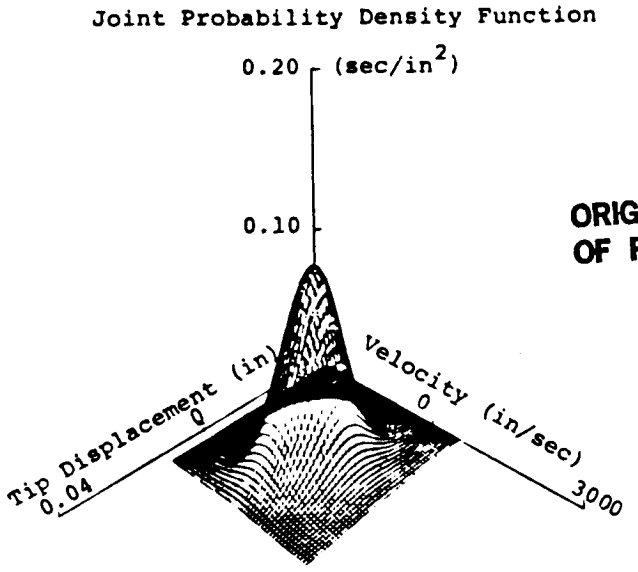

ORIGINAL PAGE IS
OF POOR QUALITY

Theoretical Joint
Probability Density Function

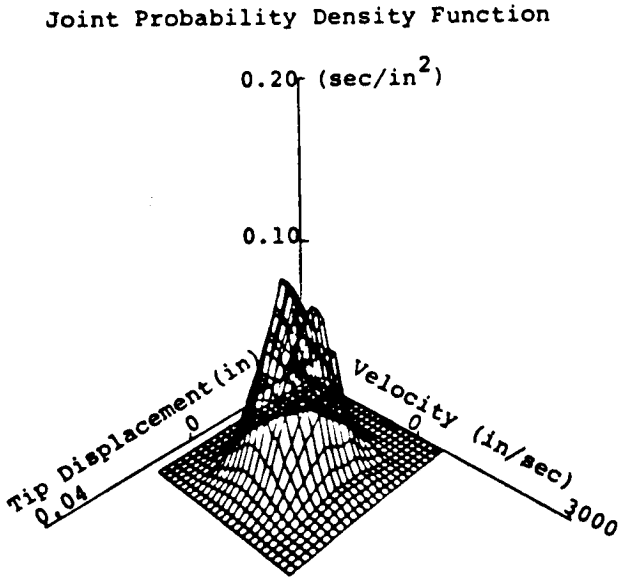

Simulated Joint
Probability Density Function

EXAMPLE 3 (MODEL 3)

QUANTIFYING UNCERTAINTIES IN THE STRUCTURAL RESPONSE OF SSME BLADES

Vinod K. Nagpal
Sverdrup Technology, Inc.
Lewis Research Center Group
Cleveland, Ohio

A probabilistic study on turbopump blades of Space Shuttle Main Engine (SSME) undertaken at NASA Lewis is reaching the three year mark. The ultimate objective of this study is to evaluate the effects of random variations, generally called uncertainties, in the geometry, material properties, loading and their probabilistic combinations on the structural response of the blade. The results obtained on geometric and material properties uncertainties demonstrate that a methodology using probabilistic structural analysis methods appears to be a powerful and unique approach to quantify uncertainties.

The application of this methodology can be extended to quantify the effects of random variations for other structural components also. Therefore, the development of the methodology has been discussed here in a rather generalized manner. This methodology consists of the following steps:

(1) The geometry and material properties can be randomly perturbed to simulate the realistic uncertainties. The simulation can be conducted using random numbers and using advanced perturbation techniques such as Monte Carlo's simulation. The random numbers can be selected to have any given probabilistic distributions which have known statistical properties. In this study, the normal distribution was selected with known mean and standard deviation.

(2) An analysis technique such as finite elements method can be used to estimate the structural response and provide means for discrete perturbations. The blade geometry and material properties were perturbed on the node and the element basis, respectively.

(3) Statistical experiment designs such as full factional design can be used to determine the effects of study variables. The advantage of using this design is that it is cost effective and provides the estimates of the effects of individual study variables and their interactions.

(4) The effects of all the study variables and their interactions can be evaluated for their significance using statistical tests. Further the probabilistic models can be developed to predict a mean response for given variations in the study variables. Probability distributions for response variables can also be developed for estimates of their range of variations. For this study, t-test, F-test, and χ^2-test were used.

To quantify the uncertainties associated with the geometry and material properties of a SSME turbopump blade, a computer code known as STAEBL was used. A finite element model of the blade used 80 triangular shell elements with 55 nodes and five degrees of freedom per node. The whole study was simulated on the computer and no real experiments were conducted. The structural response has been evaluated in terms of three variables which are natural frequencies, root (maximum) stress, and blade tip displacements.

The nodal coordinates (x, y, z) of the finite element mesh were perturbed to simulate the geometric uncertainties. The numbers of the material property matrix were perturbed for each element to simulate the material properties uncertainties. The perturbations were generated by a random number generator with preselected means and standard deviations. The magnitudes of means and standard deviations for perturbations of both geometry and material properties, in this study, were taken as ten percent or less of the original values. These magnitudes were selected based on previous experimental results and experience.

The results of the study indicate that only the geometric uncertainties have significant effects on the response. Uncertainties in material properties have insignificant effects. Also, the material properties interaction effects, which were created by variation in both material properties and geometry together have been found to have insignificant effects. A set of probabilistic models has been developed to predict the structural response for any given variations in geometry and material properties. Separate probabilistic models for only geometry variations have also been developed. Statistical tests indicate that these models are good fits.

OBJECTIVE

CONDUCT PROBABILISTIC STRUCTURAL ANALYSIS OF SSME BLADES TO QUANTIFY UNCERTAINTIES ASSOCIATED WITH:

GEOMETRY

MATERIAL PROPERTIES

WHY?

EVALUATE TOLERANCE LIMITS

- HIGHER TOLERANCE
  LOWER COST

BLADE GEOMETRY

SSME HIGH-PRESSURE FUEL TURBOPUMP
1st STAGE TURBINE BLADE

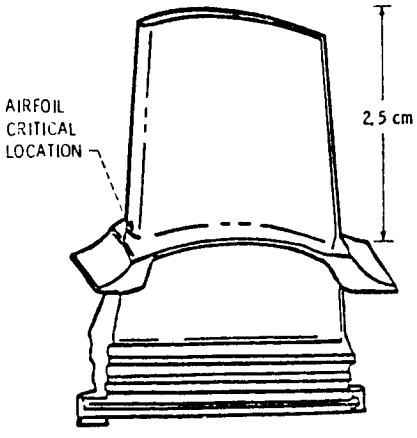

Figure 1.

METHODOLOGY

- Selected random distribution to simulate uncertainties
  Normal
- Modelled blade with finite element model
  80 Elements
  55 Nodes
- Used experiment design to perform simulation
  Full factorial design
- Analyzed response
  Probabilistic Models
  Probabilistic Distributions
  Statistical Tests

Figure 2.

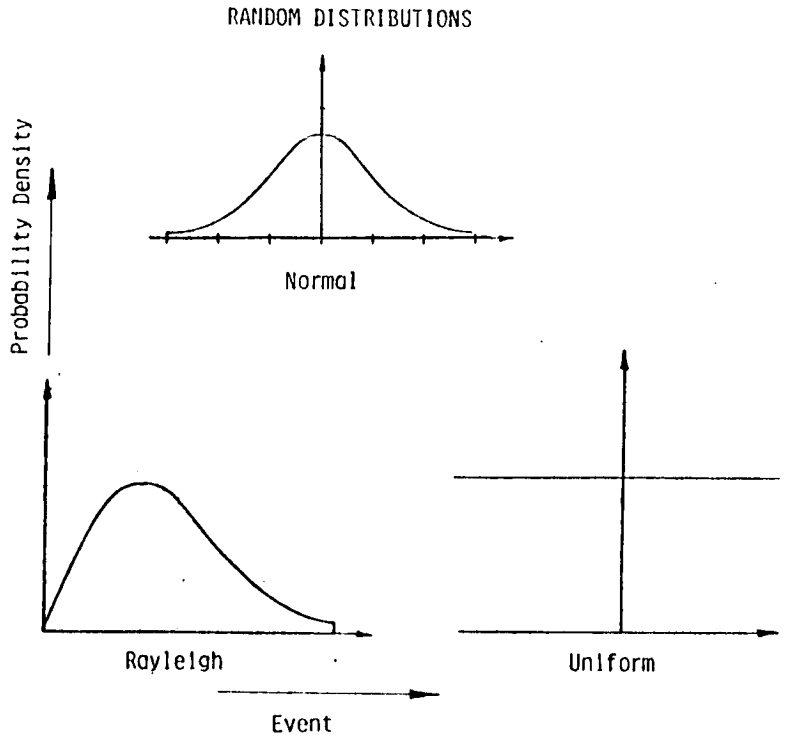

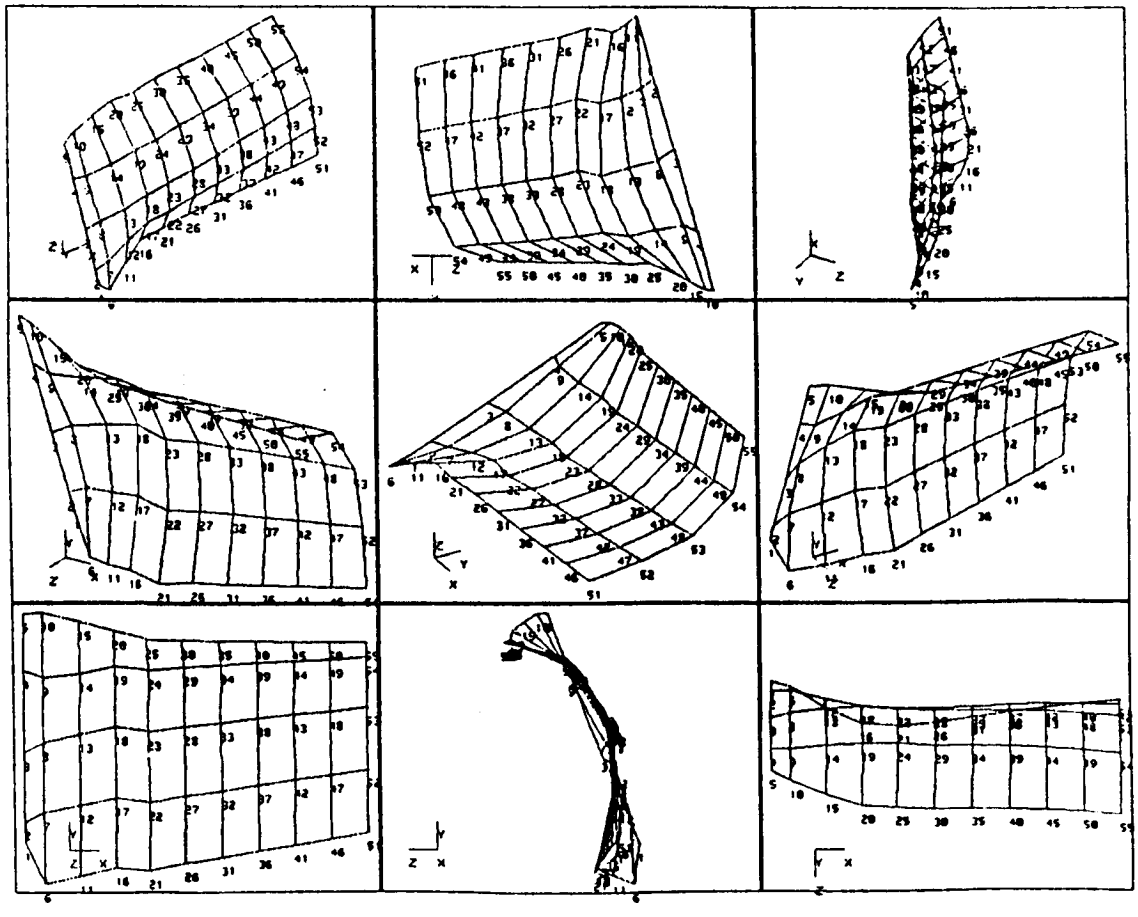

FINITE ELEMENT MODEL OF SSME BLADE

Figure 3.

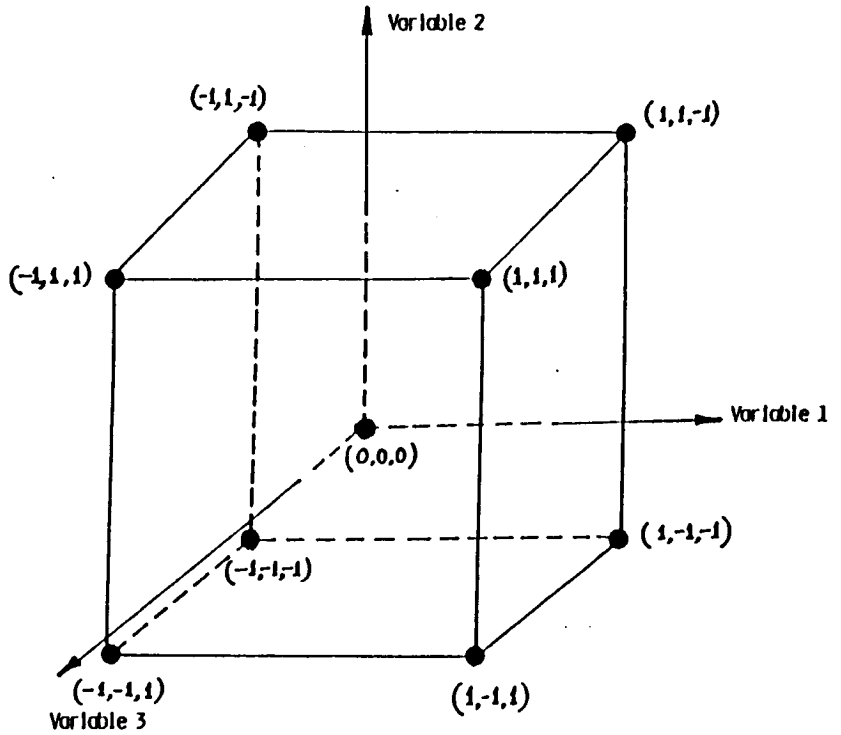

OPTIMIZED WAY OF STUDYING THREE VARIABLE EFFECTS

FULL FACTORIAL DESIGN

Figure 4.

STRUCTURAL RESPONSE

- NATURAL FREQUENCIES
  - First
  - Second
  - Third
- ROOT (MAXIMUM) STRESS
- TIP DISPLACEMENTS

Figure 5.

TABLE 1 - PROBABILISTIC MODELS - GEOMETRIC PERTURBATIONS

MODEL:

DEP. VAR. = CONSTANT + COEFF $*\mu_1$ + COEFF $*\mu_2$ + COEFF $*\mu_3$ + COEFF $*\sigma_4$ + COEFF $*\sigma_5$ + COEFF $*\sigma_6$

DEPENDENT VARIABLE	CONSTANT	COEFFICIENTS OF					
		μ_1	μ_2	μ_3	σ_4	σ_5	σ_6
FIRST FREQ.	6105.0	-832	-2915	-687	-8362	1897	-9348
SECOND FREQ.	9475.1	-1374	-2961	-408	-11398	-3869	-9095
THIRD FREQ.	15792.	-9434	27592	-7944	-17663	-4899	-44147
ROOT STRESS	63323.	49707	103320	4177	88960	-48191	283960
TIP DISPL.	.00196	.0119	.1287	.0206	-.0132	-.0419	.0067

F tests indicated that all models are good fits.

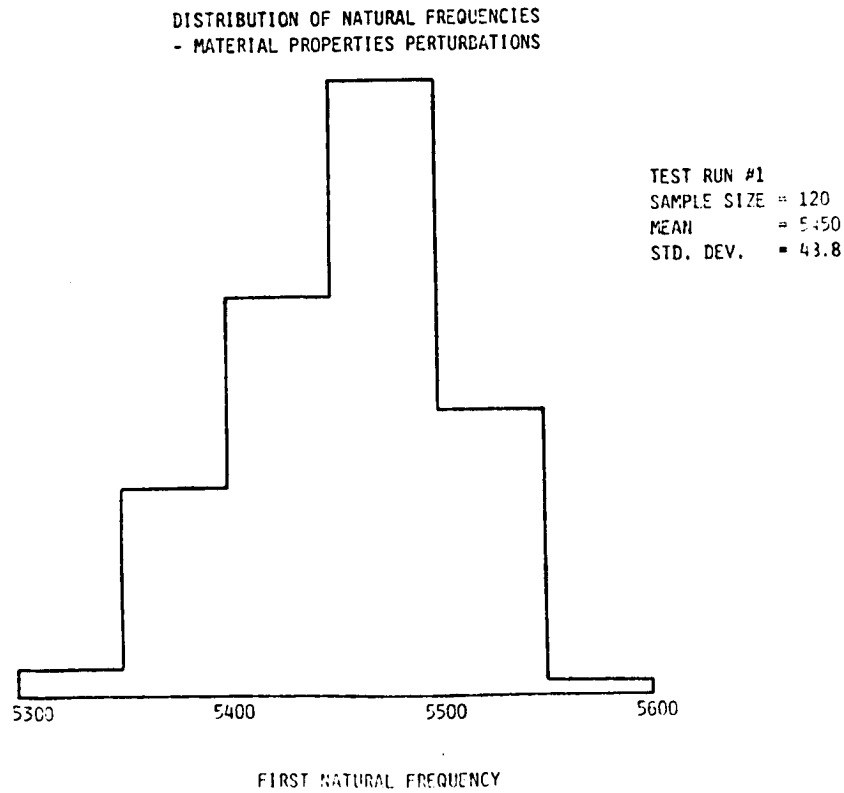

Figure 6.

STATISTICAL TESTS

- t-Test

$$t = \frac{\text{Value - Mean}}{\text{St. Dev.}}$$

- F-Test

$$F = \frac{\text{(Residual Sum of Squares)/D.F.}}{\text{(Regression Sum of Squares)/D.F.}}$$

- χ^2 Test

$$\chi^2 = \frac{(\text{Value - Mean})^2}{\text{Variance}}$$

- Plots

Figure 7.

CONCLUSIONS

- Methodology for SSME Blade has been developed and applied.
- Methodology can be extended to other structural components.
- Geometric uncertainties showed significant effect.
- Material properties uncertainties and their interactions have insignificant effects.
- Range of variation in response quantified.

Figure 8.

COMPOSITE LOAD SPECTRA FOR SELECT SPACE PROPULSION STRUCTURAL COMPONENTS*

J. F. Newell
Rocketdyne Division, Rockwell International
Canoga Park, California

The objective of this program is to develop generic load models to simulate the composite load spectra (CLS) that are induced in space propulsion system components representative of the space shuttle main engines (SSME). These models are being developed through describing individual component loads with an appropriate mix of deterministic and state-of-the-art probabilistic models that are related to key generic variables. Combinations of the individual loads are used to synthesize the composite loads spectra.

A second approach for developing the composite loads spectra load model simulation, the option portion of the contract, will develop coupled models which combine the individual load models. Statistically varying coefficients of the physical models will be used to obtain the composite load spectra.

The need for this type of technology advancement is apparent from the demand for higher performance, lighter weight, components that yield higher operating pressures, temperatures, vibration and flow loads, Figure 1. The difficulty in installation, cost, and potential for new failure mechanisms limit the required instrumentation to adequately define or verify loads. Proper quantification of loads are required to minimize adding conservatism on conservatism and to specify results so they can be accurately used for structural analysis and risk assessment.

Rocketdyne is teamed with Battelle to develop this methodology. Rocketdyne is using their background and expertise for the advancement in the loads definition and analysis methods along with the extensive SSME test database for comparitive information. Battelle is utilizing their expertise to develop an advanced probabilistic code to represent the individual loads and load spectra. Rocketdyne is packaging this total work in an easy to use expert system type code. The following discussion covers an overview and Rocketdyne's effort. Battelle's contribution is presented in a separate report.

The CLS development is a 3-year base program with a 2-year option program. The first 2 years of the base program have been completed. The effort has three major tasks: probabilistic model theory and development, code development and code validation and verification, Figure 2. Four classes of rocket engine components are being used as examples for the load development--turbine blades, transfer ducts, LOX posts and engine system ducts, Figure 3 and 4. The available SSME instrumentation for use in developing SSME related statistical data and load verification are also shown in Figure 3.

*work performed under NASA Contract NAS3-24382

The probabilistic modeling requires simulation of the individual loads summarized in Figure 5. Several shape simulations are required to characterize these loads. The start and cutoff transients include a nominal, random over nominal and spike load shape. The overall duty cycle required to define engine operating conditions is represented as a nominal shape with a random variation about the mean value. The basic nominal shapes of the duty cycle operational requirements and inlet parameter operation bounds are controlled by the engine contract requirements. These requirements are based on vehicle thrust and operation needs, Figure 6. Environments like vibration have a nominal variation dependent on a components power and/or speed, random variation from hardware geometry and test to test conditions and transient spikes from side loads, pops and chugs. The steady state dynamic loads are represented in the frequency domain for both random and sinusoidal loads, Figure 7.

Since the CLS methodology is to be applied to advanced engines, the loads are being developed from a generic basis. The use of hardware specific random variations like pump efficiency, head rise or flow resistance allow for engine to engine load variations. Accounting for variations in power level, pump speed, and engine inlet operating conditions allow for test to test variation, Figure 8. The use of key variables and appropriate physical and probabilistic models assures the methodology is applicable to variations in the SSME or to new rocket engine designs. The results obtained from the loads spectra models are being compared with available SSME engine measured results and available analytical calculations.

The probabilistic loads model being developed by Battelle is implemented as part of an expert system developed as part of the program. The expert system is a tool to generate and analyze composite loads of a rocket engine design and to supply these loads for use in either deterministic or probabilistic finite element computer codes to perform structural analysis of engine components. The probabilistic models are generic; the statistical information utilized is primarily from the SSME test database. Expert opinion and other engine background data are used where appropriate to complete the loads picture.

The knowledge-based system manages the database, provides expert knowledge relative to the generic probability loadings and generates the individual and composite loads, Figure 9. The Battelle developed ANLOAD module performs the probabilistic modeling and statistical analysis. A database system has been developed to efficiently represent the knowledge. This database system facilitates the communication between the expert system and the knowledge base. The current knowledge base contains information for SSME type engines, system type loads using the influence coefficient method, and local turbine blade load scaling methods.

The expert system is a rule based system. The rules are modularized where each module is designed to solve a particular problem or to perform a task. The load expert system LDEXPT Version 2.0, Figure 10, has rule modules for engine system dependent loads for all four components as well as selected individual local component loads. The rules so far mostly relate to overall process control and information retrieval, Figure 11. The on-going rule development is working on local individual load components and the more complex composite load spectra. Knowledge for the transfer ducts is partially developed and is being added to the system. The other two component loads are being developed.

FIGURE 1
NEED FOR PROBABILISTIC TECHNOLOGY

- INCREASED PERFORMANCE REQUIREMENTS MEAN HIGHER LOADS AND ENVIRONMENTS
- LARGE CHANGES FROM PAST EXPERIENCE BASE
- LIMITED HARDWARE AND TESTING
- DIFFICULTY IN OBTAINING LOCALIZED MEASURED DATA
- DETERMINISTIC METHODS RESULT IN LAYERED CONSERVATISM-JUDGEMENTS, ASSUMPTIONS, MIN/MAX'S
- PROBABILISTIC APPROACH FURNISHES
  - QUANTIFIED LOAD DISTRIBUTIONS
  - SENSITIVITY TO LOAD AND STRUCTURAL VARIATIONS
  - ABILITY TO PROPERLY ASSESS RISK AND FAILURE MODES

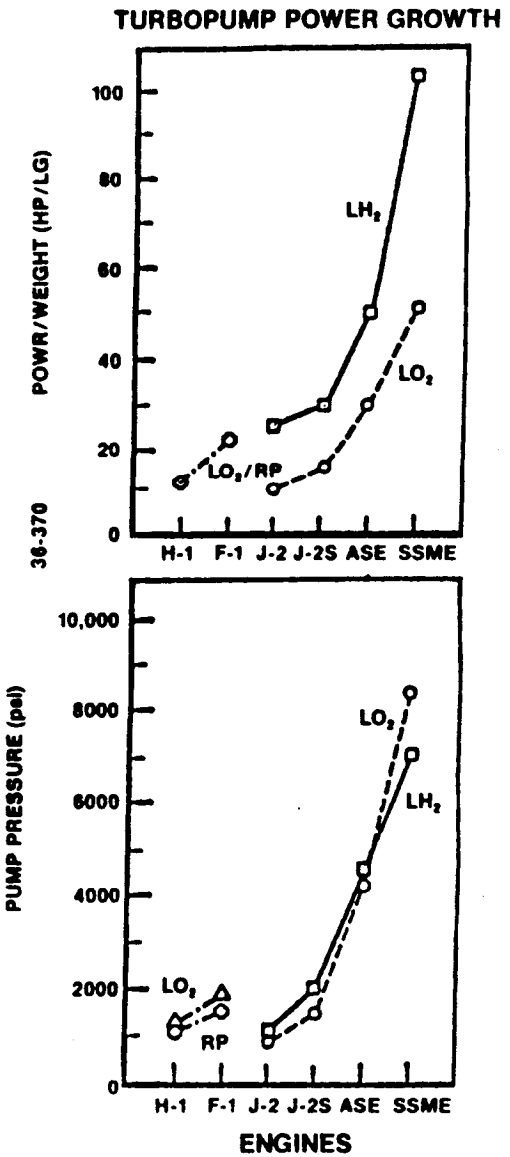

FIGURE 2

COMPOSITE LOADS SPECTRA
BASE PROGRAM

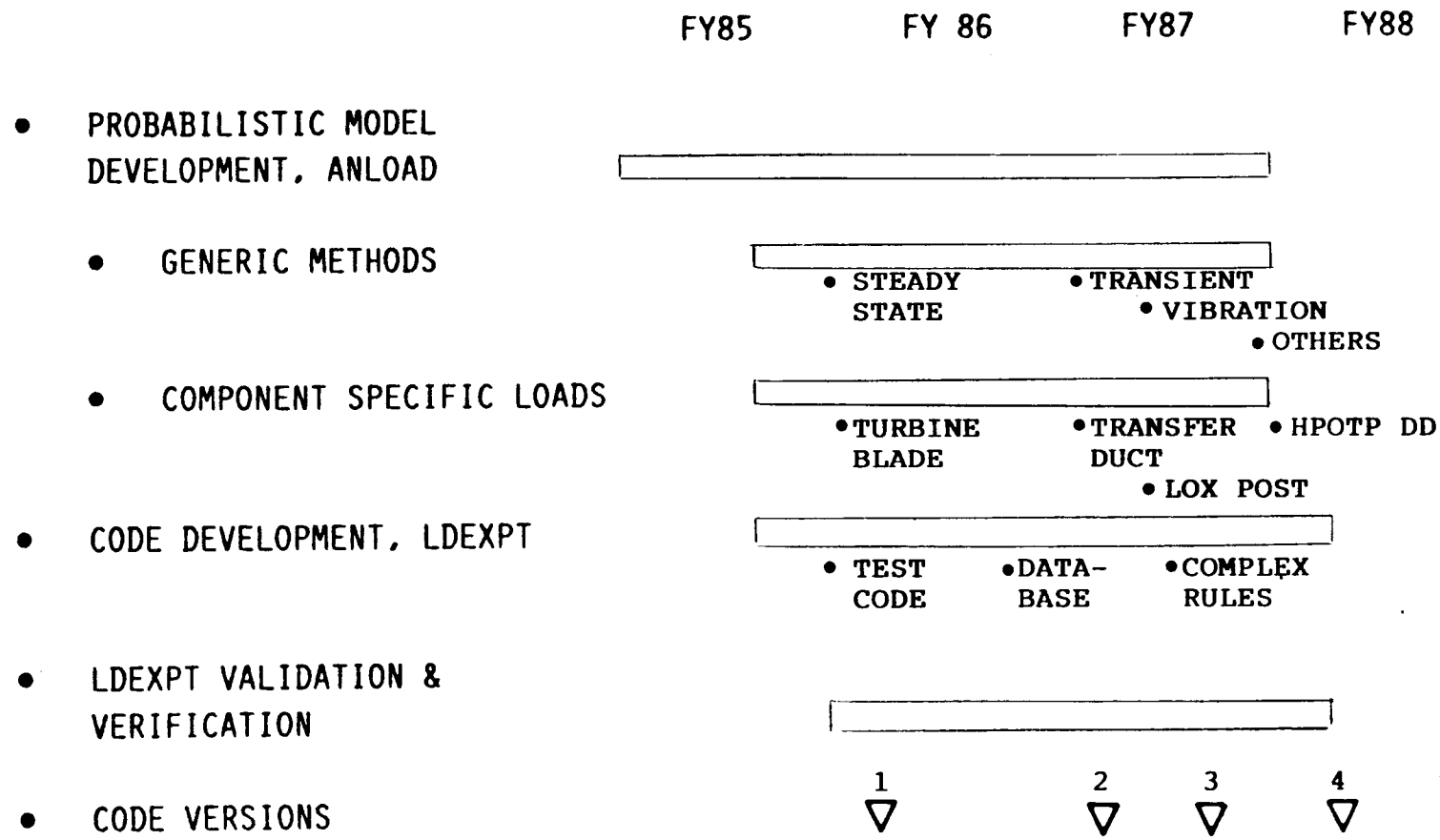

*COMPONENT IMPLEMENTATION AND
LOAD COMPLEXITY IMPROVED IN EACH CODE VERSION

FIGURE 3

CLS ANALYSIS
COMPONENTS AND STANDARD INSTRUMENTATION

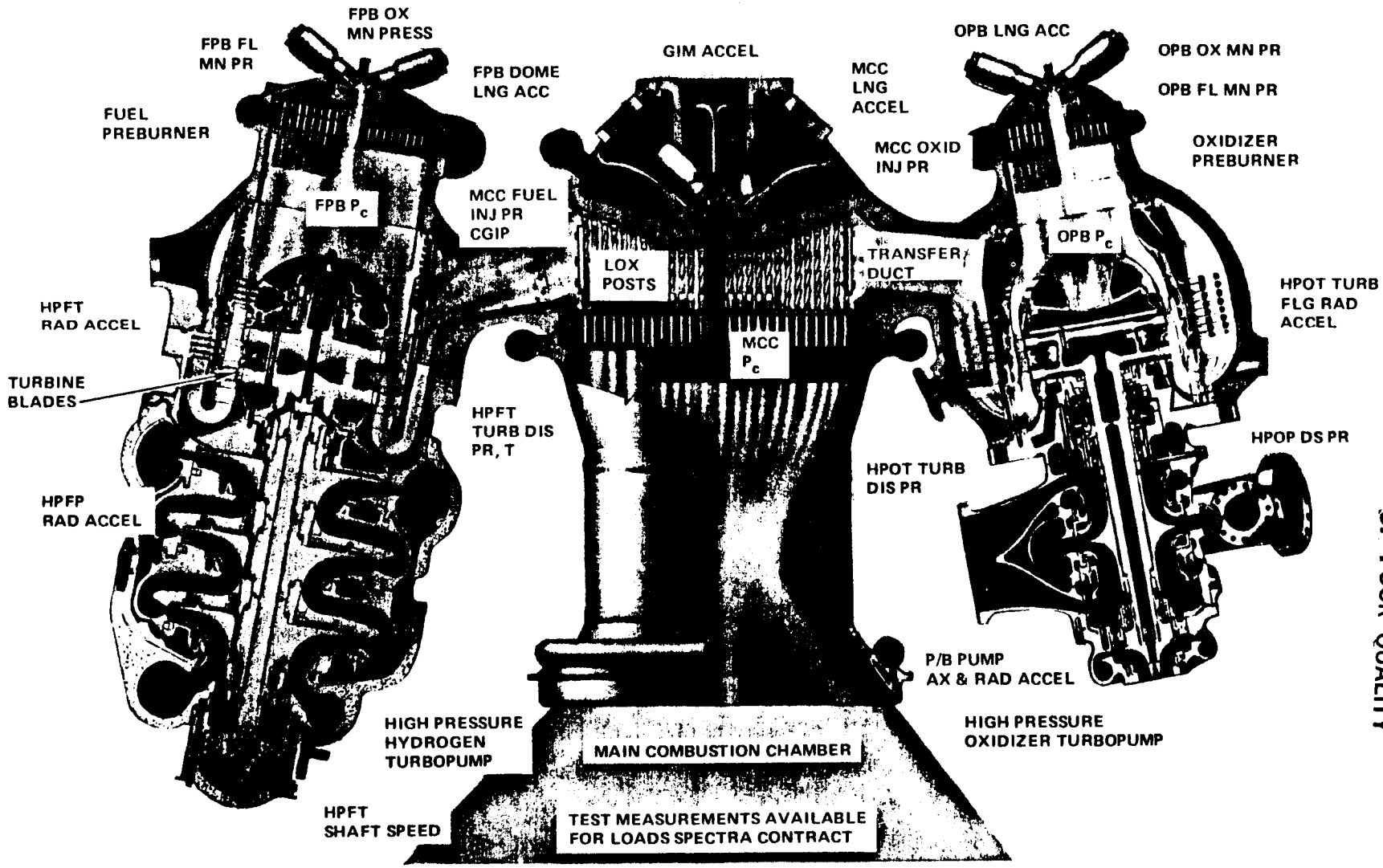

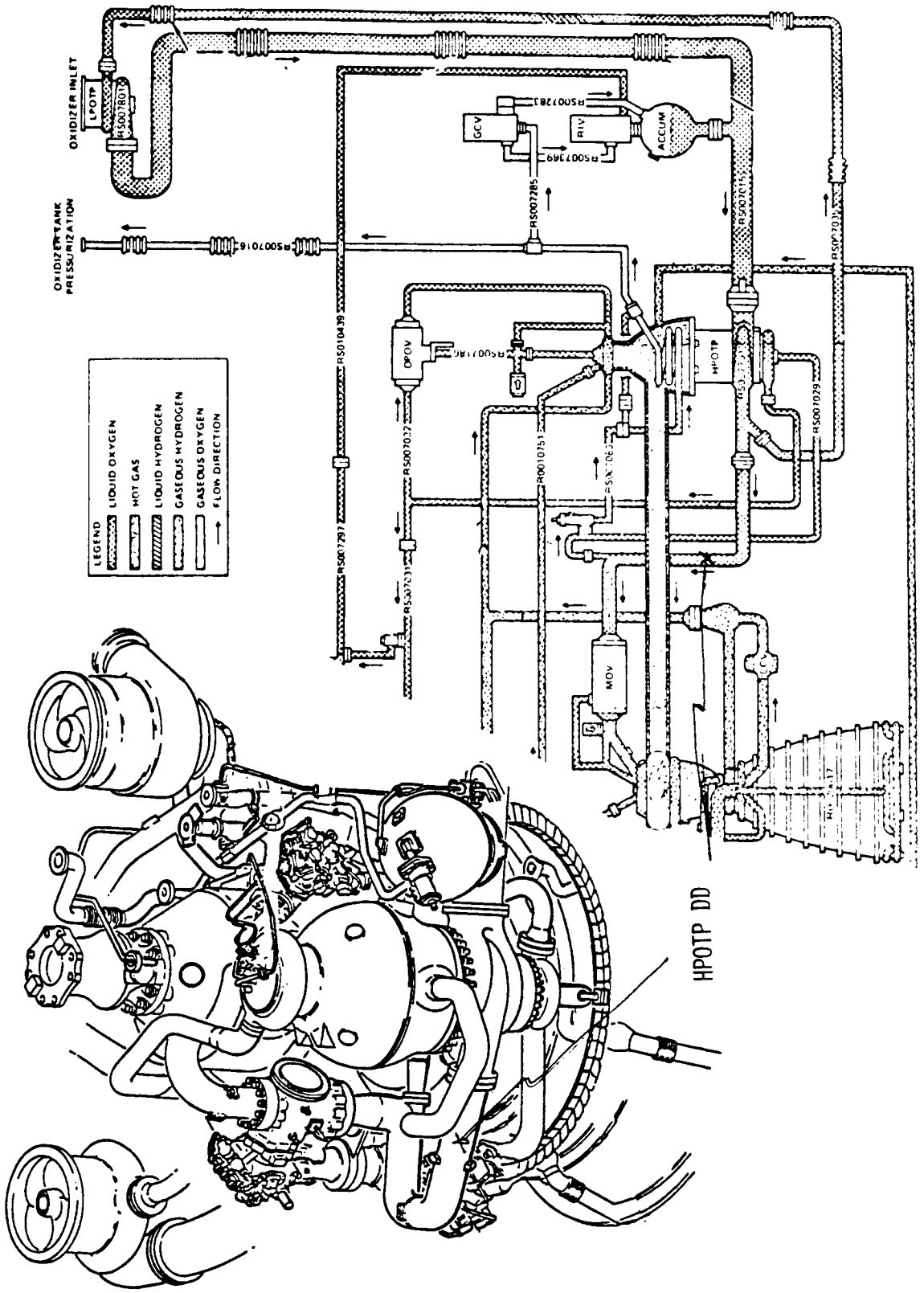

FIGURE 4
HIGH PRESSURE PUMP DISCHARGE DUCT

FIGURE 5

SUMMARY MATRIX OF INDIVIDUAL LOADS VS COMPONENTS

INDIVIDUAL LOAD	TURBINE BLADE	TRANSFER DUCT	LOX POST	HPOTPDD	LOAD FORM
• STATIC PRESSURE	X	X	X	X	DUTY CYCLE*
• DYNAMIC PRESSURE					
• CHUGGING(TRANSIENT)	-	X	-	-	AMS, STATOS
• TURBULENCE					
• SINUSOIDAL (REPEATED PULSE)	X	X			AMS, PSD, STATOS
• RANDOM	-	X	X	X	AMS, PSD
• CENTRIFUGAL	X	-	-	-	DUTY CYCLE*
• TEMPERATURE	X	X	X	X	DUTY CYCLE*
• STRUCTURAL VIBRATION					
• TRANSIENT					
• SIDELOAD	-	X	X	X	AMS, STATOS
• POPS	-	X	X	-	AMS, STATOS
• STEADY STATE					
• SINE	-	X	X	X	AMS, PSD, STATOS
• RANDOM	-	X	X	X	AMS, STATOS
• DEBRIS	X	X	X	-	HISTORY
• RUBBING	X	-	-	-	EXPERT OPINION
• INSTALLATION	-	-	X	X	EXPERT OPINION
• FAB	X	X	X	X	
• FRICTION	X	X	X	-	PSEUDO LOADS
• TOLERANCES	X	X	X	X	

*LOW FREQ. & TRANSIENT

FIGURE 6
CONTRACTURAL REQUIREMENTS

- POWER LEVEL
  - TRANSIENT
  - STEADY STATE
- MIXTURE RATIO - OXIDIZER TO FUEL MASS FLOWRATE REQUIREMENTS AT PUMP INLETS
  - PRESSURES
  - TEMPERATURES

SSME THRUST BUILD-UP LIMITS

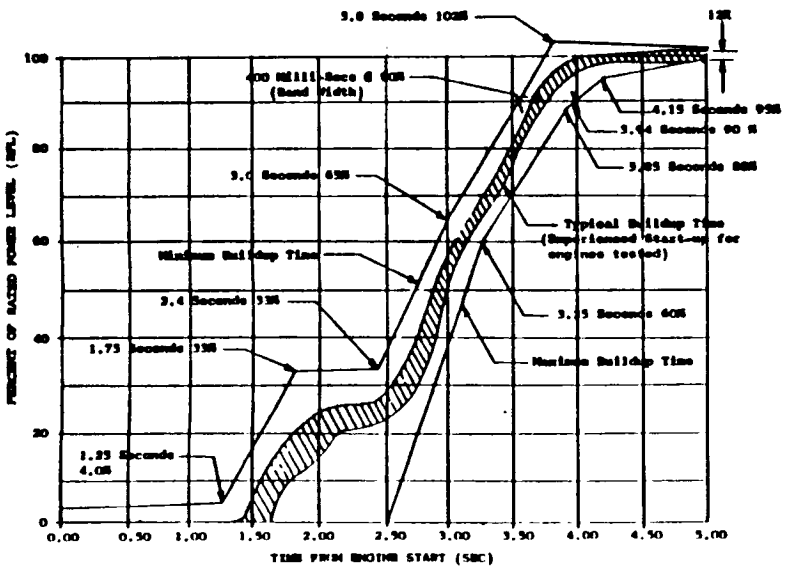

SSME FLIGHT DUTY CYCLE

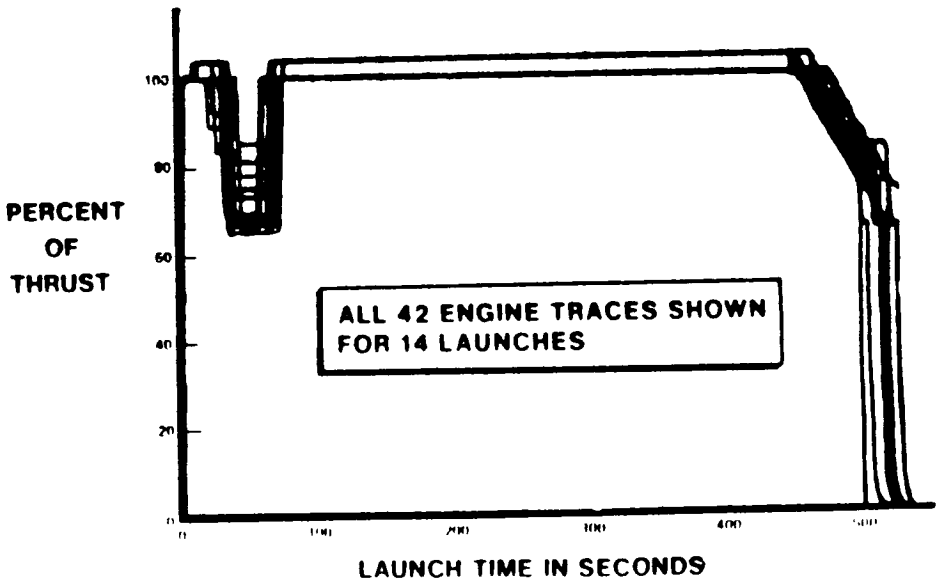

FIGURE 7

MECHANICAL VIBRATION

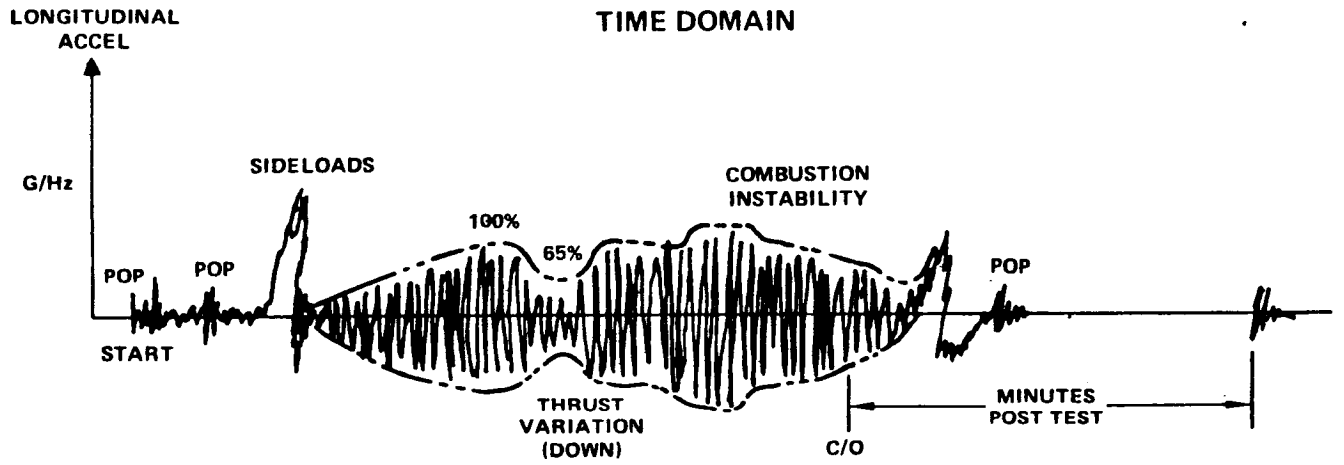

FREQUENCY DOMAIN

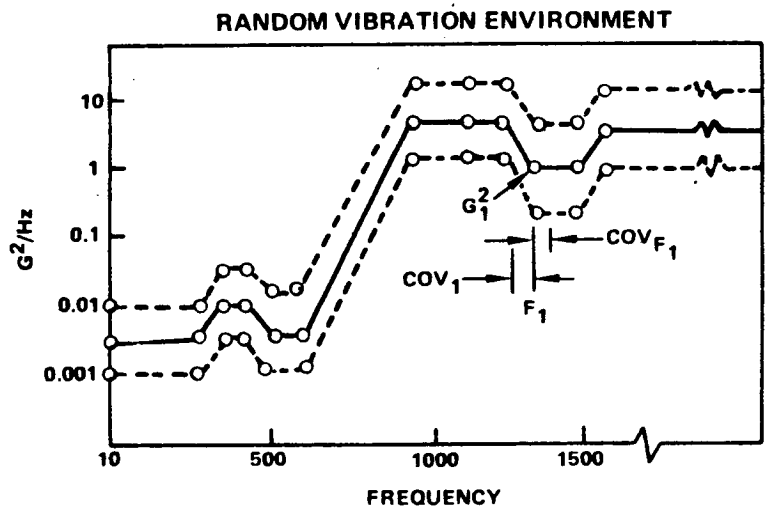

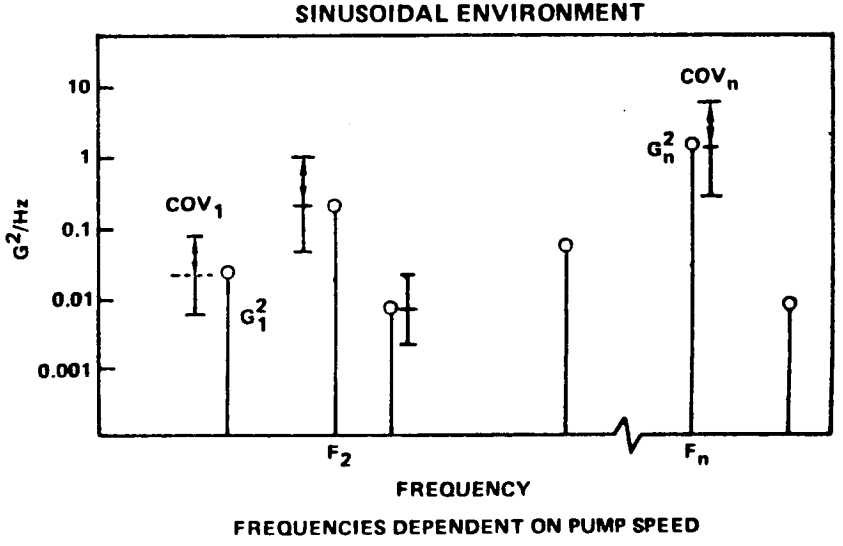

FREQUENCIES DEPENDENT ON PUMP SPEED

FIGURE 8

SYSTEM CLASS OF LOADS

- STEADY STATE
  - DIRECT VARIABLES - THRUST, INLET CONDITIONS
  - RANDOM VARIABLES - HARDWARE, TEST VARIATIONS
- TRANSIENTS
  - START AND CUTOFF CONTROLLED
  - LOCAL EFFECTS

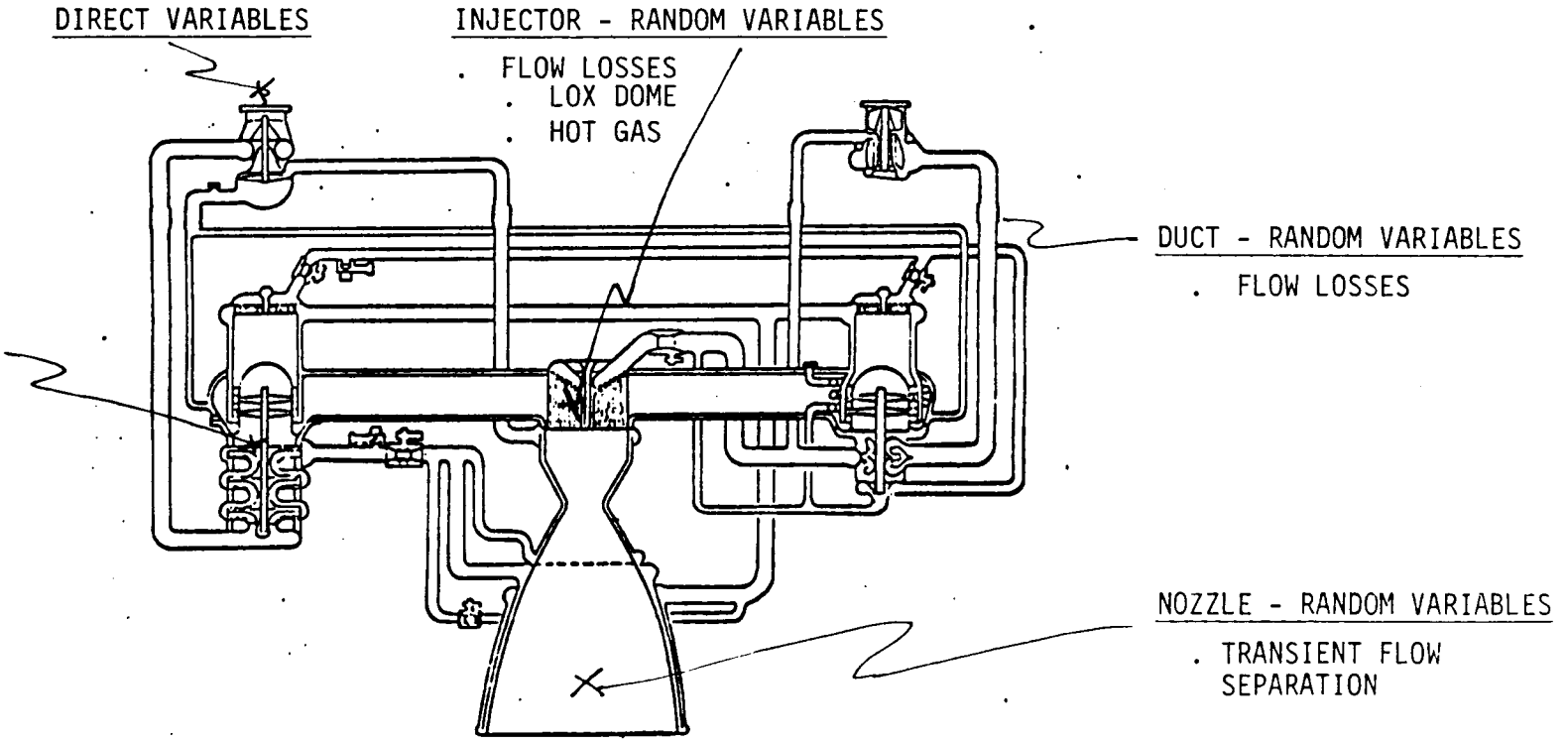

FIGURE 9
LDEXPT LOAD EXPERT SYSTEM

- EXPERT SYSTEM DRIVER
  - DECISION TREE INFERENCE
  - QUERY ON THE DATABASE KEY VARIABLES
- LOAD DATABASE SYSTEM
  - STAND-ALONG DATABASE SYSTEM
  - EXPERT SYSTEM INTERFACE
    - KEY VARIABLES ARE ATTRIBUTES OF THE EXPERT SYSTEM
    - USER/EXPERT SYSTEM SELECT OPTIONS ON KEY VALUES
- SIMPLE WORKING MEMORY MODEL
  - PASSING INFORMATIONS BETWEEN RULE MODULES
- LDEXPT RULE MODULES
  - IMPLEMENTING PROCESS AND CONTROL KNOWLEDGE
    - E.G. RETRIEVING LOAD INFORMATION
  - IMPLEMENTING PROBLEM-SOLVING KNOWLEDGE
    - E.G. SELECTING INDEPENDENT LOADS BASED ON GAINS

FIGURE 10

LDEXPT-LOAD EXPERT SYSTEM

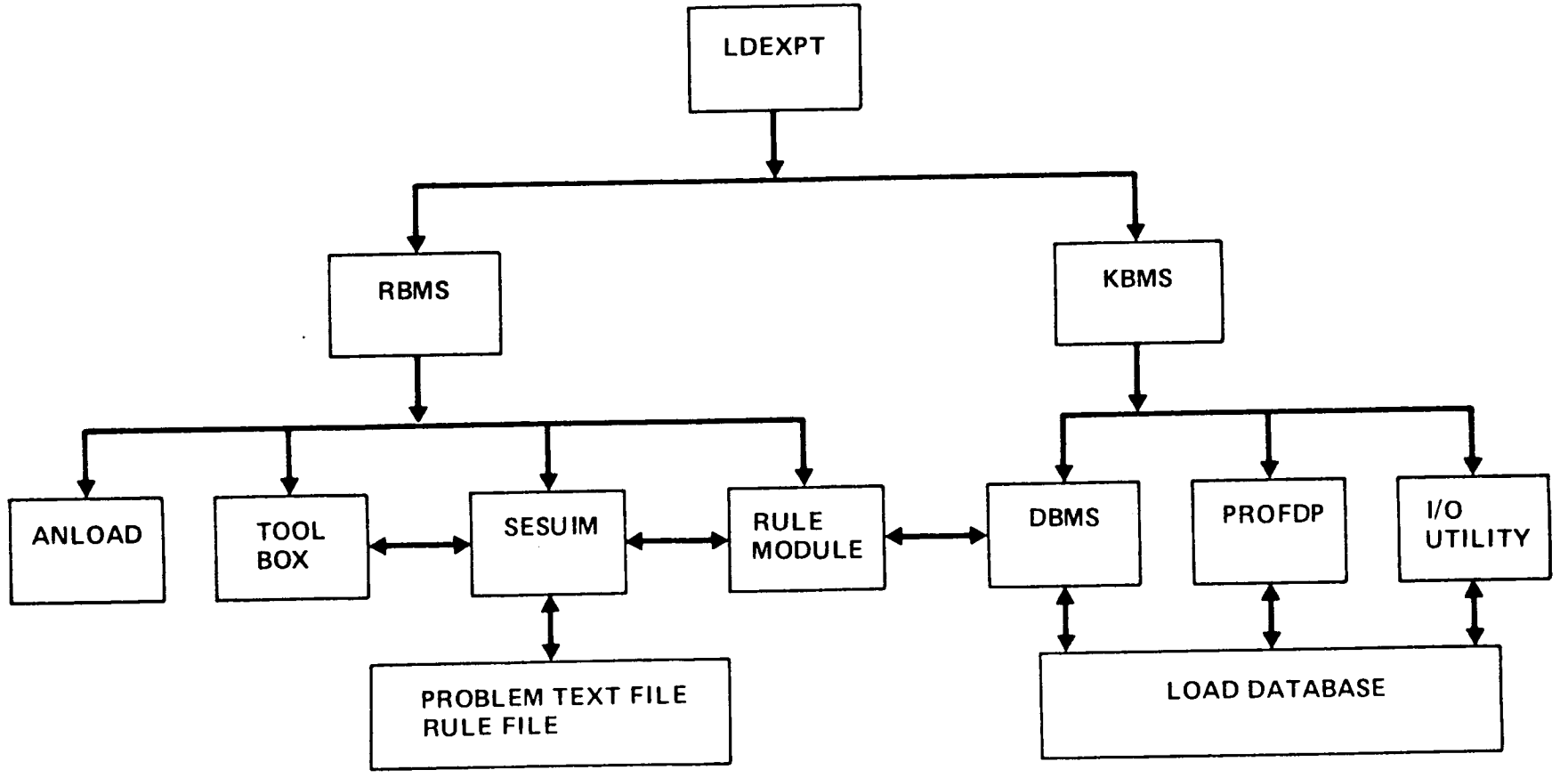

FIGURE 11
LDEXPT LOAD EXPERT SYSTEM

- RULE MODULES
  - MODULAR DESIGN FACILITATES INCREMENTAL DEVELOPMENT
  - COMMUNICATION BETWEEN RULE MODULES IS ACHIEVED WITH THE WORKING MEMORY MODEL
- EXAMPLE: RULE MODEL FOR INFLUENCE COEFFICIENT MODEL

  IF THE DEPENDENT LOAD ID IS N AND THE USER REQUESTS A POINT VALUE OF THE DEPENDENT LOAD CONTRIBUTED FROM THE M MOST INFLUENTIAL INDEPENDENT LOADS

  THEN THE EXPERT SYSTEM WILL SELECT THE M MOST INFLUENTIAL INDEPENDENT LOADS FROM THE LOAD DATABASE, RETRIEVE THE INFLUENCE COEFFICIENT SET AND PERFORM THE DETERMINISTIC INFLUENCE COEFFICIENT MODEL CALCULATION TO OBTAIN THE DEPENDENT LOAD VALUE

PROBABILISTIC LOAD MODEL DEVELOPMENT AND VALIDATION FOR COMPOSITE LOAD SPECTRA FOR SELECT SPACE PROPULSION ENGINES

R. Kurth
Battelle Memorial Institute
Columbus, Ohio

and

J.F. Newell
Rocketdyne Division, Rockwell International
Canoga Park, California

A major task of the program to develop an expert system to predict the loads on selected components of a generic space propulsion engine is the design, development, and application of a probabilistic loads model. This model is being developed in order to account for the random nature of the loads and assess the variable load ranges' effect on the engine performance.

There are several requirements of the probabilistic load model which restrict the use of some probabilistic methodologies. First, the methodology must be capable of addressing four different shapes for the sample paths in the stochastic processes describing the loads: nominal, random, spike (rare event), and periodic. This implies that the model must be capable of approximating a variety of different forms for the load processes, some, or all, of which may be non-stationary. Second, the model must be applicable to generic engines operating under a wide variety of possible mission history profiles, typified by the demanded power levels. This requirement implies that the model must be capable of dealing with both random variables, as well as stochastic processes, that may not be describable by standard distributional forms, for example bimodal behavior or discrete (on-off) processes. Also, there are sixty to seventy individual loads and/or engine parameters that can affect the composite load calculations (although, usually only ten to thirty of these are important for a single, specific composite load calculation), and, therefore, the methodology must be as efficient as possible without incurring a substantial loss of accuracy. Finally, the methodology is required to provide varying levels of accuracy, the level to be user specified.

A probabilistic model capable of addressing each of these topics has been developed. The model is based primarily on simulation methods, but also has a Gaussian algebra method (if all variables are near normal), a fast probability integrator routine (for the calculation of low probability events), and a separate, stand alone program for performing barrier crossing calculations. Each of these probabilistic methods has been verified with theoretical calculations using assumed distributional forms. The results of the these verification studies are discussed in the full presentation.

The governing philosophy for the probabilistic methodology is that each process can be described by a probability density function. To implement this philosophy for stochastic processes, approximate methods for modeling the mission history profile are needed during portions of the mission. Independent (controller), individual loads and engine parameters are treated as random variables whose distributional form and parameters are determined by the controller demanded power level (thrust). The dependent, individual loads and composite loads are then modeled by assuming a quasi-steady state system. This implies that during the power up and down, and throttle up and down phases of a mission the time step size be sufficiently small to warrant a steady state approximation, from the probabilistic point of view. That is, the physics may not be in a quasi-steady state, but it can be assumed that the loads of interest are stationary during this time. Between time steps the non-stationary loads are adjusted according to the data base information, or user supplied input. An example of the coupling of quasi-steady state and steady state phases will be discussed.

For transient events, such as engine start and cut-off, the changes in the magnitude of the loads is both large (relatively) and of short duration (one to four seconds). For these events the load profile is not assumed to be quasi-steady in order to keep the time step size relatively large and reduce the computational time. Instead, the fluctuations about the nominal response are ignored and the random nature of the transient is contained in the variable amplitude and time of occurrence. The load is modeled as a piecewise linear response over the duration of the transient. For example, in a two-stage engine, the temperature in the fuel pump is expected to have two or three spike values before settling down to a relatively steady rate of increase to the full power operation temperature level. The occurrence, or non-occurrence, of the third peak is handled statistically as a random variable, as well as the amplitude of the peak and the time at which the peak amplitude occurs. Examples of the transient model, and its coupling to other mission phase types is provided.

Because the probabilistic model is treating the problem in the time domain, special attention must be paid to periodic, or sinusoidal, loads. Since their magnitudes are usually more sensitive to frequency than they are to any time dependency (other than the time dependency of the frequencies), they are treated separately in the probabilistic model.

At this time most of the available data for the model validation has been obtained from the space shuttle main engine program. The data which has been examined thus far appears to agree, within statistically accuracy, with the model predictions obtained from the validation studies. Further testing with other engine data is planned to demonstrate the generic capability of the model. An example of a validation analysis is provided.

INTRODUCTION

Probabilistic Load Analysis

- The primary goal is the development of a probabilistic methodology that is capable of handling any generic space propulsion engine

- Requires that any anticipated distribution of engine load or parameters must be addressable by the model

- Must be able to analyze, in a manner consistent with the stochastic process being modeled, either linear or non-linear ombinations of the inputs which may be non_stationary

Probabilistic Load Model

The above points have led to the development of a model based on the following points:

- Tabulation of means, variances, and distribution types for
- Scaling laws, or expert opinion, for modifications of data base for engines currently not included
- A probabilistic model that provides varying levels of sophistication for calculating the stochastic load processes
- Capability to analyze nominal, random, or periodic loads

PROBABILISTIC LOAD MODEL

Stochastic Processes

- The stochastic load processes are modeled using PDF's to describe the individual load variables and engine parameters

- There are four primary shapes that are modeled:
  (a) Nominal
  (b) Random
  (c) Spike
  (d) Peridoic

- Because the load is a stochastic process there are three different methods for displaying the results:
  (a) Nominal plot
  (b) Sample function plot
  (c) Probability tables of exceeding specified load levels

PROBABILISTIC LOAD MODEL
(continued)

Individual loads

- Probability density functions
- Data analysis, or calculated using engine influence coefficient

Composite loads

- User supplied:
  Mission history profile
  Accuracy required
  Output desired

- Composite load is calculated from the probabilistic method selected from the input accuracy needed and the desired output

Non–stationary processes

- Computer program decides if the individual loads are non–stationary (This option can be suppressed). If they are not stationary, then new distribution parameters are calculated based on the current power level

- Relatively small time step is used to approximate a stationary process over the time increment

Probabilistic Methodology

- Methodology based primarily on simulation methods

- Gaussian algebra, fast probability integrator (Wirsching and Wu), and barrier crossing methods are also available for specialized calculations

- Distribution fitting subroutine is included in the model to provide summary statistics on the stochastic processes or random variables

Displayed Output

- Discrete load level, with its associated probability
- Updated distributions for the individual load (where warranted) and composite loads at specified times
- Interface with printer plot or LOTUS plotting packages
- All output is stored on a file called DPD.OUT

Data Base Update

- If data analysis for individual load has been performed, it is inserted in the data base (not currently automated)
- The output for the composite load will be cataloged so that future users may simply refer to this analysis without having to re–do the entire calculation

Probabilistic Model Flowchart

Model Input and Set-up

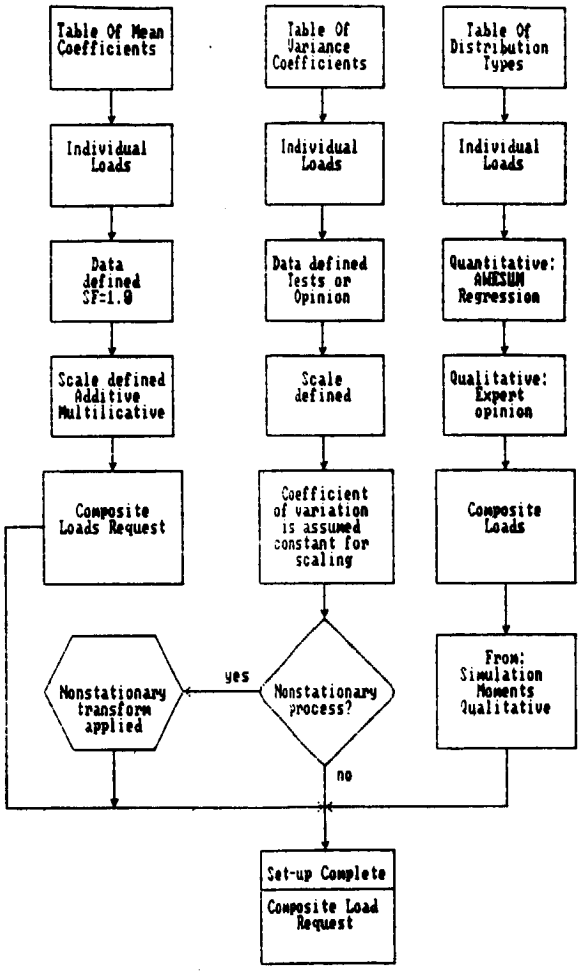

Probabilistic Model Flowchart

Model Calculations

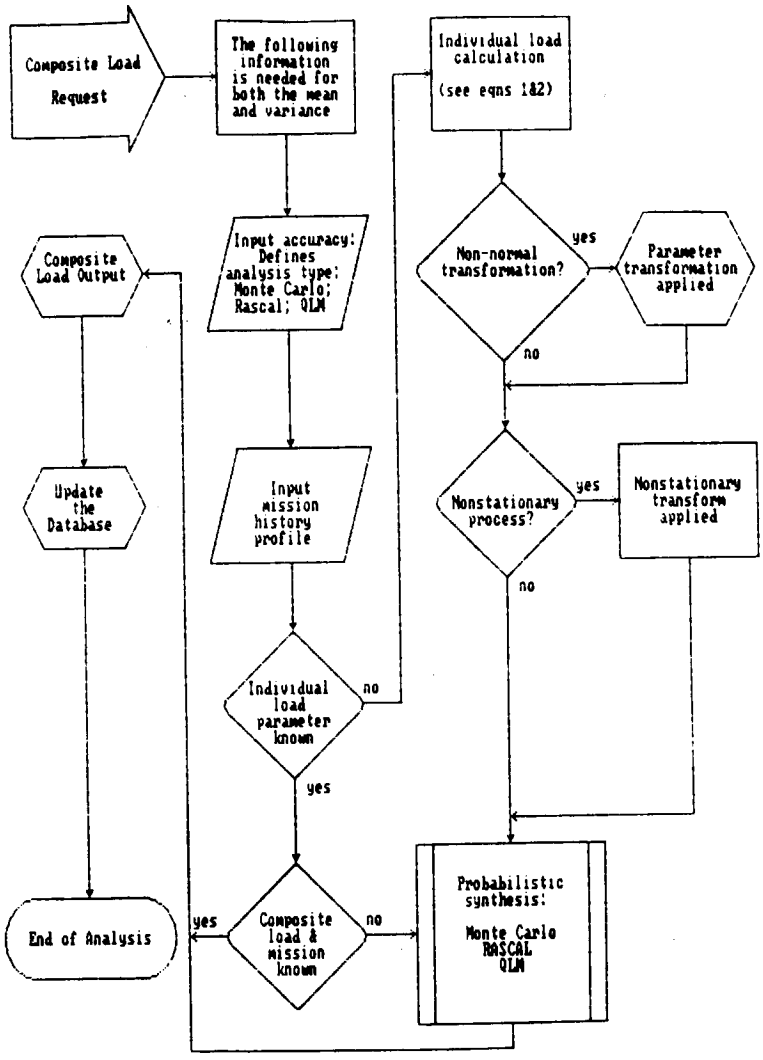

Sample Calculation I

RASCAL Verification

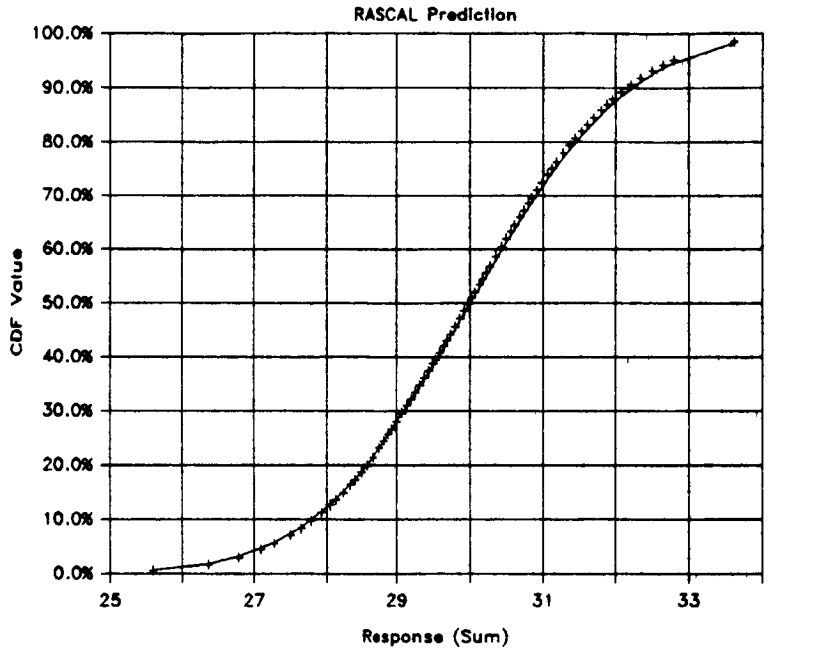

- Sum of three normal variables N(10, 1)
- Known mean of 30 and variance of 3
- Prediction obtained from the 1% to 99% values of the CDF is within 0.02% relative error of the theoretical distribution

Sample Calculation II
Low Probability Calculations

RASCAL Prediction: Failure Probability

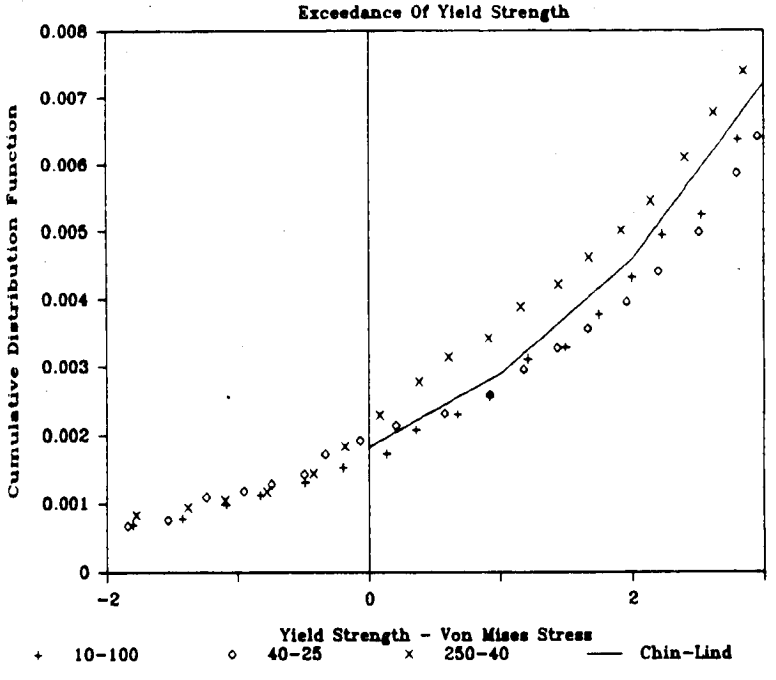

- Pressure vessel failure probability model used because previous analysis is available for comparison
- Fast probability integerator (Wirsching and Wu)
- RASCAL and FPI predictions closely agree

Sample Calculation III

Transient Load Model

Transient Temeperature Model

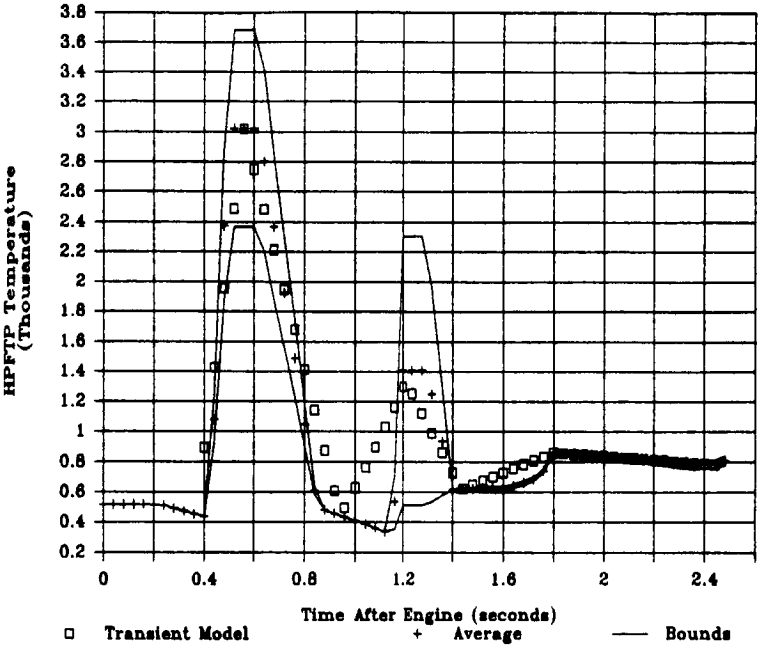

- Frequency of:
  - Number of peak amplitudes
  - Magnitude of peak amplitudes
  - Timing of peak amplitudes
- Piecewise linear model is used
- Plot compares model to ensemble average for the verification.

Sample Calculation IV

Transient Model Validation

Transient Temeperature Model

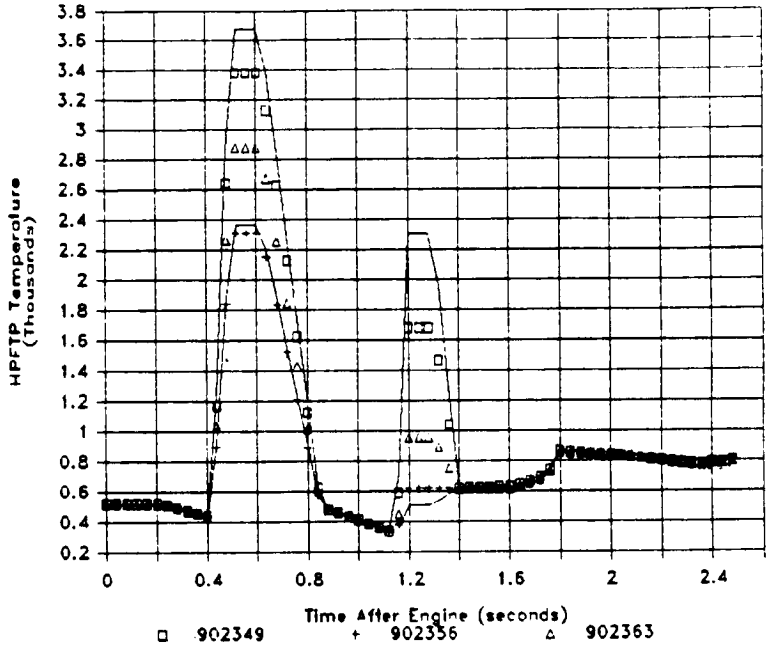

- SSME HPFTP data was examined for data sets that spanned the the possible range of sample paths
- Plot compares transient model and three selected test sets
- Comparison appears very good

Sample Calculation V

Mission Phase Linking

Transient Temeperature Model

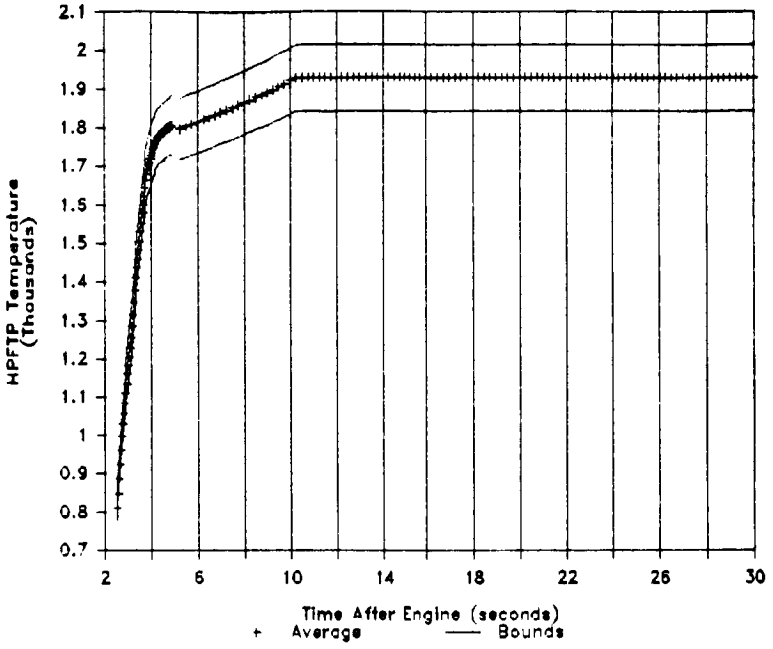

- Transient spike values not shown
- Influence function only valid above 65% rated power level
- Extrapolation used to move from the end of the tranmsient data set to the beginning of the quasi-steady phase
- Agreement between the point reached from extrapolation and the 65% level for temperature is very good

SUMMARY

- A probabilistic load model has been developed that is capable of addressing all portions of the mission profile
- The model can address constant, random, spike, and periodic load forms
- Comparisons to date have shown the model to work well in comparison to available data

STRUCTURAL TAILORING USING THE SSME/STAEBL CODE*

Robert Rubinstein
Sverdrup Technology, Inc.
Lewis Research Center Group
Cleveland, Ohio

Space Shuttle Main Engine (SSME) blades are subject to severe thermal, pressure, and forced vibration environments. An SSME blade design must meet tight clearance, fatigue life, and stress limit constraints. Because of the large number of potentially conflicting constraints, a "manual" design procedure may require many time-consuming iterations. Structural optimization provides an automated alternative. Any number of analyses, design variables, and constraints can be incorporated in a structural optimization computer code. This idea has been applied to develop the code SSME/STAEBL, which is a stand-alone code suitable for automated design of SSME turbopump blades.

SSME/STAEBL was developed by systematically modifying and enhancing the STAEBL (Structural Tailoring of Engine Blades) code developed by Pratt and Whitney under contract to NASA Lewis Research Center. STAEBL was designed for application to gas turbine blade design. Typical design variables include blade thickness distribution and root chord. Typical constraints include resonance margins, root stress, and root to chord ratios. In this program, the blade is loaded by centrifugal forces only.

Additions and modifications of STAEBL included in SSME/STAEBL include (1) thermal stress analysis, (2) gas dynamic (pressure) loads, (3) temperature dependent material and thermal properties, (4) forced vibrations, (5) tip displacement constraints, (6) single crystal material analysis, (7) blade cross section stacking offsets, (8) direct time integration algorithm for transient dynamic response. Capabilities are also included which permit data transfer from finite element models and stand-alone analysis.

Several design optimization studies have been completed using an SSME blade design to test these various capabilities. Optimization studies have been completed to test the influence of thermal and pressure loads and temperature dependent properties on optimal blade design. Comparison between designs optimized under centrifugal loads only and under centrifugal, thermal, and pressure loads with temperature dependent blade properties shows that the additional loads require additional weight to meet all design constraints. The difference between the designs can be attributed to material property temperature dependence, which in this case forces a much tighter root stress constraint.

Design optimization studies for a blade made of a typical single crystal material showed relatively little effect of crystal axis orientation. This

---

*Work performed under NASA Lewis Task Order No. 5207.

study was dominated by a root stress constraint which was violated by the initial design. It was found that root stress is influenced much less by crystal orientation than by the geometric design variables. The result is that the optimized design is found by adjusting the blade geometry significantly, but the crystal axis orientation insignificantly. Of course, in blade designs dominated by natural frequency constraints in particular, a different conclusion could obtain.

Optimization studies were undertaken to assess the influence of blade cross-section offsets on optimal design. These offsets are defined as the differences between the blade cross section centers of gravity and a straight line perpendicular to the engine axis. Blade designers use these variables to balance centrifugal and pressure loads. In a typical optimization study, the initial design violated the root stress constraint. Root stress is extremely sensitive to offset variables, and the optimized design recommended a significant change in stacking.

It can be concluded that structural optimization provides a practical and flexible approach to SSME blade design. The general structure of optimization algorithms allows many design variables, constraints, loads, and analysis options to be incorporated in the optimization procedure. In the design optimization studies reported here, which were dominated mainly by root stress constraints, it was found that temperature dependent properties can require additional weight in the optimized design, mainly by reducing the yield stress. Crystal axis orientation was relatively unimportant design variable in these studies. Blade cross-section stacking offsets were shown to have very significant effect on root stress-dominated designs. This conclusion agrees with the general experience of blade designers.

OBJECTIVE

Apply structural optimization methods to

SSME blade design.

STRUCTURAL TAILORING OF ENGINE BLADES (STAEBL)

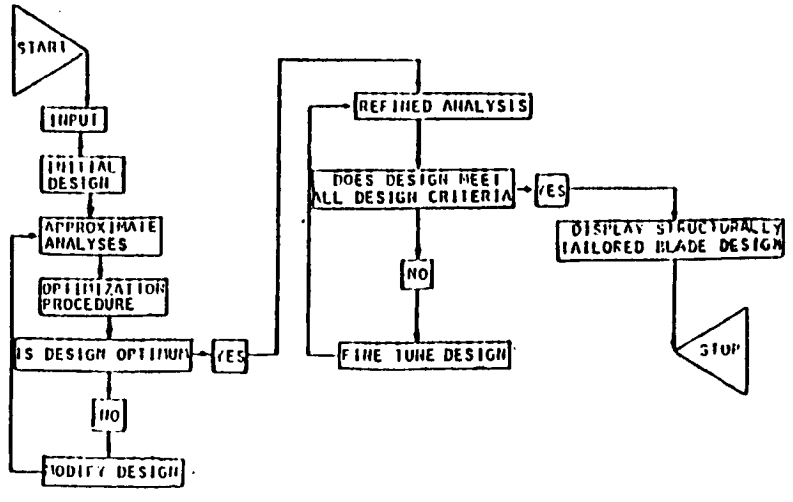

STAEBL FLOW CHART

OPTIMIZATION STUDY - SSME TURBOPUMP BLADE

COMPARISON BETWEEN INITIAL AND OPTIMIZED DESIGN

INITIAL DESIGN			OPTIMIZED DESIGN UNDER CENTRIFUGAL LOADS ONLY		
%SPAN	THK (IN)	CHD (IN)	% SPAN	THK (IN)	CHD (IN)
0.	.233	1.041	0.	.224	.890
50.	.138	.804	50.	.082	.681
100.	.092	.761	100.	.065	.650
NATURAL FREQUENCIES (CPS)					
	3562.			3454.	
	4383.			4868.	
	7916.			7969.	
ROOT STRESS (KSI)		83.		108.	
TIP DISPLACEMENTS					
UNTWIST (DEG)		2.28		2.80	
UNCAMBER (DEG)		1.22		0.70	
TIP EXT (IN)		.0211		0.0027	
BLADE WEIGHT (LB)		.056		.043	
NUMBER OF BLADES		62		73	
STAGE WEIGHT (LB)		3.50		3.14	

OPTIMIZATION STUDY - SSME TURBOPUMP BLADE

EFFECT OF THERMAL, PRESSURE LOADS AND FORCED VIBRATION ON OPTIMAL DESIGN

CENTRIFUGAL LOADS ONLY, TEMPERATURE INDEPENDENT PROPERTIES			REPRESENTATIVE THERMAL, PRESSURE LOADS TEMPERATURE DEPENDENT PROPERTIES		
% SPAN	THK (IN)	CHD (IN)	% SPAN	THK (IN)	CHD (IN)
0.	.224	.890	0.	.228	.890
50.	.082	.681	50.	.082	.681
100.	.065	.650	100.	.077	.650
NATURAL FREQUENCIES (CPS)					
	3454.			3174.	
	4868.			4438.	
	7969.			8835.	
ROOT STRESS (KSI)		108.		65.	
TIP DISPLACEMENTS					
UNTWIST (DEG)		2.8		2.9	
UNCAMBER (DEG)		0.7		1.5	
TIP EXT (IN)		0.0027		0.0209	
FORCED RESPONSE MARGINS		.000		.592	
		.000		.557	
		.000		.010	
BLADE WEIGHT (LB)		.043		.044	
NUMBER OF BLADES		73		73	
STAGE WEIGHT (LB)		3.14		3.18	

SINGLE CRYSTAL ANALYSIS

EFFECT OF CRYSTAL ORIENTATION ON OPTIMAL DESIGN

	CRYSTAL ALIGNED WITH ROOT CHORD		CRYSTAL ALIGNED 45° TO ROOT CHORD	
% SPAN	THK. (IN)	CHD. (IN)	THK. (IN)	CHD. (IN)
0	.23	.89	.23	.89
50	.11	.69	.08	.69
100	.06	.65	.06	.65
FREQUENCIES (CPS)	5110.		5079.	
	6851.		6847.	
	13540.		13870.	
ROOT STRESS (KSI)	63.		65.	
STAGE WEIGHT (LB)	3.26		3.15	
CRYSTAL ORIENTATION EULER ANGLES				
α	.89 E-3		45.00	
β	.57 E-2		-.20 E-1	
γ	-.51 E-3		.48 E-2	

SINGLE CRYSTAL ANALYSIS

GRADIENT OF ROOT STRESS CONSTRAINT AT FIRST ITERATION

VARIABLE	GRADIENT
THICKNESS 1	-.24
THICKNESS 2	-.16
THICKNESS 3	.01
THICKNESS 4	.04
THICKNESS 5	.01
ROOT CHORD	1.55
EULER ANGLES	
α	.02
β	-.01
γ	.00

Optimization Study including blade stacking design variables

Initial Design			Final Design		
Z span	thk	chd	Z span	thk	chd
0.	.233	1.041	0.	.226	.890
50.	.138	.804	50.	.134	.688
100.	.092	.761	100.	.091	.650

blade stacking

A = 0.	B = 0.	A = -.0012	B = .0078
C = 0.	D = 0.	C = .0013	D = .0095

Root Stress

82. ksi	74 ksi.

z axis along span, blade length = L

Δx = x displacement from center of gravity

Δy = y displacement from center of gravity

$$\Delta x = A\,(z/L) + B\,(z/L)^2$$

$$\Delta y = C\,(z/L) + D\,(z/L)^2$$

Comparison between effects of thickness, root chord, and blade stacking on root stress.

Optimization run with root stress constraint violated by initial design

Design Variable		Gradient of Root Stress
	thk 1 (root)	-.21
	thk 2	-.25
	thk 3	.00
	thk 4	.02
	thk 5 (tip)	.00
	root chord	1.28
blade stacking	A	9.20
	B	8.77
	C	2.39
	D	2.82

NONISOTHERMAL ELASTO-VISCO-PLASTIC RESPONSE OF SHELL-TYPE STRUCTURES*

G.J. Simitses, R.L. Carlson, and R. Riff
Georgia Institute of Technology
Atlanta, Georgia

The prediction of inelastic behavior of metallic materials at elevated temperatures has increased in importance in recent years The operating conditions within the hot section of a rocket motor or a modern gas turbine engine present an extremely harsh thermomechanical environment. Large thermal transients are induced each time the engine is started or shut down. Additional thermal transient from an elevated ambient, occur whenever the engine power level is adjusted to meet flight requirements. The structural elements employed to construct such hot sections, as well as any engine components located therein, must be capable of withstanding such extreme conditions. Failure of a component would, due to the critical nature of the hot section, lead to an immediate and catastrophic loss in power and thus cannot be tolerated. Consequently, assuring satisfactory long term performance for such components is a major concern for the designer.

Traditionally, this requirement for long term durability has been a more significant concern for gas turbine engines than for rocket motors. However, with the advent of reusable space vehicles, such as the Space Shuttle, the requirement to accurately predict future performance, following repeated elevated temperature operation, must now be extended to include the more extreme rocket motor application.

A mathematical model and solution methodologies for analyzing structural response of thin, metallic shell-type structures under large transient, cyclic or static thermomechanical loads have been developed. Among the system responses, which are associated with these load conditions, are thermal buckling and creep buckling. Thus, geometric as well as material-type nonlinearities (of high order) can be anticipated and have been considered in the development of the mathematical model. Furthermore, this was accommodated in the solution procedures.

A complete true ab-inito rate theory of kinematics and kinetics for continuum and curved thin structures, without any restriction on the magnitude of the strains or the deformation, was formulated. The time dependence and large strain behavior are incorporated through the introduction of the time rates of the metric and curvature in two coordinate systems; a fixed (spatial) one and a convected (material) coordinate system. The relations between the time derivative and the covariant derivatives (gra-

---

*This work was performed under NASA Grant No. NAG3-534.

dients) have been developed for curved space and motion, so that the velocity components supply the connection between the equations of motion and the time rate of change of the metric and curvature tenors.

The metric tensor (time rate of change) in the convected material coordinate system is linearly decomposed into elastic and plastic parts. In this formulation, a yield function is assumed, which is dependent on the rate of change of stress, metric, temperature, and a set of internal variables. Moreover, a hypoelastic law was chosen to describe the thermoelastic part of the deformation.

A time and temperature dependent viscoplastic model was formulated in this convected material system to account for finite strains and rotations. The history and temperature dependence were incorporated through the introduction of internal variables. The choice of these variables, as well as their evolution, was motivated by phenomenological thermodynamic considerations. The nonisothermal elastic-viscoplastic deformation process was described completely by "thermodynamic state" equations.

The procedure employed permits the rates of the field formulation to be interpreted as increments in the numerical solution. This is particulary convenient for the construction of a finite element models together with incremental boundary condition histories. Finite element formulation was developed for curved beams and shells. The element matrixes were derived directly from the incrementally formulated equations using tensor oriented procedure.

Finite element solution of any boundary-value problem involves the solution of the equilibrium equation (global) together with the constitutive equation (local). Both equations are solved simultaneously in a step by step manner. The incremental form of the global and the local equation can be achieved by taking the integration over the incremental time step $\Delta t=t_{j+1}-t_j$. The rectangular rule has been applied to execute the resulting time integration.

For structures with unstable deformation paths (snap-buckling phenomenon), accurate and efficient description of the motion of the structure was obtained by inclusion of the inertia forces.

Applications: The response of a clamped circular arch and of a cylindrical panel were studied. The shallow circular clamped arch subjected to a single central concentrated load, as shown in Fig. 1, was analyzed. The material chosen for the numerical experimentation is the carbon steel C-45 (DIN 1720) with $E = 10^7$ psi, $\nu = 0.3$ and $\sigma_y = 2.7 \cdot 10^4$ psi at room temperature.

The arch response, the deflection time history and the influence of temperature on the arch response are shown in Figs. 2,3 and 4, respectively.

A thin cylindrical shell panel simply supported on all sides, made of the same material as the arch, and subjected to in-plane loads along the generators as shown in Fig. 5 was also studied.

The deflection time history of the panel is shown in Fig 6, for a value of $N_{\beta\beta} = 20$ lbs/in. This load is well below the critical (buckling) load for the geometry which is 42.15 lbs/in.

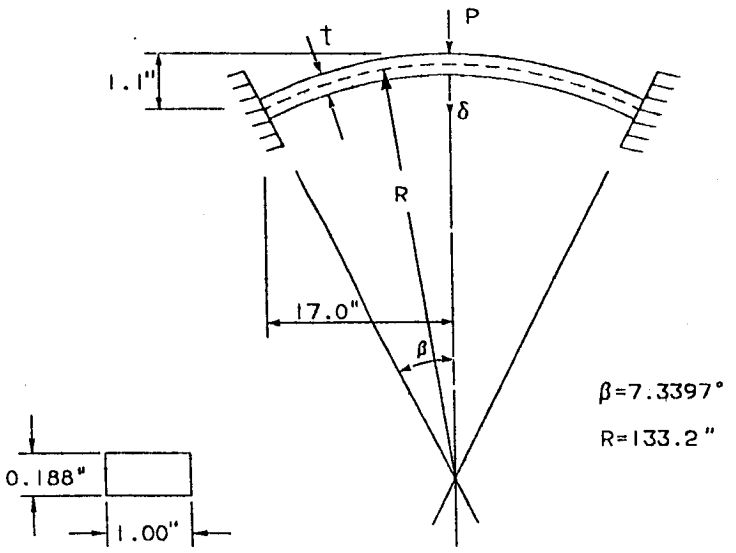

FIG. 1 CLAMPED CIRCULAR ARCH

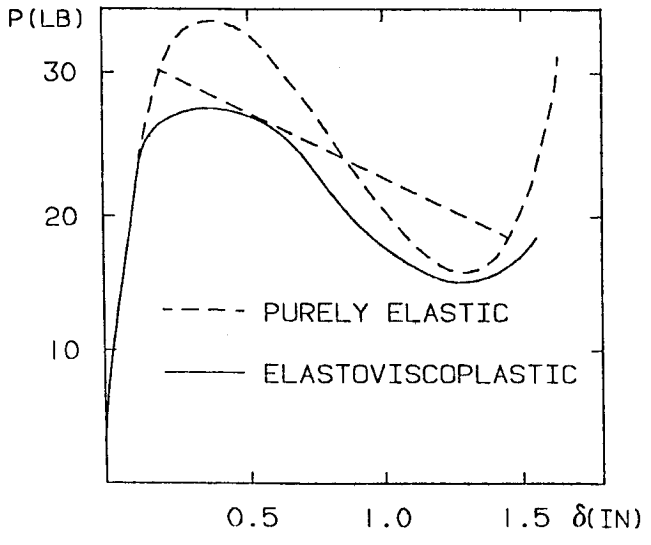

FIG. 2 THE ARCH RESPONSE

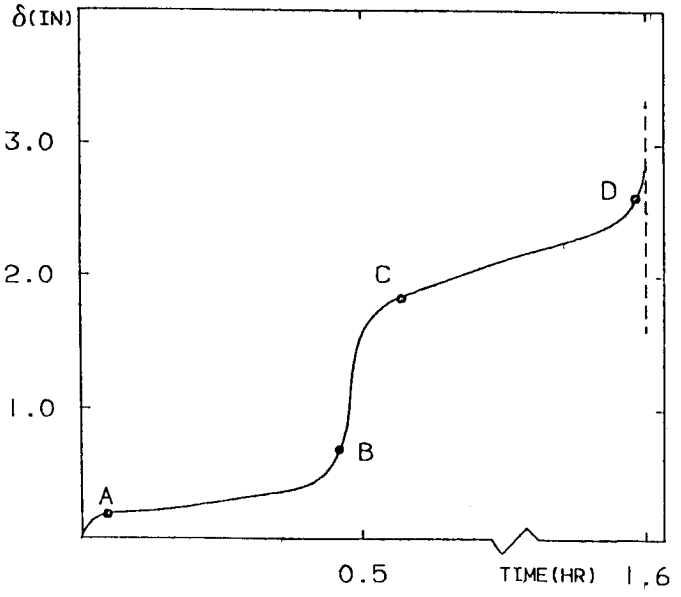

FIG. 3 DEFLECTION TIME HISTORY

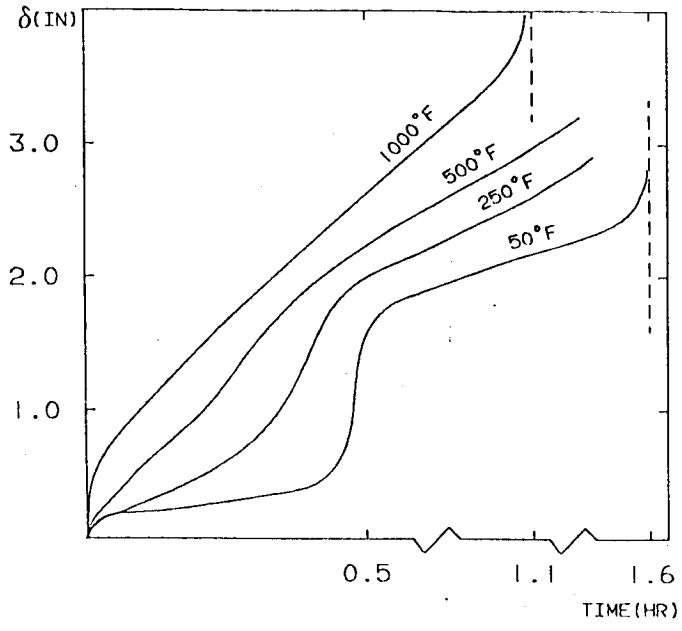

FIG. 4 THE INFLUENCE OF TEMPERATURE

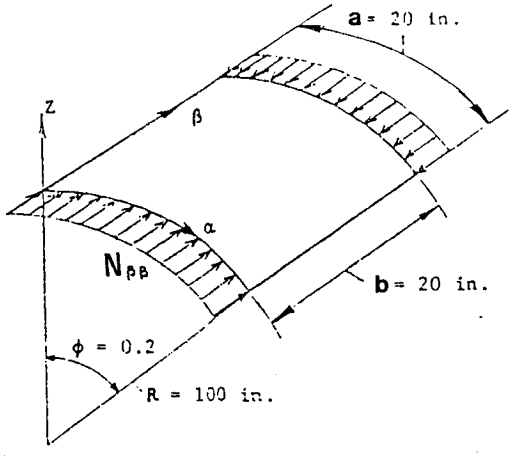

FIG. 5 CYLINDRICAL PANEL

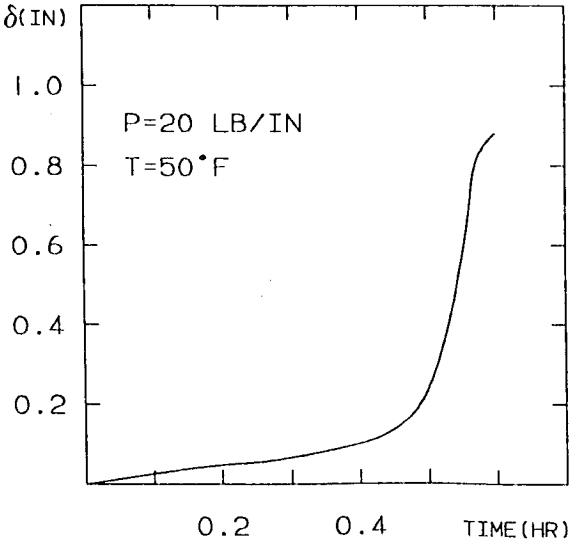

FIG. 6 CYLINDER PANEL CREEP RESPONSE

DYNAMIC CHARACTERISTICS OF SINGLE CRYSTAL SSME BLADES

L.A. Moss and T.E. Smith
Sverdrup Technology, Inc.
Middleburg Heights, Ohio

The SSME High Pressure Fuel Turbopump (HPFTP) blades are currently manufactured using a Directionally Solidified (DS) material, MAR-M-246+Hf. However, a necessity to reduce the occurrence of fatigue cracking within the DS blades has lead to an interest in the use of a Single Crystal (SC) material, PWA-1480.

A study was initiated to determine the dynamic characteristics of the HPFTP blades made of SC material and find possible critical engine order excitations. This study examined both the first and second stage drive turbine blades of the HPFTP. The dynamic characterization was done analytically as well as experimentally. The analytical study examined the SC first stage HPFTP blade dynamic characteristics under typical operating conditions. The blades were analyzed using MSC/NASTRAN and the finite element model shown in Figure 1. Two operating conditions, 27500 RPM and 35000 RPM, were investigated. Each speed had a unique blade temperature distribution. Bench experiments were conducted to determine the non-rotating natural frequencies and mode shapes.

Parametric studies were done varying the crystal orientation with respect to the blade. Crystal orientation was important because of the anisotropic nature of the material. Youngs Modulus was greatest along the crystal's <111> direction. The crystal <111> direction was referenced within the blade according to its projected rotate angle and tilt angle shown in Figure 2. The SC blades were initially analyzed at a tilt angle of 54.74 degrees such that its crystal growth direction was aligned in the blades' span direction, similar to the DS blade.

For the first three modes the frequency appeared to be least dependent on the crystal rotation angle. For the same modes the crystal tilt angle had a greater influence on the modal frequencies as shown in Figure 3. For modes four through six the crystal rotate angle had a more significant effect on natural frequencies as shown in Figure 4.

Campbell diagrams were constructed with the following critical engine orders determined by Rocketdyne; 11, 13, 15, 24, 26, 28, and 41. The modal analysis results for the SC blades were found to be worse than the DS when considering the engine order

interferences (see Figures 5 and 6). These results indicated critical engine order crossings may occur over the first three modes of the SC blades.

Additional investigations attempted to determine an optimum crystal orientation which would most effectively avoid the above interferences. The procedure was to vary the orientation of the crystals <111> direction between the extremes. The extremes would be strongest crystal direction either blade spanwise or chordwise. The best orientation when considering the a +/- 5% deviation of excitation frequency occurred at a tilt angle of 90 degrees and a rotate angle of 0 degrees (see Figure 7). It appears that for any orientation, the third mode interference will exist (Figure 8).

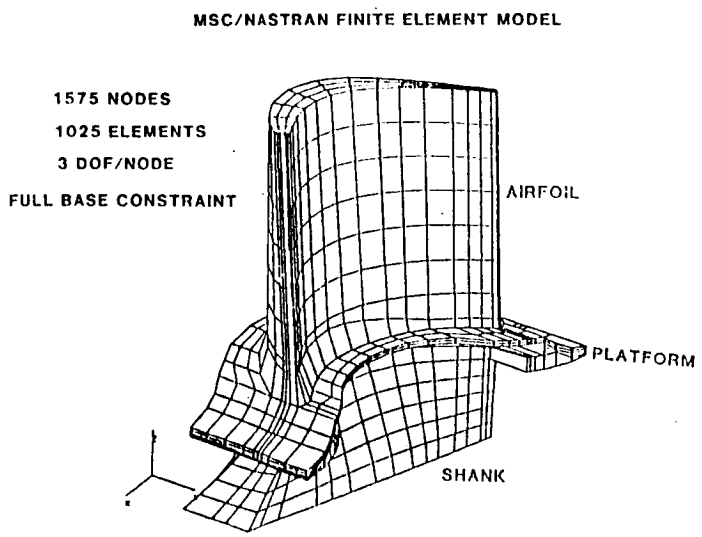

FIGURE 1

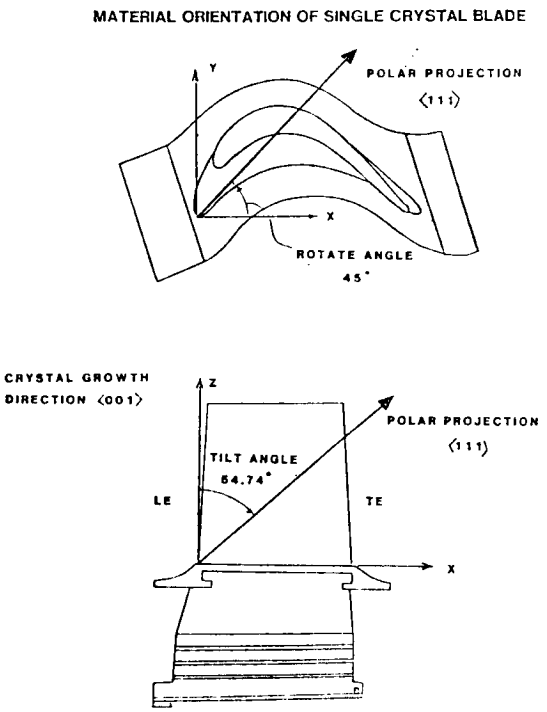

FIGURE 2

SSME HPFTP - 1st Stage Blade
PWA-1480; 35000 RPM; Taf=1400 F. and Tsh=1200 F.
1st Mode

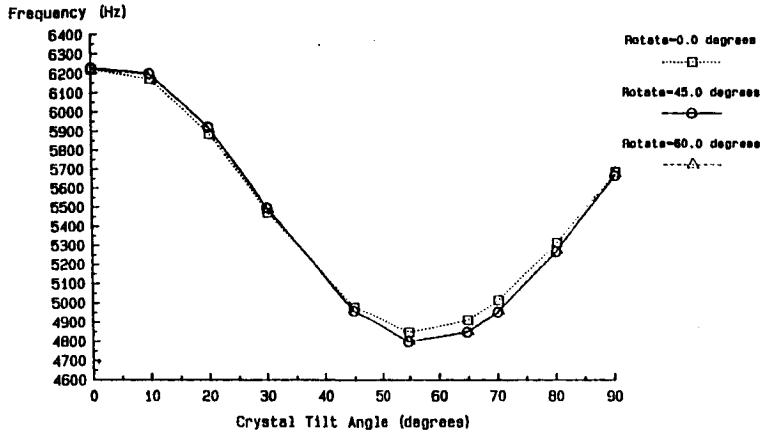

FIGURE 3

SSME HPFTP - 1st Stage Blade
PWA-1480; Nonrotating; 70 degress F.
4th Mode

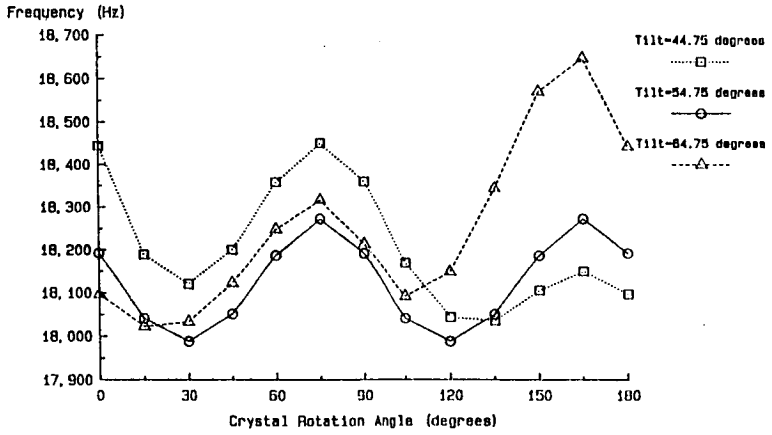

FIGURE 4

SSME HPFTP - 1ST STAGE BLADE
CAMPBELL DIAGRAM; DS MAR-M-246 Hf MATERIAL

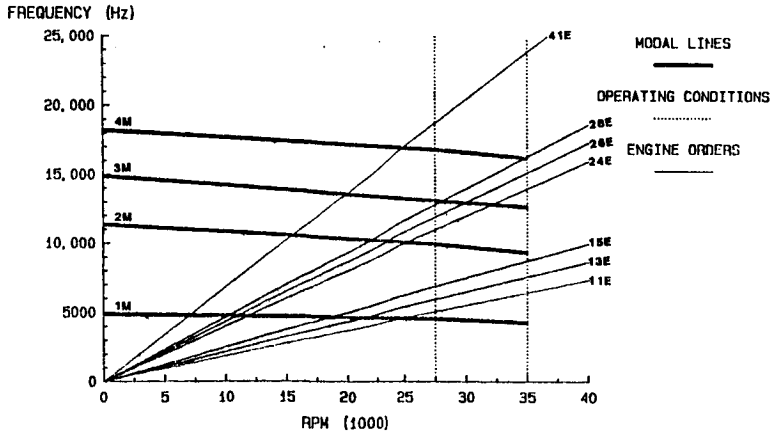

FIGURE 5

SSME HPFTP - 1ST STAGE BLADE
CAMPBELL DIAGRAM; PWA-1480 MATERIAL
SC ORIENTATION; TILT=54.74, ROTATE=0.0

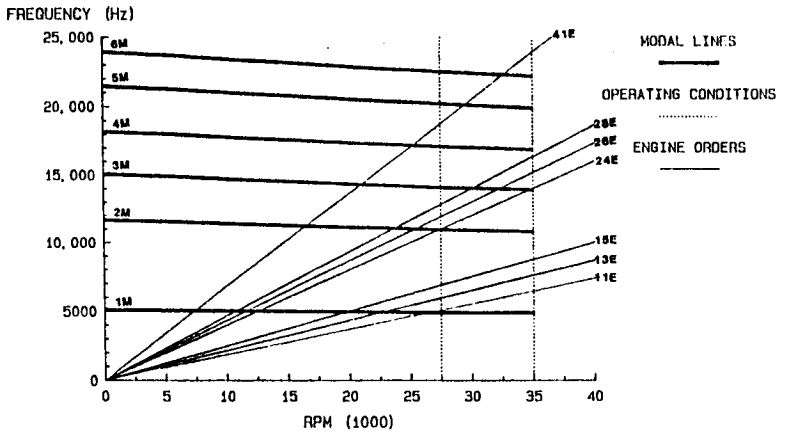

FIGURE 6

SSME HPFTP - 1ST STAGE BLADE
CAMPBELL DIAGRAM; PWA-1480 MATERIAL
SC ORIENTATION; TILT=90.00, ROTATE=00.0

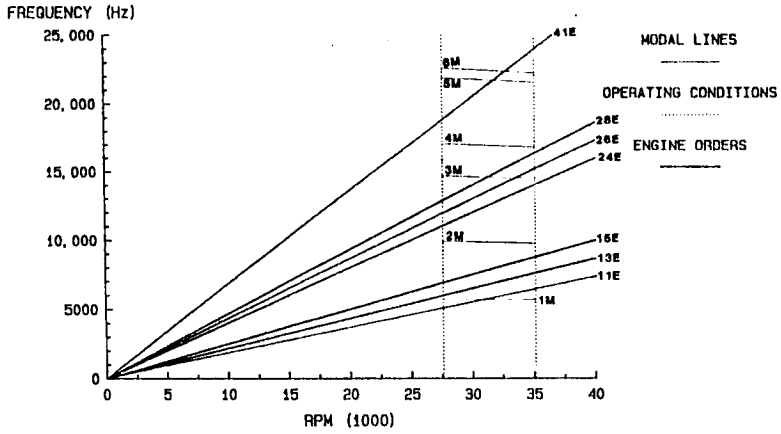

FIGURE 7

SSME HPFTP - 1st Stage Blade
PWA-1480; 35000 RPM; Taf=1400 F. and Tsh=1200 F.
3rd Mode

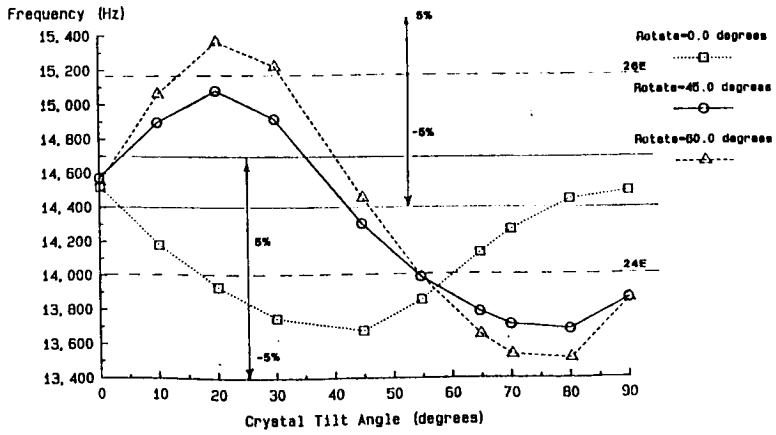

FIGURE 8

SSME BLADE DAMPER TECHNOLOGY

Robert E. Kielb
NASA Lewis Research Center
Cleveland, Ohio

and

Jerry H. Griffin
Carnegie-Mellon University
Pittsburgh, Pennsylvania

Before 1975 turbine blade damper designs were based on experience and very simple mathematical models. Failure of the dampers to perform as expected showed the need to gain a better understanding of the physical mechanism of friction dampers. Over the last 10 years research on friction dampers for aeronautical propulsion systems has resulted in methods to optimize damper designs.

The first-stage turbine blades on the SSME high-pressure oxygen pump have experienced cracking problems due to excessive vibration. A solution is to incorporate a well-designed friction dampers to attenuate blade vibration. The subject study, a cooperative effort between NASA Lewis and Carnegie-Mellon University, represents an application of recently developed friction damper technology to the SSME high-pressure oxygen turbopump.

The major emphasis of study was the contractor's design known as the two-piece damper. Damping occurs at the frictional interface between the top half of the damper and the underside of the platforms of the adjacent blades. The lower half of the damper is an air seal to retard airflow in the volume between blade necks.

A bench test apparatus was developed to conduct an extensive set of experiments on the two-piece damper. The bench test apparatus was successful. The normal load was applied through a fishhook-pulley-weights system. The weights were varied from 0.25 to 70 lb. The blade support was tuned to simulate blade natural frequencies at pump operating temperatures and speeds (approximately 9.5 KHz for the edgewise bending mode). The excitation system consisted of an electromagnet and a small chip of transformer iron mounted on the blade. Blade response, measured with a miniature accelerometer, was up to 700 G's tip acceleration, 0.1-mil tip displacement, and 1700-psi stress at the crack location.

Analytical models were fit to the experimental data and used to extrapolate the results to pump operating conditions. These extrapolations show that the best thickness for the two-piece damper is 0.047 in. and that the performance can be improved by reducing the width by 15 percent. Even with these improvements, the performance is poor. An example of predicted damper performance (pump conditions) is attached. The linear portion of the curve, emanating from the origin, is where the damper is locked and not functioning. The curved portion, beginning at an input level of 3 lbf, is where the damper starts to slip. The optimum condition is when the damper slips for approximately one-

half of the vibratory cycle. Since the stress required to crack the blade is estimated to be between 5000 and 10000 psi, we conclude that the damper is not working in the range of interest and is a poor design.

Two other damper designs were considered. A design, known as the X-damper, was found to be a poorer performer than the two-piece damper. A tip damper design was found to have excellent performance.

Whirligig tests are inconclusive concerning two-piece damper performance. However, these results strongly imply that the parameter controlling blade vibrations is tip clearance. Large tip clearance results in high stresses.

The hot-fire test results from MSFC are the only one which imply that the two-piece damper is effective in reducing stresses. Although this may be the case, the lack of cracked blades may be due to something other than the two piece dampers. For example, if the tip clearances on the blades in the hot-fire test are relatively tight, the blades would have low stresses without dampers.

In summary, the two-piece and X-dampers are poor performers. The tip damper is a good performer and should be more actively pursued. Because of the unknowns associated with tip clearance, the hot-fire test should not be used as a justification to incorporate the two piece damper into production. Additional testing should be conducted to understand the role of tip clearance on blade response.

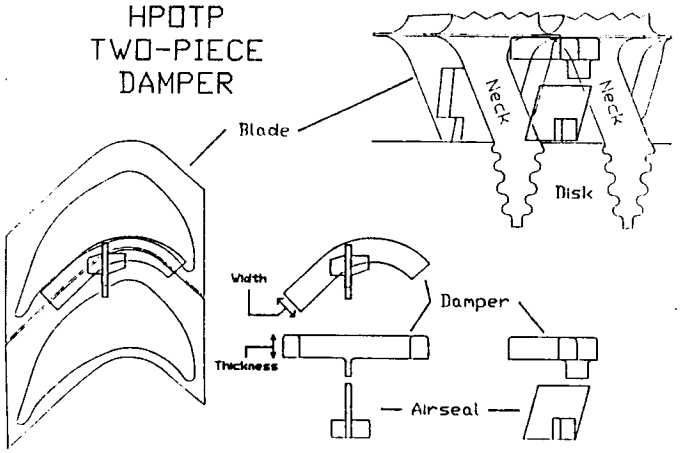

Figure 1.

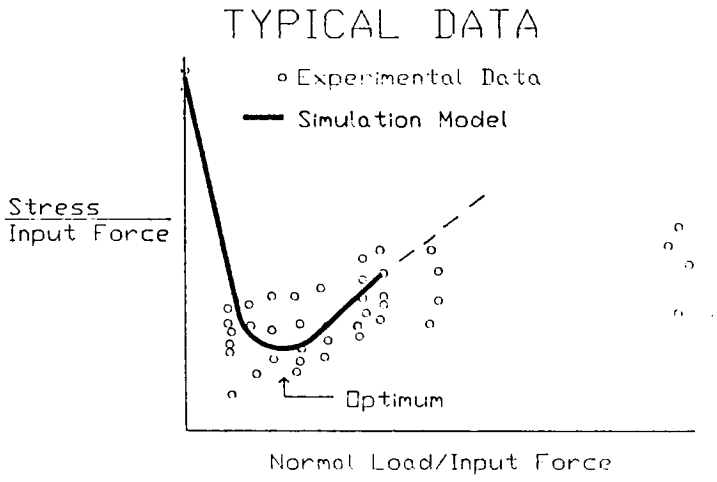

Figure 2.

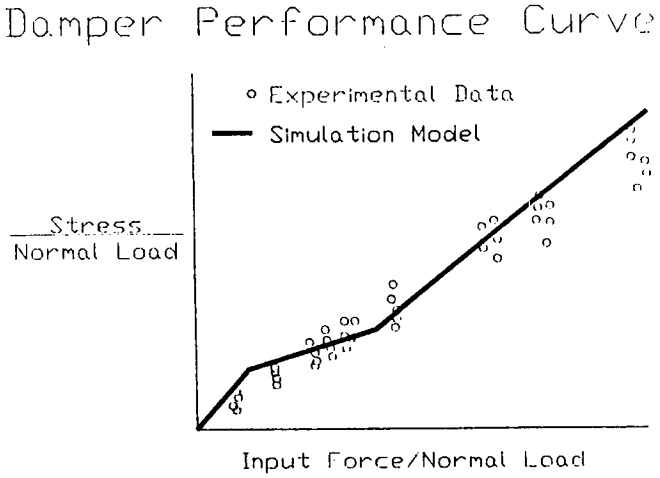

Figure 3.

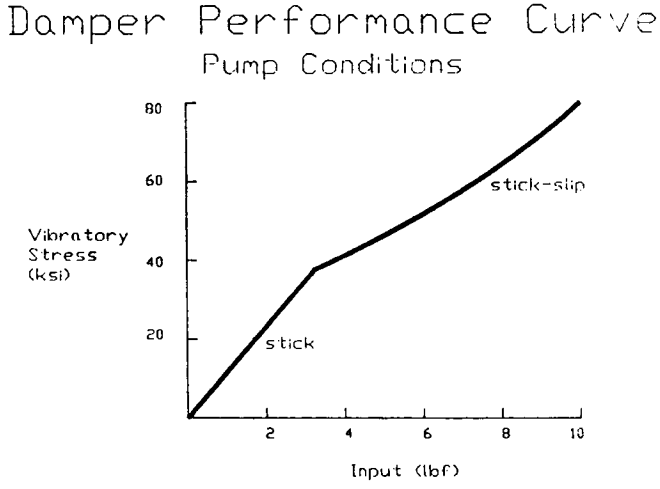

Figure 4.

DEVELOPMENT OF AN INTEGRATED BEM FOR HOT FLUID-STRUCTURE INTERACTION

G.F. Dargush and P.K. Banerjee
State University of New York at Buffalo
Buffalo, New York

The design of hot-section components such as those in SSME is generally accomplished by examining the solid and the fluid individually. Typically, the analysis that is required to support the design process is performed by separate groups using different techniques and computer codes. For a solid, a two-step approach is undertaken, a thermal analysis to determine the temperature profile using either a finite difference or a finite element method and the subsequent stress analysis by finite element method.

The finite element method for stress analysis has reached a very high level of maturity and sophistication. Principal codes have comprehensive facilities for material and geometric nonlinearities, inhomogeneity, anistropy, as well as considerable flexibility, in the specification of boundary conditions. A similar development of boundary element is well on the way as a part of the host program and has already proven to be extremely attractive and cost effective for both linear and nonlinear stress analyses problems.

Computational fluid dynamics is, however, at a much less developed stage. The governing equations are highly nonlinear and coupled. Finite difference method dominates the scene primarily due to its simplicity and consequently one has to pay a price for this simplicity. Extremely dense grids are required near boundary and in regions of high velocity gradients. Varying requirements of discretization in the flow field, boundary layer, etc. can often lead to stability and accuracy problems. Finite element methods have also been applied recently, but it also suffers from the same restrictions.

There is therefore a need to examine an alternative approach that considers the fluid flow and the solid deformation as a coupled problem using boundary element method. Since this method uses boundary equations,

it would be easier to develop a coupled analysis and since the nonlinearities in the fluid are primarily confined to regions, it may be possible to develop an efficient and cost effective solution.

METHOD OF ANALYSIS

Because the problem is essentially a coupled one, any separate treatment of each part (fluid and solid) would require the introduction of a complex set of artificially devised boundary conditions at the common interface to take care of the complex flow and heat transfer phenomenon. The problem is schematically depicted in Figure 1, where the solid region is subjected to pressure (p), temperature (T) resulting in displacements (u) and stresses. The flow of fluid from both inside the solid and outside is governed by the velocity (v), pressure (p) and temperature (T) as well as the boundary displacement (u).

A boundary integral representation for the entire coupled problem has been recently completed. The formulation is based on the fundamental analytical solution of the Navier-Stokes equation for the fluid velocity in an infinite domain. This fundamental solution was obtained by decomposing the Navier-Stokes equation into vorticity and dilation transport equations. A boundary integral formulation involving convolutions in time was then constructed in which the convective terms appear in the volume integral.

The entire fluid formulation has been implemented and the linear part of the viscous flow is already giving good results. It is hoped to get some nonlinear flow problems working within the next few months. Figure 2 shows 4 boundary elements and 1 cell representation for the couette flow problem and Figure 3 shows that the exact analytical solution is reproduced by such a simple discretization. It is therefore likely that viscous flow at a high Reynolds number could be efficiently solved by this method.

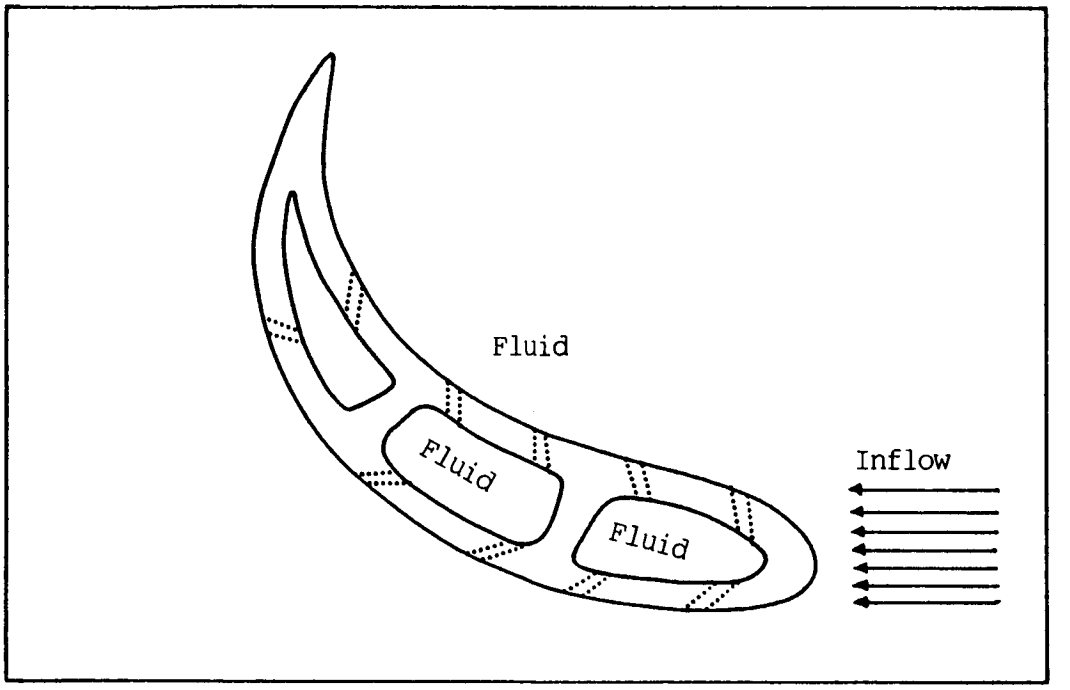

FIGURE 1

HOT FLUID STRUCTURE INTERACTION

BOUNDARY ELEMENT MESH

COUETTE FLOW

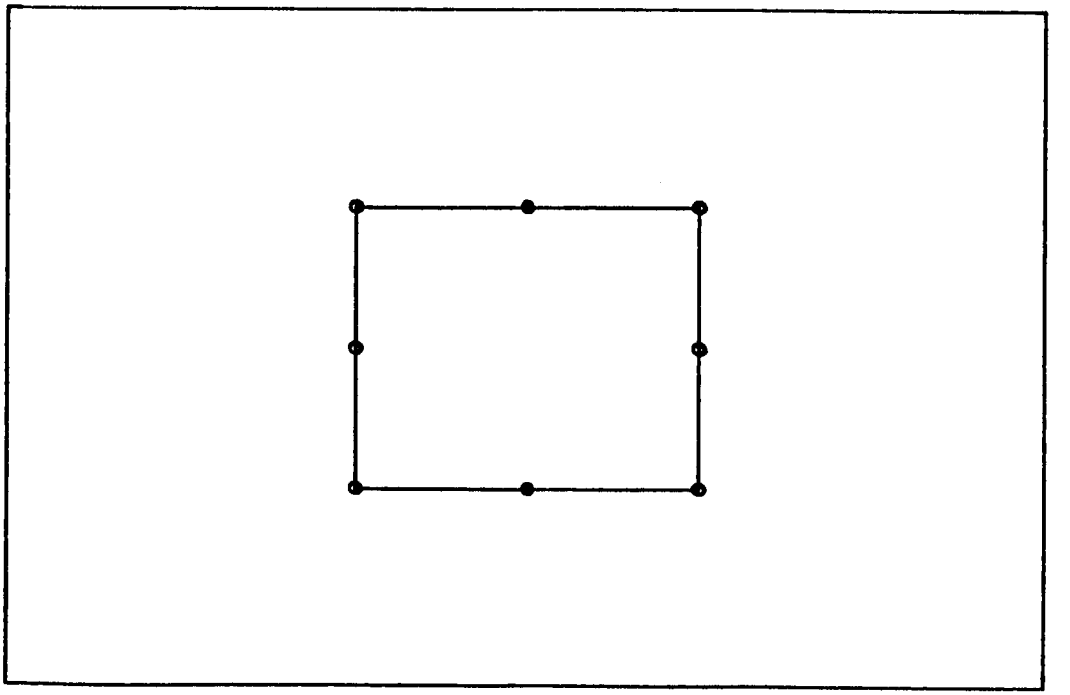

FIGURE 2

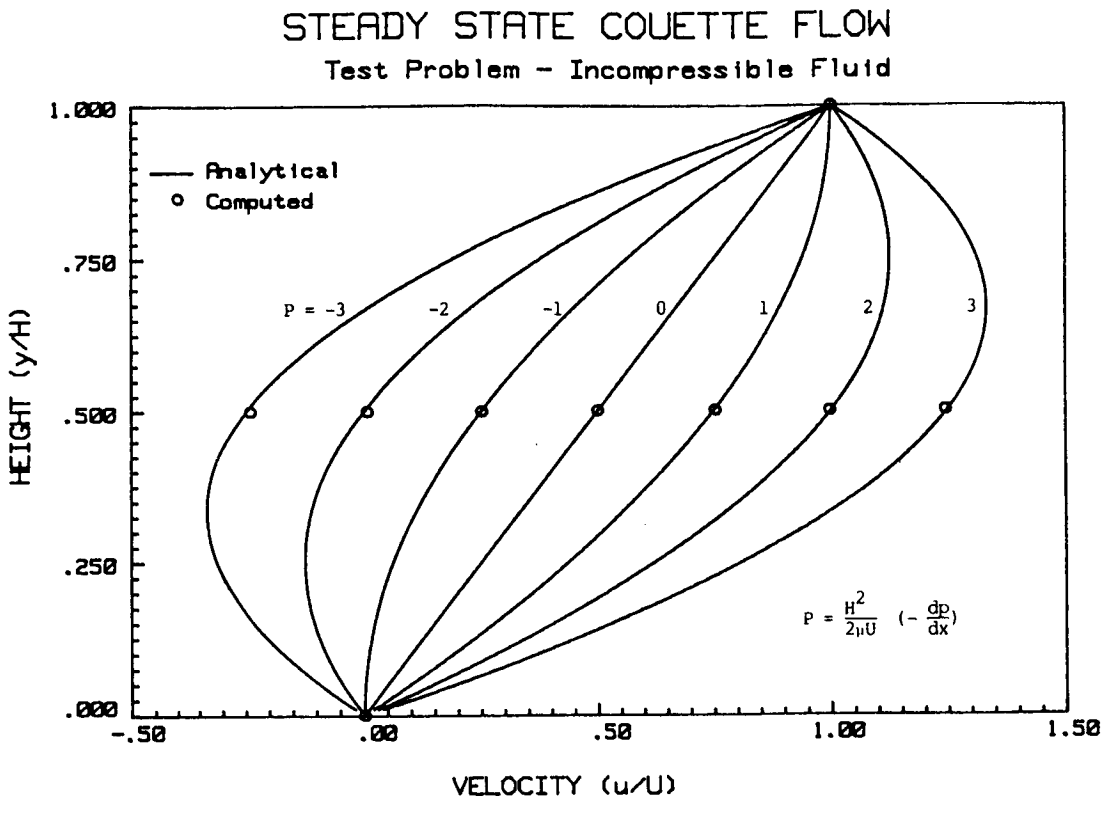
STEADY STATE COUETTE FLOW
Test Problem - Incompressible Fluid
Analytical
Computed
P = -3
-2
-1
0
1
2
3
$P = \frac{H^2}{2\mu U}\left(-\frac{dp}{dx}\right)$
1.000
.750
.500
.250
.000
HEIGHT (y/H)
-.50
.00
.50
1.00
1.50
VELOCITY (u/U)

FIGURE 3

1. Report No.	2. Government Accession No.	3. Recipient's Catalog No.
NASA CP-2471		

4. Title and Subtitle	5. Report Date
Structural Integrity and Durability of Reusable Space Propulsion Systems	6. Performing Organization Code: 553-13-00
7. Author(s)	8. Performing Organization Report No.: E-3512
	10. Work Unit No.
9. Performing Organization Name and Address: National Aeronautics and Space Administration, Lewis Research Center, Cleveland, Ohio 44135	11. Contract or Grant No.
12. Sponsoring Agency Name and Address: National Aeronautics and Space Administration, Washington, D.C. 20546	13. Type of Report and Period Covered: Conference Publication
	14. Sponsoring Agency Code

15. Supplementary Notes

16. Abstract

A two-day conference on the structural integrity and durability of reusable space propulsion systems was held on May 12 and 13, 1987, at the NASA Lewis Research Center. Presentations were made by industry, university, and government researchers organized into four sessions: aerothermodynamic loads; instrumentation; fatigue, fracture, and constitutive modeling; and structural dynamics. The principal objectives of the conference were to disseminate research results to date and future plans in each of the four areas. This publication contains the extended abstracts and visual material presented during the conference.

17. Key Words (Suggested by Author(s))	18. Distribution Statement
Earth-to-orbit proportion; Reusable rocket systems; Aerothermodynamic loads; Fatigue; Constitutive modeling; Instrumentation	Unclassified - unlimited STAR Category 20

19. Security Classif. (of this report)	20. Security Classif. (of this page)	21. No. of pages	22. Price*
Unclassified	Unclassified	232	A11

*For sale by the National Technical Information Service, Springfield, Virginia 22161